

DOKUZ EYLÜL UNIVERSITY
GRADUATE SCHOOL OF NATURAL AND APPLIED
SCIENCES

DESIGN OF OPTICAL CHEMICAL
NANOSENSORS FOR DETERMINATION OF
SOME SELECTED CATIONS AND ANIONS IN
AQUEOUS SAMPLES AND EVALUATION OF
THE INTERFERENCE EFFECTS

by
Sibel KAÇMAZ

July, 2012
iZMiR

**DESIGN OF OPTICAL CHEMICAL
NANOSENSORS FOR DETERMINATION OF
SOME SELECTED CATIONS AND ANIONS IN
AQUEOUS SAMPLES AND EVALUATION OF
THE INTERFERENCE EFFECTS**

**A Thesis Submitted to the
Graduate School of Natural and Applied Sciences of Dokuz Eylül University
In Partial Fulfillment of the Requirements for the Degree of Doctor of
Philosophy in Chemistry, Analytical Chemistry Program**

**by
Sibel KAÇMAZ**

**July, 2012
İZMİR**

Ph.D. THESIS EXAMINATION RESULT FORM

We have read the thesis entitled “**DESIGN OF OPTICAL CHEMICAL NANOSENSORS FOR DETERMINATION OF SOME SELECTED CATIONS AND ANIONS IN AQUEOUS SAMPLES AND EVALUATION OF THE INTERFERENCE EFFECTS**” completed by **SİBEL KAÇMAZ** under supervision of **PROF. DR. KADRIYE ERTEKİN** and we certify that in our opinion it is fully adequate, in scope and in quality, as a thesis for the degree of Doctor of Philosophy.



Prof. Dr. Kadriye ERTEKİN

Supervisor



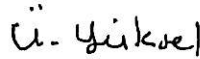
Prof. Dr. M. Yavuz ERGUN

Thesis Committee Member



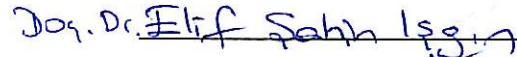
Yard. Doç. Dr. Aylin ALBAYRAK

Thesis Committee Member




Prof. Dr. Ümran YÜKSEL

Examining Committee Member



Examining Committee Member



Prof. Dr. Mustafa SABUNCU
Director

Graduate School of Natural and Applied Sciences

ACKNOWLEDGMENTS

I would like to express my sincere gratitude to my supervisor Prof. Dr. Kadriye ERTEKİN for providing the fascinating subject, for her valuable support during this thesis and for the great working conditions at our laboratory.

Besides my advisor, I would like to thank the rest of my thesis committee: Prof. Dr. M. Yavuz ERGUN and Yard. Doç. Dr. Aylin ALBAYRAK for their encouragement, valuable suggestion, guidance through out the work.

I gratefully acknowledge that my personal funding was provided by the Scientific Research Council of Turkey (TUBITAK) (Multi-Disciplinary Earthquake Researches in High Risk Regions of Turkey Representing Different Tectonic Regimes–TURDEP Project) and Center for Earthquake Research (DAUM) of Dokuz Eylul University.

I would like to thank to help of my flatmate, Süendam KUNİ.

Finally, I would like to thank to my parents and especially to my mother Pakize KAÇMAZ, my father Hayrettin KAÇMAZ and my sister Dr. Hülya KAÇMAZ for their tolerant attitude to my working effort during the elaboration of this dissertation and for their incessant support and understanding during all the years of my studies.

Sibel KAÇMAZ

**DESIGN OF OPTICAL CHEMICAL NANOSENSORS FOR
DETERMINATION OF SOME SELECTED CATIONS AND ANIONS IN
AQUEOUS SAMPLES AND EVALUATION OF THE INTERFERENCE
EFFECTS**

ABSTRACT

In this thesis, we designed original optical chemical nanosensors exploiting electrospun nanofibrous materials for optical sensing of silver (I), mercury (II), iron (III), hydroxyl, calcium (II) and copper (II) ions at sub-nanomolar levels in aqueous samples.

Poly(methyl methacrylate) and ethyl cellulose were used as polymeric materials together with appropriate fluoroionophores and other additives. Cation and /or anion sensing nanomaterials were fabricated by electrospinning that the most convenient way to make a nano-scale continuous polymer uses a high static voltage to draw the fiber from a liquid polymer. Sensors were based on the change in the fluorescence signal intensity of all employed ionophore. The offered nanosensors allow determination of ions in a large linear working range. The preliminary results of Stern–Volmer analysis show that the sensitivities of electrospun nanofibrous membranes to detect ions are 10-100-fold higher than those of the thin film based sensors. The extraordinary sensitivities can be attributed to the high surface area of the nanofibrous membrane structures that provided faster sensor dynamics in applications. In all of the sensor designs, sensor performance characteristics such as the response time, long-short term stabilities, reversibility, limit of detection, linear concentration range, repeatability and interference effects also have been studied.

Last of all, we have successfully combined the nanoscale electrospun fiber materials with optical sensing technology exploiting appropriate fluoroionophores for subnanomolar sensing of ions without interference effects.

Keywords: Optical nanosensor, anion-cation sensors, fluorescence, spectrofluorometer, fiber optic prob, electrospinning, ionic liquid.

SULU ÖRNEKLERDE BAZI SEÇİLMİŞ KATYON VE ANYONLARIN TAYİNİNE YÖNELİK OPTİK KİMYASAL NANOSENSÖR TASARLANMASI VE GİRİŞİM ETKİLERİNİN DEĞERLENDİRİLMESİ

ÖZ

Bu tezde, Gümüş (I), Civa (II), Demir (III), Hidroksil, Kalsiyum (II) ve Bakır (II) iyonlarının, su örneklerinde nanomolar altı düzeylerde tayinine yönelik olarak orjinal optik kimyasal nanosensörler tasarlanmıştır.

Polimerik malzemeler olarak poli(metil metakrilat) ve etil selüloz'un yanında uygun floroanyonforlar ve diğer katkı maddeleri birarada kullanılmıştır. Katyon ve/veya anyonları algılayıcı nanomalzemeler elektroegirme yöntemiyle üretilmiştir. Elektro egirme yöntemi, yüksek bir statik voltajın kullanılmasıyla, sıvı bir polimerden nano boyutta sürekli polimerik fiber yapmak için en uygun yoldur. Sensörler, kullanılan bütün iyonoforların floresans sinyal şiddetinde yaptığı değişikliğe dayanmaktadır. Önerilen nanosensörler, iyonların tayini için oldukça büyük bir doğrusal çalışma aralığı sağlamaktadır. Stern-Volmer analizi sonuçlarına göre, iyonları algılamada ince film tabanlı sensörlere kıyasla elektro-egirme ile üretilmiş nanofiberler membranların hassasiyetlerinin 10–100-kat daha fazla olduğu görülmüştür. Bu olağanüstü duyarlılığın, nanofiber yapıların daha yüksek yüzey alanına sahip olmasından kaynaklandığı ve uygulamalarda daha hızlı bir sensör dinamiği sağladığı düşünülmektedir. Tüm sensör tasarımlarında, sensör yanıtı, uzun-kısa dönem kararlılığı, rejenere edilebilirliği, tayin limiti, doğrusal çalışma aralığı, tekrarlanabilirlik ve girişim etkileri gibi sensör performans özellikleri de incelenmiştir. Sonuç olarak, girişim etkileri olmadan ve nanomolar altı düzeylerde iyonları tayin edebilmek için, elektro-egirme yöntemi ile üretilmiş uygun iyonoforları içeren nanoboyutta fiber malzemeler optik sensör teknolojisi ile başarılı bir şekilde kombine edilmiştir.

Anahtar kelimeler: Optik nanosensörler, anyon-katyon sensörleri, floresans, spektrofotometre, fiber optik sensör, elektro-egirme, iyonik sıvı.

CONTENTS	pages
Ph.D. THESIS EXAMINATION RESULT FORM	ii
ACKNOWLEDGMENTS	iii
ABSTRACT.....	iv
ÖZ	v
CHAPTER ONE - INTRODUCTION	1
1.1 Chemical Composition and Constituents of Water	1
1.1.1 A summary of techniques for Chemical Analysis of Water	3
1.2 Optical Chemical Sensing Approach	4
1.2.1 Classification of Sensors.....	6
1.2.2 Fiber optic	7
1.2.2.1 Sensing Modes and Fiber-Optic Assemblies	8
1.2. 3 A Short View to the Optical Chemical Sensors.....	9
CHAPTER TWO - ELECTROSPINNING AND NANOFIBER	12
2.1 Nanotechnology and Nanomaterials.....	12
2.2 Electrospinning for Polimeric Nanofiber	13
2.3 Electrospun Nanofibrous Membranes for Sensors.....	16
CHAPTER THREE - EXPERIMENTAL METHOD AND INSTRUMENTATION	17
3.1 Reagents	17
3.2 Structural Specification of Ionophores	19
3.3 Fabrication of Electrospun Nanofibers.....	23

3.4 Thin Film Fabrication.....	25
3.5 Electrospinning Apparatus	26
3.6 Apparatus and Experimental Setup	26
3.7 Rtils as Polymer Electrolytes	28
3.8 Stoke’s Shift and Quantum Yield Calculations.....	30
3.9 Stern-Volmer Analysis	33

CHAPTER FOUR - EMISSION BASED SUB-NANOMOLAR SILVER SENSING WITH ELECTROSPUN NANOFIBERS..... 35

4.1 Introduction	35
4.2 Spectral Characterization of Fluoroionophore	37
4.2.1 Absorption Spectra Related Characteristics	37
4.2.2 Emission Spectra Related Characteristics.....	38
4.2.3 Quantum Yield Calculations.....	39
4.3 SEM Images of Electrospun Membranes	44
4.4 pH Dependency of the M-AZM Dye.....	47
4.5 Silver Uptake and Fluorescence Based Response	51
4.6 Stern–Volmer Analysis	54
4.7 Response and Detection Limit.....	56
4.8 Selectivity Studies and Interference Effects.....	58
4.9 Conclusion.....	59

CHAPTER FIVE - SUB-NANOMOLAR SENSING OF IONIC MERCURY WITH POLYMERIC ELECTROSPUN NANOFIBERS 60

5.1 Introduction	60
5.2 Photocharacterization of Fluoroionophore	62

5.3 Quantum Yield Calculations	64
5.4 SEM images of electrospun membranes	65
5.5 Dissociation Constant (pKa) Calculations of Indicator Dye In EC Matrix.....	66
5.6 Response to Mercury Ions	67
5.7 Stern-Volmer Analysis	71
5.8 Effect of pH on Hg (II) response	72
5.9 Selectivity Studies, Regeneration And Interference Effects	73
5.10 Conclusion.....	75

**CHAPTER SIX - DEVELOPMENT OF OPTICAL CHEMICAL SENSOR
BASED ON POLYMER NANOFIBERS FOR Ag (I) ION DETECTION..... 77**

6.1 Introduction	77
6.2 Investigation of the Photophysical Properties of the Present Indicator Dye	78
6.3 Fluorescence Quantum Yield Calculation.....	80
6.4 SEM Images	81
6.5 Detection of pK _a for TM-AZM	83
6.6 Response to Ag (I) Ions in Thin Film and Nanofiber Form.....	86
6.7 Evaluation of Effect of pH on Ag (I) Response and Interference Effects.....	90
6.8 Stern-Volmer Analysis and Determination of K _{sv} Constant	92
6.9 Reversibility Performance	93
6.10 Conclusion.....	93

**CHAPTER SEVEN - FLUORESCENT Fe³⁺ SENSING AT FEMTO-MOLAR
LEVEL WITH FUNCTIONAL ELECTROSPUN NANOFIBERS..... 94**

7.1 Introduction	94
------------------------	----

7.2 Spectral Evaluation, Photostability and Fluorescence Quantum Yield Calculations	97
7.3 SEM Displays	100
7.4 Explanation of Effect of pH on the response for Fe ³⁺	101
7.5 Dynamic Working Range and Fe ³⁺ Response	102
7.6 Stern-Volmer Analysis	105
7.7 Specification of Selectivity and Interference Effect	107
7.8 Response Time, Regeneration and Reproducibility	108
7.9 Conclusion	110

CHAPTER EIGHT - FIBER OPTIC HYDROXYL (OH) SENSING WITH LONG WAVELENGTH EXCITABLE IONOPHORE DOPED IN NANOFIBERS 111

8.1 Introduction	111
8.2 Photocharacterization of Newly Synthesized BCDA Dyes and Assesment of Quantum Yield	112
8.3 SEM Images of Electrospun Membranes	116
8.4 Discussions Related to Possible Sensing Mechanism of BCDA	117
8.5 pKa Calculations of BCDA in EtOH	119
8.6 pKa Calculations of BCDA in EC Matrix	121
8.7 Dynamic Working Range and Sensor Response	123
8.8 Possible Intereference Effects	124
8.9 Conclusion	125

CHAPTER NINE - DESIGN OF A NOVEL FLUORESCENT OPTICAL SENSOR USING NANOFIBROUS MEMBRANES FOR Ca (II)..... 127

9.1 Introduction	127
9.2 Spectral Evaluation of Newly Synthesized DMK-OFD-BIS Dye and Quantum Yield Calculations	129
9.3 pKa Calculations of DMK-OFD-BIS in EC Matrix.....	132
9.4 SEM Images of Electrospun Membranes	133
9.5 Interference Effects	135
9.6 Effect of pH on the Calcium Response	136
9.7 Dynamic Working Range and Ca (II) Response	136
9.8 Conclusion.....	141
CHAPTER TEN - A NOVEL FLUORESCENT QUENCHING-BASED Cu (II) NANOSENSOR.....	143
10.1 Introduction	143
10.2 Spectral Evaluation of the DMK-OFD-7 Dye.....	146
10.3 Calculation of Fluorescence quantum yield (θ_F)	148
10.4 pKa Calculations of DMK-OFD-7 in EC Matrix.....	149
10.5 Photostability Study	151
10.6 Investigation of Interference Effects	152
10.7 Effect of pH on the Copper Response	153
10.8 Dynamic Working Range and Cu (II) Response.....	154
10.9 Stern-Volmer Analysis	158
10.10 SEM Images of Electrospun Membranes.....	160
10.11 Conclusion.....	161
CHAPTER ELEVEN - CONCLUSIONS.....	162
REFERENCES.....	165

CHAPTER ONE

INTRODUCTION

1.1 Chemical Composition and Constituents of Water

Water may contain various types' natural and different concentrations of dissolved, colloidal or suspended constituents.

Water in its most basic form is simply a molecule made up of two hydrogen atoms and an oxygen atom. However, water's dynamics through the hydrologic cycle adds many different substances, particularly mineral content, as dissolved solids. The mineral content in water consists of things our bodies need to be healthy and make tasteful the drinking water. The natural waters containing up to 0,1 % of dissolved substances, are named stale, from 0,1 up to 2,5 % - mineralised, from 2,5 up to 5 % - as waters with sea saltiness, more than 5 % - brine. The majority of salts of acids and bases can also be dissolved in water. The solutions of these substances are electrolytes (taken from http://water157.narod.ru/clear/root_e.htm).

The list of the main dissolved mineral components of natural waters include the ions Na^+ , K^+ , Ca^{2+} , Mg^{2+} , H^+ , Cl^- , HCO_3^- , CO_3^{2-} , SO_4^{2-} and gases O_2 , N_2 , CO_2 and H_2S . In small amounts such ions contain: Fe^{2+} , Fe^{3+} , Mn^{2+} , Br^- , I^- , F^- , BO_2^- , HPO_4^{2-} , SO_3^{2-} , HSO_4^- , $\text{S}_2\text{O}_3^{2-}$, HS^- , HSiO_3^- , HSO_3^- and gases CH_4 , Ar , He , Rn . Other substances are in water in the smaller amounts. Under the contents of the weighed substances and painted huminous substances, we distinguish highly coloured and highly turbid water. Except for the painted organic impurities, there are also colourless organic substances at natural waters - the products of life process of microorganisms and combinations acting with wastewater. In natural waters contain hydrocarbons, chlorids and sulfits of alkaline metals in the greatest amounts; their nitrates, nitrits and salts of other acids in smaller ones (taken from http://water157.narod.ru/clear/root_e.htm). Table 1.1 shows dissolved constituents in natural water classified by relative abundance.

Table 1.1 Dissolved constituents in natural water classified by relative abundance (Greenberg, Cleasceri, & Eaton, 1992)

Major constituents (1.0 to 1000 mg/L)	
Cations	
Sodium (Na ⁺)	high levels often associated with pollution
Calcium (Ca ²⁺)	Cause hardness when combined with HCO ⁻³ , CO ₂ ⁻³ , SO ₂ ⁻⁴ etc. - Ca ²⁺ normally below 15 mg/L
Magnesium (Mg ²⁺)	- Ca ²⁺ can be above 100 mg/L in carbonate-rich rocks - Mg ²⁺ normally between 1 and 50 mg/L depending upon rock type
Potassium (K ⁺)	generally low (<10) in natural fresh waters
Anions	
Hydrojencarbonate (HCO ₃ ⁻)	normally ranges from 25 to 400 mg/l
Sulfate (SO ₄ ²⁻)	is normally between 2 and 80 mg/l
Chloride (Cl ⁻)	is normally less than 40 mg/l in unpolluted waters
Silica	

Minor constituents (0.01 to 10.0 mg/L)	
Cations	
Boron	
Iron	
Potassium	
Strontium	
Anions	
Carbonate (CO ₃ ²⁻)	in fresh waters is normally dilute (<10 mg/l)
Fluoride	< 1 mg/L
Nitrate	is significant in some areas

Table 1.1 Dissolved constituents in natural water classified by relative abundance (Greenberg, Clesceri, & Eaton, 1992)

Trace constituents (< 0.1 mg/L)			
Aluminum	Antimony	Arsenic	Barium
Beryllium	Bismuth	Bromide	Cadmium
Cerium	Cesium	Chromium	Cobalt
Copper	Gallium	Germanium	Gold
Indium	Iodide	Lanthanum	Lead
Lithium	Manganese	Molybdenum	Nickel
Niobium	Phosphate	Platinum	Radium
Rubidium	Ruthenium	Scandium	Selenium
Silver	Thallium	Thorium	Tin
Titanium	Tungsten	Uranium	Vanadium
Yttrium	Zinc		Zirconium

1.1.1 A summary of techniques for Chemical Analysis of Water

The detection and quantification of cations and anions in waters are one of the important issues for scientists in worldwide. Thus, scientists are intensively continuing their work on developing new techniques for determination of anions and cations.

A number of techniques have been developed over the years for cations and anions analysis, including spectrophotometric (Rosha, Martelli, & Reis, 2004), capillary ion electrophoresis (Romano, & Krol, 1993), capillary electrophoresis(CE) by using indirect-UV detection (Hiissa, Siren, Kotiaho, Snellman, & Hautajarvi,

1999), ion Chromatography (Jackson, 2001), Atomic absorption spectrometry (AAS) (Arienzo, & Capasso, 2000; Chen, & Teo, 2001; Sperling, Xu, & Welz, 1992), inductively coupled plasma (ICP), graphite furnace atomic absorption spectroscopy (GFAAS), inductively coupled plasma emission or mass spectrometry (ICP-ES, ICPMS) (Chen, Megharaj, & Naidu, 2007; Forstner, & Wittmann, 1981; Liang, Qin, Hu, Peng, & Jiang, 2001; Merian, 1991; Fresenius, Quentin, & Schneider, 1988), High Performance Liquid Chromatography (HPLC) (Crafts, Bailey, Plante, & Acworth, 2009), total reflection X-ray fluorimetry (TXRF) (Klockenkampfer, 1997) and anodic stripping voltammetry (ASV).

Only some of them have found application in routine analysis. Detection limits for cation analysis in watery samples are 10^{-7} and 10^{-14} M for FAAS and GFAAS respectively. The GFAAS offers good limits of detection, but is an expensive and difficult method. Inductively coupled plasma emission-mass spectrometry is quite expensive and requires well educated users. Anodic stripping voltammetry only serves for analysis of limited number of cations.

As a result, most of these techniques are generally requiring expensive equipment, sample pretreatment, and/or analyte preconcentration steps. However, with respect to these techniques, optical chemical sensors have many advantages due to be a simple, rapid, inexpensive, selective and sensitive method. Because of these advantages, studies on optical sensor design have become one of the most popular fields of analytical chemistry.

1.2 Optical Chemical Sensing Approach

Chemical sensing using optics is under extensive research all over the world and many optical chemical sensors are finding increasing application in industry, environmental monitoring, medicine, biomedicine, chemical analysis, critical care, industrial hygiene, process controls, product quality controls, human comfort controls, emissions monitoring, automotive, clinical diagnostics, home safety alarms,

homeland security and, more recently. Chemical sensors have defined in different manners.

According to Baldini, '*Chemical sensors are miniaturized analytical devices that can deliver real-time and on-line information on the presence of specific compounds or ions in complex samples.*' In the easiest and simplest case, a sensor probe is inserted into the sample of interest to obtain an analytical signal that can be converted into a concentration unit (Baldini, Chester, Homola, & Martelucci, 2006).

The following definition is given by an IUPAC commission on sensors.

“A chemical sensor is a device that transforms chemical information ranging from the concentration of a specific sample component to total composition analysis into analytical useful signal. The chemical information mentioned above may originate from a chemical reaction of the analyte or from a physical property of the system investigated. A chemical sensor is an essential component of an analyser. In addition to the sensor, the analyser may contain that perform the following functions: sampling, sample transport, signal processing, data processing” (Wolfbeis, 1991). An analyzer may be an essential part of an automated system. The analyzer working according to a sampling plan as a function of time acts as a monitor (Hulanicki, Geab, & Ingman, 1991).

Chemical sensors contain two basic functional units: a receptor part and a transducer part. Some sensors may include a separator, which is, for example, a membrane. In the *receptor* part of a sensor, the chemical information is transformed into a form of energy, which may be measured by the transducer. The *transducer* part is a device capable of transforming the energy carrying the chemical information about the sample into a useful analytical signal. The transducer as such does not show selectivity. In the receptor part of a chemical sensor, a chemical interaction takes place, in which a chemical reaction with participation of the analyte gives rise to the analytical signal (Hulanicki, Geab, & Ingman, 1991).

1.2.1 Classification of Sensors

Sensors can be classified in many different ways. They may be classified according to the principle of operation of transducer in two main groups as “physical” and “chemical” sensors. They also can be divided into sub groups as optical, electrochemical, electrical, mass sensitive, magnetic and thermometric devices (Hulanicki, Geab, & Ingman, 1991).

Optical devices transform changes of optical phenomena, which are the result of an interaction of the analyte with the receptor part. This group may be further subdividing according to the type of optical properties, which have been exploited in chemical sensors:

- a) Absorbance**, measured in a transparent medium, caused by the absorptivity of the analyte itself or by an indirect reaction with some proper indicator.
- b) Reflectance** is measured in non-transparent moiety, usually using an immobilized indicator.
- c) Luminescence**, based on the measurement of the intensity of light emitted after an excitation or a chemical reaction in the receptor system.
- d) Fluorescence**, measured as the positive emission effect upon exposure to irradiation. Also, selective quenching of fluorescence may be the basis of such devices.
- e) Refractive index**, measured as the result of a change in solution composition. This may include also a surface plasmon resonance effect.
- f) Optothermal effect**, based on a measurement of the thermal effect caused by light absorption.
- g) Light scattering**, based on effects caused by particles of definite size present in the sample.

The application of many of these phenomena in sensors became practice by the help of the optical fibres in various configurations. Such devices have also been called optodes. It should be emphasized that fibre optics now commonly used in technical devices (Hulanicki, Geab, & Ingman, 1991).

Fiber optics serves analytical sciences in several ways. First, they enable optical spectroscopy to be performed on sites inaccessible to conventional spectroscopy, over large distances. Second, fiber optics, in being waveguides, in particular evanescent wave spectroscopy. Fibers are available now with transmissions over a wide spectral range from UV to near infrared.

1.2.2 Fiber optic

A fiber-optic cable consists of two concentric layers, called the core and the cladding, as illustrated in Figure 1.1. The core and cladding have different refractive indices n_1 , and n_2 , respectively.

The refractive index of the core, n_1 , is always greater than the index of the cladding, n_2 . Therefore, light is guided through the core, and the fiber acts as an optical waveguide. Figure 1.1 shows the propagation of light through the fiber-optic cable using the principle of total internal reflection (Alwayn, 2004).

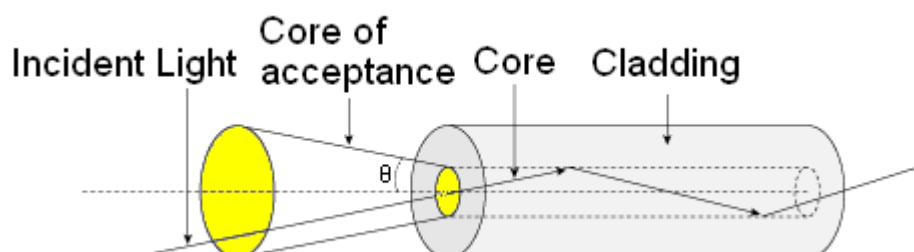


Figure 1.1 The propagation of light through the fiber-optic cable using the principle of total internal reflection.

Fiber-optic cable consists of a plastic or glass core surrounded by a layer of cladding material (see Figure 1.1). The difference in refractive indices between these two components enables the cables to act in accordance with the principle of total internal reflection (Alwayn, 2004).

The optical fiber also has a numerical aperture (NA). The NA is given by the following formula:

$$NA = \sin \theta = (n_1^2 - n_2^2)^{1/2} \quad (1.1)$$

To ensure that the signals reflect and travel correctly through the core, the light must enter the core through an acceptance cone derived by rotating the acceptance angle about the cylindrical fiber axis. The size of the acceptance cone is a function of the refractive index difference between the core and the cladding. There is a maximum angle from the fiber axis at which light can enter the fiber so that it will propagate, or travel, in the core of the fiber. The sine of this maximum angle is the NA of the fiber (Alwayn, 2004).

An optical fiber may be made up of either glass or plastic. Glass optical fibers consist of a bundle of very thin glass strands, each typically measuring 0.051 mm (0.002 in.) diameter. A flexible stainless steel–armored sheath or a polyvinyl-chloride jacket (PVC) to protect the bundle of cladded fibers can be used. Glass fiber bundles can withstand corrosive environment and harsh operating temperatures as high as 450°F (Biala, 2001).

1.2.2.1 Sensing Modes and Fiber-Optic Assemblies

Fiber-optic sensor systems can also be concluded as a derivative of photoelectric sensing technology. The photoelectric sensing modes (diffuse reflective, through-beam, retroreflective) are also available for fiber optics. The two types of fiber-optic assemblies that corresponds these sensing modes are *individual* and *bifurcated*, respectively (Biala, 2001).

The bifurcated mode, as shown in Figure 2.1 consists of two different cables combining in one end. One is interfaced with the light source and is used to guide light beam towards a sensing agent. The other is attached to the receiver of the remote sensor and is used to guide light beam from the sensing agent back to the detector. The emitter and detector cables are positioned opposite each other. Sensing is achieved when the light beam that comes from the light source is changed in intensity upon exposure to analyte.

A bifurcated fiber-optic assembly is used for both diffuse reflective and retroreflective sensing approaches. In contrast to an individual cable, a bifurcated

cable combines the emitter and the receiver cable assemblies in one assembly. The emitter and receiver fibers are laid side-by-side along the length of the cable and are randomly mixed at the sensing point, an ideal configuration for applications that require a compact sensing tip. When a sensing material immobilized in front of the tip of the bifurcated cable, light from the emitter cable excites the sensing agent and back into the receiver of the remote sensor via the receiver arm, and therefore, detection is achieved (Biala, 2001).

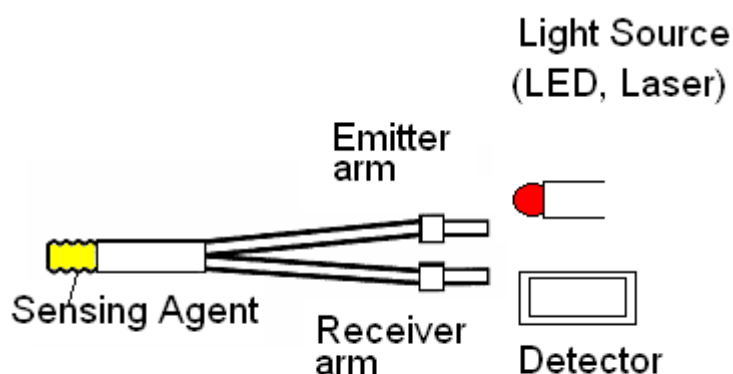


Figure 2.1 Those who need to use a single cable assembly to both illuminate and view an object greatly benefit from the bifurcated fiber-optic cable assembly. Here, the emitter and the receiver strands are laid side by side along the length of the cable.

1.2. 3 A Short View to the Optical Chemical Sensors

As mentioned earlier, an optical chemical sensor is a device that measures a physical quantity or the concentration of a chemical or biochemical species and converts it into a signal, which can be read by an observer or by an instrument. The most widely used basic measuring techniques in optical chemical sensors are optical absorption and luminescence, but sensors based on other optical parameters, such as refractive index and dispersion, have also been developed. However, sometimes the term “sensor” is being used to refer to a molecular probe or a pH indicator.

The alternative use of optical fibers in various spectroscopic applications has grown, especially during the past 10-15 years. In recent designs, the fiber optic probes were incorporated with spectroscopic instruments, which eliminate the need for traditional cuvettes for measurements. The probe can be immersed in a beaker, water bath, and enclosed pipe or can be interfaced with any suitable platform containing solid sample. In such kind of designs, light source and detector systems of the conventional spectroscopic instruments are being used together with fiber optics.

Optical fibers have many uses in remote sensing. In some applications, the instrumentation can be designed independently simply containing a proper light source, bifurcated optical fibers, detector and signal processor. Sometimes the sensor may be itself an optical fiber. In other cases, fiber is used to connect a non-fiber optic sensor platform to a measurement system. Depending on the application, optical fiber may be used because of its small size, or the fact that no electrical power is needed at the remote location. Conceptual basis of optical sensor design relies on absorption and emission based spectroscopic techniques. Therefore results of the huge number of absorption or emission based experimental studies can be beneficial in early stages of optical sensor design. Optical chemical sensors are mainly composed of a polymer matrix material, an ion carrier and an indicator dye or a combined form of the carrier and dye; chromoionophore or more specifically fluoroionophore; that acts as a fluorescent probe.

Aside from instrumentation, probably, the most challenging aspect of an optical chemical sensor design is the planning of the indicator chemistry which covers proper choice of analyte-specific indicator and compatible matrix material where the reagent dye can be adsorbed, covalently or electrostatically immobilized, or simply encapsulated that is also permeable to the analyte.

In order to perform an efficient immobilization of the indicator in the support matrix, the indicator must be soluble and stable in the chosen material. Commonly used polymer based matrix materials in optical chemical sensor design include polystyrene, polyvinyl chloride, polymethyl methacrylate, polydimethyl siloxanes,

polytetrafluoroethylenes, polymers for molecular imprinting, organic conductive polymers, hydrogel-plasticizer emulsions and cellulose derivatives such as ethyl cellulose. The sol-gel process and different types of glassy materials also provide relatively suitable support matrix for the immobilization of analyte-sensitive reagents.

Recently, with advances in materials fabrication and better understanding of the characteristics of the ionic liquids (IL), ILs is being used in optical sensor design as matrix material or additive. Understanding of the availability of ILs is a novel development in this area and future applications looks like promising.

CHAPTER TWO

ELECTROSPINNING AND NANOFIBER

2.1 Nanotechnology and Nanomaterials

Nanotechnology may be defined as examination, production and development of nanometer-sized materials. Towards macroscopic scale to nano-scale, increases surface area / volume ratio for materials and this increase cause more of different and unexpected mechanical and electrical properties in materials. For this reason, recent studies in the field of nanoscience and nanotechnology have attracted much attention and it can be applied to all aspects of science and engineering (Haghi, & Zaikov, 2011; He, Liu, Mo, Wan, & Xu, 2008). The importance of *nanotechnology* as an emerging technology has been recognised that was launched, with an investment of over \$1 billion in nanotechnology research over the past few years (Naschie, Chaos, Solitons, & Fractals, 2006).

Nanomaterials have about 100 nm and below in size that showing a number of features is unique because of their size.

Nanomaterials divided into two groups that organic and inorganic. Inorganic nanomaterials cannot be included carbon structures and it includes other elements. Organic nanomaterials are nanostructures, which include element of carbon in the composition (Miller, Seratto, & Cardences, 2006).

The properties of materials can be different at the nanoscale for two main reasons: First, nanomaterials have a relatively larger surface area when compared to the same mass of material produced in a larger form. This can make materials more chemically reactive (in some cases materials that are inert in their larger form are reactive when produced in their nanoscale form), and affect their strength or electrical properties. Second, quantum effects can begin to dominate the behaviour of matter at the nanoscale - particularly at the lower end - affecting the optical, electrical and magnetic behaviour of materials.

Nanomaterials are usually classified as dimensional in literature. According to this classification (Miller, Seratto, & Cardences, 2006);

- 0-D nanomaterials (nanoparticles)
- 1-D nanomaterials (nanotubes, nanowire, Nanofiber)
- 2-D nanomaterials (nanofilm)

One-dimensional nano-structures such as Nanofiber, nanotubes (hollow fiber) and nanofiber-filled are among the most interesting topics in nanotechnology, because of their unique and many of excellent properties (Velez, 2005).

Nanofibres can be described as diameter a micron and below fibers. Today, Nanofiber production realized many ceramic and polymer materials using various production methods (Ramarkrishra, Fujihara, Teo, Lim, & Ma, 2005).

An apparent aspect is the remarkably large surface-to-volume ratio of nanomaterials. Therefore, the research and development of nanofibres has gained much prominence in recent years due to the promising applications in the field emission-based flat panel displays, semiconducting devices, chemical sensors, ultra-sensitive electromechanical devices, medical, engineering and defence fields (Haghi, & Zaikov, 2011).

2.2 Electrospinning for Polimeric Nanofiber

There are various approaches for fabrication of nanofibres. Each of these methods leads to fibers with different properties and carachteristics. They can be listed as follows.

Drawing technology for producing micro/nanofibres using a micropipette with a diameter of a few micrometres; template synthesis of carbon nanotubes, nanofibre arrays and electronically conductive polymer nanostructures; and thermally induced

phase separation method for producing nanoporous nanofibres. Electrospinning is the cheapest and the most straightforward way to produce nanomaterials. Electrospun nanofibres are of indispensable importance for the scientific and economic revival of developing countries (Haghi, & Zaikov, 2011; He et. all, 2008).

In addition to, Electrospinning is a highly versatile method to process solutions or melts (mainly of polymers) into continuous fibres with diameters ranging from a few micrometers to a few nanometers. This technique is applicable to virtually every soluble or fusible polymer. The polymers can be chemically modified and tailored with additives ranging from simple carbon-black particles to complex species such as enzymes, viruses, and bacteria. Dependent upon a multitude of molecular, process, and technical parameters. The method provides access to entirely new materials, which may have complex chemical structures (Haghi, & Zaikov, 2011).

Structured polymer fibres with diameters in the range from several micrometres down to tens of nanometres are of considerable interest for various kinds of applications. It is now possible to produce a low-cost, high-value, high-strength fibre from a biodegradable and renewable waste product for easing environmental concerns (He et. all, 2008).

Electrospinning is a novel process for producing superfine fibres by forcing a viscous polymer, composite, sol–gel solution or melt through a spinneret with an electric field to a droplet of the solution, most often at a metallic needle tip (Figure 2.1). The electric field draws this droplet into a structure called a Taylor cone (Taylor, 1964). If the viscosity and surface tension of the solution are appropriately tuned, varicose break-up is avoided (if there is varicose break-up, then electrospray occurs) and a stable jet is formed.

Taylor cone: A Taylor cone is caused by equilibrium between the electronic force of the charged surface and the surface tension. A higher applied voltage leads to an elongated cone; when it exceeds its threshold voltage, a jet is emanated (Taylor, 1964).

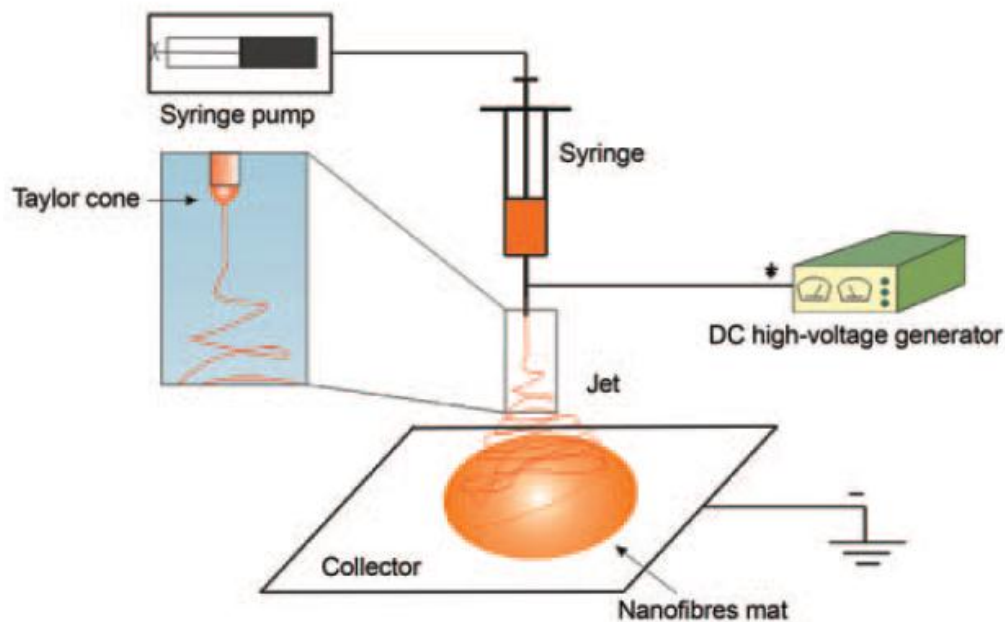


Figure 2.1 The most frequently used electrospinning set-up. (He et al., 2008)

Electrospinning traces its roots to electrostatic spraying. Electrospinning now represents an attractive approach for polymer biomaterials processing, with the opportunity for control over morphology, porosity and composition using simple equipment. Because electrospinning is one of the few techniques to prepare long fibres of nano- to micro-metre diameter, great progress has been made in recent years (He et. all, 2008).

Electrospun fibrous can be used in the following applications: nonwoven fabrics, reinforced fibres, support for enzymes, drug delivery systems, fuel cells, conducting polymers and composites, photonics, sensorics, medicine, pharmacy, wound dressings, filtration, tissue engineering, catalyst supports, fibre mats serving as reinforcing component in composite systems, and fibre templates for the preparation of functional nanotubes, to name just a few (He et. all, 2008).

2.3 Electrospun Nanofibrous Membranes for Sensors

Increasing demand of new approaches toward highly sensitive detection techniques in the field of sensor has led to an intensive interest in the nanostructured material such as nanofibers.

The role of sensors is to transform physical or chemical responses into an electrical signal based on the targeted application. So far, electrospun polymer nanofibers have been investigated as gas sensors, chemical sensors, optical sensors and biosensors. It is considered that high sensitive sensors can be assembled by nanofibers, which possess high surface to volume ratio. Except sensitivity of sensors, quick response time for subjective analyte is also expected to for nanofiber sensors. The principle of nanofiber sensors is to utilize the chemical or physical reaction between a targeted material and a sensing material. Furthermore, the sensors convert the result of those chemical or physical phenomena to the optical or electrical output and finally quantitative measurement of the detected materials is conducted.

Electrospun polymer nanofibers used in various sensor applications as gas (Ding, Kim, Shiratori, & Miyazaki, 2004; Ding, Yamazaki, & Shiratori, 2004; Gouma, 2003; Liu, Kameoka, Czaplewski, & Craighead, 2004), chemical (Kwoun, Lee, Han, Ko, 2000; Kwoun, Lee, Han, Ko, 2001), optical sensor (Celin, Pandit, Kapoor, & Sharma, 2003; Lee, Ku, Wang, Samuelson, Kumar, 2002; Wang et al., 2002) and biosensors (Lala, Ramaseshan, Ramakrishna, 2005; Ramarkrishra, Fujihara, Teo, Lim, & Ma, 2005; Wang et al., 2004).

CHAPTER THREE

EXPERIMENTAL METHOD AND INSTRUMENTATION

3.1 Reagents

All solvents and the other used chemicals were of analytical grade and purchased from Merck, Fluka, and Riedel. The polymers ethyl cellulose (EC) and poly(methyl methacrylate) (PMMA) were purchased from Acros and Aldrich companies, respectively. The plasticizer, dioctyl phthalate (DOP) was supplied from Aldrich. The ionic liquid (RTIL), 1-ethyl-3-methylimidazolium tetrafluoroborate (EMIMBF₄) and potassium tetrakis-(4-chlorophenyl) borate (PTCPB) were supplied from Fluka. Solvents of the spectroscopic studies were used without further purification. Aqueous solutions were prepared with freshly deionized ultra pure water (specific resistance >18 MΩcm, pH 5.5) from a Millipore reagent grade water system.

For metal ion tests, metal solutions (Ag⁺, Al³⁺, Ba²⁺, Ca²⁺, Co²⁺, Cr³⁺, Cu²⁺, Fe³⁺, Fe²⁺, Hg₂²⁺, Hg²⁺, Li⁺, K⁺, Mn²⁺, Mg²⁺, Na⁺, NH₄⁺, Ni²⁺, Pb²⁺, Sn²⁺ and Zn²⁺ were used. The standard metal solutions were prepared from their 0.1 M stock solutions by using the metal salts of AgNO₃, Al(NO₃)₃.9H₂O, BaCl₂.2H₂O, Co(NO₃)₂.6H₂O, Cr(NO₃)₃.9H₂O, Cu(NO₃)₂.3H₂O, Hg₂(NO₃)₂, Hg(NO₃)₂, Fe(SO₄)₂.7H₂O, Fe(NO₃)₃.9H₂O, SnCl₂, MnCl₂.4H₂O, NiCl₂.6H₂O, Pb(NO₃)₂, Zn(NO₃)₂.6H₂O, NaHCO₃, NaCl, KNO₃, MgSO₄, Ca(NO₃)₂.6H₂O, HNO₃, NaOH, LiCl, NH₄NO₃ was from Merck. All standards were diluted with 0.01 M acetic acid/acetate buffer of used pH.

The pH of the solutions were monitored by use of a digital pH-meter (ORION) calibrated with standard buffers of pH 12.00, 7.00 and 4.00 at 25±1 °C. All of the experiments were carried out at room temperature; 25 °C

In all of the studies, ultra pure water of Millipore was used. Deionised water, generated by a Milli-Q deionised water unit, which had a resistance better than 18.2 µcm, was used for the preparation of all the solutions.

Preparation of 0.01 M acetic acid/acetate buffer; 0.572 mL of acetic acid ($d=1.05$ and 17.48 Molar) were dissolved in 950 mL ultra pure water. The solution was titrated to pH 5 at the lab temperature of 20 °C either with 0.1 M HCl or 0.1 M NaOH as needed. The resulting solution was made up to 1000 ml with ultra pure water in a volumetric flask. The buffer solutions in the range of pH 4.0-6.0 were prepared by the same way by adjusting to the desired pH.

Preparation of 0.005 M acetic acid / acetate buffer; 0.286 mL of acetic acid ($d=1.05$ and 17.48 Molar) were dissolved in 950 mL ultra pure water. The solution was titrated to pH 5.0 at the lab temperature of 20°C either with 0.1 M HCl or 0.1 M NaOH as needed. The resulting solution was made up to 1000 ml with ultra pure water in a volumetric flask. The buffer solutions in the range of pH 4.0-6.0 were prepared by the same way by adjusting to the desired pH.

Preparation of 0.005 M H_3PO_4 buffer; 0.285 mL ($d=1.71$ and 14.83 Molar) of phosphoric acid were dissolved in 950 mL ultra pure water. The solution was titrated to pH 2.0 at the lab temperature of 20°C either with 0.1 M HCl or 0.1 M NaOH as needed. The resulting solution was made up to 1000 ml with ultra pure water in a volumetric flask. The buffer solutions in the range of pH 2.0-3.0 were prepared by the same way by adjusting to the desired pH.

Preparation of 0.005 M NaH_2PO_4 / Na_2HPO_4 buffer; 0.78 g of $NaH_2PO_4 \cdot 2H_2O$ (MW=156.01) and 1.79 g of $Na_2HPO_4 \cdot 12H_2O$ (MW=358.14) were dissolved in 950 mL ultra pure water. The solution was titrated to pH 7.0 at the lab temperature of 20 °C either with 0.1 M HCl or 0.1 M NaOH as needed. The resulting solution was made up to 1000 ml with ultra pure water in a volumetric flask. The buffer solutions in the range of pH 7.0-9.0 and 10-12 were prepared by the same way by adjusting to the desired pH.

3.2 Structural Specification of Ionophores

The silver sensitive fluorescent ionophore (explained into detail in chapter 4), 1,2-bis (4- methoxybenzylidene) hydrazine (M-AZM) (see Figure 3.1) was synthesized in our laboratories according to the literature method and characterized with ¹H NMR and IR based data (Ambroziak, & Szypa, 2007; Grigoras, & Antonoaia, 2005; Méalares, & Gandini, 1996).

Mp: 165 °C, IR: 2926 (CH), 1625 (C N), ¹H NMR: 3.78 (s, 6H, 2× OCH₃), 7.01–7.09 (m, 4H, ArH), 7.79–7.86 (m, 4H, ArH), 8.37 (s, 1H, ArCH N), 8.41 (s, 1H, ArCH N)

Synthesis and ¹H NMR characterization of the subjective molecule was performed by Professor Y. ERGUN.

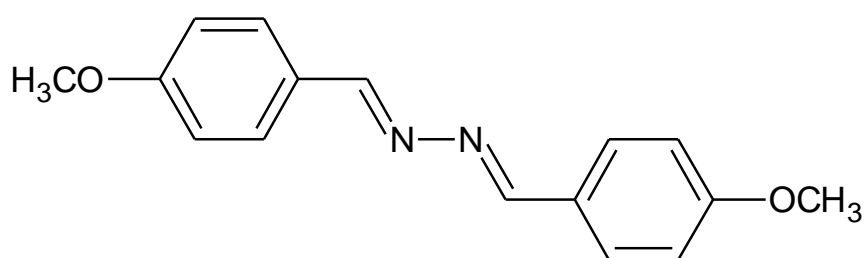


Figure 3.1 Structure of the silver sensitive fluoroionophore, 1,2-bis(4 methoxybenzylidene)hydrazine (M-AZM)

The mercury sensitive fluorescent ionophore (explained into detail in chapter 5), (4-(dimethylamino)benzaldehyde2-[[4-cyanophenyl] methylene]hydrazone (DC-AZM) (See figure 3.2) dye has been performed in our laboratories from Professor Y. ERGUN according to the literature information and characterized with ¹H NMR and IR based data (Ambroziak, & Szypa, 2007; Derinkuyu, Ertekin, Oter, & Ergun, 2010; Grigoras, & Antonoaia, 2005; Méalares, & Gandini, 1996).

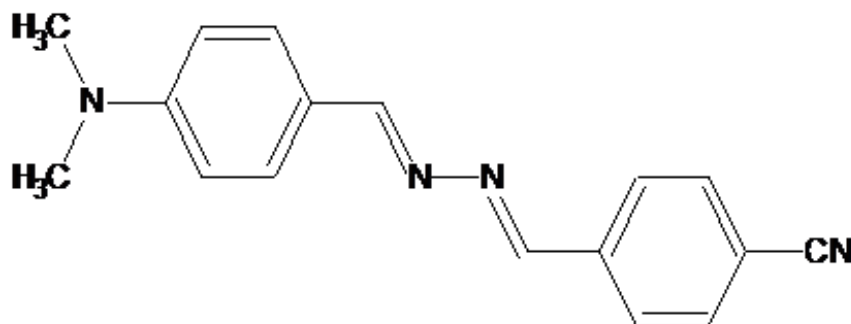


Figure 3.2 Structure of the mercury sensitive fluoroionophore, (4-(dimethylamino) benzaldehyde2-[[4-cyanophenyl] methylene] hydrazone (DC-AZM)

The other silver sensitive fluorescent ionophore was obtained from Professor Y. ERGUN (explained into detail in chapter 6). The 4,4'-[hydrazone-1,2-dilidendimethylidene]bis(N,N-dimethylaniline (TM-AZM) (see Figure 3.3) dye was synthesized in our laboratories according to the literature method and characterized with ^1H NMR and IR based data (Ambroziak, & Szypa, 2007; Grigoras, & Antonoaia, 2005; Méalares, & Gandini, 1996).

The ^1H NMR and IR based measurements were performed by Professor Y. ERGUN.

IR (KBr): 2909 (C-H), 1598 (C=N) cm^{-1} . ^1H -NMR (400 MHz, d_6 -DMSO): δ 2.97 (s, 12H, 4xCH₃), 6.66 (d, 4H, J=8.4 Hz, 4x ArH), 7.57 (d, 4H, J=8.8 Hz, 4x ArH), 8.41 (s, 2H, -N=CH), GC-MS [M]⁺= 294.3, mp=265.2 $^{\circ}\text{C}$.

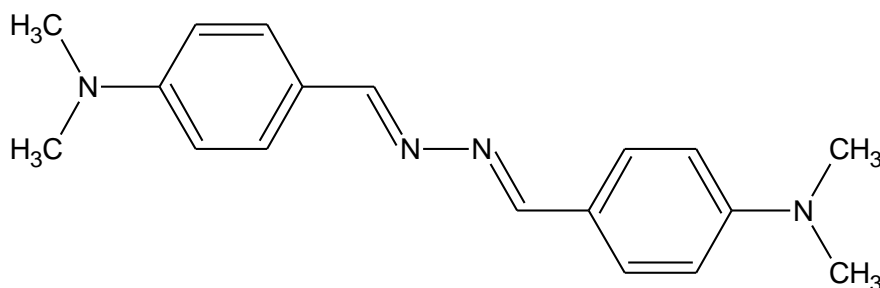


Figure 3.3 Structure of the silver sensitive fluoroionophore 4,4'-[hydrazone-1,2-dilidendimethylidene]bis(N,N-dimethylaniline (TM-AZM)

The iron sensitive fluorescent ionophore (explained into detail in chapter 7), N'-(4-cyanobenzylidene)isonicotinohydrazide (CBINH) (see Figure 3.4) was synthesized in our laboratories by Professor Y. ERGUN in a similar way to the literature (Bottari et. all. 2000) and characterized with ^1H NMR and IR based data.

mp: 253°C, **IR**(KBr): 3479 (NH), 2222 (CN), 1663 (C=O), 1607 (C=N) cm^{-1} , **^1H -NMR** (400 MHz, d_6 -DMSO): δ 7.74 (d, 2H, $J=8.0$ Hz, ArH), 7.84 (d, 2H, $J=7.4$ Hz, ArH), 8.03 (d, 2H, $J=8.0$ Hz, ArH), 8.1 (bs, 1H, NH), 8.57 (s, 1H, N=CH), 8.92 (d, 2H, $J=7.6$ Hz, ArH).

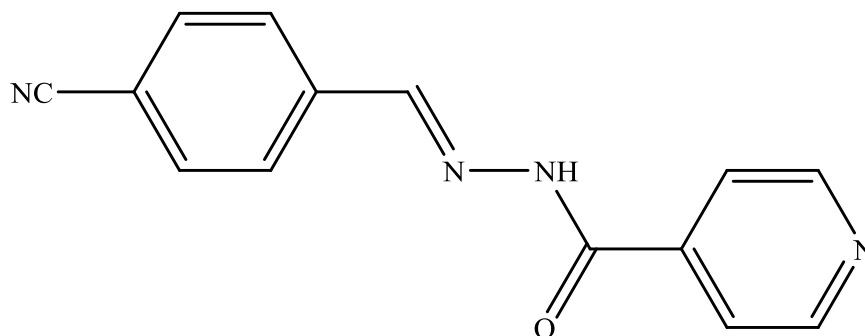


Figure 3.4 Structures of the iron sensitive fluoroionophore N'-(4-cyanobenzylidene)isonicotinohydrazide (CBINH)

The hydroxyl (OH^-) sensitive fluorescent ionophore (explained into detail in chapter 8), 9-butyl-bis-3-(4-(dimethylamino)phenyl)allylidene)-9H-carbazole-3,6-diamine(BCDA) (see Figure 3.5) was synthesized in our laboratories by Professor Y. ERGUN and studies regarding IR and NMR related data of the newly synthesized molecules are on going.

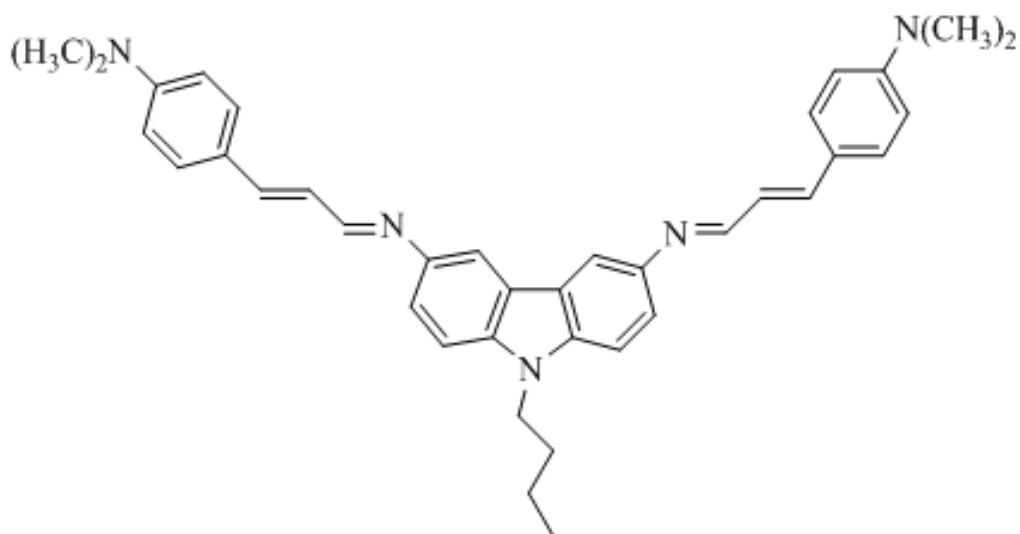


Figure. 3.5 Structures of the hydroxyl sensitive fluoroionophore, 9-butyl-bis-3-(4-(dimethylamino)phenyl)allylidene)-9H-carbazole-3,6-diamine (BCDA)

The calcium sensitive fluorescent ionophore (in chapter 9), DMK-OFD-BIS; 2,2'-{1,2-phenylenebis[nitrilomethylylidene]} diphenol (see Figure 3.6) was synthesized in University of Ege by Prof. Dr. Engin ÇETİNKAYA and studies regarding IR and NMR related data of the synthesized molecules are on going.

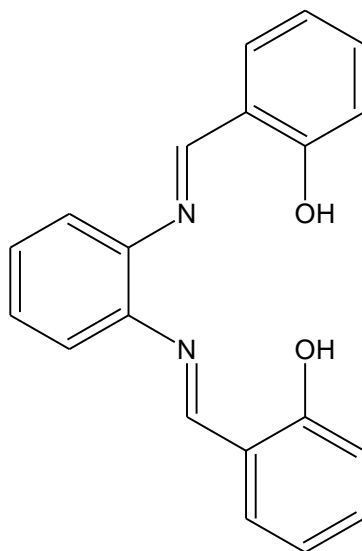


Figure 3.6 Structure of calcium sensitive molecule, **DMK-OFD-BIS**; 2,2'-{1,2-phenylenebis[nitrilomethylylidene]} diphenol

The copper sensitive fluorescent ionophore (in chapter 10), DMK-OFD-7, 2-[[2-(2-aminophenyl)imino]methyl]-4,6-di-*tert*-butylphenol (see Figure 3.7) were synthesized in University of Ege by Prof. Dr. Engin ÇETİNKAYA. Studies regarding IR and NMR related data of the synthesized molecules are on going.

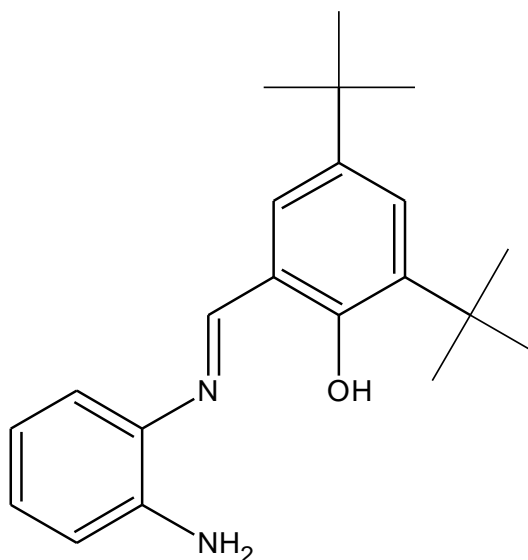


Figure 3.7 Structure of copper sensitive molecule, **DMK-OFD-7**; 2-[[2-(2-aminophenyl) imino]methyl]-4,6-di-*tert*-butylphenol

3.3 Fabrication of Electrospun Nanofibers

The sensing composites were prepared by mixing 240 mg of polymer (PMMA or EC), 192 mg of plasticizer (Dioctyl phthalate, DOP), 48 mg of RTIL and 1 to 5 mg of ionophore, equivalent amount of potassium tetrakis (4-chlorophenyl) borate (PTCPB) in 2.0 mL of THF or DCM: EtOH (25.75) solvent systems. We referred these mixtures as cocktails. The prepared cocktails contained 50% PMMA or EC, 40% plasticizer and 10% IL by weight. Chemical structures of the exploited polymers, plasticizers, lipophilic anionic additive, and RTIL were shown in Figure 3.8.

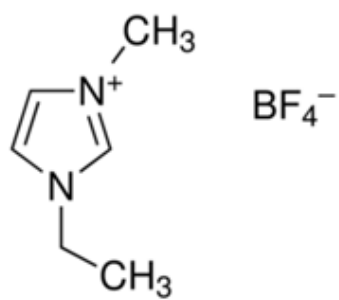
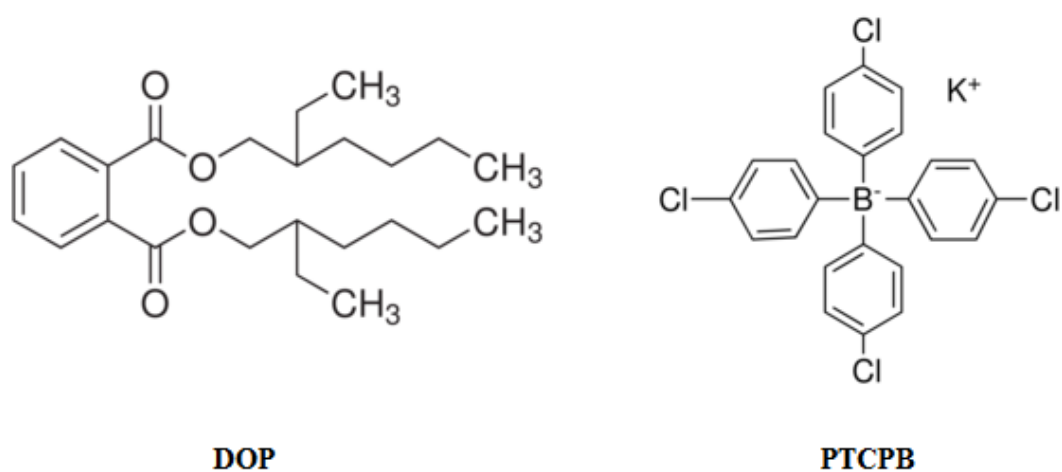
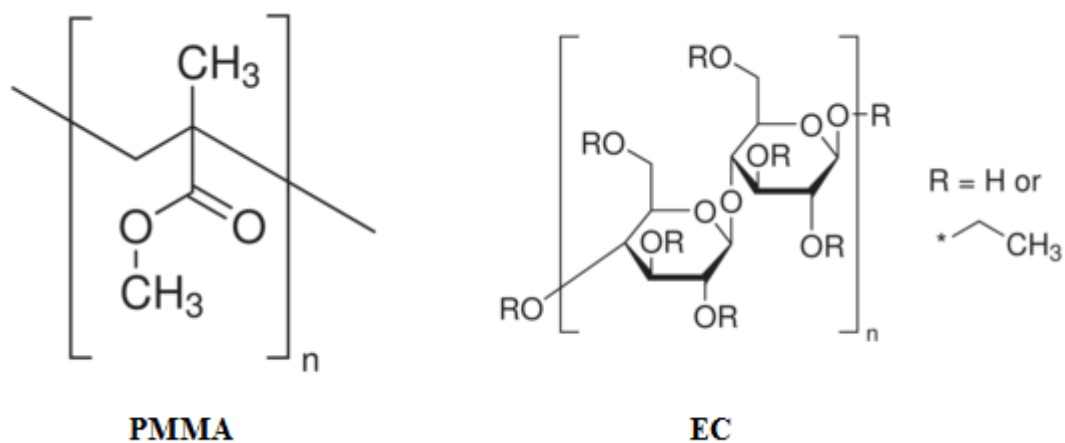


Figure 3.8 Structures of PMMA, EC, DOP, PTCPB and RTIL

Electrospinning was used to fabricate optical chemical sensing materials. The electrospinning conditions were optimized in order to form bead-free PMMA (Poly (methyl methacrylate)) or EC (Ethyl cellulose) based continuous nanofibers by varying the concentrations of plasticizer, PMMA or EC and RTILs (1-Ethyl-3-methylimidazolium tetrafluoroborate) in the composites. The concentration of RTIL was varied from 5% up to 50% w/w, with respect to the content of PMMA or EC. It was found that the presence of the RTILs in the PMMA solutions facilitates the electrospinning of bead-free nanofibers from the lower polymer concentrations. This behavior can be attributed to the high conductivity and proper viscosity of the RTIL doped precursor polymer solutions.

For the fabrication of nanofibers, the polymer solution was taken in a hypodermic syringe and an electric potential of 25 kV was applied between the needle of the syringe and the substrate in the form of aluminum foil. The distance between the needle and the electrode was 10 cm while the diameter of the needle was 0.40 mm. The solution flow rate was maintained at 0.5 mL/h using the syringe pump.

When the high voltage applied, the charged polymer solution overcame the surface tension of the liquid and a stream of polymer jet was produced. The solvent evaporated and very fine fibers were completely coated on the clean aluminum foil. The surface morphology of the nanofibers was studied using SEM instrument (6060-JEOL JSM). The nanofibers either on aluminum substrate or in bulk form were fixed in the flow cell and the excitation or emission spectra were recorded.

3.4 Thin Film Fabrication

The thin films were prepared employing the same composition for electrospun nanofibers. The resulting composites were spread onto a 125 μm polyester support (Mylar TM type) with a spreading device. Thickness of the films was measured using Tencor Alpha Step 500 Prophyloimeter and was found to be 5.11 μm . This result was an average of eight measurements and exhibited a Standard deviation of ± 0.08 . Each sensing film was cut to 1.2cm diameter, fixed in the flow cell, and the excitation or emission spectra were recorded.

3.5 Electrospinning Apparatus

The homogeneous PMMA or EC solutions were placed in a 10 mL plastic syringe fitted with a metallic needle of 0.4mm of inner diameter. The syringe is fixed vertically on the syringe pump (Top Syringe Pump Top-5300) and the electrode of the high voltage power supply (Gamma High Voltage ES30) was clamped to the metal needle tip. Schematic structure of the electrospinning apparatus is shown in Figure 3.9.

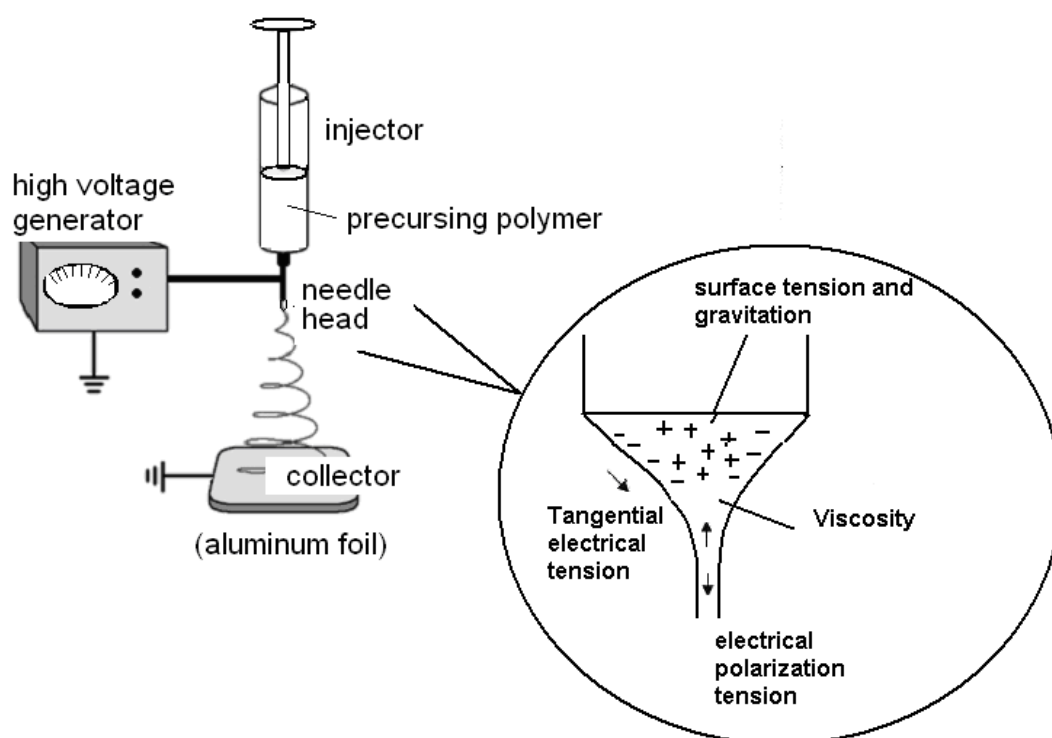


Figure 3.9 Schematic structures of the employed electrospinning apparatus

3.6 Apparatus and Experimental Setup

Absorption spectra were recorded using a Shimadzu 1601 UV-Visible spectrophotometer.

Steady state fluorescence emission and excitation spectra were measured using Varian Cary Eclipse Spectrofluorometer with a xenon flash lamp as the light source.

The fiber optic components were obtained from Varian. Metal response measurements were carried out with fiber optic probe (2m long) and solid sample tip

accessories constructed on the spectrofluorometer and were executed by flow system. The flow cell was made from polytetrafluoroethylene (PTFE) in the atelier of University of Ege. For instrumental control, data acquisition and processing the software package of the spectrofluorometer was used.

pH measurements were recorded with a ORION pH meter. In all of the studies ultra pure water of Millipore was used.

Setup of fiber optical system; The fiber optical sensor was constructed with the commercial accessories of Varian Cary Eclipse Spectrofluoremeter: Eclipse Fibre optic coupler, Fluorescence remote read probe (2 metres), Probe tip for solid measurements and Probe tips for liquid measurements (10 mm and 20 mm length tips). This method also allows the examination of samples remote from the instrument. The installation steps are:

- ***The fibre optic coupler*** is an accessory that enables the use of a fiber optic probe with Carry Eclipse spectrofluoremeter. After the removal of the sample compartment of the Carry Eclipse, the fibre optic coupler was stabilized to the same position by the help of the screws.
- ***The fiber optic probe*** was connected to the coupler accessory by inserting the two connector ends into the two key holds.
- ***The probe tips*** were screwed onto the end of the probe. Due to the phase of the sample (solid or liquid), either a solid sample probe tip or a liquid sample probe tip were used.
- To ensure that the fibre optic system will operate at maximum performance, it is necessary to optimize the efficiency with which light passes through the coupling device before experimentation begins. The alignment was done by using the software of the instrument.

The flow system with fiber optic; Metal response measurements were carried out with fiber optic probe (2m long) and solid sample tip accessories constructed on the spectrofluorometer. For instrumental control, data acquisition and processing the software package of the spectrofluorometer was used. The tip of the bifurcated fiber optic probe was interfaced with a sensing film in a buffer containing 300 μ L flow cell (Figure 3.10). The flow cell was equipped with a four channel Ismatec Reglo Analog peristaltic pump. Analyte solutions or buffers were transported by the peristaltic pump via tygon tubing of 2.06 mm i.d. (Figure 3.10)

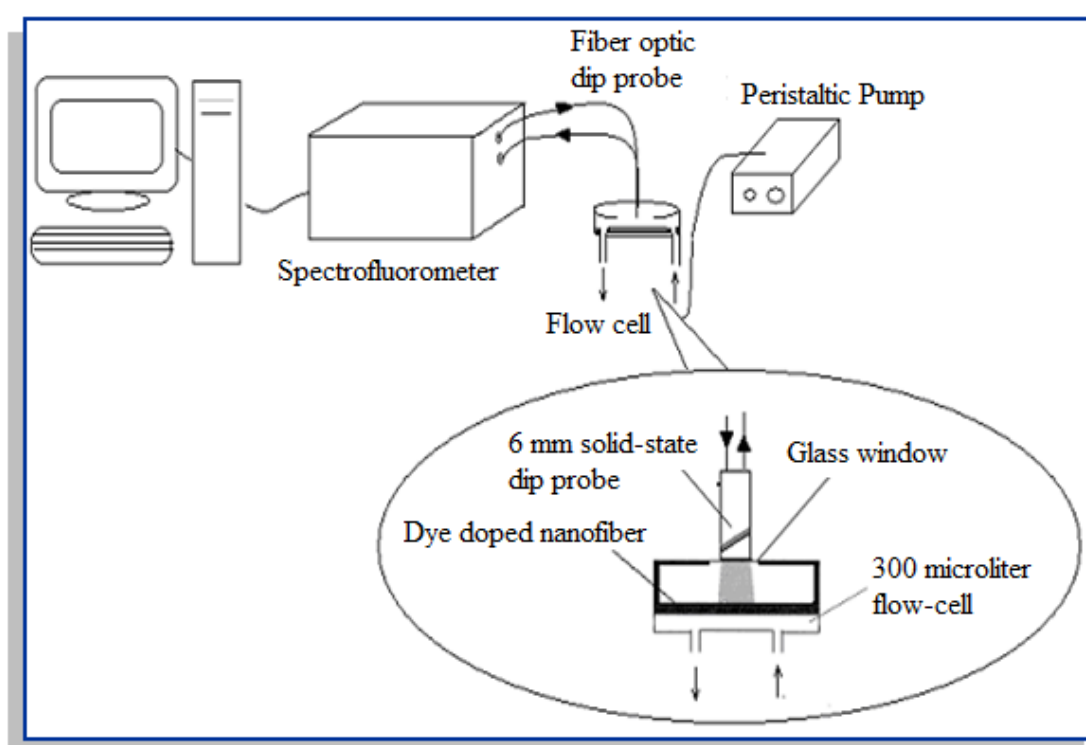


Figure 3.10 Instrumental set-up used for dye-doped nanofiber measurements

3.7 Rtils as Polymer Electrolytes

At the initial stage of the electrospinning process, the polymer solution is hanged by its surface tension at the end of the syringe needle. When a sufficiently large electric voltage is applied, the solution at the tip of the needle becomes stretched to form a cone because of coupled effects of the electrostatic repulsion within the charged droplet and attraction to a grounded electrode of opposite polarity. As the strength of the electric field is increased, the charge overcomes the surface tension,

and at a critical voltage, fine jet is ejected from the apex of the cone (Gibon, Schreuder-Gibson, & Rivin, 2001; Reneker, & Chun, 1996).

In order to perform this process, the polymer solution should have a certain electrical conductivity. On the other hand, to achieve true electrical conductivity in polymers one must add compatible electrically conductive additives into the polymer. Ionic liquids are very new matrix materials as polymer electrolytes. Unlike traditional solvents, which can be described as molecular liquids, ionic liquids are composed of ions.

Recently, Cheruvally et. all. (2007) utilized ionic liquids together with dissolved lithium salt as new polymer electrolytes for electrospinning process. They produced lithium batteries employing the poly (vinylidene fluoride-co-hexafluoropropylene) as the basic polymeric component.

In this thesis, we have demonstrated that it is possible to electrospin the EC and PMMA based composite fibers in presence of non-volatile room temperature ionic liquid (RTIL); EMIMBF₄. The employed RTIL was chosen as polymer electrolyte due to its high ionic conductivity, thermal and chemical stability, non-volatile, non-flammable and low toxicity characteristics (Cheruvally et. all. 2007; Galinski, Lewandowski, & Stepniak, 2006). Additionally, the IL also enhances photostability of the used ionophore in the polymer matrix acting as a sink for acidic or basic species from the ambient air of the laboratory (Oter, Ertekin, Topkaya, & Alp, 2006; Oter, Ertekin, & Derinkuyu, 2008).

We exploited the RTILs as additives in the polymer matrices with two purposes. One of them was to provide a reasonable electrical conductivity in the precursor polymer solution during electrospinning. The other was to provide a chemically stable microenvironment for the chromoionophore. By this way, we could obtain enhanced stability and longer storage time for polymer-doped fluoroionophores.

The RTIL containing EC matrix provided a highly stable and spectroscopically available microenvironment for the ionophore dyes. Although the imidazolium based

ionic liquids have non-negligible absorption and intrinsic fluorescence in the visible region of the electromagnetic spectrum, the observed fluorescence of the ionic liquids studied was negligible in the excitation and emission wavelength ranges of the indicator dyes and did not limit the sensing ability of ionophore dye in any way. The schematic structures of the ionic liquid are shown in Figure 3.11.

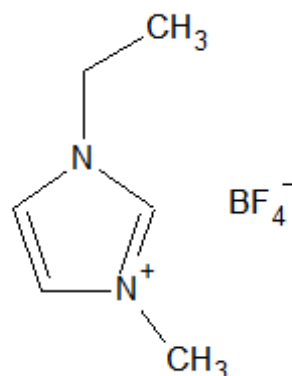


Figure 3.11 Structures of the polymer additive, ionic liquid; 1-ethyl-3-methylimidazolium tetrafluoroborate (EMIMBF₄).

3.8 Stoke's Shift and Quantum Yield Calculations

Fluorescence is one type of luminescence that is the emission of light from any substance and occurs from electronically excited states. Fluorescence spectral data are generally presented as emission spectra. Emission spectra vary widely and are dependent upon the chemical structure of the fluorophore and the solvent in which it is dissolved. Stoke's Shift and Quantum yield is Characteristics of Fluorescence Emission (Lakowicz, 1999; Parker, 1968; Schmidt, 1994).

The energy of emission is typically less than that of absorption. Thus, the law of Stokes states that the fluorescence is shifted to higher wavelengths relatively to absorption (Stoke's Shift). As already mentioned, emission usually occurs from the

lowest excited state, but higher excited states are reached by absorption. The phenomenon is known as Stokes Shift can be caused by: energy losses due to relaxation to ground vibrational states, solvent effects, excited state reactions, complex formation and energy transfer (Lakowicz, 1999; Parker, 1968; Schmidt, 1994).

The fluorescence quantum yield is an intrinsic property of a fluorophore and is important for the characterization of novel fluorescent probes. When a fluorophore absorbs a photon of light, an energetically excited state is formed. The fate of this species is varied, depending upon the exact nature of the fluorophore and its surroundings, but the result is deactivation (loss of energy) and return to the ground state.

The fluorescence quantum yield (Φ_F) is the ratio of photons absorbed to photons emitted through fluorescence. In other words, the quantum yield gives the probability of the excited state being deactivated by fluorescence rather than by another, non-radiative mechanism.

$$\Phi_F = \text{photons}_{\text{em}} / \text{photons}_{\text{abs}} \quad (3.1)$$

For calculation of fluorescence quantum yield values (Φ_F) of the employed dyes, we used the comparative William's method that the most reliable method for recording of Φ_F (Williams, Winfield, & Miller, 1983).

Comparative William's method involves the use of well characterised standard samples with known Φ_F values. Essentially, solutions of the standard and samples with identical absorbance at the same excitation wavelength can be assumed to be absorbing the same number of photons. Hence, a simple ratio of the integrated fluorescence intensities of the two solutions (recorded under identical conditions) will yield the ratio of the quantum yield values. Since Φ_F for the standard sample is known, it is trivial to calculate the Φ_F for the sample.

According to this method, the standards should be chosen to ensure they absorb at the excitation wavelength of choice for the test sample, and, if possible, emit in a similar region to the test sample. In order to minimise re-absorption effects (Dhami et al., 1995) absorbances in the 10 mm fluorescence cuvette should never exceed 0.1 at and above the excitation wavelength. Above this level, non-linear effects may be observed due to inner filter effects, and the resulting quantum yield values may be perturbed. This maximum allowable value of the recorded absorbance must be adjusted depending upon the path length of the absorption cuvette being used (for example, 10 mm = 0.1 maximum, 20 mm = 0.2 maximum etc).

In this thesis, firstly, we recorded the UV-vis absorbance spectrum of the solvent background for the chosen sample and standard (see Table 3.1) and noted down the absorbance at the excitation wavelengths. Secondly, we recorded the fluorescence spectrum of the same solutions. We used standard 10 mm path length fluorescence and absorption cuvettes for running the fluorescence and absorbance measurements. The UV-vis absorption (absorbance ≤ 0.10 at the excitation wavelength) and corrected fluorescence emission spectra were recorded for three or more solutions with increasing concentrations of the sample and the standard. Thirdly, we calculated the integrated fluorescence intensities (that is, the area of the fluorescence spectrum) from the fully corrected fluorescence spectrum and plotted graphs of integrated fluorescence intensity vs absorbance. Finally, the gradient of the plots were later used in the quantum yield calculations according to the following equation;

$$\Phi_X = \Phi_{ST} \left(\frac{\text{Grad}_X}{\text{Grad}_{ST}} \right) \left(\frac{\eta_X^2}{\eta_{ST}^2} \right) \quad (3.2)$$

Where the subscripts *ST* and *X* denote standard and test respectively, Φ is the fluorescence quantum yield, *Grad* the gradient from the plot of integrated fluorescence intensity vs absorbance and n is the refractive index of the solvent.

Table 3.1 Used Standard Materials and Their Literature Quantum Yield Values (Lakowicz, 1999; Scaiano, 1989)

Compound	Solvent	Literature Quantum yield	Emission range / nm
Quinine sulfate	0.1M H ₂ SO ₄	0.54	400–600
HPTS	Acidic Water	1.00	400-650
Rose Bengal	Basic Ethanol	0.11	550-750

3.9 Stern-Volmer Analysis

Fluorescence quenching refers to any process that decreases the fluorescence intensity of a sample. There are a wide variety of quenching processes that include excited state reactions, molecular rearrangements, ground state complex formation, and energy transfer. Quenching experiments can be used to determine the accessibility of quencher to a fluorophore, monitor conformational changes, monitor association reactions of the fluorescence of one of the reactants changes upon binding. There are two basic types of quenching: static and dynamic (collisional). Both types require an interaction between the fluorophore and quencher. In the case of dynamic quenching the quencher must diffuse to the fluorophore during the lifetime of the excited state. Upon contact the fluorophore returns to the ground state without emission of a photon. In the case of static quenching a complex forms between the fluorophore and the quencher, and this complex is non-fluorescent. The formation of this complex does not rely upon population of the excited state (Lakowicz, 1999).

In a solution, the quantitative measure of fluorescence quenching is described by the Stern–Volmer constant, K_{sv} ,

$$(I_0/I) = 1 + K_{sv}[Q] \quad (3.3)$$

In Eq. (3.3), I_0 and I are the intensities of fluorescence in the absence and in the presence of the quencher, respectively. The equation reveals that I_0/I increases directly proportional to the concentration of the quencher. When all other variables are kept constant, the higher the K_{sv} , the lower the concentration of quencher required to quench the fluorescence. In a heterogeneous medium, such as in polymer films, a negative deviation from the linear Stern–Volmer equation occurs at high quencher concentration (Bacon, & Demas, 1987; Carraway, Demas, DeGraff, & Bacon, 1991).

CHAPTER FOUR

EMISSION BASED SUB-NANOMOLAR SILVER SENSING WITH ELECTROSPUN NANOFIBERS

4.1 Introduction

The silver content of environmental samples has increased day by day with increasing use of silver compounds in industry, medicine and technology. Silver is widely used in medicine because of its wide-spectrum antimicrobial activity, which arises from the chemical properties of its ionized form, Ag (I). Different forms of silver are found in functional products for water purification, biofilms, dental treatment water, bandages, pool water, integrated into fabric for medicinal benefits and numerous others. Today exposure to silver compounds is widespread owing to the use of soluble silver formulations (Chambers, Krieger, Kay, & Stroud, 1974; Environment Protection Agency (EPA), 1980; Kimura, Yajima, Tatsumi, Yokoyama, & Oue, 2000). Consequently, design of chemosensors targeting Ag (I) cations is very important. A number of fluorescent chemosensors for silver ion have been designed and tested (Coskun, & Akkaya, 2005; Iyoshi, Taki, & Yamamoto, 2008; Kandaz, Güney, & Senkal, 2009; Shamsipur, Alizadeh, Hosseini, Caltagirone & Lippolis, 2006; Szigeti et al., 2006; Topal, Gürek, Ertekin, Yenigul, & Ahsen, 2010; Wang, Xue, Qian, & Jiang, 2010). Most of these studies have been performed in the solution phase. Studies performed in liquid phase provide valuable information for researchers. Nevertheless, the integration of sensing ionophores with solid-state components is necessary for better detection limits. Additionally, development of new approaches toward highly sensitive detection techniques is still very important for the researchers working in the field of analytical chemistry.

In optical chemical sensing approach, sensitivity varies inversely proportional with dimensions. Miniaturization attempts and nanotechnology applications allowed improvements in functionality, sensitivity and response time of the sensors. Consequently, nanoscale structures should be combined with optical chemical sensing approaches (Wang et. all., 2002). Here we have successfully combined the

nanoscale electrospun fiber materials with optical sensing technology for silver detection at femtomolar levels. Electrospinning, the most convenient way to make a nano-scale continuous polymer, uses a high static voltage to draw the fiber from a liquid polymer. As a jet of charged fluid polymer sprays out the bottom of a needle, an electric field forces the stream to spin, stretching the fiber lengthwise so its diameter becomes as little as 10 nm. The fiber forms a thin membrane as it hits the electrically conductive substrate below the needle. These electrospun membranes have a unique combination of stretchiness and strength, and are easy to handle, making them suitable for a wide variety of applications. Electrospun nano-fibrous membranes can have approximately 1–2 orders of magnitude more surface area than that found in continuous thin films (Gibon, Schreuder-Gibson, & Rivin, 2001; Reneker, & Chun, 1996). It is expected that this large amount of functional surface area has the potential to provide unusual high sensitivity and fast response time in sensing applications.

In this study, matrix materials of poly(methyl methacrylate) (PMMA) and ethyl cellulose (EC) were used to produce nanofibrous and continuous “silver sensing thin films”. Optical nano-fibrous membrane chemical sensors were fabricated by electrospinning technique. The methoxy azomethine ionophore, 1,2-bis(4-methoxybenzylidene)hydrazine (M-AZM) (Figure 4.1) was chosen as the fluorescent indicator due to the strong absorbance, high quantum yield, large Stoke’s shift and excellent photostability. The electrospun nano-fibers were characterized using scanning electron microscopy (SEM) and their average diameters were evaluated. To our knowledge this is the first attempt using the fluoroionophore-doped electrospun nano-fibrous materials for silver sensing at femtomolar level (Kacmaz et. all., 2011).

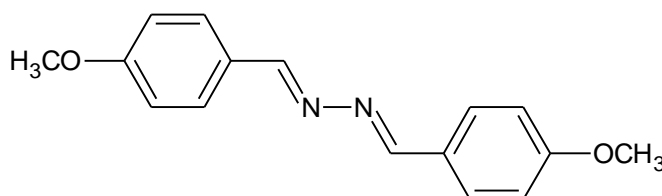


Figure 4.1 Structures of the silver sensitive fluoroionophore, 1,2-bis(4-methoxybenzylidene)hydrazine (M-AZM)

4.2 Spectral Characterization of Fluoroionophore

4.2.1 Absorption Spectra Related Characteristics

Absorption spectra of the compound were acquired in dilute solutions of THF, (To: EtOH), DCM, DMF, and in polymers of EC and PMMA in thin film form. In the survey of matrix effects, it was apparent that the immobilization of the ionophore in polymers produced dramatic spectral changes (see Figure 4.2). Upon immobilization, the absorption peak around 330 nm was broadened and an intense shoulder appeared around 400 nm as shown in Table 4.1. The ionophore exhibited very efficient absorbance and high molar extinction coefficients around 330 nm and 400 nm in all the employed solvents and solid matrices, respectively. In agreement with Ref. (Derinkuyu, Ertekin, Oter, Denizalti, & Cetinkaya, 2008), molar extinction coefficients (ϵ) of M-AZM in polymer matrices were increased about 2.5-fold, with respect to the (ϵ) values observed in the solution phase (see Table 4.1). These data can be taken as proofs that the M-AZM dye absorbs better when immobilized in EC or PMMA matrices.

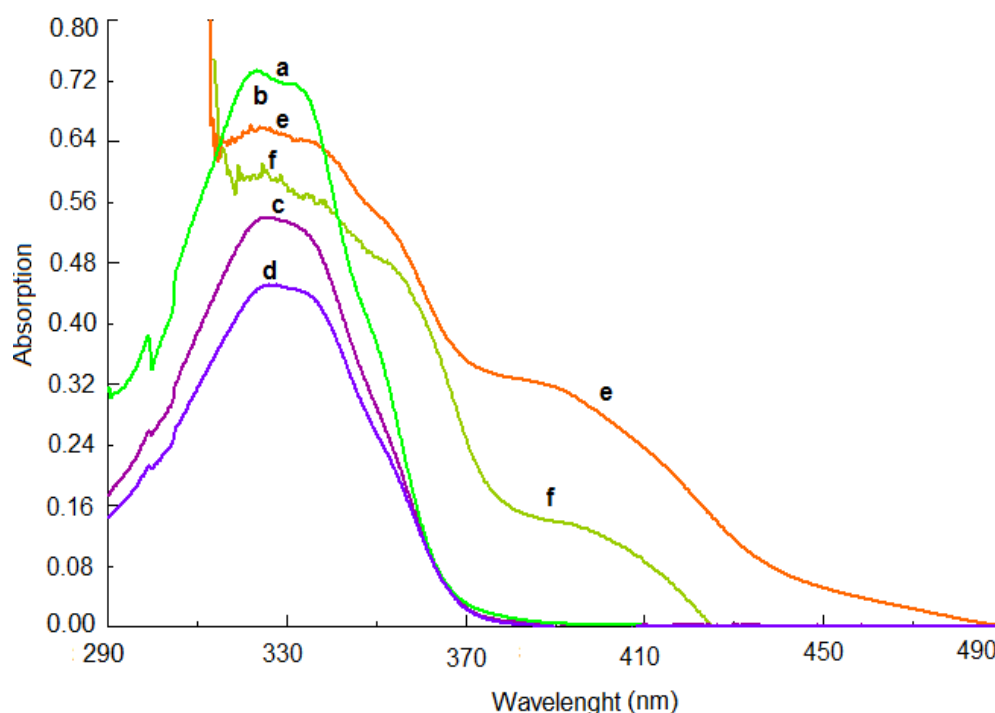


Figure 4.2 Absorption spectra of the dilute solution of M-AZM-dye (a) in THF, (b) To:EtOH, (c) DCM, (d) DMF, (e) in EC (approximately 2 mmol dye/kg polymer) (f) in PMMA

Table 4.1 UV–vis spectra related data of the M-AZM ionophore in the solvents of EtOH, DCM, THF and toluene/ethanol mixture (80:20), DMF and in solid matrices of PMMA and EC.

Compound	Solvent/Matrix	n(refractive index)	λ^1_{abs}	λ^2_{abs}	$\epsilon_{\text{max}}(\lambda^1_{\text{abs}})$	$\epsilon_{\text{max}}(\lambda^2_{\text{abs}})$
M-AZM	EtOH	1.3590	--	--	--	--
	DCM	1.4241	328	--	54000	--
	THF	1.4070	325	--	73400	--
	To: EtOH	1.4694	330	--	68800	--
	DMF	1.4305	330	--	44900	--
	EC	1.4790	333	395	100948	49068
	PMMA	1.4893	329	400	153890	34975

4.2.2 Emission Spectra Related Characteristics

The similar solvent and solid phase studies were repeated for fluorescence measurements. The emission peaks of M-AZM were acquired in optically dilute solutions around 390 nm. However when immobilized in polymers they appeared around 460 nm (see Figure 4.3). Immobilization into the solid phase caused dramatic red shift and enhanced fluorescence, which can be attributed to the rigidity of the molecule in this moiety.

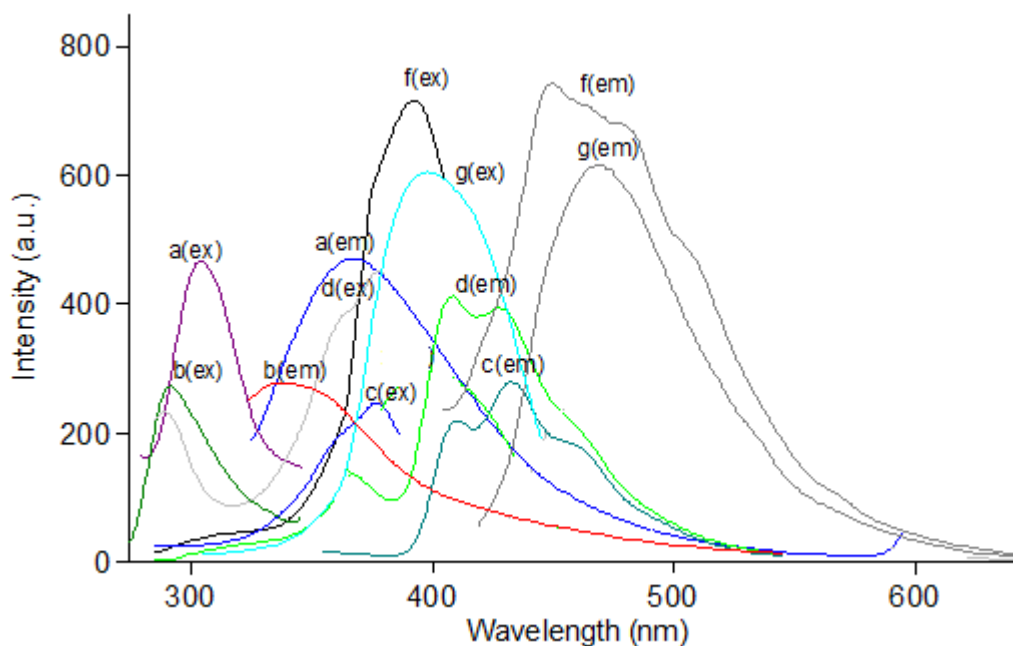


Figure 4.3 Excitation / emission spectra of the dilute solution and matrices of M-AZM-dye (a) in THF, (b) To:EtOH, (c) DCM, (d) DMF, (e) in EC (approximately 2 mmol dye/kg polymer) (f) in PMMA.

4.2.3 Quantum Yield Calculations

The fluorescence quantum yield of M-AZM in THF, EC and PMMA matrices was calculated by William's Method (Williams, Winfield, & Miller, 1983). The Williams method and the calculation of quantum yield values were explained into detail in Chapter 3.

For this purpose, the emission spectra of five different concentrations of reference standards (HPTS and QUININE SULFATE) were recorded by exciting at 390 and 348 nm for solid and solution phases, respectively (see Figure 4.4 and 4.5). By similar way, the emission spectra of the five different concentrations of the M-AZM dye were recorded (see Figure 4.6, Figure 4.7 and Figure 4.8).

The integrated fluorescence intensities were plotted *vs* absorbance for the reference standard, and the dye. The ratio of gradients of the plots is important and proportional to the quantum yield. The linearized plots of the dye in THF, EC and PMMA matrices can be described by the equations and the relevant correlation

coefficients of $[y= 48119x, R^2= 0.9910]$, $[y=101521x, R^2= 0.9936]$, and $[y=129999x, R^2=0.9966]$, respectively. For quantum yield standard; HPTS, and QUININE SULFATE the equations are $[y=4136512x, R^2=1.0; y = 470972x, R^2= 0.9965]$. The data are also shown in Table 4.2.

Fluorescence quantum yield of M-AZM in EC and PMMA, $\phi_F = 0.030$ and 0.039 has increased about 25-fold, with respect to ϕ_f of M-AZM in THF, and, molar extinction coefficient of M-AZM in EC and PMMA matrix, $\epsilon = 100948$ and 153890 , has increased about 2.5- fold, with respect to ϵ of M-AZM in THF. These data can be taken as proofs that the dye molecule M-AZM fluoresces better in immobilized EC and PMMA matrix.

Table 4.2 Quantum yield related data for M-AZM in THF, EC and PMMA matrices

Dye	Refractive index, n	Equations of plots	Gradient Of the plots	Quantum Yield, ϕ_F
HPTS (in water)	1.3328	$y = 4136512x$	4136512	1
QUININE SULFATE (in water)	1.3328	$y = 470972x$	470972	0.546
M-AZM (in THF)	1.4070	$y = 48119x$	48119	1.2×10^3 (calculated)
M-AZM (in EC)	1.4790	$y = 101521x$	101521	0.030 (calculated)
M-AZM (in PMMA)	1.4893	$y = 129999x$	129999	0.039 (calculated)

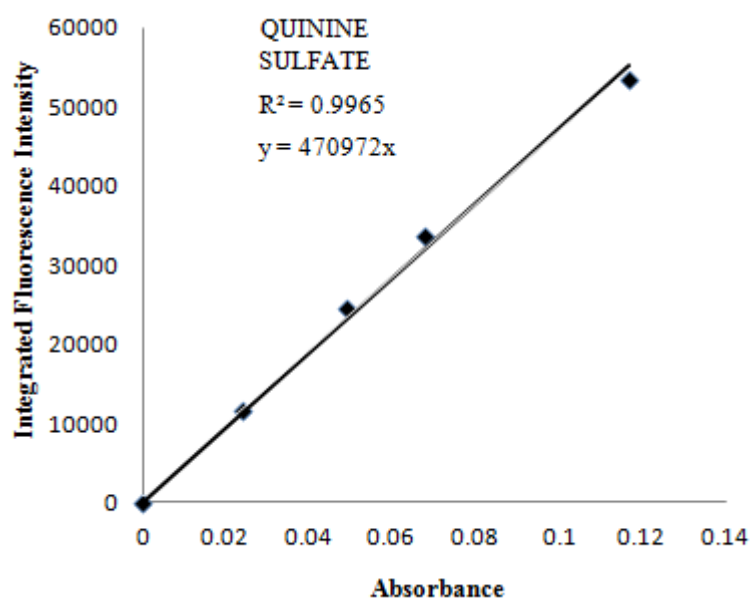


Figure 4.4 The integrated fluorescence intensities vs absorbance values of QUININE SULFATE in water (excitation at 348 nm).

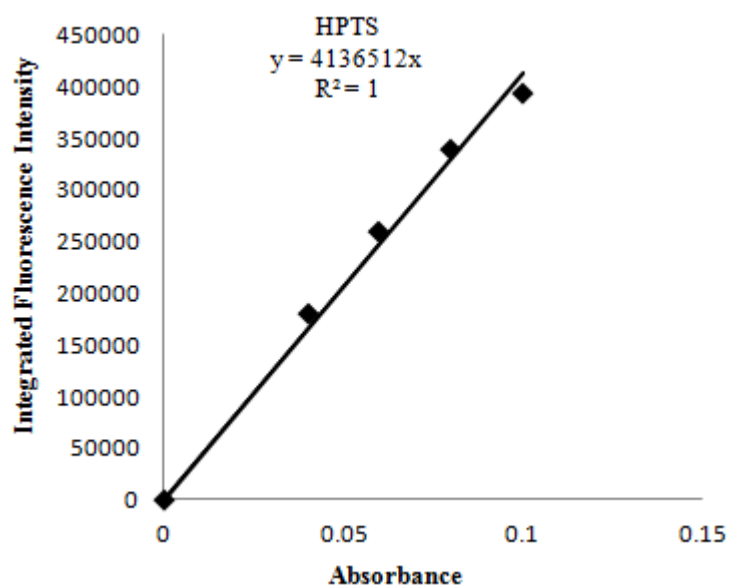


Figure 4.5 The integrated fluorescence intensities vs absorbance values of HPTS in water (excitation at 390 nm).

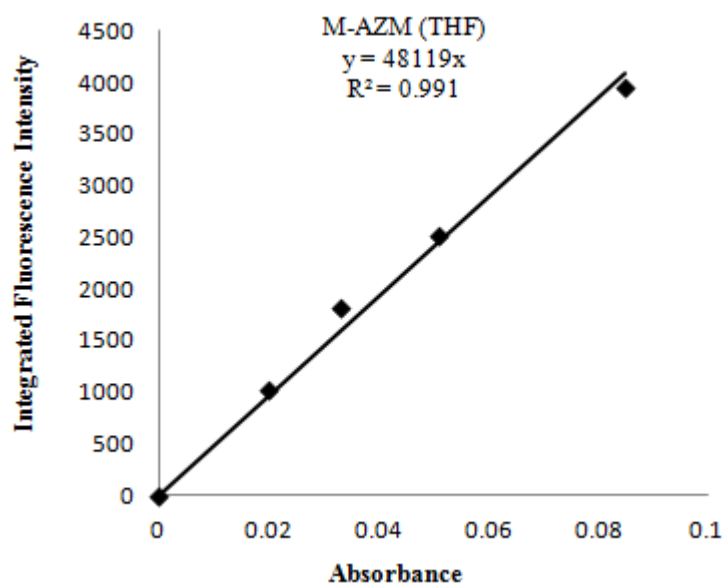


Figure 4.6 The integrated fluorescence intensities vs absorbance values of M-AZM dye in THF (excitation at 320 nm).

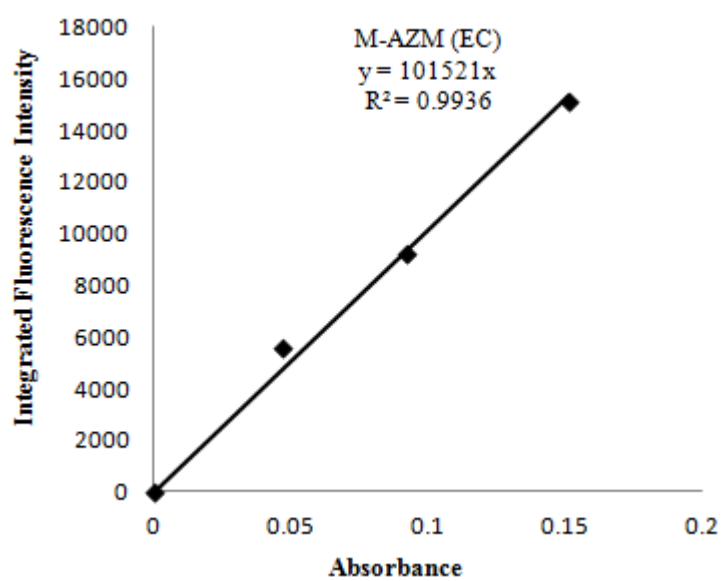


Figure 4.7 The integrated fluorescence intensities vs absorbance values of M-AZM dye in EC matrix (excitation at 380 nm).

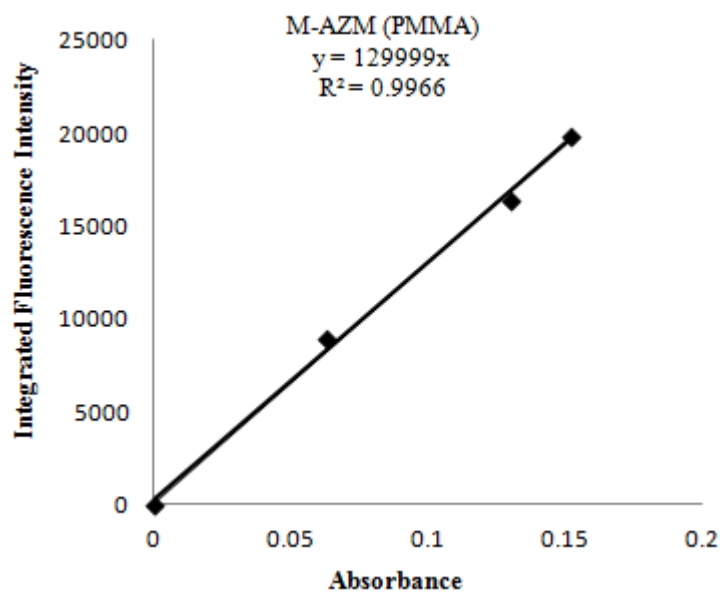


Figure 4.8 The integrated fluorescence intensities vs absorbance values of M-AZM dye in PMMA matrix (ex. at 395 nm).

The dye displayed enhanced fluorescence emission quantum yield and longer excitation wavelength in immobilized forms compared to the (ϕ_f) values recorded in THF. There were no dramatic changes in the Stoke's shifts (see Table 4.3). The observed red shift of absorption and emission of M-AZM, and, approximately 25-fold increase of the (ϕ_f) in EC or PMMA can be attributed to the enhanced conjugation in immobilized polymer phase by hindrance of vibrational rotational motions.

Table 4.3 The excitation–emission spectra related characteristics of the M-AZM acquired in conventional solvents, and in thin film form of PMMA and EC.

Compound	Matrix	λ_{\max}^{em}	λ_{\max}^{ex}	$\Delta\lambda_{ST}$ (Stoke's shift)	ϕ_F (Quantum yield)
M-AZM	DCM	393	300	93	1.2×10^{-3} in THF
	THF	380	310	70	
	To:EtOH	365	300	65	
	DMF	393	300	93	
	EC	460	380	80	0.030
	PMMA	470	395	75	0.039

4.3 SEM Images of Electrospun Membranes

The SEM images of PMMA and EC based electrospun membranes at various magnifications are denoted in Figure 4.9 and Figure 4.10, respectively. The membrane has a 3-D structure with a random fiber orientation that is evenly distributed on the substrate. It can be seen from Figure 4.9 and Figure 4.10 that the diameters of the fibers were in the range of 326 and 527 nm. The same figure also reveals that the diameters of some nanofibers were smaller than these values. For instance, some nanofibers possess approximately 100 nm and less than this value.

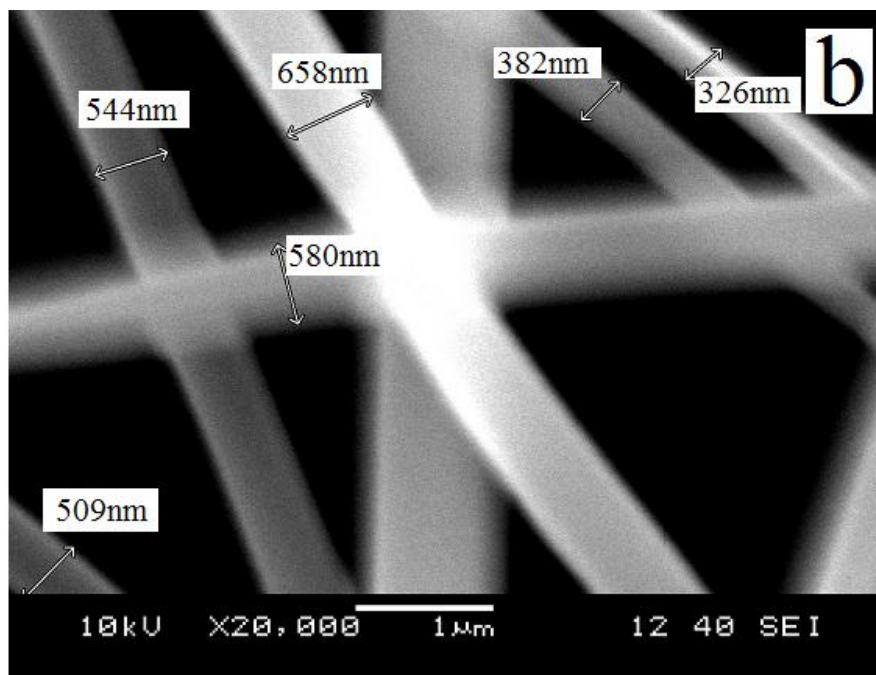
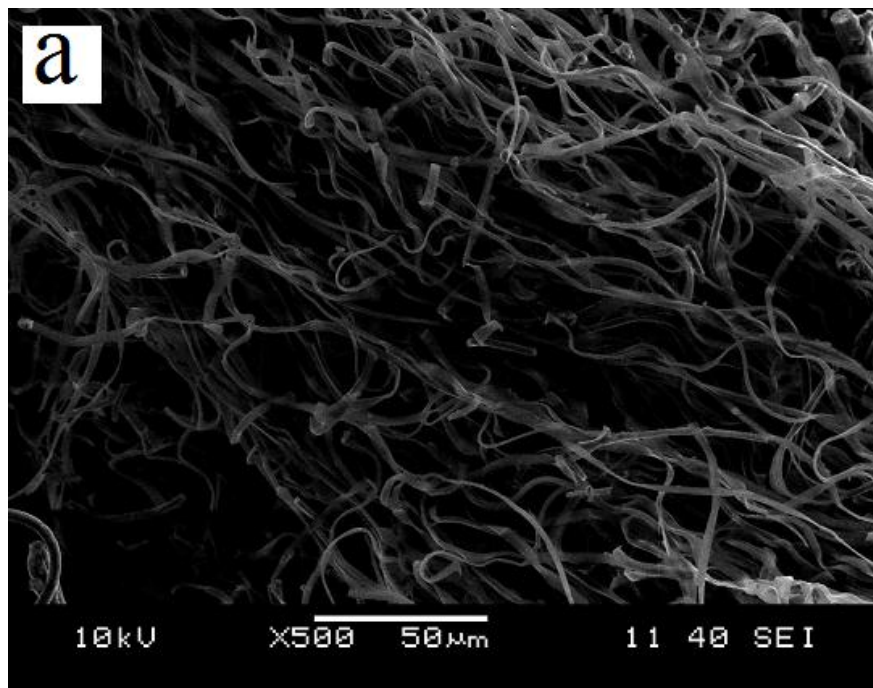


Figure 4.9 SEM images of electrospun membranes; (a) and (b); PMMA based nanofibers at different magnifications such as $\times 500$, $\times 20\,000$.

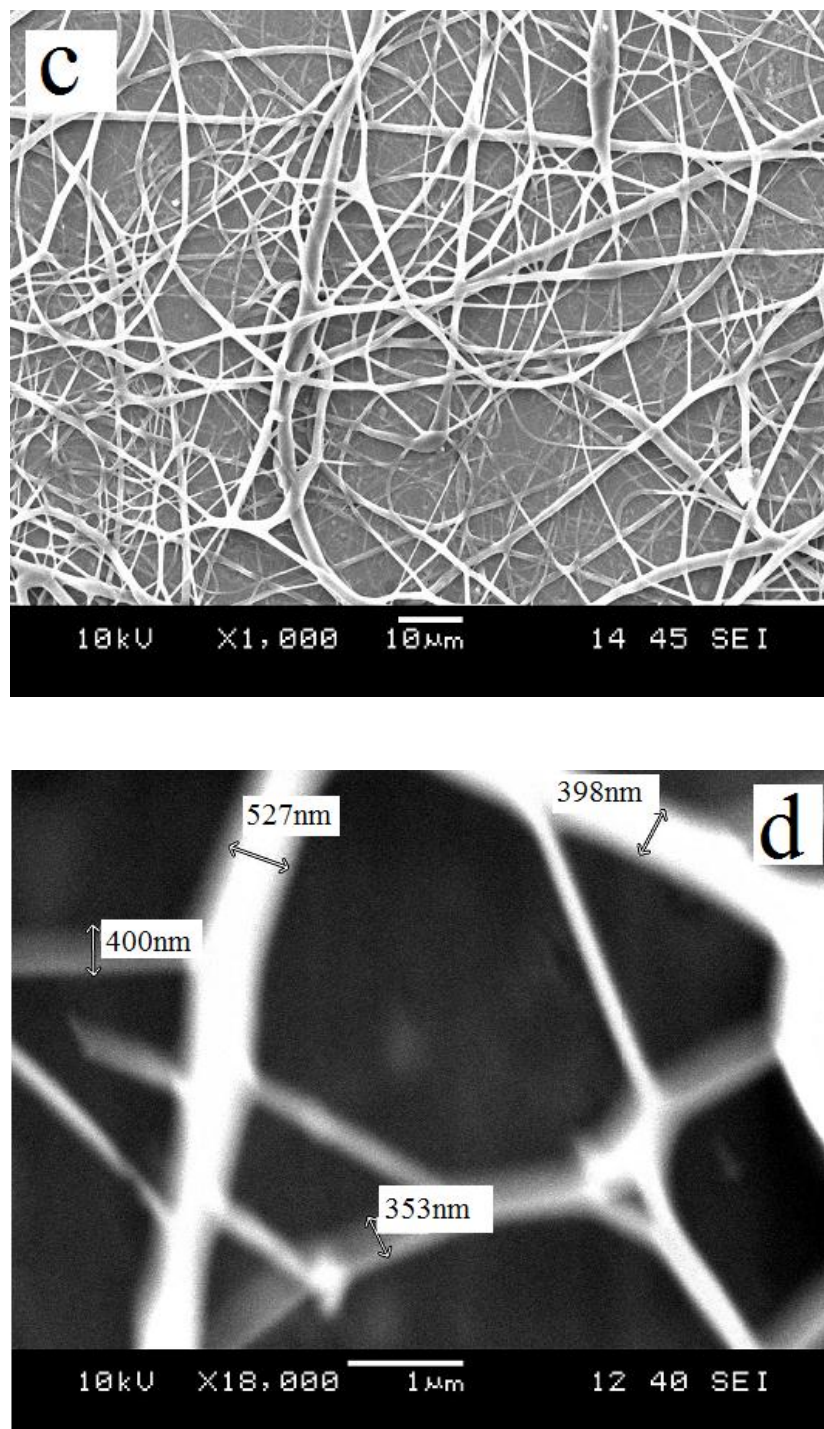


Figure 4.10 SEM images of electrospun membranes; (c) and (d); EC based nanofibers at different magnifications such as $\times 1\,000$ and $\times 18\,000$.

4.4 pH Dependency of the M-AZM Dye

The pH dependence of the dye doped thin films and electrospun nanofibers was investigated in the pH range of 2.0–7.0 in silver free and silver containing solutions. Buffer solutions were prepared with 0.01M CH₃COOH, 0.01 NaOH, and 0.01M NaH₂PO₄ at desired pH. The preparation procedures for the buffer solutions were given in Chapter 3. In silver-free studies the dye exhibited significant pH dependency around pH 5.0. For further metal ion sensing studies we employed buffered solutions keeping the pH constant at pH 4.5.

The absorption maximum of the thin film form of M-AZM in EC at 320 nm decreased meanwhile the λ_{max} at 400 nm increased as the pH of the buffers varied from 7.0 to 2.0 exhibiting an isobestic point around 375 nm.

In contrast, the emission and excitation maxima of M-AZM in EC at 470 and 400 nm decreased as the pH of the buffer varied from 7.0 to 2.0. The pH dependence of the dye is probably due to the protonation-deprotonation equilibria of the central nitrogen groups. Figure 4.11 and 4.12, shows the pH dependency of the membrane in silver-free buffer solutions in the pH range of 7.0 - 2.0. Similar behavior was also observed in absorption spectrum recorded in PMMA matrices. In case of PMMA, the isobestic point was appeared at 370 nm. Figure 4.13 and 4.14 reveals pH induced absorption and emission spectral behavior of M-AZM in PMMA.

The pKa values of the fluoroionophore dye were calculated by using non linear fitting algorithm of Gauss- Newton-Marquardt method (Mills, & Chang, 1992) both in EC and PMMA matrices and were found to be pKa= 4.77 and pKa= 4.60, respectively. The Gauss- Newton-Marquardt equation is as follows;

$$pKa = pH + \log [(I_x - I_b)/(I_a - I_x)] \quad (4.1)$$

where I_a and I_b are the intensities of acidic and basic forms and I_x is the intensity at a pH near to the pKa.

$$pKa = 4.5 + \log[(740-268)/(995-740)]$$

$$\text{pKa} = 4.5 + \log [1.85]$$

$$\text{pKa} = 4.77 \quad (\text{for indicator immobilized EC})$$

$$\text{pKa} = 4.5 + \log[(498-85)/(829-498)]$$

$$\text{pKa} = 4.5 + \log [1.25]$$

$$\text{pKa} = 4.60 \quad (\text{for indicator immobilized PMMA})$$

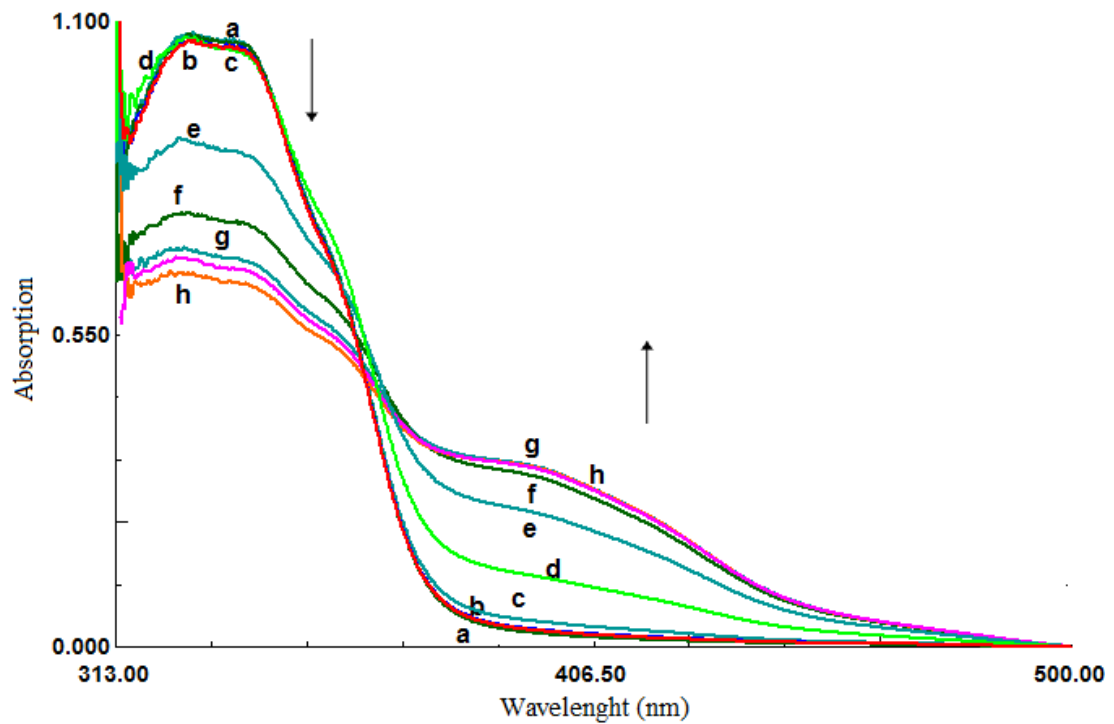


Figure 4.11 pH induced absorption spectra of the M-AZM doped EC membrane after exposure to buffer solutions in the pH range of 7.0–2.5 (a) pH=7.0-6.5 (b) pH=6.0 (c) pH= 5.5 (d) pH= 5.0 (e) pH= 4.5 (f) pH= 4.0 (g) pH= 3.5-3.0 (h) 2.5 (pKa=4.77).

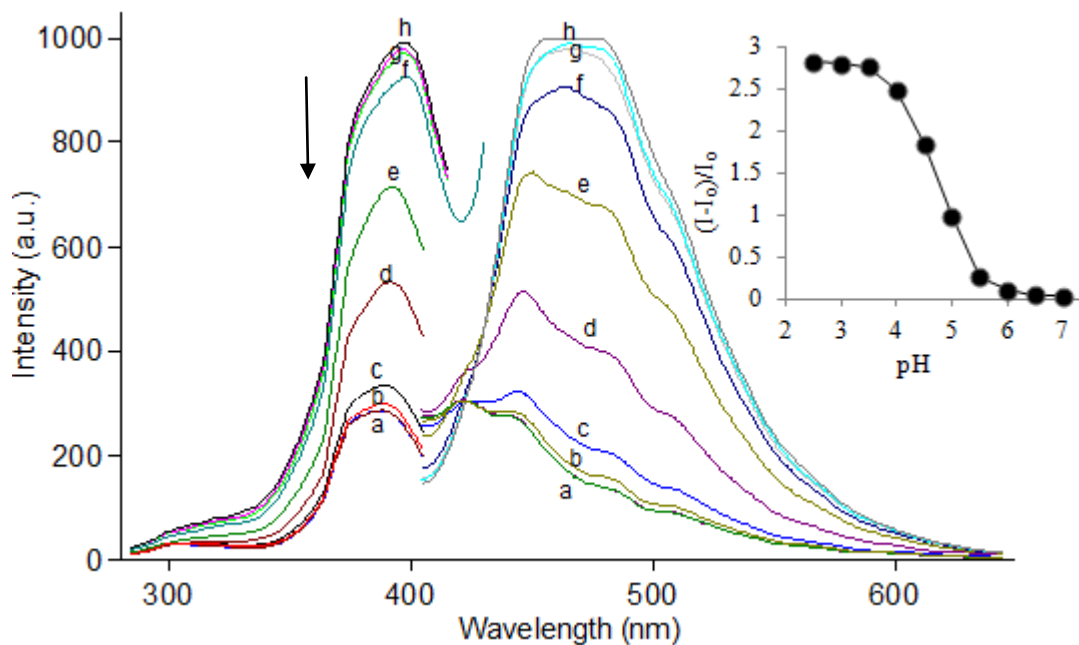


Figure 4.12 pH induced emission characteristics and sigmoidal calibration curve of M-AZM doped EC membrane in the pH range of 7.0–2.5 (a) pH=7.0–6.5 (b) pH=6.0 (c) pH= 5.5 (d) pH= 5.0 (e) pH= 4.5 (f) pH= 4.0 (g) pH= 3.5–3.0 (h) 2.5 (pKa=4.77).

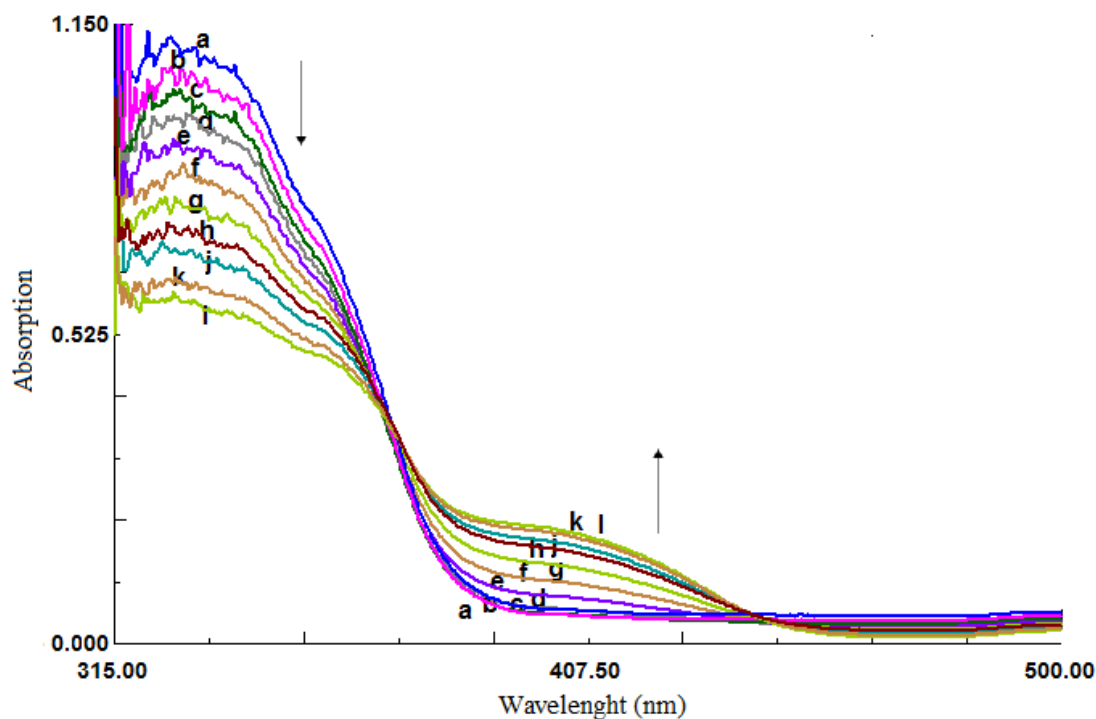


Figure 4.13 pH induced absorption spectra of the M-AZM doped PMMA membrane after exposure to buffer solutions in the pH range of 7.0–2.0 (a) pH=7.0 (b) pH= 6.5 (c) pH= 6.0 (d) pH= 5.5 (e) pH= 5.0 (f) pH= 4.5 (g) pH= 4.0 (h) pH= 3.5 (j) pH= 3.0 (k) pH= 2.5 (k) pH= 2.0 (pKa=4.60).

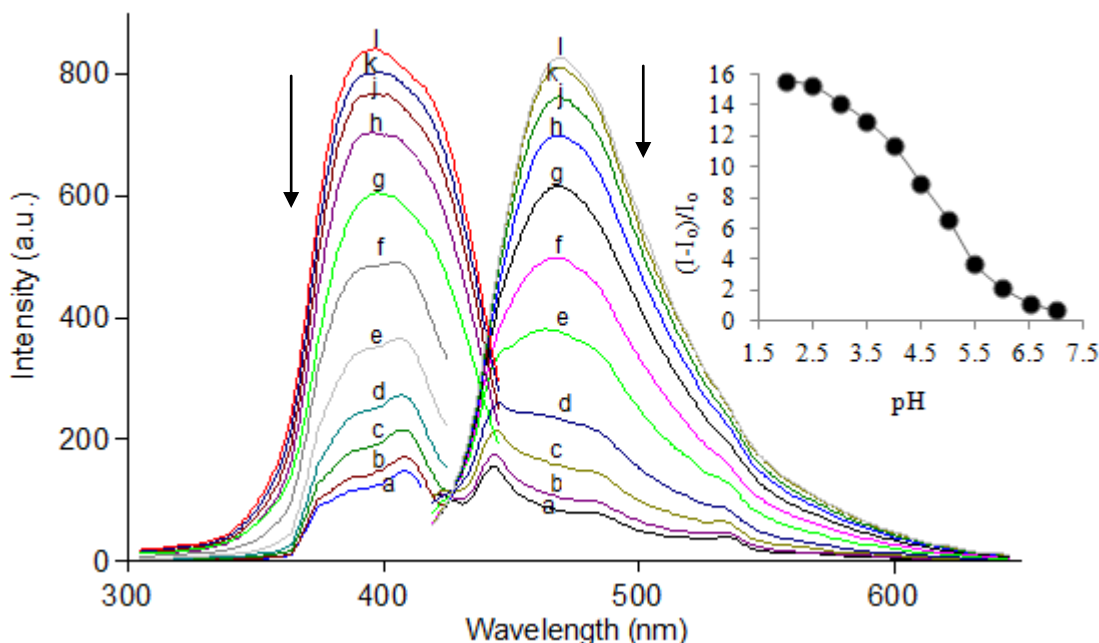


Figure 4.14 pH induced emission characteristics and sigmoidal calibration curve M-AZM doped PMMA membrane after exposure to buffer solutions in the pH range of 7.0–2.0 (a) pH=7.0 (b) pH= 6.5 (c) pH= 6.0 (d) pH= 5.5 (e) pH= 5.0 (f) pH= 4.5 (g) pH= 4.0 (h) pH= 3.5 (j) pH= 3.0 (k) pH= 2.5 (k) pH= 2.0 ($pK_a=4.60$).

For further metal ion sensing studies; the effect of pH on the interaction of M-AZM ionophore with Ag (I) ions was investigated between pH 2.5 and 7.0 at fixed metal concentration, $10^{-5} \text{ mol L}^{-1}$. As can be seen from Figure 4.15, the relative signal change; $(I_0 - I)/I_0$ produced by the Ag (I) ions was high enough and stable around pH 4.5.

Distribution of the chemical species in the working conditions was theoretically checked with chemical equilibrium software programme (Visual MINTEQ) at pH 4.5 in presence of acetate ions ($\text{CH}_3\text{COO}^- (\text{aq})$: 35.6%, $\text{CH}_3\text{COOH}(\text{aq})$: 64.4% and $\text{Ag}^+(\text{aq})$: 100.0%). Due to the excellent silver solubility, acetic acid/acetate buffered solutions of pH 4.5 were chosen further studies.

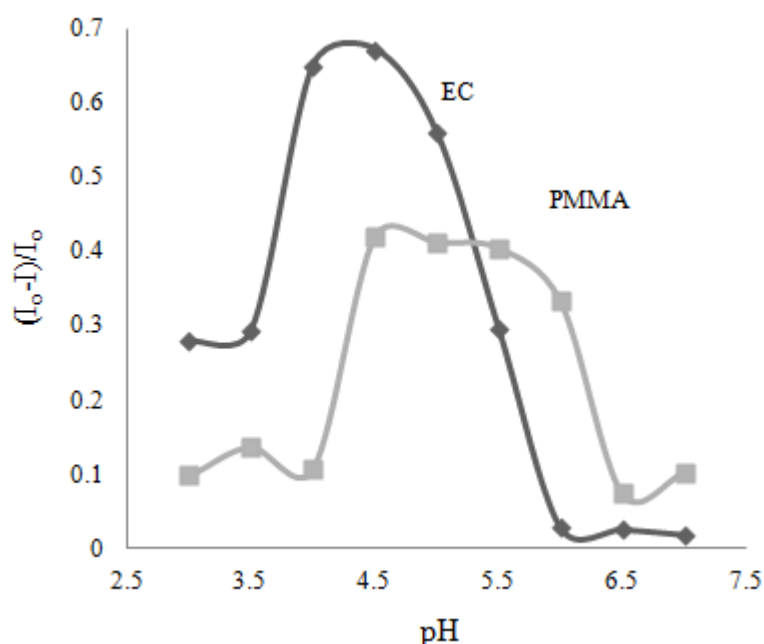


Figure 4.15 pH dependency of the M-AZM doped nanofibers in the presence of 10^{-5} mol L⁻¹ Ag (I) ions between pH 2.5 and 7.0.

4.5 Silver Uptake and Fluorescence Based Response

When doped into modified PMMA and EC matrices along with the anionic additive, potassium tetrakis-(4-chlorophenyl) borate, the M-AZM dye becomes a Ag (I) selective probe. In this system, silver ions are selectively extracted into the nanofibers (or thin films) by the anionic additive meanwhile potassium ions diffuse from the membrane into the aqueous phase due to the mechanism of ion exchange. Physical aspect of the response mechanism of M-AZM dye can be explained by the following ion-exchange pathway shown in Eq. 4.2

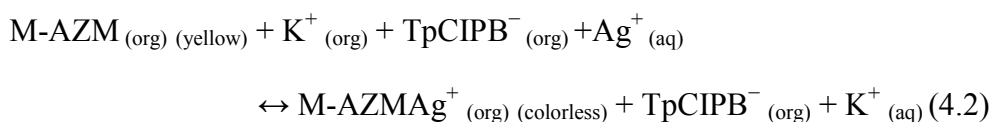


Figure 4.16- I and II shows the change in fluorescence spectra of PMMA based thin film and electrospun materials as a function of different concentrations of silver ions. Fluorescence sensing investigations reveal that, in both matrices, compared to

continuous thin films, electrospun films exhibited enhanced reactivity, larger linear analytical ranges and better sensitivity.

The intensity decrease is known to be due to the quenching of the M-AZM by Ag (I) ions. In many instances the fluorophore can be quenched both by collisions and by complex formation. The intensity based data (I_0/I) or $(I_0 - I)/I_0$ exhibiting an upward-concave curvature toward the y-axis is the evidence of combined quenching both by collisions (dynamic quenching) and by complex formation (static quenching) with the same quencher (Lakowicz, 1999). In case of dynamic quenching because the collision between the quencher and the fluorophore affects only the excited state of the fluorophore, no changes in the absorption or excitation spectrum are expected. On the contrary, the formation of ground-state complex in static quenching will perturb the absorption spectra of the fluorophore. Thus, by careful examination of the absorption or excitation spectrum, one can attempt to distinguish static and dynamic quenching. Figure 4.16 depicts the excitation–emission spectrum of M-AZM dye in the absence and presence of Ag (I) ions (see spectrum “a” and others) in PMMA matrices.

The excitation band at 390 nm exhibited a decrease in signal intensity upon exposure to Ag (I) ions and an accompanying band broadening. Variation of color of M-AZM dye from yellow to colorless reveal the formation of a non-fluorescent complex with Ag (I) in the ground state. When the linear shape of the fluorescence intensity based response data were evaluated together, the quenching mechanism between M-AZM and Ag (I) can be concluded as “static quenching”. Upon exposure to Ag (I) ions, the EC based thin films and electrospun materials exhibited very similar results to PMMA in terms of fluorescence signal change and working range (see Figure 4.17-I and II). From the figures, it can be concluded that in EC matrix, compared to continuous thin films, electrospun films exhibited enhanced reactivity, larger linear analytical ranges and better sensitivity. In the insets of Figure 4.17 I and II, linearized calibration plots for the concentration range of 10^{-12} - 10^{-6} M Ag (I) and 10^{-14} - 10^{-7} M Ag (I) were shown for thin film and nanofiber forms, respectively.

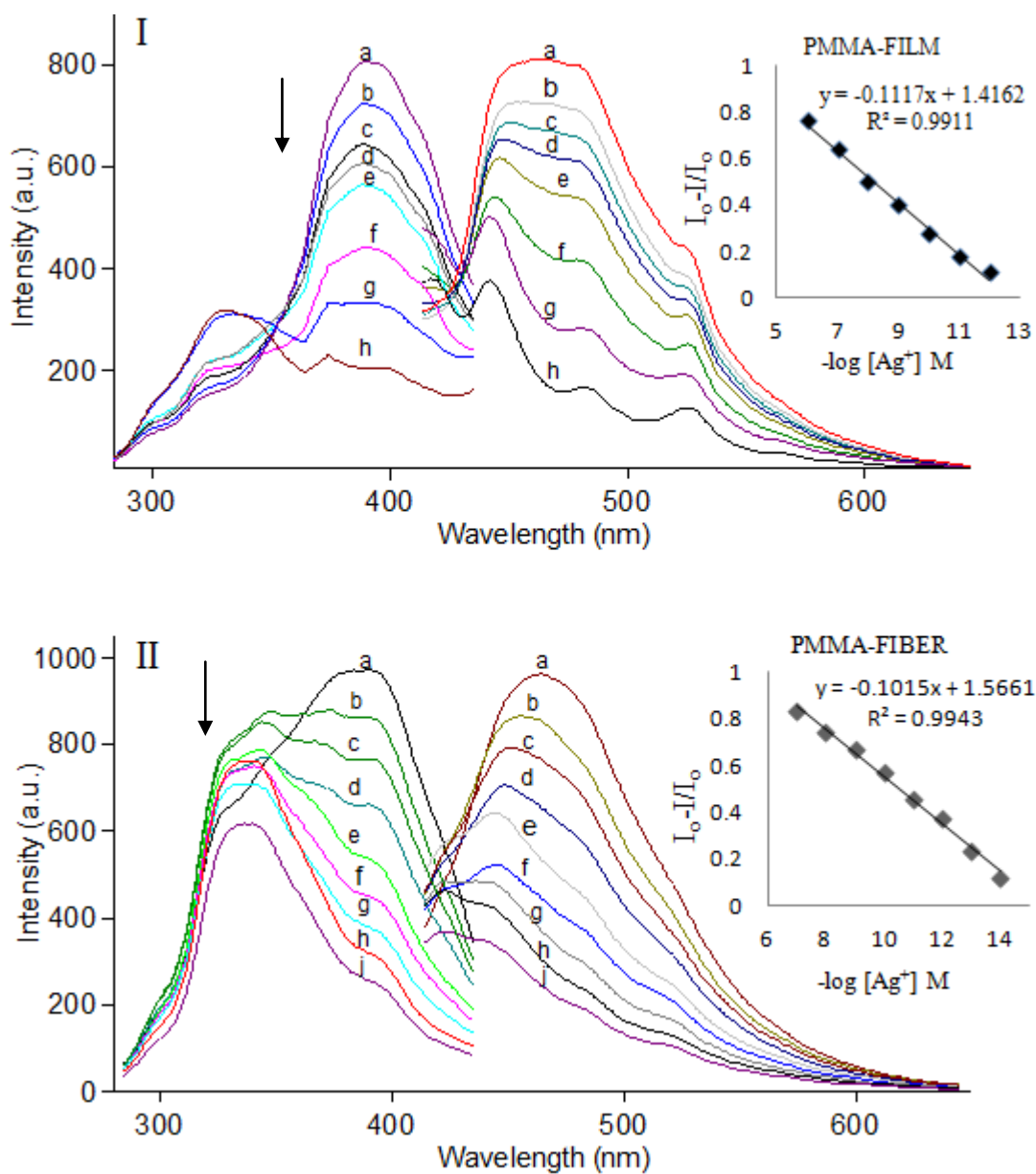


Figure 4.16 **I**. Fluorescence response of the M-AZM-doped PMMA based thin film to Ag (I) ions at pH 4.5. (a) Ag-free buffer (b) 10^{-12} , (c) 10^{-11} , (d) 10^{-10} , (e) 10^{-9} , (f) 10^{-8} , (g) 10^{-7} , (h) 10^{-6} M Ag(I), Inset: Calibration plot for the concentration range of 10^{-12} - 10^{-6} M Ag (I). **II**. Response of the PMMA based nanofiber to Ag (I) ions at pH 4.5. (a) Ag-free buffer, (b) 10^{-14} , (c) 10^{-13} , (d) 10^{-12} , (e) 10^{-11} , (f) 10^{-10} , (g) 10^{-9} , (h) 10^{-8} , (j) 10^{-7} M Ag (I), Inset: Linearized calibration plot for the concentration range of 10^{-14} - 10^{-7} M Ag (I).

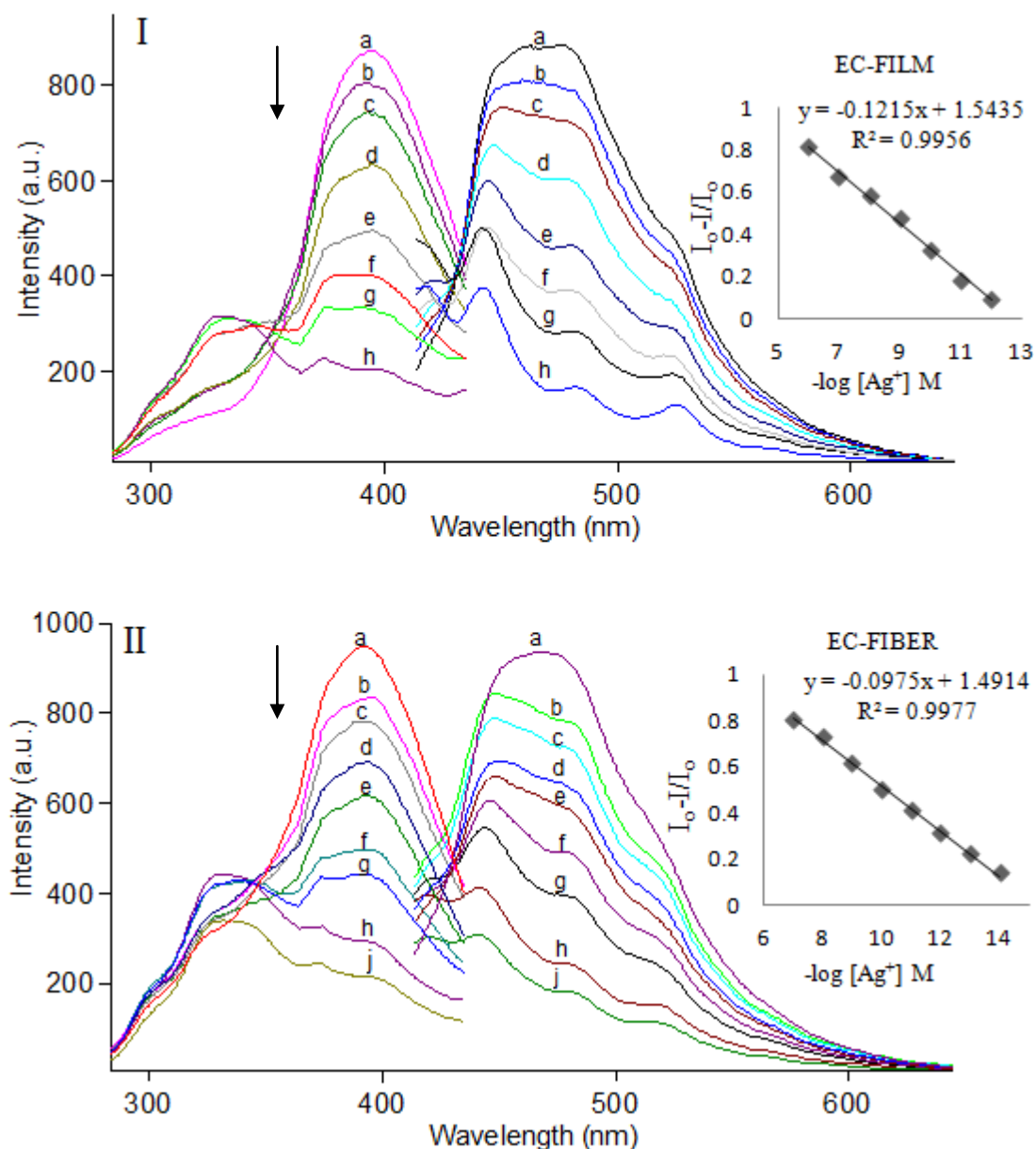


Figure 4.17 **I**. Excitation-emission based response of the dye-doped EC based thin film to Ag (I) ions at pH 4.5. (a) Ag-free buffer, (b) 10^{-12} , (c) 10^{-11} , (d) 10^{-10} , (e) 10^{-9} , (f) 10^{-8} , (g) 10^{-7} , (h) 10^{-6} M Ag(I), Inset: Calibration plot for the concentration range of 10^{-12} - 10^{-6} M Ag (I). **II**. Response of the EC based nanofiber to Ag (I) ions at pH 4.5. (a) Ag-free buffer, (b) 10^{-14} , (c) 10^{-13} , (d) 10^{-12} , (e) 10^{-11} , (f) 10^{-10} , (g) 10^{-9} , (h) 10^{-8} , (j) 10^{-7} M Ag (I), Inset: Linearized calibration plot for the concentration range of 10^{-14} - 10^{-7} M Ag (I).

4.6 Stern–Volmer Analysis

In a solution, the quantitative measure of fluorescence quenching is described by the Stern–Volmer constant, K_{sv} . These definitions were given into detail in Chapter 3.

The data obtained by gathering Stern–Volmer analysis for each electrospun and continuous thin film are shown in Table 4.4. For quencher concentrations in the range of 1.0×10^{-14} to 1.0×10^{-7} M, linear plots concentration versus I_0/I are obtained showing an excellent Stern–Volmer relationship. Stern–Volmer constants (K_{sv}) of the electrospun films, calculated from slopes of the plots were found to be 1.0×10^{10} (M^{-1}) and 1.1×10^{10} (M^{-1}) for EC and PMMA nanofibers, respectively. These values are 11 and 100-fold greater than that obtained from the continuous thin films of PMMA and EC, respectively (see Table 4.4, Figure 4.18 and Figure 4.19).

The calculated K_{sv} values reveal important practical consequences. The sensitivity of the quenching process is enhanced by controlling the quencher diffusion rate to fluorophores via the nano-structural properties of the electrospun sensing films. Additionally this type of nano-structure provides higher surface area-to-volume ratio than that of continuous thin films (Deitzel, Kleinmeyer, & Tan, 2001).

Table 4.4 The Stern-Volmer plot related data of PMMA and EC based electrospun nanofibers and thin films.

Indicator dye	Matrix /form	Linear Stern Volmer Equation	K_{sv} constant(M^{-1})
M-AZM	EC/ nanofiber	$y = 1.0E+10x + 1$	1.0×10^{10}
	PMMA/nanofiber	$y = 1.1E+10x + 1$	1.1×10^{10}
	EC / thin film	$y = 9.0E+08x + 1$	9.0×10^8
	PMMA/ thin film	$y = 1.0E+08x + 1$	1.0×10^8

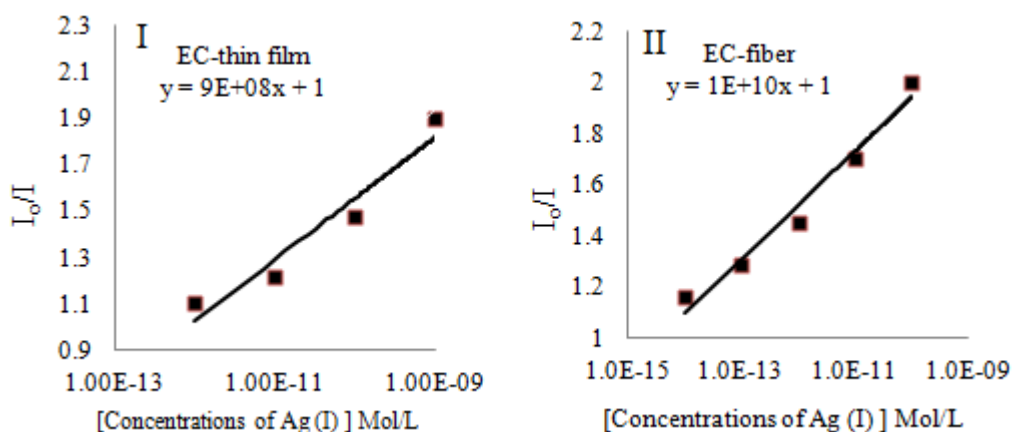


Figure 4.18 Stern-Volmer plots of EC based thin film (I) and electrospun nanofibers (II) as a function of different quencher concentrations.

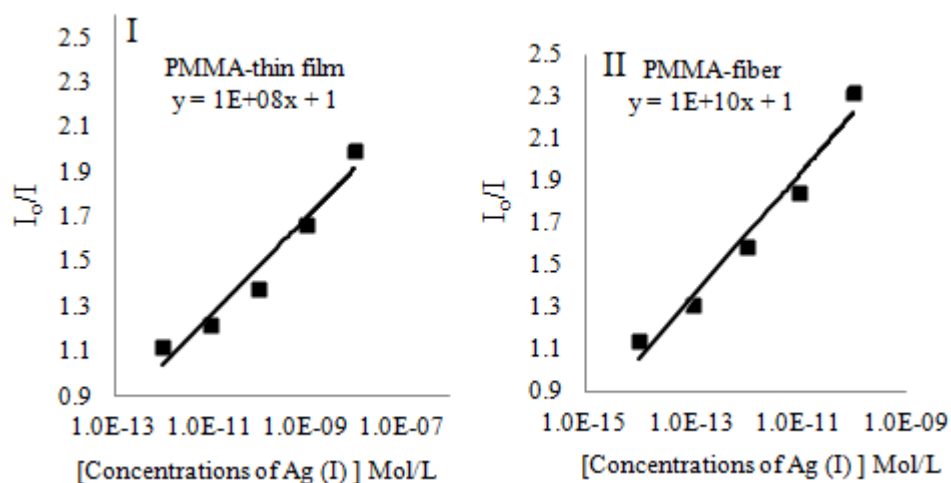


Figure 4.19 Stern-Volmer plots of PMMA based thin film (I) and electrospun nanofibers (II) as a function of different quencher concentrations.

4.7 Response and Detection Limit

The M-AZM doped electrospun nanofibers demonstrated a linear response over range of 1.0×10^{-14} to 1.0×10^{-7} M for Ag (I) ions. The tested sensor compositions exhibited large relative signal change, excellent linearity and very good sensitivity to Ag (I) ions. To our knowledge this is the largest reported linear working range and highest sensitivity among other fluorescence based silver sensing designs (Coskun, &

Akkaya, 2005; Iyoshi, Taki, & Yamamoto, 2008; Kandaz, Güney, & Senkal, 2009; Koca, Gonca, & Gül, 2008; Topal, Gürek, Ertekin, Yenigul et al., 2010; Topal, Gürek, Ertekin, Atilla et. all., 2010; Wang et al., 2010; Yarasir, Kandaz, Senkal, Koca, & Salih, 2007; Zhu, Fu, & Wong, 2008).

It should be remembered that, linear response offers many advantages over quadratic calibration curves such as interpolation and extrapolation. In this work, due to the compatibility of the acquired data, the ordinary least-squares (OLS) regression model was employed for the fit of the calibration curves. The regression results yielded an absolute linear response with coefficients of regression (R^2) of 0.9977 and 0.9943 for PMMA and EC electrospun nanofibers, respectively (see Table 4.5, Figure 4.16 and 4.17).

The detection limit was determined as the concentration of Ag (I) that would give a signal three times the standard deviation of the blank signal which corresponded to 0.46 and 0.34 fmol (4.60×10^{-16} M and 3.40×10^{-16} M) silver ion for electrospun EC and PMMA films, respectively. The detection limits of 190 and 198 fmol were calculated for continuous thin film form of the same compositions. For 10 successive determinations of 0.46 and 0.36 fmol/L Ag (I), relative standard deviations were obtained 5.5% and 4.8%, respectively. The results demonstrated that the functionalized nanoporous electrospun films could improve both the sensitivity and the reproducibility.

The stability of M-AZM ionophore in the employed matrix materials was excellent and when stored in the ambient air of the laboratory there was no significant drift in signal intensity after 7 months.

Table 4.5 Calibration related characteristics of PMMA and EC based electrospun nanofibers and thin films

Indicator Dye	Matrix /Form	Linear Range (Ag(I) Mol/L)	Regression Coefficient (R ²)	LOD (Molar)	LOD (femto molar)
M-AZM	EC/nanofiber	1.0×10 ⁻¹⁴ to 1.0×10 ⁻⁷	0.9977	4.60×10 ⁻¹⁶	0.46
	PMMA/nanofiber	1.0×10 ⁻¹⁴ to 1.0×10 ⁻⁷	0.9943	3.40×10 ⁻¹⁶	0.34
	EC / thin film	1.0×10 ⁻¹² to 1.0×10 ⁻⁶	0.9956	1.90×10 ⁻¹³	190
	PMMA/ thin film	1.0×10 ⁻¹² to 1.0×10 ⁻⁶	0.9911	1.98×10 ⁻¹³	198

4.8 Selectivity Studies and Interference Effects

Measuring Ag (I) concentrations in drinking water, groundwater or environmental samples with indicators may be difficult due to the competitive binding of Ca²⁺, K⁺, Mg²⁺ and other cations. In order to examine the response of the M-AZM ionophore to potential interfering cations, the sensor films were treated with 10⁻³ M concentrations of Li⁺, Na⁺, K⁺, Ca²⁺, Ba²⁺, Mg²⁺, NH₄⁺, Ni²⁺, Co²⁺, Cu²⁺, Pb²⁺, Al³⁺, Cr³⁺, Mn²⁺, Sn²⁺, Hg⁺, Hg²⁺, Zn²⁺, Fe²⁺ and Fe³⁺ ions at pH 4.5 in acetic acid/acetate buffer solutions.

It can be concluded from Figure 4.20 that the PMMA based sensing membrane is capable of determining silver ions with a high selectivity over others. Nonetheless, the response to Sn²⁺ is markedly different from the response to other metal ions and fluorescence of M-AZM is affected appreciably by Sn²⁺ at concentrations of ≥10⁻³ mol L⁻¹. The interference effects of the anions; F⁻, Cl⁻, Br⁻, NO₃⁻, NO₂⁻, SO₄²⁻ and PO₄³⁻ were also tested. Relative signal changes of less than 5% were observed for EC and PMMA doped films at pH 4.5.

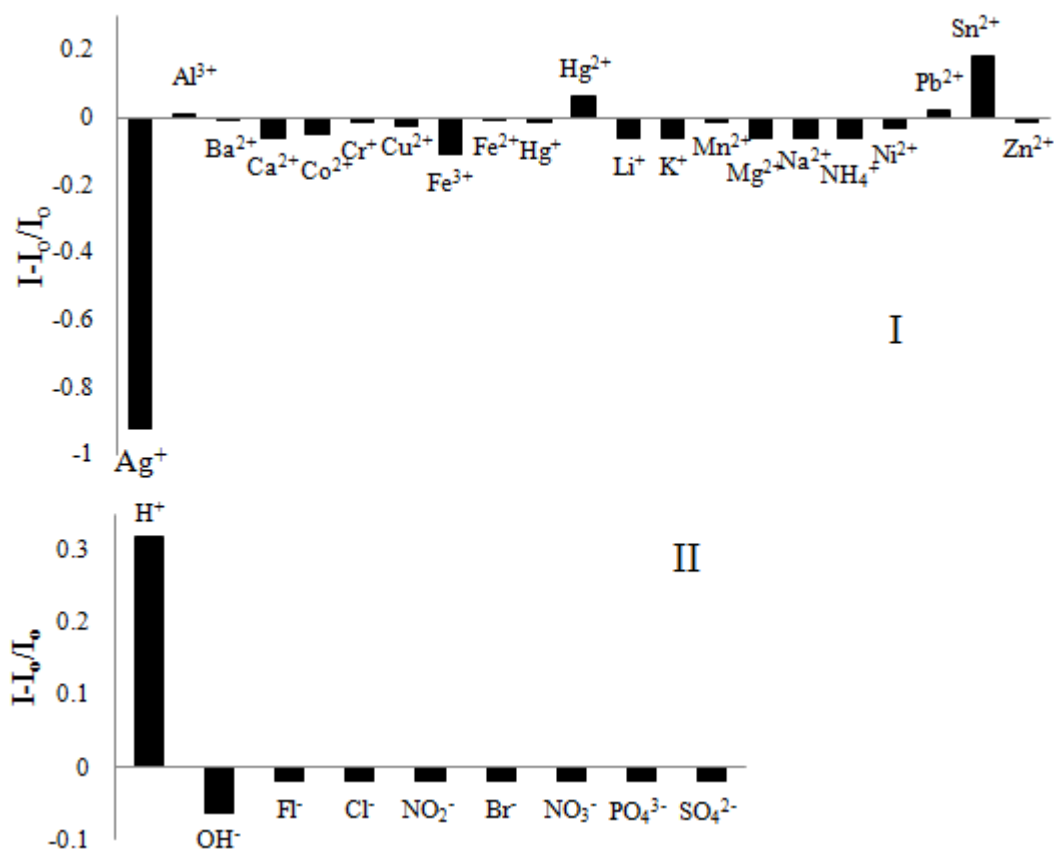


Figure 4.20 **I**: Metal ion response of PMMA based nanofibers at pH 4.5. **II**: anion response of the same composition near neutral solutions.

4.9 Conclusion

Electrospinning resembles a promising, simple, and an effective method for fabricating polymer based chemosensors. With respect to continuous thin films, electrospun nanomaterials, provided enhanced sensitivity and reactivity in emission based silver sensing.

The fluorophore M-AZM is shown to be a highly selective reagent for the determination of silver (I) ion at sub-nanomolar level. The fluorescence of M-AZM is statically quenched by silver (I) ions. A dynamic working range of silver (I) determination from 1.0×10^{-14} to 1.0×10^{-7} M with a limit of detection of 3.40×10^{-16} M was obtained.

CHAPTER FIVE

SUB-NANOMOLAR SENSING OF IONIC MERCURY WITH POLYMERIC ELECTROSPUN NANOFIBERS

5.1 Introduction

Heavy metals or soft metals like Hg (II), Pd (II) and Cd (II) are trace metals. High concentration exposure is not necessary to produce a state of toxicity in the human body or tissues and, over time, they can reach toxic concentration levels. Therefore design of chemosensors targeting ionic mercury at sub nanomolar level is very important. In recent years a number of fluorescent chemosensors for Hg (I) and Hg (II) have been designed and tested (Cano-Raya, Fern'andez-Ramos, G'omez-S'Anchez, & Capit'An-Vallvey, 2006; Ertekin, Oter, Ture, Denizalti, & Cetinkaya, 2009; Fana et al., 2009; Harris, Pickering, & George, 2003; Kuswandia, & Narayanaswamy, 2001; Lv et al. 2008; Murkovic, & Wolfbeis, 1997; Selid, Xu, Collins, Face-Collins, & Zhao, 2009; Wan et al., 2009; Yari, & Papi, 2009; Yuan et al., 2007; Zhu et al., 2008). In most of these designs, a mercury selective chromoionophore was exploited. The sensing agent was functional either in solution or in embedded form in a polymer matrix.

In the optical chemical sensing of mercury, the thin film approach has been used many times. Such sensors with thickness in the range of 1–30 μm provided enhanced robustness, reversibility, stability and sensitivity with respect to the sensing studies realized in solution phase. On the other hand, preparation and use of nanomaterials is a current research topic of interest in different scientific and technological areas including sensor technologies due to its promising properties. The usage of nano scale sensing materials is expected to offer good results in comparison to sensing films prepared with the same composition. Although there have been limited number of works regarding sensor applications of nanomaterials, a former study of Wang et al. (2002) encouraged us to work in this way, who reported the usage of electrospun nanofibrous membranes as fluorescence quenching-based optical sensors for metal ions and 2,4-dinitrotoluene (DNT). In this work a fluorescent polymer, poly (acrylicacid)-poly (pyrene methanol) (PAA-PM), was used as a sensing material.

A few years later, Wang and co-workers (2004) fabricated more sensitive optical sensors by combining the techniques of electrospinning and electrostatic adsorption. A fluorescent probe, hydrolyzed poly[2-(3-thienyl) ethanol butoxy carbonyl-methyl urethane], was electrostatically assembled onto the surface of cellulose acetate electrospun nanofibrous membranes. The fluorescence of these membranes can be quenched by extremely low concentrations (ppb) of methyl viologen (MV^{2+}) and cytochrome *c* (cyt *c*) in aqueous solutions.

Liu, Kameoka, Czaplewski, & Craighead (2004) used a nonlithographic deposition process to form single polymeric nanowire chemical sensors. Oriented polyaniline nanowires, with diameters on the order of 100 nm, were deposited on gold electrodes. The devices showed a rapid and reversible resistance change upon exposure to NH_3 gas at concentrations as low as 0.5 ppm.

Manesh, Santhosh, Gopalan, & Kwang-Pill Lee (2007) prepared the nanofibrous membrane of the composite consisting of poly(vinylidene fluoride) and poly(aminophenylboronic acid) (PVdF/PAPBA-NFM). The PVdF/PAPBA-NFM displayed linear response in detection of glucose for the concentration range of 1 to 15mM with a response time of less than 6 s.

Up to now, the reported works regarding optical chemical sensor applications of electrospun nanofibers is very rare. Here we have successfully combined the nano-scale electrospun fiber materials with optical sensing technology for detection of ionic mercury at subnanomolar levels. In this work, the analyte sensitive fluoroionophore (azomethine dye), ionic liquid and ethyl cellulose (EC) combination were used together to produce electrospun nanofibers. The nano-fibrous materials were fabricated by electrospinning technique. In an earlier set of investigations we used the azomethine molecule as a proton driven molecular switch (Derinkuyu et al. 2010). During these studies another point we discovered was the selective response of this dye to Hg (I) and Hg (II) ions. Here we present the chemosensing ability of the fluorescent methoxy azomethine ionophore; (4-(dimethylamino)benzaldehyde2-[[4-cyanophenyl]methylene]hydrazone (DC-AZM) to mercury ions. The dye was

also chosen due to the strong absorbance, high quantum yield, large Stoke's shift and excellent photostability. The electrospun nano-fibers were characterized using scanning electron microscopy (SEM) and their average diameters were evaluated. To our knowledge this is the first attempt using the fluoroionophore-doped EC based electrospun nano-fibrous materials for mercury sensing at subnanomolar level (Kacmaz et al., 2012). The DC-AZM dye, responds both of the common oxidation states of mercury; Hg (I) and Hg (II) at pH of interest. However, in this work we focused on sensing of Hg (II); the most abounded form of mercury. Schematic structure of the employed dye molecule is shown in Figure 5.1.

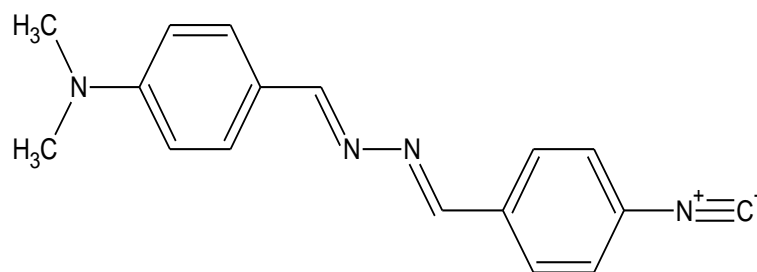


Figure 5.1 Schematic structures of the mercury sensitive fluoroionophore DC-AZM; (4-(dimethylamino) benzaldehyde2-[[4 cyanophenyl] methylene] hydrazone dye.

5.2 Photocharacterization of Fluoroionophore

For spectral characterization of the DC-AZM, absorption excitation and corrected emission spectra were recorded in the solvents of EtOH, DCM, THF and toluene/ethanol (To:EtOH; 80:20) mixture and in PMMA and EC matrices (see Figure 5.2 and 5.3).

The UV-Vis spectroscopy related data (absorption maxima; λ_{Abs} , and molar extinction coefficient; ϵ), were shown in Table 5.1. DC-AZM exhibited very efficient absorbance and high molar extinction coefficients around 492 nm and 494 nm in PMMA and EC matrices. In agreement with literature (Derinkuyu et al., 2008) molar extinction coefficients (ϵ_{max}) of DC-AZM were increased in PMMA and EC with respect to (ϵ_{max}) of DC-AZM in solution phase (see Table 5.1). These data can

be taken as proofs that DC-AZM molecules absorb better in plasticized PMMA and EC matrices. The excitation-emission spectra and the related data of the DC-AZM are shown in Figure 5.3 and Table 5.2.

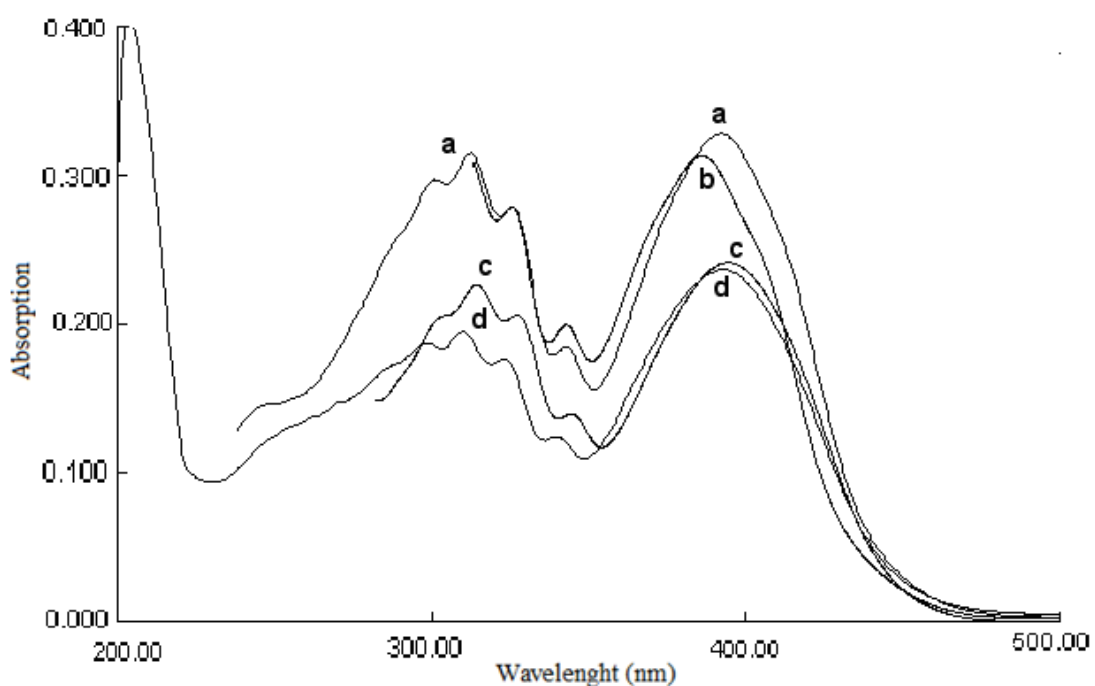


Figure 5.2 Absorption spectra of the DC-AZM dyes (10^{-6} M dye or 2 mM dye/kg polymer). a) DCM b) THF c) To: EtOH d) EtOH

Table 5.1 UV-Vis spectra related data of DC-AZM in the solvents of EtOH, DCM, THF and toluene/ethanol mixture (80:20) and in solid matrices, EC and PMMA

Compound	Solvent/Matrix	λ^1_{abs}	λ^2_{abs}	$\epsilon_{\text{max}}(\lambda^1_{\text{abs}})$	$\epsilon_{\text{max}}(\lambda^2_{\text{abs}})$
DC-AZM	EtOH	310	394	19500	23600
	DCM	312	393	31500	32800
	THF	--	387	--	65000
	To: EtOH	314	395	22600	24100
	EC	390	494	32165	40486
	PMMA	390	490	247332	161686

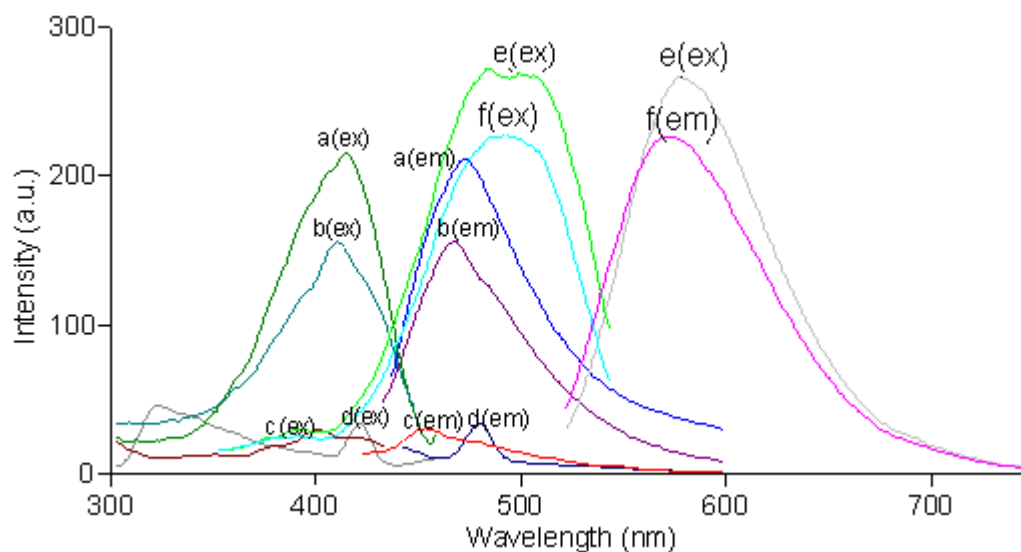


Figure 5.3 Excitation and corrected emission spectra of the DC-AZM dye (10^{-6} M dye or 2 mM dye/kg polymer) a) EtOH b) To: EtOH (80:20) c) DCM d) THF e) EC f) PMMA.

Table 5.2 The excitation–emission spectra related characteristics of the DC-AZM acquired in conventional solvents, and in thin film form of PMMA and EC.

Compound	Matrix	λ_{\max}^{em}	λ_{\max}^{ex}	$\Delta\lambda_{ST}$ (Stoke's shift)	ϕ_F (Quantum yield)
DC-AZM	EtOH	473	415	58	1.9×10^{-3} in EtOH
	DCM	454	400	54	
	THF	480	420	60	
	To:EtOH	468	410	58	
	EC	572	500	72	0.3805
	PMMA	570	500	70	0.8532

5.3 Quantum Yield Calculations

The absorbance and corrected emission spectra of five different concentrations of reference standard Rose Bengal ($\lambda_{ex} = 525$ nm, quantum yield (ϕ_F) = 0.11 in alkaline ethanol) and DC-AZM compound were recorded for fluorescence quantum yield calculations. The integrated fluorescence intensities were plotted vs absorbance for the reference standards and the DC-AZM compound in EC and PMMA matrices (see Figure 5.4). The gradients of the plots are proportional to the quantity of the quantum yield of the studied molecules. The equations of the plots are $y = 43846x$; $R^2 =$

0.9985 for reference standard, $y = 128195x$; $R^2 = 0.9976$ for DC-AZM dye in EC and $y = 391118x$; $R^2 = 0.9927$ for DC-AZM dye in PMMA. Quantum yield (ϕ_f) values were calculated according to the given equation in Chapter 3 as 0.0019 in ETOH, 0.3805 in EC and 0.8532 in PMMA.

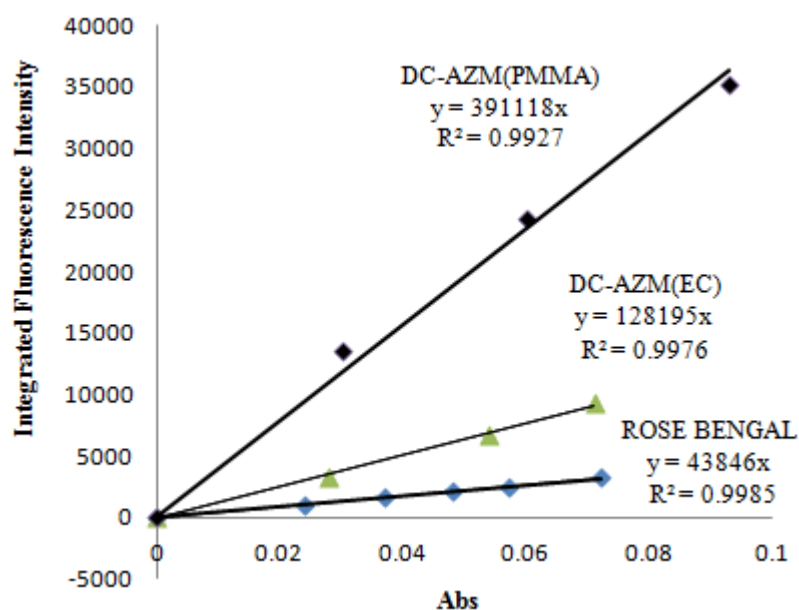


Figure 5.4 The integrated fluorescence intensities vs absorbance for the reference standard; Rose Bengal in in alkaline ethanol, the DC-AZM dye in EC and DC-AZM dye in PMMA matrices.

5.4 SEM images of electrospun membranes

The scanning electron microscope (SEM) images of an electrospun membrane are shown in Figure 5.5. The fiber diameters were approximately 400 to 685 nm.

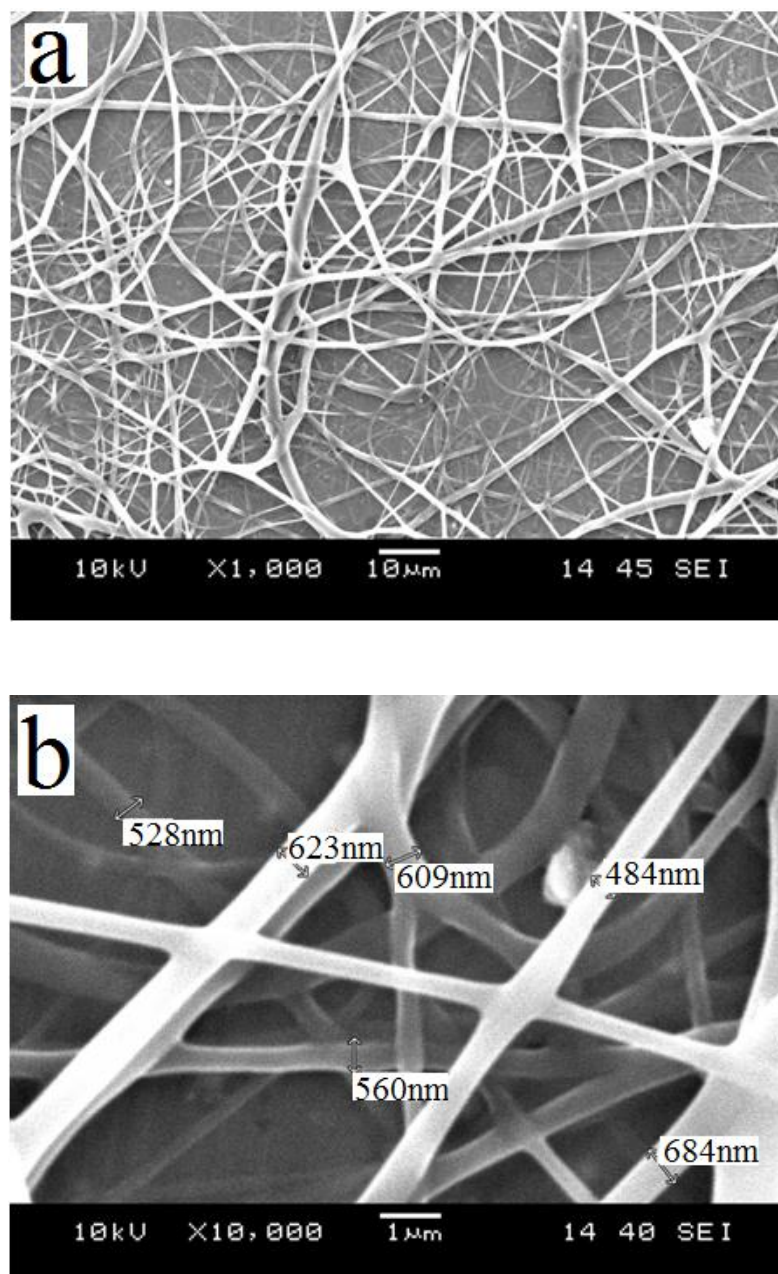


Figure 5.5 SEM images of EC based electrospun nanofibers (a) and (b); EC based nanofibers at different magnifications such as $\times 1000$ and $\times 10000$.

5.5 Dissociation Constant (pKa) Calculations of Indicator Dye In EC Matrix

The knowledge of dissociation constant (pK_a) of dye is of fundamental importance in order to provide information on chemical reactivity range of the indicator dye. So, determination of the acidity constant has been performed in EC matrix. pH induced emission-excitation spectra of DC-AZM doped EC matrix were

recorded in the pH range of 6.50-11.00. Dye doped-EC thin film was exposed to buffered solutions at different pH values, and after each expose, pH values of the media were recorded (see Figure 5.6). Here a relative signal change of approximately 100% has been reached. Figure 5.6 shows the plot of emission-excitation intensity of DC-AZM doped EC matrix versus measured pH values. pKa values were found as 7.57. Given pKa values were calculated by using non-linear fitting algorithm of Gauss–Newton–Marquardt equation; $pK_a = pH + \log [(I_x - I_b)/(I_a - I_x)]$

$$pK_a = 7.5 + \log [(165-1)/(303-165)]$$

$$pK_a = 7.5 + \log [1.19]$$

$$pK_a = 7.57 \quad (\text{for indicator immobilized EC})$$

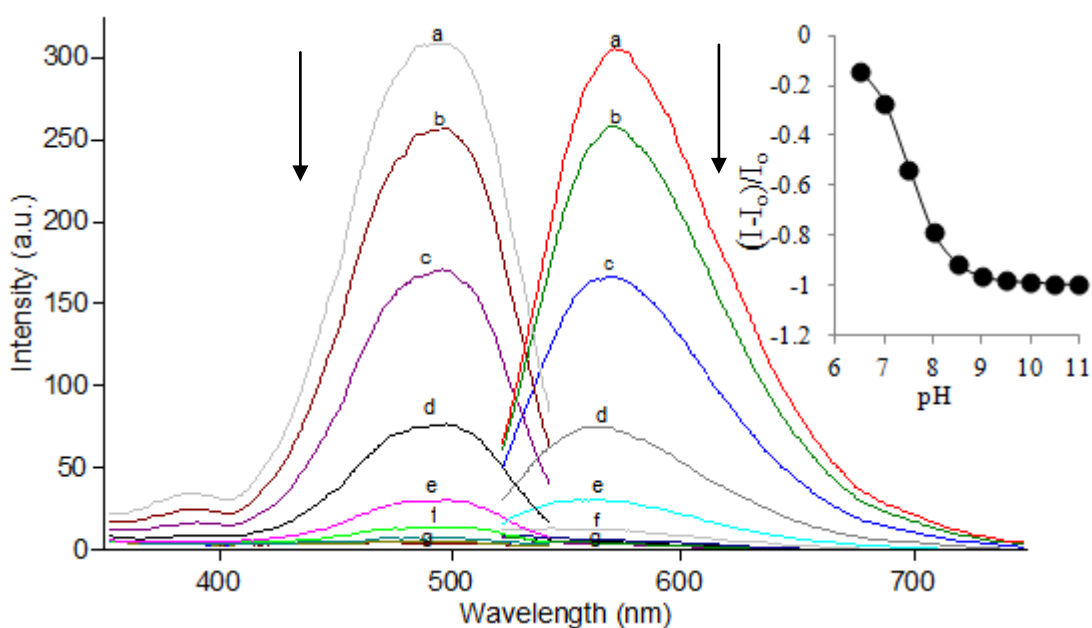


Figure 5.6 pH induced emission characteristics and sigmoidal calibration curve of DC-AZM doped EC membrane in the pH range of 6.5–11.0 (a) pH=6.5 (b) pH=7.0 (c) pH= 7.5 (d) pH= 8.0 (e) pH= 8.5 (f) pH= 9.0 (g) pH= 9.5-10.0- 10.5-11.0 (pKa=7.57).

5.6 Response to Mercury Ions

When doped into modified EC matrices along with the anionic additive; potassium tetrakis- (4-chlorophenyl) borate; the DC-AZM dye becomes a Hg (II) selective probe. In this system, Hg (II) ions are extracted into the polymer phase by

the anionic additive meanwhile two of potassium ions diffuse from the membrane into the aqueous phase via the mechanism of ionexchange due to the electroneutrality consideration. Same principle is valid in uptake of Hg (I) ions into the polymeric EC matrix. Physical aspect of the ion-exchange pathway can be explained by the following equation.

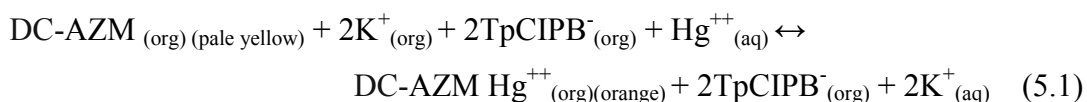


Figure 5.7-I and II shows the change in fluorescence spectra of thin film and electrospun materials as a function of different concentrations of mercury ions, respectively. The observed intensity decrease at 572 nm is known to be due to the quenching of the DC-AZM dye by Hg (II) ions.

A number of processes can lead to quenching. These processes can occur during the excited state lifetime of the fluoroionophore. For example collisional quenching, energy transfer, charge transfer reactions or they may occur due to formation of complexes in the ground state. Sometimes the fluorophore can be quenched both by collisions and by complex formation in the same time. A correlation between quencher concentration and intensity based data (I_0/I) exhibiting an upward-concave curvature toward the y-axis is the evidence of combined quenching both by collisions (dynamic quenching) and by complex formation (static quenching) with the same quencher (Lakowicz, 1999). In case of dynamic quenching, the collision between the quencher and the fluorophore affects only the excited state of the fluorophore. No changes in the absorption or excitation spectrum are expected. On the contrary, the formation of ground-state complex in static quenching will perturb the absorption spectra of the fluorophore. Thus, by careful examination of the absorption spectrum, one can distinguish static and dynamic quenching.

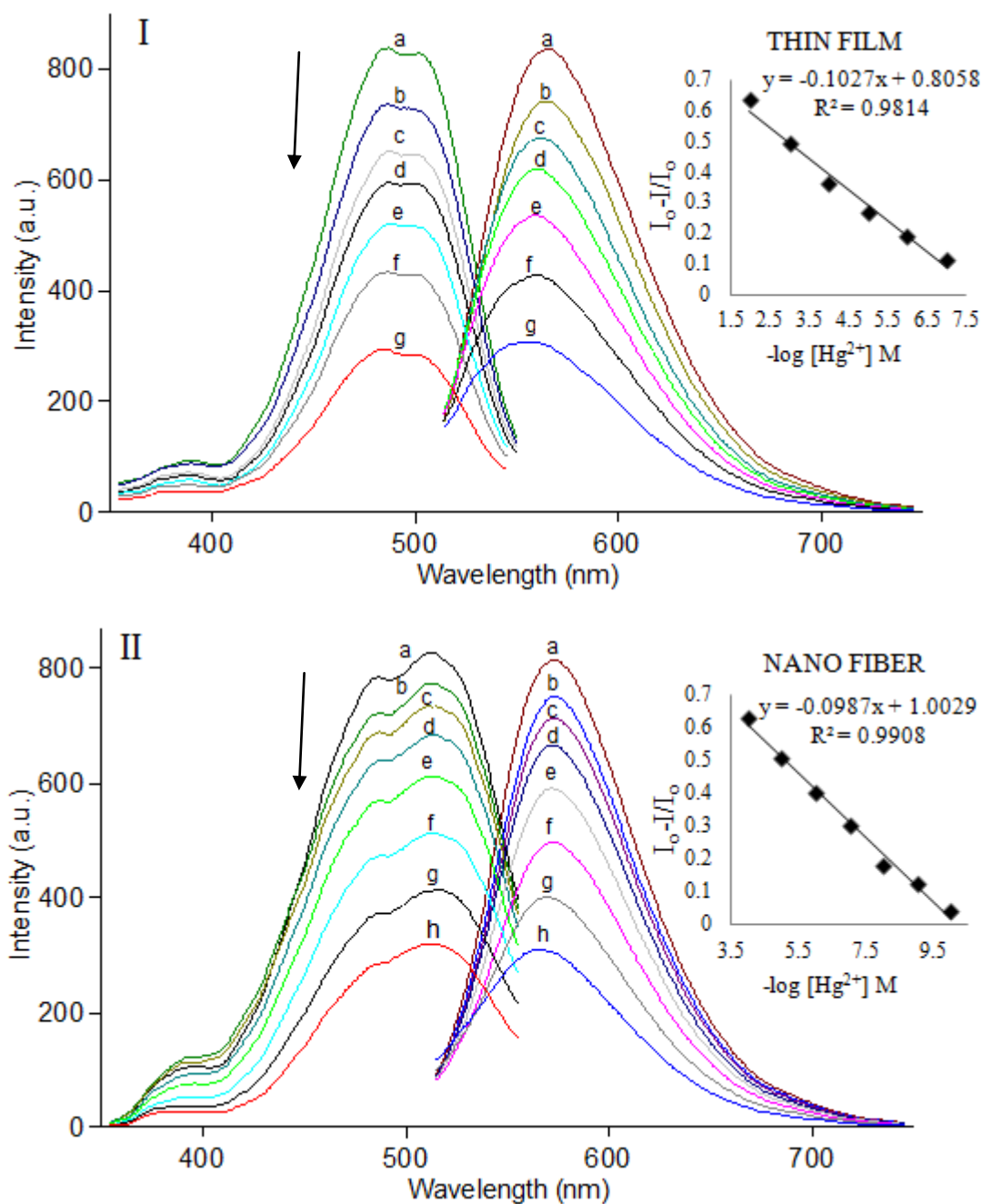


Figure 5.7- I. Fluorescence response of the DC-AZM-doped EC based thin film to Hg (II) ions at pH 4.0. (a) Hg-free buffer (b) 10^{-7} , (c) 10^{-6} , (d) 10^{-5} , (e) 10^{-4} , (f) 10^{-3} , (g) 10^{-2} M Hg(II), Inset: Calibration plot for the concentration range of 10^{-7} - 10^{-2} M Hg (II). **II.** Response of the EC based nanofiber to Hg (II) ions at pH 4.0. (a) Hg-free buffer, (b) 10^{-10} , (c) 10^{-9} , (d) 10^{-8} , (e) 10^{-7} , (f) 10^{-6} , (g) 10^{-5} , (h) 10^{-4} M Hg (II), Inset: Linearized calibration plot for the concentration range of 10^{-10} - 10^{-4} M Hg (II).

Figure 5.8 shows the absorption spectrum of the DC-AZM dye in the absence and presence of Hg (II) ions. The absorption band around 400 nm exhibited a dramatic decrease in signal intensity upon exposure to Hg (II) and an accompanying spectral

shift of 80 nm. Variation of absorption spectra and an accompanying discernible color change of DC-AZM dye from pale yellow to orange reveal the formation of a non-fluorescent complex with Hg (II) in the ground state. When the linear shape of the fluorescence intensity based response and absorption spectroscopy related data were evaluated together, the quenching mechanism between DC-AZM and Hg (II) can be concluded as “static quenching” (see inset of Figure 5.7).

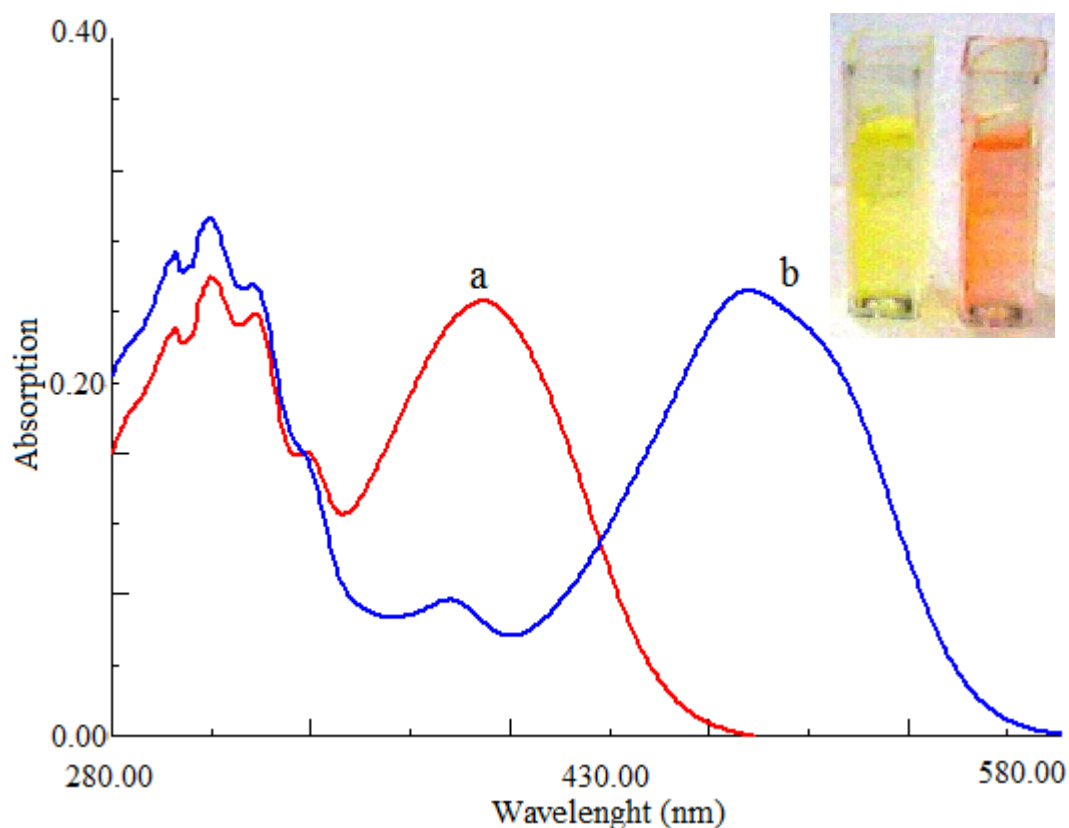


Figure 5.8 Absorption spectrum of the DC-AZM dye in ethanol (a) Hg (II) free , (b) in presence of 5×10^{-5} M Hg (II)

The DC-AZM doped eletrospun nanofibers demonstrated a linear response over the concentration range of 1.0×10^{-10} - 1.0×10^{-4} Mol.L⁻¹ for Hg (II) ions. The tested sensor compositions exhibited large relative signal change (65%), excellent linearity and very good sensitivity to Hg (II) ions. The regression results yielded an absolute linear response with coefficients of regression (R^2) of 0.9908 for EC electrospun nanofibers. (see Table 5.3, Figure 5.7-II).

The detection limit was determined as the concentration of Hg (II) that would give a signal three times the standard deviation of the blank signal which corresponded to 0.07 nM (7.2×10^{-11} M) ion for EC based electrospun nanofiber. The detection limits of 14.4 nM were calculated for continuous thin film form of the same compositions. In all cases the reported LOD values are without sample preconcentration. The offered technique permit determination of mercury ions with a very high sensitivity and detection limits of 100 to 1000 times better than those obtainable with classical flame AAS and/or graphite furnace – AAS. The employed technique looks like competing with atomic fluorescence spectroscopy (AFS) and ICP-MS in terms of detection limits.

Table 5.3 Calibration characteristics of EC based electrospun nanofibers and thin films

Indicator Dye	Matrix /form	Conc. Range (Hg(II) Mol/L)	Regression Coefficient (R^2)	LOD (Molar)	LOD (nM) (nanomolar)
DC-AZM	EC/nanofiber	10^{-10} to 10^{-4}	0.9908	7.20×10^{-11}	0.07
	EC / thin film	10^{-7} to 10^{-2}	0.9814	1.44×10^{-8}	14.4

The stability of DC-AZM ionophore in the employed matrix material was excellent and when stored in the ambient air of the laboratory there was no significant drift in signal intensity after 4 months.

5.7 Stern-Volmer Analysis

The data obtained by gathering Stern-Volmer analysis results for electrospun and continuous thin films were shown in Table 5.4. For quencher concentrations in the range of 1.0×10^{-10} - 1.0×10^{-4} Mol.L⁻¹ linear plots between concentration of quencher and I_0/I are obtained showing an excellent Stern-Volmer relationship with electrospun nanofibers. Stern- Volmer constants (K_{sv}) of the electrospun films, calculated from slopes of the plots were found to be 1.09×10^5 (M⁻¹) and 1.02×10^3 (M⁻¹) for nanofiber and continuous thin film respectively. The (K_{sv}) of the electrospun film is approximately 100 fold greater than that of the (K_{sv}) obtained from the

continuous thin film. (see Table 5.4, Figure 5.9 -I and Figure 5.9-II). The calculated K_{sv} values reveal important practical consequences. The sensitivity of the quenching process is enhanced by controlling the quencher diffusion ability and rate to fluorophores via the nano-structural properties of the sensing agents. Additionally, the recorded response time for the electrospun nanofibers is approximately 1 minute which is at least 5 times better than that of the response times measured for thin films.

Table 5.4 The Stern-Volmer plots related data of EC based electrospun nanofibers and thin films

Indicator Dye	Matrix /form	Linear Stern Volmer Equation	K_{sv} Constant(M^{-1})
DC-AZM	EC / nanofiber	$y = 109297x + 1$	1.09×10^5
	EC / thin film	$y = 1018.2x + 1$	1.02×10^3

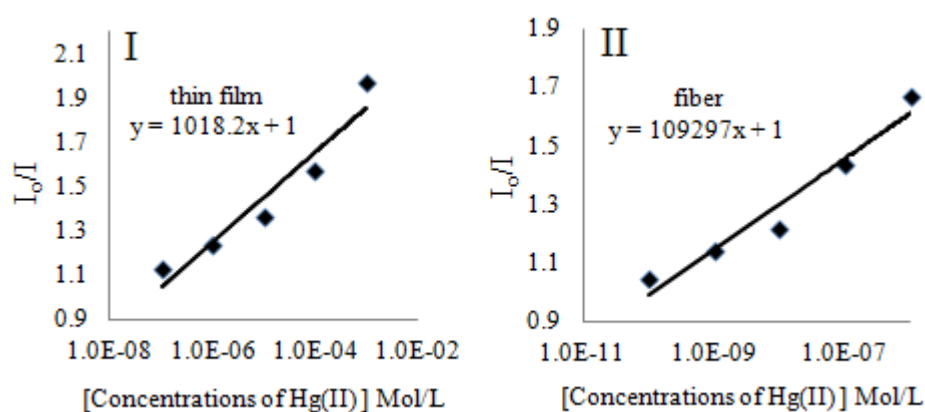


Figure 5.9 The Stern Volmer plot of EC based **I**: thin films and **II**: electrospun nanofibers

5.8 Effect of pH on Hg (II) response

The effect of pH on the sensing performance of dye doped thin films and electrospun nanofibers was investigated at fixed metal ion concentration; 5×10^{-3} mol L^{-1} between pH 3.0 – 6.0. Buffer solutions were prepared with 0.01 M CH_3COOH and 0.01 M NaH_2PO_4 at desired pH. As can be seen from Figure 5.10, the relative

signal change; $(I_0-I)/I_0$ produced by the Hg (II) ions was high enough and stable around pH 4.0.

Distribution of the Hg (II) related chemical species in the working conditions was also checked with chemical equilibrium software programme (Visual MINTEQ) at pH 4.0 in presence of acetate ions. $[(\text{CH}_3\text{COO}^-_{(\text{aq})}: 1\%, \text{CH}_3\text{COOH}_{(\text{aq})}: 99\%, \text{Hg}(\text{OH})_{2(\text{aq})}; 31.3\%, \text{Hg}^{2+}_{(\text{aq})}; 50.1\% \text{ and } \text{Hg}(\text{OH})^+_{(\text{aq})}; 18.6\%]$ Due to the solubility considerations, acetic acid/ acetate buffered solutions of pH 4.0 was chosen further studies.

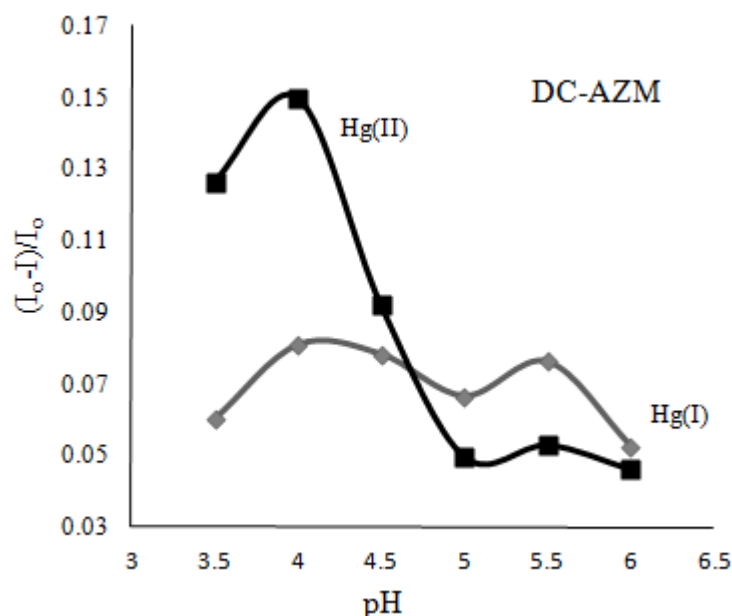


Figure 5.10 pH dependency of DC-AZM dye in presence of mercury ions between pH 3.0-6.0

5.9 Selectivity Studies, Regeneration And Interference Effects

In order to examine the response of the DC-AZM to possible interfering cations, the sensing agents were treated with 5×10^{-3} M concentrations of Ag^+ , Al^{3+} , Ba^{2+} , Ca^{2+} , Co^{2+} , Cr^{3+} , Cu^{2+} , Fe^{3+} , Fe^{2+} , Hg_2^{2+} , Hg^{2+} , Li^+ , K^+ , Mn^{2+} , Mg^{2+} , Na^+ , NH_4^+ , Ni^{2+} , Pb^{2+} , Sn^{2+} and Zn^{2+} ions in acetic acid/acetate buffer solutions at pH 4.0. From Figure 5.11-I, it can be concluded that, the sensing membrane is capable of determining mercury ions (Hg^{2+}) with a high selectivity over other ions. The

fluorescence was dramatically quenched in the presence of Hg (II) at 572 nm exhibiting a relative signal change (RSC) ratio of 70%. However, the response to Zn^{2+} is markedly different from the response to other metal ions and fluorescence of DC-AZM is affected appreciably by Zn^{2+} , Fe^{3+} and Mn^{2+} at concentrations of $\geq 10^{-3}$ mol L⁻¹.

The interference effects of the anions; OH^- , F^- , Cl^- , Br^- , NO_3^- , NO_2^- , SO_4^{2-} and PO_4^{3-} were also tested (See Figure 5.11-II). Among them, the hydroxide ion looks like a potential interferent. However, this sensing system will not be influenced by OH^- anion since pH 4 was chosen as working pH.

Relative signal changes of less than 5% were observed for EC doped films at pH 4.0.

A selectivity comparison of Hg (I) over Hg (II) in separate solutions was also investigated. The response of the DC-AZM dye upon interaction with Hg (I) and Hg (II) was measured at fixed Hg (I) or Hg (II) concentrations at pH 4.0. The DC-AZM dye was found to be effectual in selective binding of both Hg (I) and Hg (II) with respect to other possible interferants. However, a speciation was not possible.

The reversibility of the nanofibers was checked by washing the used optodes with 0.1 mol L⁻¹ EDTA solutions at pH: 2 and 0.1 mol L⁻¹ HCl for regeneration purposes. The results showed that the nanofibers could not be regenerated and each fiber can be used as a disposable sensor for single shot analysis.

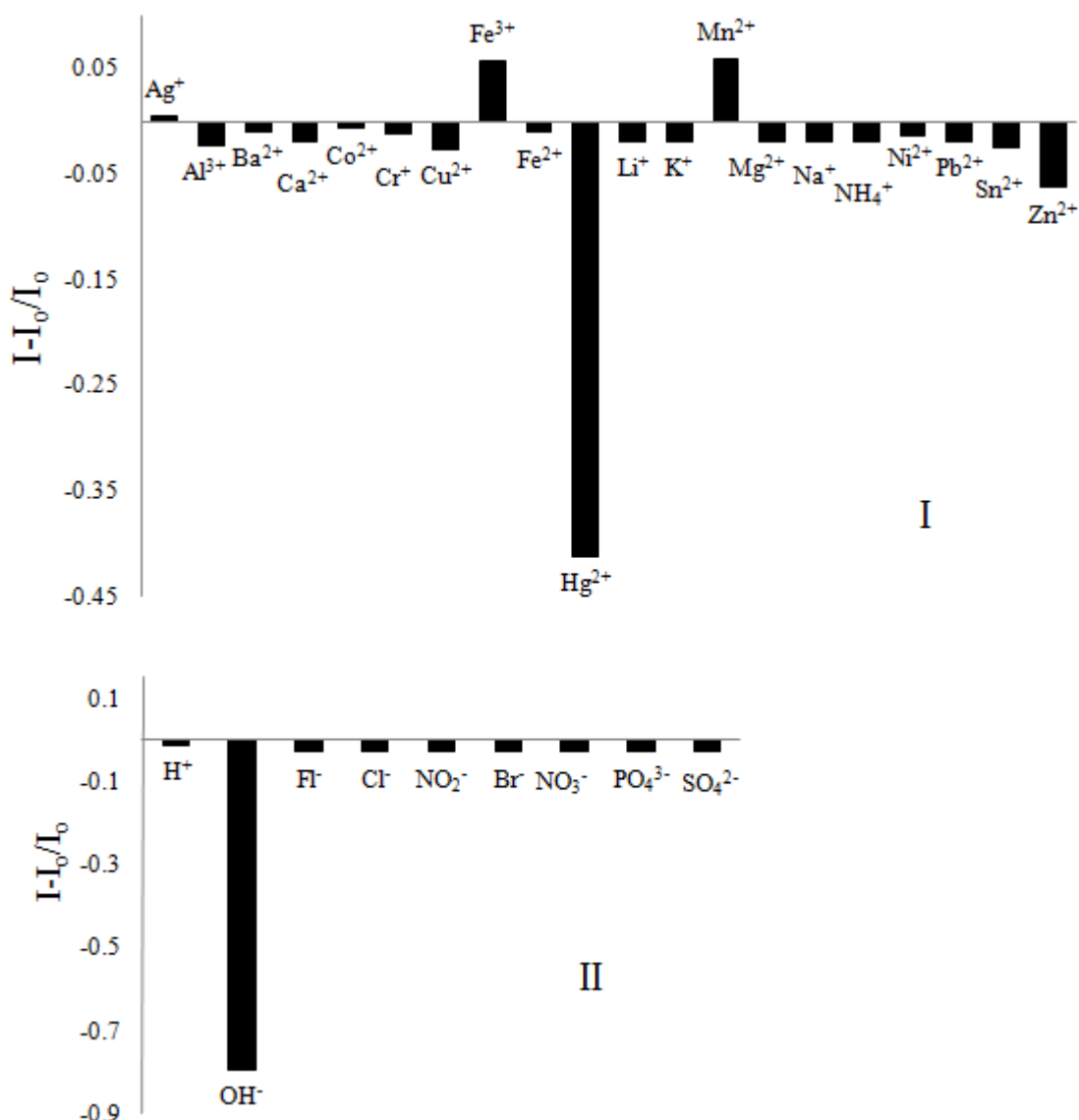


Figure 5.11 **I**. Metal-ion response of EC based DC-AZM at pH 4 **II**. Anions response of the same composition near neutral solutions. Results were plotted as relative fluorescence changes; $(I-I_0)/I_0$

5.10 Conclusion

Usage of nanomaterials looks like a promising, simple, and an effective method for fabricating optical chemical sensor devices. With respect to continuous thin films, electrospun nanofibers offered enhanced sensitivity, lower LOD values and reactivity in optical chemical sensing of Hg (II). In this work, we tested an EC doped selective fluorescent molecular probe in form of nanofiber for Hg (II) ion sensing. The DC-AZM dye was used for the first time as a fluoroionophore in the optical sensing of mercury (II) ions. The EC based nanofibers can be used at pH 4.0 for quantitative

determination of Hg (II) in the concentration range of 1.0×10^{-10} - 1.0×10^{-4} Mol. L⁻¹. A quite good LOD (0.07 nM) was reached. The mercury levels as low as 0.01 and 0.07 nM can be measured with the offered system. The offered LOD value is better than that of the earlier reported sensor responses (Cano-Raya et al., 2006; Ertekin et al., 2009; Fana et al., 2009; Harris, Pickering & George, 2003; Kuswandia & Narayanaswamy, 2001; Lv et al. 2008; Murkovic & Wolfbeis, 1997; Selid et al., 2009; Wan et al. 2009; Yari & Papi, 2009; Yuan et al., 2007; Zhu et al., 2008).

CHAPTER SIX

DEVELOPMENT OF OPTICAL CHEMICAL SENSOR BASED ON POLYMER NANOFIBERS FOR Ag(I) ION DETECTION

6.1 Introduction

Results of the studies performed in liquid phase provide valuable information for researchers; however, they remain far from applications in sensor technology at this stage. The integration of liquid components with solid state optics is not practical and molecule-based solid state approaches employing polymeric media should be developed. On the other hand, the development of new approaches toward highly sensitive detection techniques remains a major challenge in the field of chemical sensing. Therefore, considerable effort has been made to increase the surface area of the sensing interface in chemical sensors. In this context, recently, a number of ultrasensitive fluorescent optical sensors for a variety of analytes have been demonstrated; new strategies are still being developed (Chen et al., 1999; Fan, Plaxco, & Heeger, 2002; Yang, & Swager, 1998)

Electrospinning is a relatively simple and versatile method for creating high-surface-area polymeric fibrous membranes. In a typical process, a large static voltage is applied to a polymer solution to generate fine jets of solution that dry into an interconnected membrane like web of small fibers (Reneker, & Chun, 1996). Electrospun fibres can be functionalized by the use of proper indicator and auxiliary additives for desired purposes.

Here we have successfully combined nano-scale electrospun fiber materials with optical sensing technology for Ag⁺ ions detection. A series of Ag⁺ sensitive nanofibers with various compositions of poly-methyl-methacrylate (PMMA), ethyl cellulose (EC), plasticizer and ionic liquid (1-ethyl-3-methylimidazolium tetrafluoroborate) were produced and characterized by Scanning Electron Microscopy (SEM). The Ag⁺ sensitive dye (TM-AZM) dyes has been used as sensing agent (see Figure 6.1).

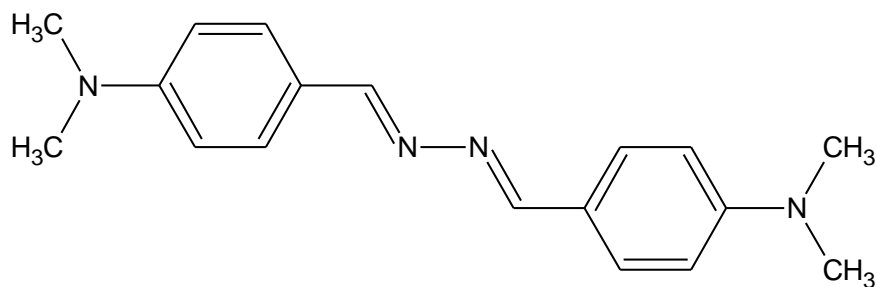


Figure 6.1 4,4''-[hydrazine-1,2-dilidenedimethylidene]bis(N,N-dimethylaniline (TM-AZM)

6.2 Investigation of the Photophysical Properties of the Present Indicator Dye

The photophysical properties of the indicator dye were investigated in different solvents. For this purpose, absorption, excitation and corrected emission spectra were recorded in the solvents of EtOH, DCM, THF and toluene/ethanol (To: EtOH; 80:20) mixture and solid matrix of EC and PMMA. The photophysical constants such as quantum yield, molar extinction coefficients and Stock's shift values were calculated. The indicator dye with high quantum yield can be excited with visible light are better for the design of fiber optical sensors (see Figure 6.2 and 6.3). The UV-Vis spectroscopy related data (absorption maxima; λ_{Abs} , and molar extinction coefficient; ϵ), were shown in Table 6.1 and 6.2. TM-AZM dye exhibited very efficient absorbance and high molar extinction coefficients around 492 nm and 488 nm in PMMA and EC matrices. In agreement with literature molar extinction coefficients (ϵ_{max}) of TM-AZM were increased in PMMA and EC with respect to (ϵ_{max}) of TM-AZM in solution phase (see Table 6.1, Table 6.2). These data can be taken as proofs that TM-AZM molecules absorb better in plasticized PMMA and EC matrices.

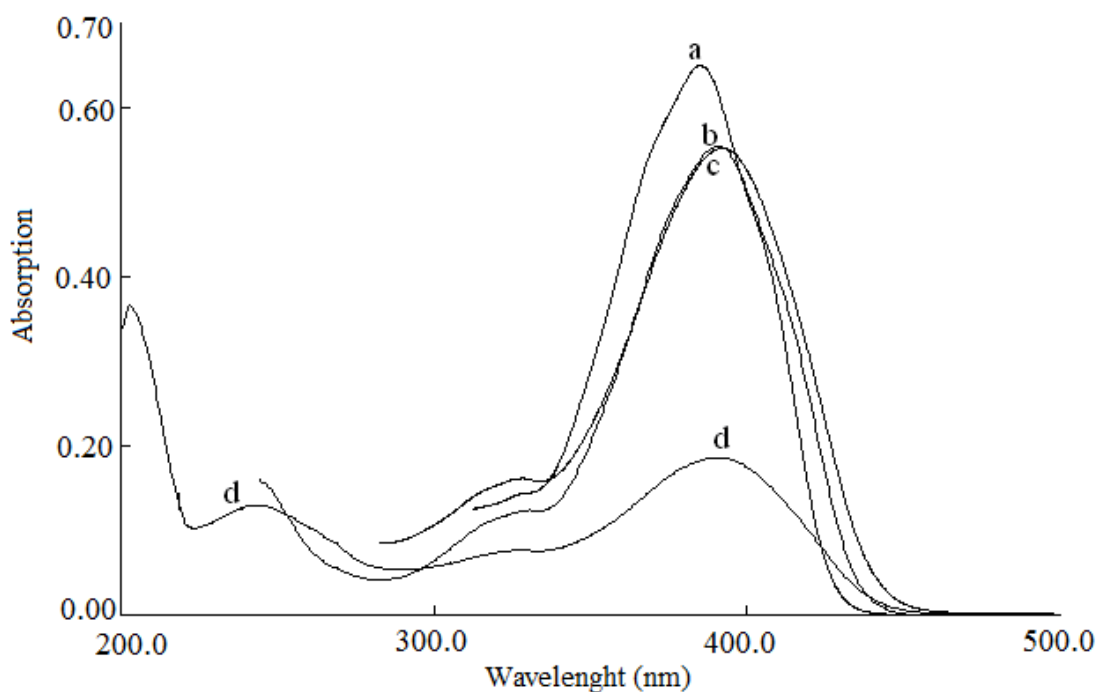


Figure 6.2 Absorption spectra of the TM-AZM dyes (10^{-6} M dye or 2 mM dye/kg polymer). a) THF b) DCM c) To: EtOH d) EtOH

Table 6.1 UV-Vis spectra related data of TM-AZM in the solvents of EtOH, DCM, THF and toluene/ethanol mixture (80:20) and in solid matrices of EC and PMMA

Compound	Solvent/Matrix	λ^1_{abs}	λ^2_{abs}	$\epsilon_{\text{max}}(\lambda^1_{\text{abs}})$	$\epsilon_{\text{max}}(\lambda^2_{\text{abs}})$
TM-AZM	EtOH	243	391	12900	18600
	DCM	244	391	15800	55200
	THF	--	385	--	65000
	To: EtOH	--	391	--	55200
	EC	388	488	96045	84100
	PMMA	389	492	236964	167640

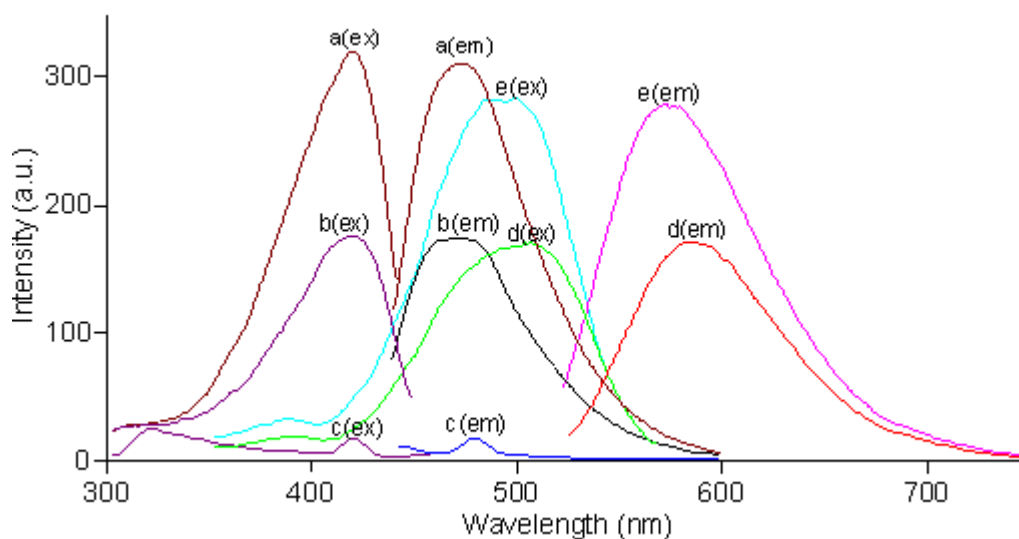


Figure 6.3 Excitation and corrected emission spectra of the TM-AZM dye (10^{-6} M dye or 2 mM dye/kg polymer). a) EtOH b) To:EtOH (80:20) c) THF d) PVC e) EC.

Table 6.2 The excitation–emission spectra related characteristics of the DC-AZM acquired in conventional solvents, and in thin film form of PMMA and EC.

Compound	Matrix	λ_{\max}^{em}	λ_{\max}^{ex}	$\Delta\lambda_{ST}$ (Stoke's shift)	ϕ_F (Quantum yield)
TM-AZM	EtOH	473	420	53	4.2×10^{-3} in EtOH
	DCM	--	--	--	
	THF	466	422	44	
	To:EtOH	469	422	47	
	EC	580	505	75	0.2336
	PMMA	565	495	70	0.7967

6.3 Fluorescence Quantum Yield Calculation

For calculation of fluorescence quantum yield, the absorbance and corrected emission spectra of five different concentrations of reference standard Rose Bengal ($\lambda_{ex} = 525$ nm, quantum yield (ϕ_F) = 0.11 in alkaline ethanol) and TM-AZM compound were recorded. The integrated fluorescence intensities were plotted vs

absorbance for the reference standards and the TM-AZM compound in EC and PMMA matrices (see Figure 6.4).

The gradients of the plots are proportional to the quantity of the quantum yield of the studied molecules. The equations of the plots are $y = 43846x$; $R^2 = 0.9985$ for reference standard, $y = 78698x$; $R^2 = 0.9958$ for DC-AZM dye in EC and $y = 363888x$; $R^2 = 0.9964$ for DC-AZM dye in PMMA. Quantum yield (ϕ_f) values were calculated according to the given equation in Chapter 3 and were found to be 0.0042 in ETOH, 0.2336 in EC and 0.7967 in PMMA.

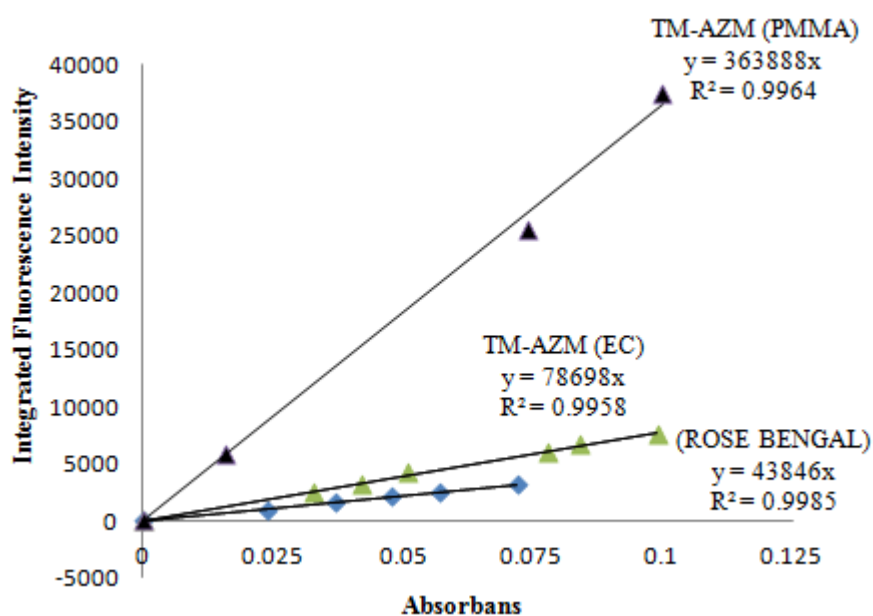


Figure 6.4 The integrated fluorescence intensities vs absorbance for the reference standard; Rose Bengal in alkaline ethanol, the TM-AZM dye in EC and TM-AZM dye in PMMA matrices.

6.4 SEM Images

Electrospinning was performed at 25 kV voltage and at 0.3 mL/h flow rate. SEM micrograph of EC and PMMA based nanofibers were shown in Figure 6.5 and Figure 6.6, respectively. The membrane has a 3-D structure with a random fiber orientation that is evenly distributed on the substrate. The fiber diameters were measured

between 708-912 nm for 40% DOP, 10% IL and 50% EC containing composites and 730-980 nm for same PMMA containing composites.

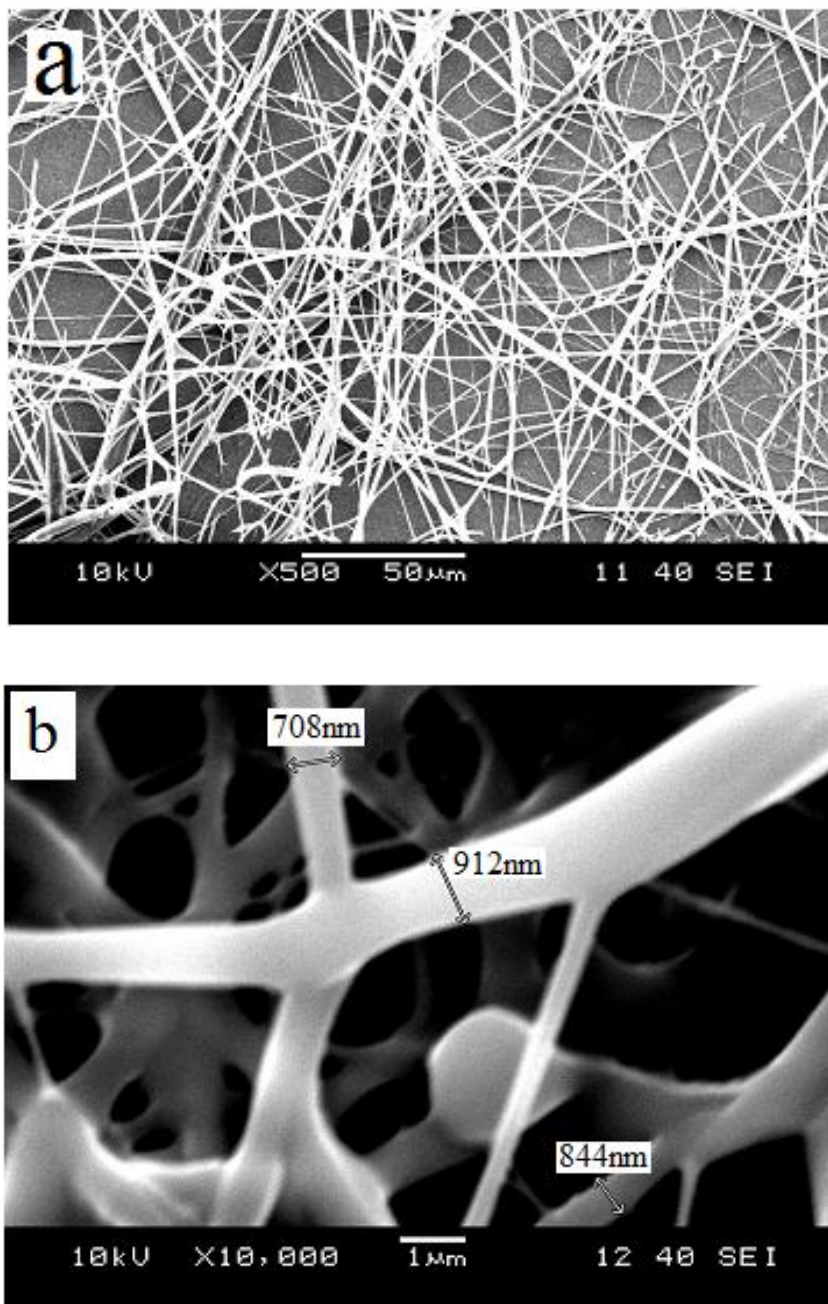


Figure 6.5 SEM images of electrospun membranes; (c) and (d); EC based nanofibers at different magnifications such as $\times 500$ and $\times 10,000$.

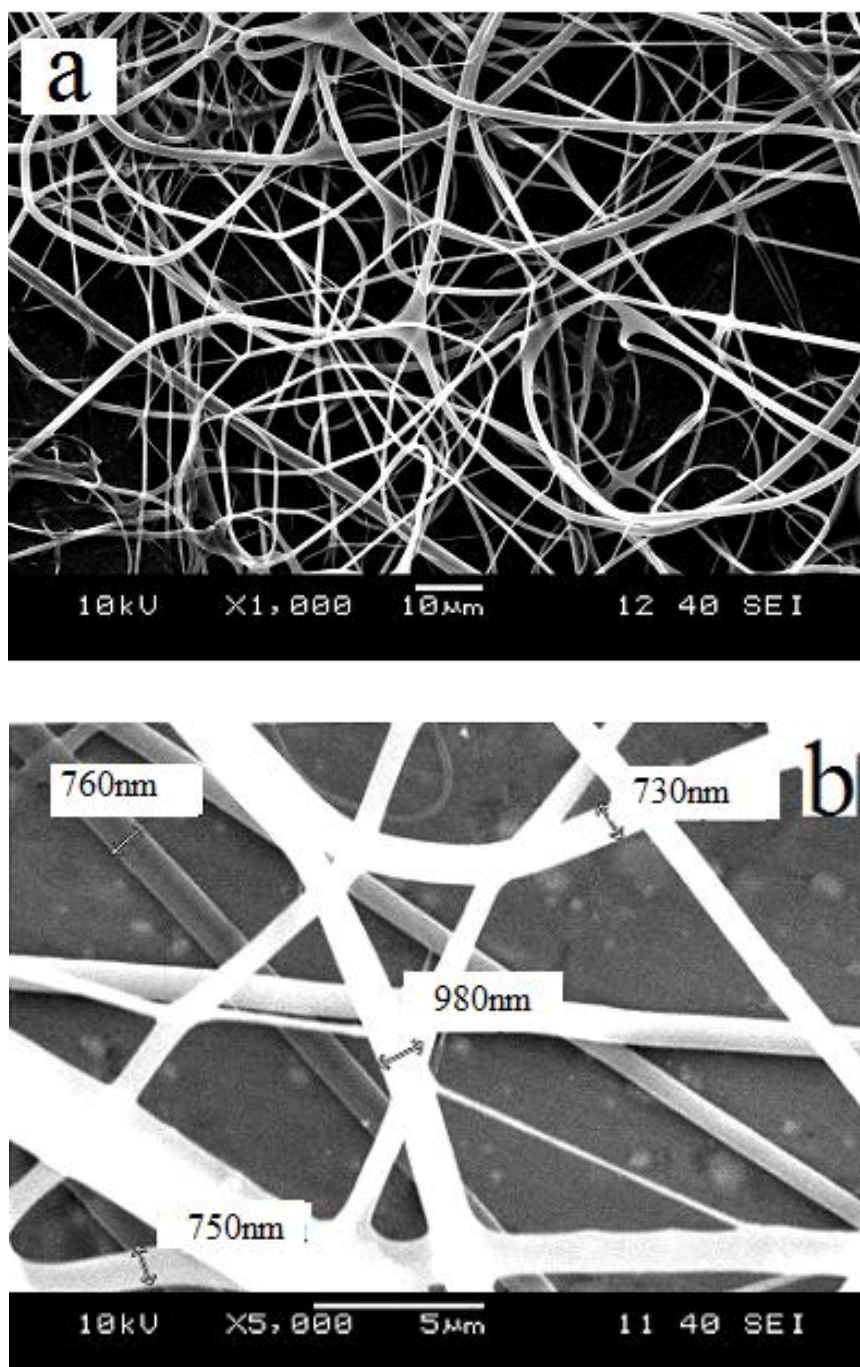


Figure 6.6 SEM images of electrospun membranes; (a) and (b); PMMA based nanofibers at different magnifications such as $\times 1\,000$, $\times 5\,000$.

6.5 Detection of pK_a for TM-AZM

The knowledge of acidity constants (pK_a) of dyes is of fundamental importance in order to provide information on chemical reactivity range of the dyes. For this

reason, the absorption and emission based pH induced response of TM-AZM were investigated in EC and PMMA matrix.

The immobilized TM-AZM reversibly responded to H⁺ ions in PMMA and EC. The relative signal change of absorption spectra of the TM-AZM was monitored after addition of certain concentrations of buffered solutions at different pH ranges.

pH induced absorption spectra of TM-AZM doped PMMA membrane in the pH range of 7.00-12.00 were shown in Figure 6.7. Fluorescence spectra of TM-AZM doped PMMA and EC membrane and related emission based sigmoidal response (pH versus $(I-I_0)/I_0$) were shown in Figure 6.8 and 6.9, respectively.

The acidity constants were calculated via the following equation;

$$pK_a = pH + \log [(I_x - I_b)/(I_a - I_x)]$$

The pKa values were found to be 10.03 and 7.68 for TM-AZM in PMMA and EC, respectively.

$$pK_a = 10.00 + \log [(264-187)/(336-264)]$$

$$pK_a = 10.00 + \log [1.07]$$

$$pK_a = 10.03 \text{ (for indicator immobilized PMMA)}$$

$$pK_a = 7.75 + \log [(197-8)/(417-197)]$$

$$pK_a = 7.75 + \log [0.86]$$

$$pK_a = 7.68 \text{ (for indicator immobilized EC)}$$

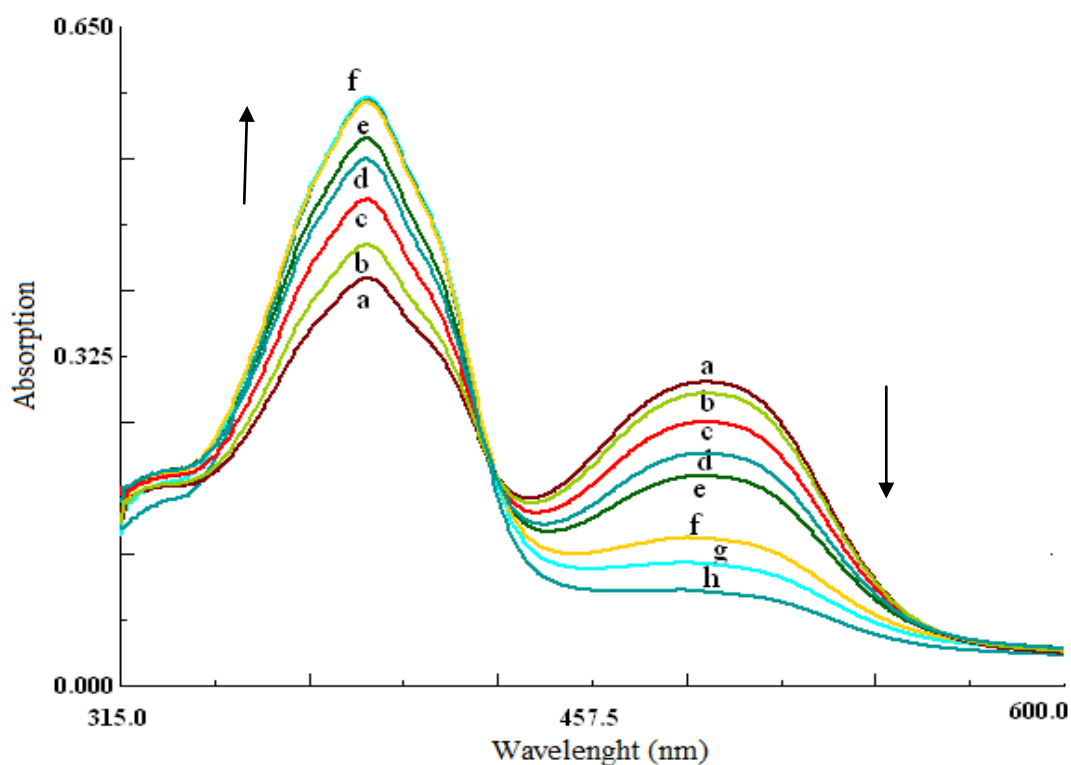


Figure 6.7 pH induced absorption spectra of the TM-AZM doped PMMA membrane after exposure to buffer solutions in the pH range of 7.0–12.0 pH= (a) 7.0-7.5 (b) 8.0 (c) 8.5 (d) 9.0 (e) 9.5 (f) 10.0 (g) 10.5-11.0 (h) 11.5-12.0 ($pK_a=10.03$)

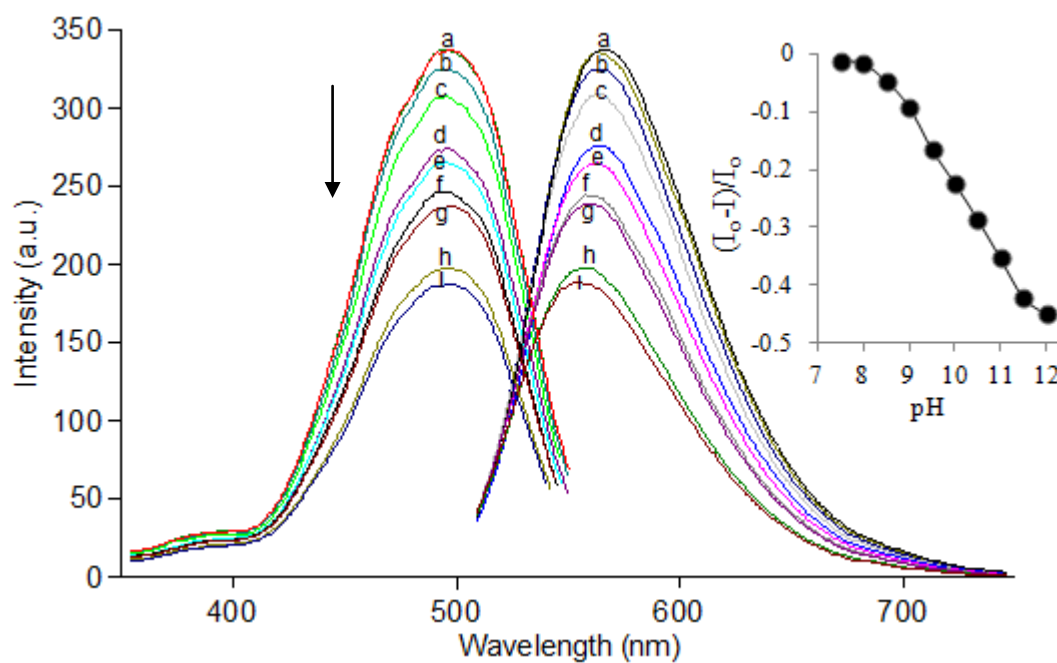


Figure 6.8 pH induced emission characteristics and sigmoidal calibration curve of TM-AZM doped PMMA membrane in the pH range of 7.0–12.0 pH= (a) 7.0-7.5 (b) 8.0 (c) 8.5 (d) 9.0 (e) 9.5 (f) 10.0 (g) 10.5-11.0 (h) 11.5-12.0 ($pK_a=10.03$)

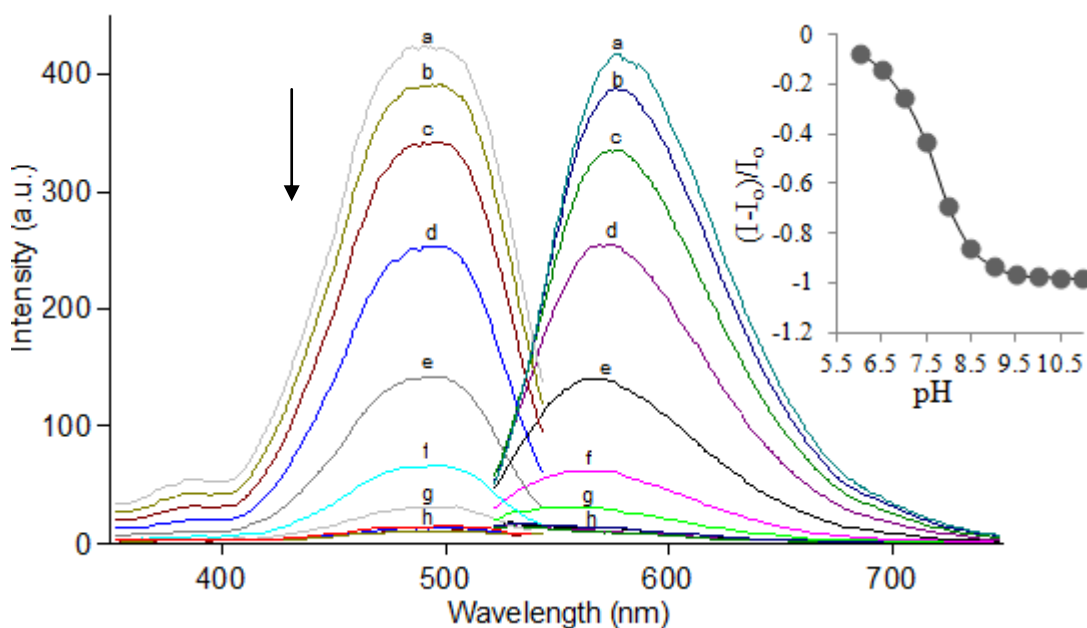


Figure 6.9 pH induced emission characteristics and sigmoidal calibration curve of TM-AZM doped EC membrane in the pH range of 6.0–11.0 pH= (a) 6.0 (b) 6.5 (c) 7.0 (d) 7.5 (e) 8.0 (f) 8.50 (g) 9.0 (h) 9.5-10.0- 10.5- 11.0 (pKa=7.68)

6.6 Response to Ag (I) Ions in Thin Film and Nanofiber Form

The TM-AZM dye contains nitrogen atoms in its structure as possible interaction sites for silver ions. The TM-AZM dye becomes a Ag (I) selective nanosensor; whenever doped into plasticized EC or PMMA nanofiber along with the anionic additive; potassium tetrakis-(4-chlorophenyl) borate.

The TM-AZM dye-doped EC and PMMA nanofiber exhibited spectacular fluorescence intensity quenching upon exposure to Ag^+ ions at pH 6.0. The dynamic response to Ag^+ ions were monitored as a decrease in the relative fluorescence intensity in at 580 and 565 nm as the nanofiber was exposed to buffer solutions containing different concentrations of Ag^+ , respectively. Figure 6.10-I-II and 6.11 I-II reveals response of the sensing agent to Ag^+ ions in the concentration range of 3.51×10^{-07} - 1.43×10^{-02} and 10^{-7} - 10^{-2} M in PMMA and EC nanofibers, respectively.

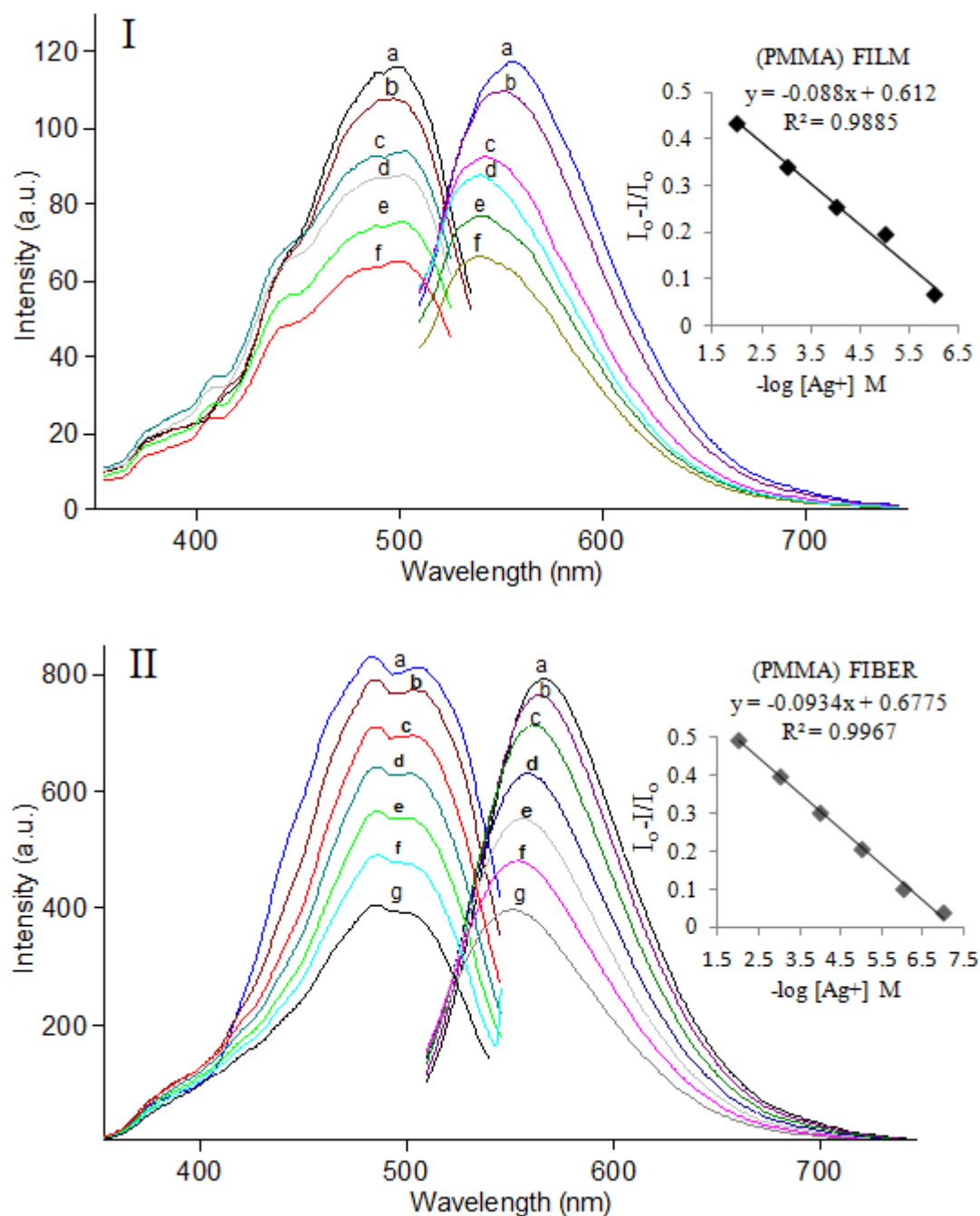


Figure 6.10 **I**. Fluorescence response of the TM-AZM-doped PMMA based thin film to Ag (I) ions at pH 6.0. (a) Ag-free buffer (b) 10^{-6} , (c) 10^{-5} , (d) 10^{-4} , (e) 10^{-3} , (f) 10^{-2} M Ag(I), Inset: Calibration plot for the concentration range of 10^{-6} - 10^{-2} M Ag (I). **II**. Response of the EC based nanofiber to Ag (I) ions at pH 6.0. (a) Ag-free buffer, (b) 10^{-7} , (c) 10^{-6} , (d) 10^{-5} , (e) 10^{-4} , (f) 10^{-3} , (g) 10^{-2} M Ag (I), Inset: Linearized calibration plot for the concentration range of 10^{-7} - 10^{-2} M Ag (I).

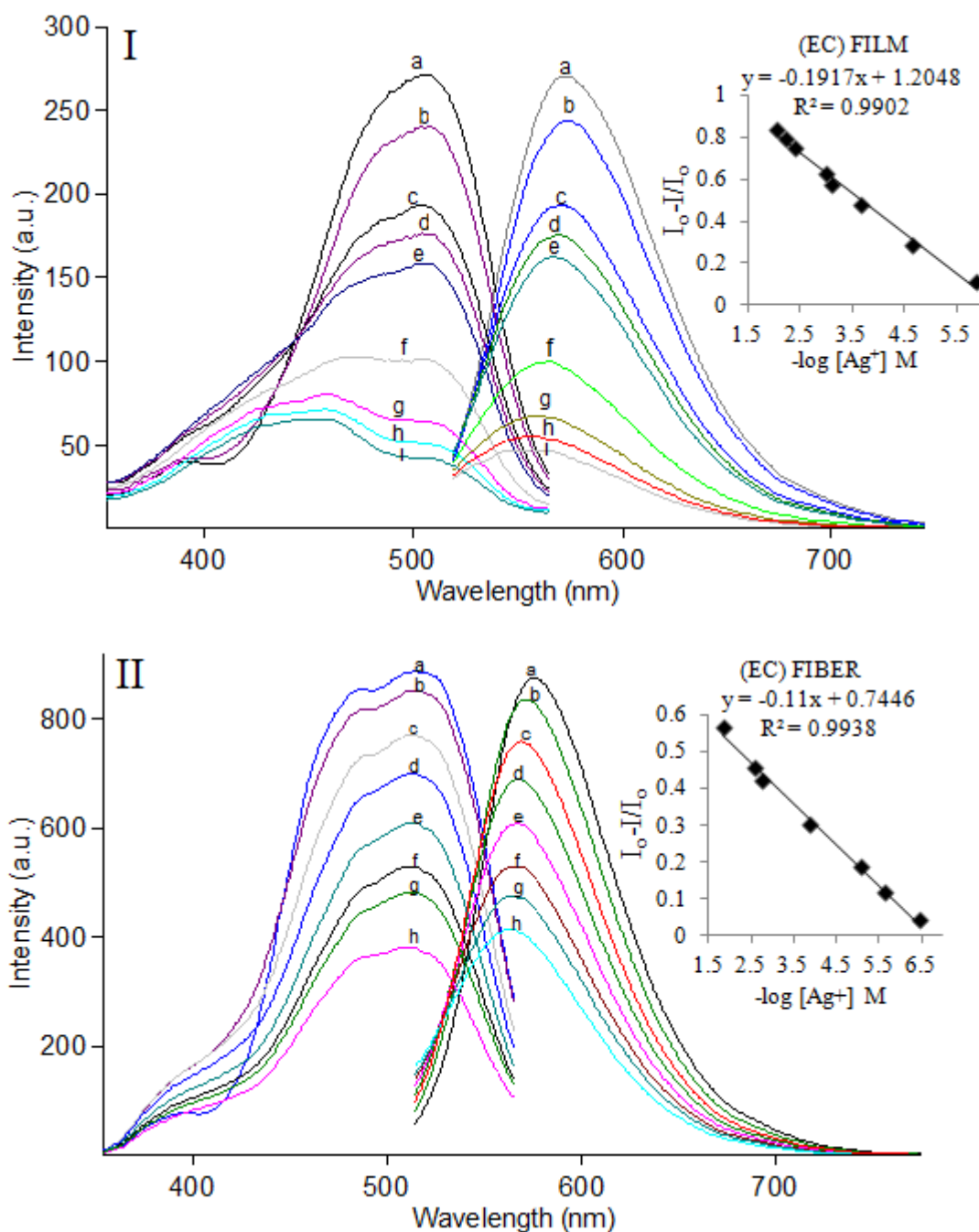


Figure 6.11 **I**. Fluorescence response of the TM-AZM-doped EC based thin film to Ag (I) ions at pH 6.0. (a) Ag-free buffer (b) 1.35×10^{-6} , (c) 2.25×10^{-5} , (d) 2.20×10^{-4} , (e) 7.98×10^{-4} , (f) 1×10^{-3} , (g) 4×10^{-3} , (h) 6×10^{-3} , (i) 9×10^{-3} M Ag(I), Inset: Calibration plot for the concentration range of 1.35×10^{-6} - 9×10^{-3} M Ag (I). **II**. Response of the EC based nanofiber to Ag (I) ions at pH 6.0. (a) Ag-free buffer, (b) 3.51×10^{-7} , (c) 2.34×10^{-6} , (d) 8.46×10^{-6} , (e) 1.37×10^{-4} , (f) 1.76×10^{-3} , (g) 2.50×10^{-3} , (h) 1.43×10^{-2} M Ag (I), Inset: Linearized calibration plot for the concentration range of 3.51×10^{-7} - 1.43×10^{-2} M Ag (I).

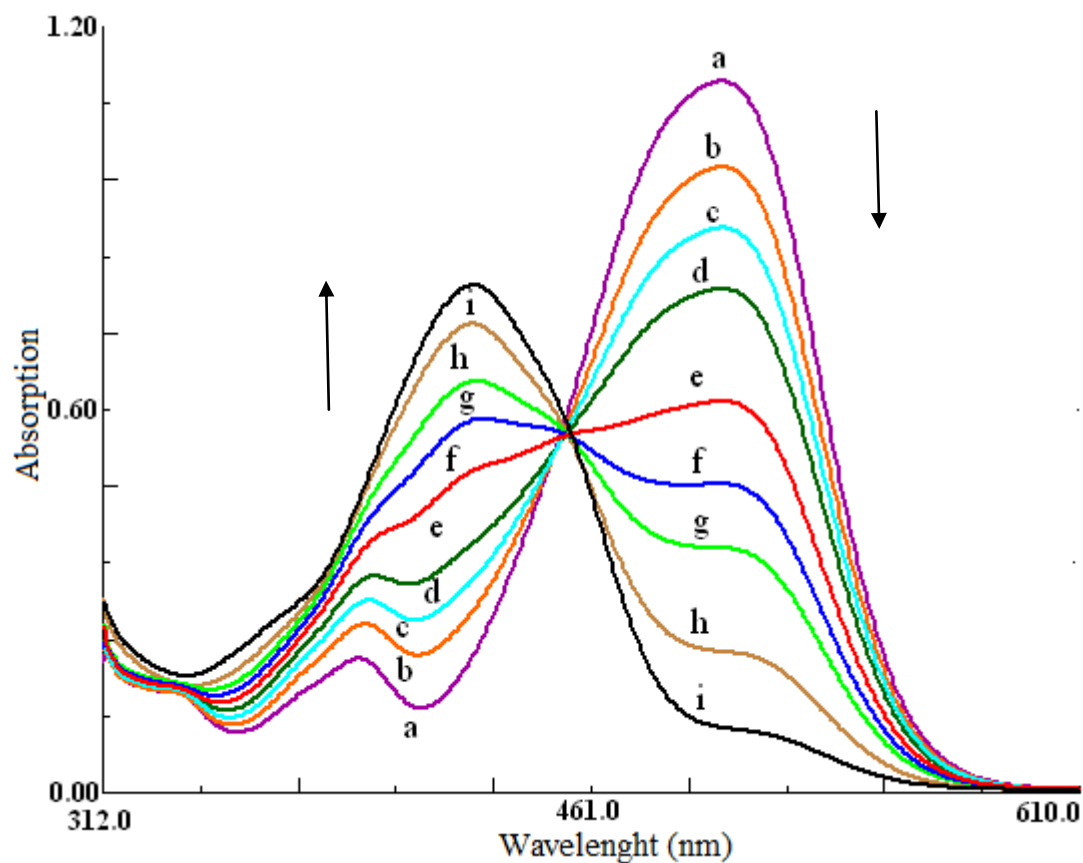


Figure 6.12 Absorption based response of the TM-AZM-doped EC based thin film to Ag (I) ions at pH 6.0. (a) Ag-free buffer (b) 1.35×10^{-6} , (c) 2.25×10^{-5} , (d) 2.20×10^{-4} , (e) 7.98×10^{-4} , (f) 1×10^{-3} , (g) 4×10^{-3} , (h) 6×10^{-3} , (i) 9×10^{-3} M Ag(I), Inset: Calibration plot for the concentration range of 1.35×10^{-6} - 9×10^{-3} M Ag (I).

Table 6.3 Calibration characteristics of PMMA and EC based electrospun nanofibers and thin films.

Indicator Dye	Matrix /form	Linear Range (Hg(II) Mol/L)	Regression Coefficient (R^2)	LOD (Molar)
TM-AZM	EC/nanofiber	3.51×10^{-7} to 1.43×10^{-2}	0.9938	1.59×10^{-7} M
	PMMA/nanofiber	1.0×10^{-7} to 1.0×10^{-2}	0.9967	5.10×10^{-8} M
	EC / thin film	1.35×10^{-6} to 9.0×10^{-3}	0.9902	5.70×10^{-7} M
	PMMA/ thin film	1.0×10^{-6} to 1.0×10^{-2}	0.9885	2.20×10^{-7} M

6.7 Evaluation of Effect of pH on Ag (I) Response and Interference Effects

The sensor nanofibers were examined in terms of cross-sensitivity to other ion permeability by immersing the nanofiber in buffer solutions with pH values at 5. Except of Hg ions, no change in signal intensity was observed, which is proof for the specificity of the system for Ag⁺ (see Figure 6.13)

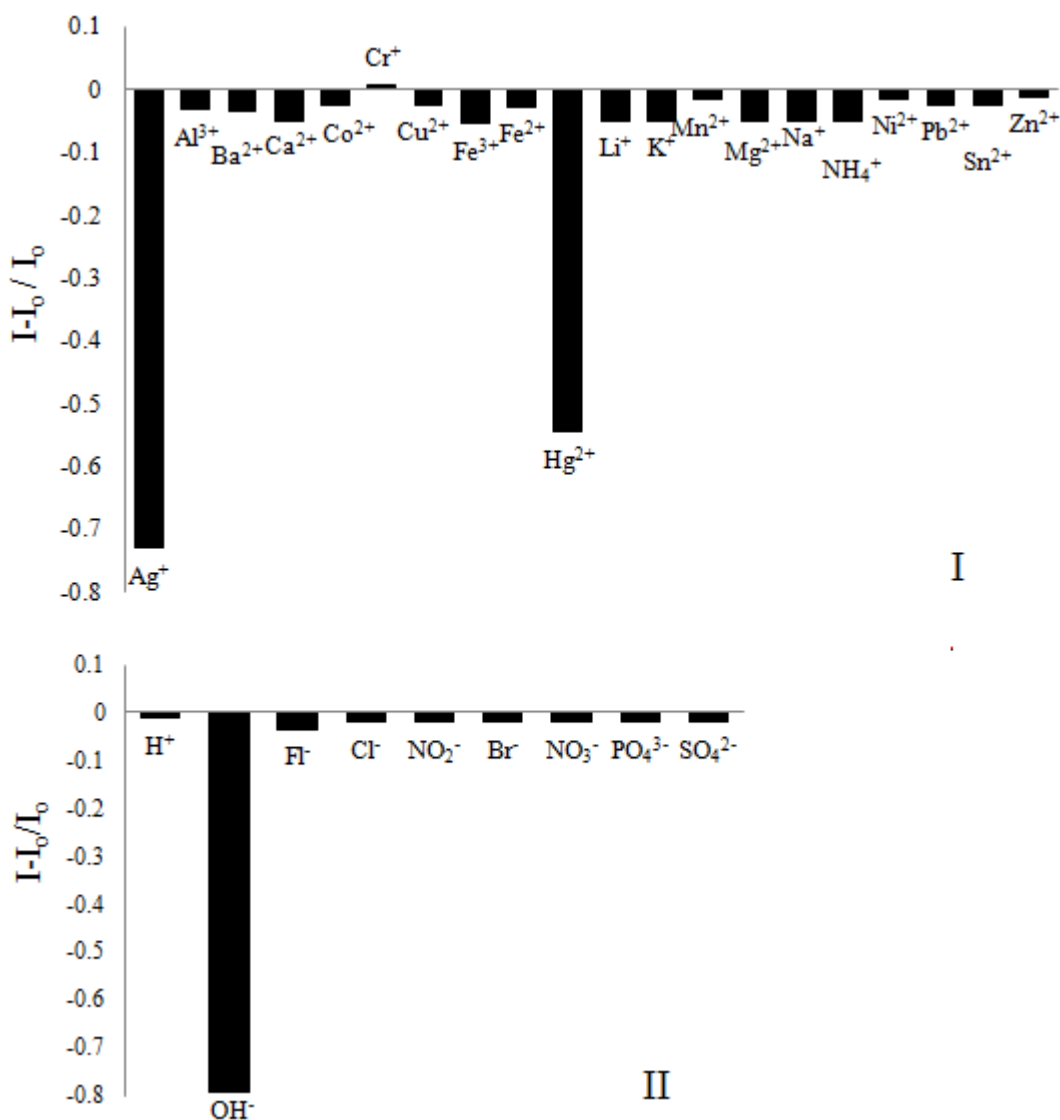


Figure 6.13 **I.** Metal-ion response of EC based TM-AZM at pH 6. **II.** Anion response of the same composition near neutral solutions. Results were plotted as relative fluorescence changes; $(I-I_0)/I_0$

For further evaluation of interference degree, the effect of pH on the sensing performance of dye doped thin films and electrospun nanofibers was investigated with Ag (I), Hg (II) and Hg (I) at fixed metal concentration; $5 \times 10^{-3} \text{ mol L}^{-1}$ between pH 3.5 – 6.0. As can be seen from Figure 6.14, the relative signal change; $(I_0 - I)/I_0$ produced by the Ag (I) ions was high enough and stable around pH 6.0.

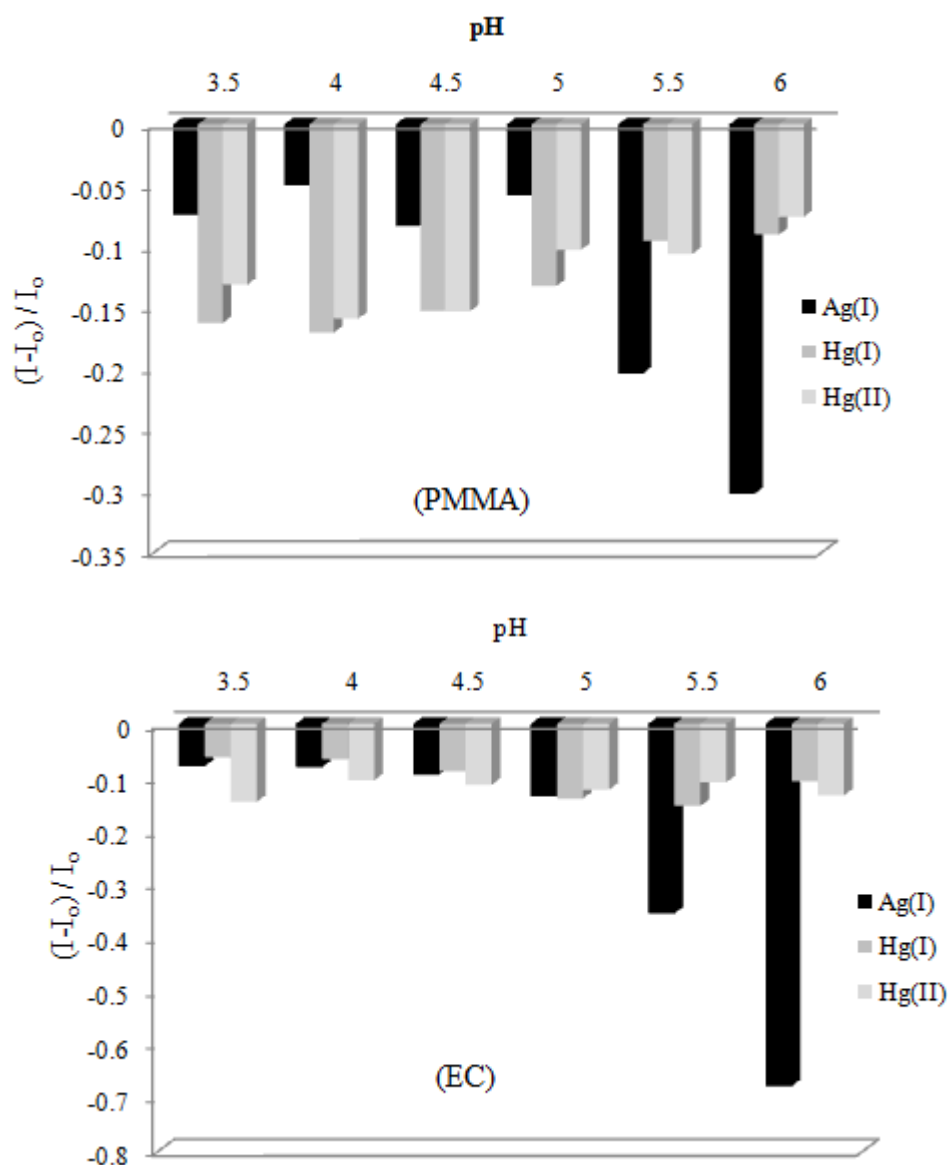


Figure 6.13 pH dependency of the TM-AZM doped PMMA and EC based nanofibers in the presence of $10^{-5} \text{ mol L}^{-1}$ Ag (I) ions stable between pH 3.5 and 6.0.

6.8 Stern-Volmer Analysis and Determination of Ksv Constant

The data obtained by gathering Stern-Volmer analysis results for electrospun and continuous thin films were shown in Table 6.4. Stern-Volmer constants (K_{sv}) of the electrospun films, calculated from slopes of the plots were found to be 2.54×10^3 (M^{-1}) and 4.22×10^2 (M^{-1}) for nanofiber and continuous thin film in EC and 7.01×10^2 (M^{-1}) and 8.2×10^1 (M^{-1}) respectively. The (K_{sv}) of the electrospun film is approximately 10 fold greater than that of the (K_{sv}) obtained from the continuous thin film. (see Table 6.4, Figure 6.15 I-II and 6.16 I-II). The calculated K_{sv} values reveal important practical consequences. The sensitivity of the quenching process is enhanced by controlling the quencher diffusion ability and rate to fluorophores via the nano-structural properties of the sensing agents.

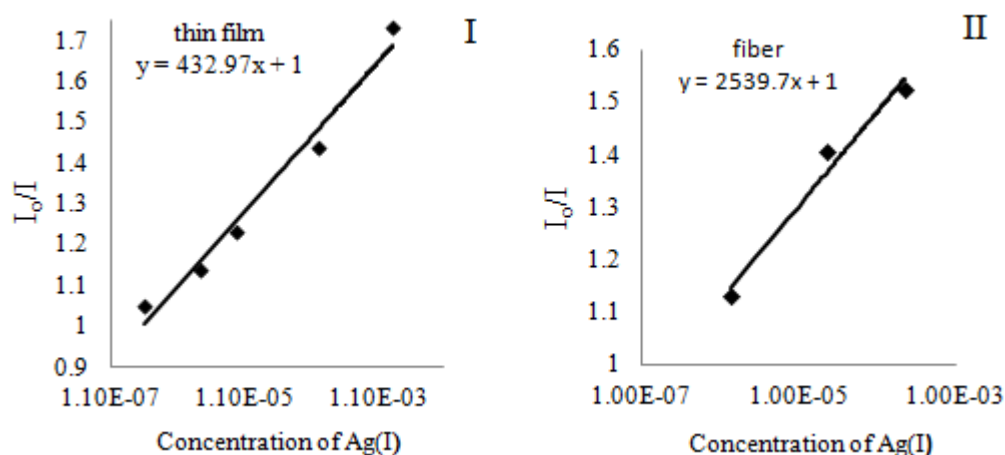


Figure 6.15 The Stern Volmer plot of EC based **I**: thin films and **II**: electrospun nanofibers

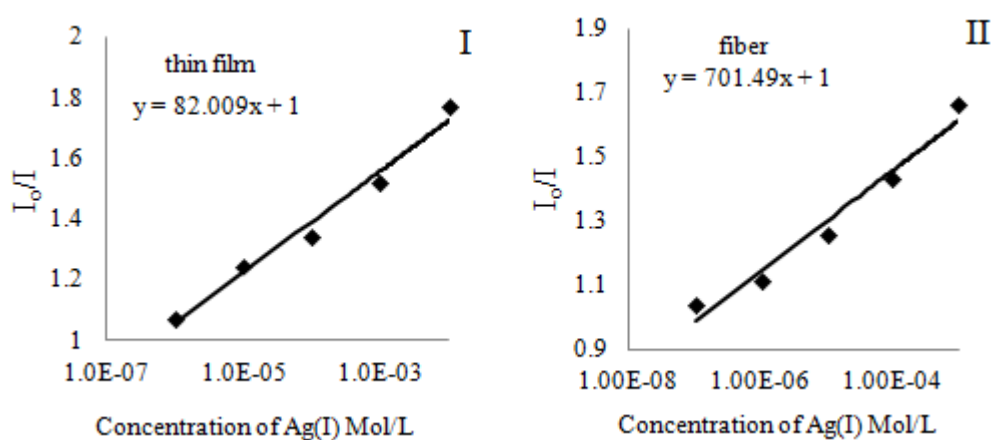


Figure 6.16 The Stern Volmer plot of PMMA based **I**: thin films and **II**: electrospun nanofibers

Table 6.4 The Stern Volmer plot and Ksv Constant of PMMA and EC based electrospun nanofibers and thin films.

Indicator Dye	Matrix /form	Linear Regression Equation	Ksv Constant
TM-AZM	EC/ nanofiber	$y = 2539.7x + 1$	$2.54 \cdot 10^3$
	PMMA/nanofiber	$y = 701.49x + 1$	$7.01 \cdot 10^2$
	EC / thin film	$y = 432.97x + 1$	$4.32 \cdot 10^2$
	PMMA/ thin film	$y = 82.009x + 1$	$8.2 \cdot 10^1$

6.9 Reversibility Performance

The reversibility of the nanofiber was checked by washing the used optodes with 0.1 mol L⁻¹ EDTA solutions at pH: 2 and 0.1 mol.L⁻¹ HCl were also tested for regeneration purposes. The results showed that the nanofibers could not be regenerated and each fiber can be used as a disposable sensor for single shot analysis.

6.10 Conclusion

In the last years, the interest for the production of polymer fibers ranging from 100 nm to 1 mm has grown. These materials have many applications in industrial field for their characteristic, like stability, and the easy and reproducible mechanism for the fiber growth. Here, a new kind of optical Ag⁺ nanosensor is presented that is based on the changes in the fluorescence intensity of a novel dye. The TM-AZM dye was used for the first time as a fluoroionophore in the optical silver sensing. The quantum yield of the dye in EC and PMMA is reasonably high (0.23 and 0.79, respectively). The TM-AZM dye doped nanofibers in EC and PMMA can be used at pH 6.0 for quantitative determination of Ag (I) in the concentration range of 3.51×10^{-7} to 1.43×10^{-2} and 1.0×10^{-7} to 1.0×10^{-2} mol L⁻¹ with an outstanding high selectivity, whereas mercury (II) was the only interferent.

CHAPTER SEVEN

FLUORESCENT Fe³⁺ SENSING AT FEMTO-MOLAR LEVEL WITH FUNCTIONAL ELECTROSPUN NANOFIBERS

7.1 Introduction

Selective determination of trace amounts of Fe³⁺ ions has a vital importance in chemical, physiological, environmental and industrial samples. Today, various sophisticated instrumental techniques are exploited for the determination of trace amounts of iron. Alternatively, many promising chemosensing systems have been designed utilizing the molecular framework of quinazolinone (Zhang, Chenga, Zhang, Shen, & Yu, 2007), thiocyanate (Pons, Forteza, & Cerd, 2005), imino-dinaphthalen based ionophores (Babakhanian et al., 2010), pyoverdin (Pulido-Tofin˜o, Barrero-Moreno, & Pe´rez-Conde, 2000) benzofuran (Oter, Ertekin, Kirilmis, Koca, & Ahmedzade, 2007) fluorescent Schiff bases (Oter, Ertekin, Kılincarslan, Ulusoy, & Cetinkaya, 2007), phenanthroline (Jezek, Dilleen, Haggett, Fogg, & Birchi, 2007) and other numerous chromogenic and fluorescent receptors (Gupta, Jain, Agarwal, & Maheshwari, 2007; Lohani, & Lee, 2010; Motlagh, Taher, & Ahmadi, 2010). In some of these approaches absorption or emission based response of a chromoionophore molecule resulting from interaction with Fe³⁺ ions in solution phase (Jung, Singh, Lee, & Jang, 2010; Lin, Long, Yuan, Cao, & Feng, 2009; Hu et. all, 2011) were monitored as analytical signal. These investigations provided valuable information for chemosensing of Fe³⁺ ions. Sometimes, indicators proposed for detection of Fe³⁺ exhibited weak or strong responses to other cations. Over the last two decades researchers began to use the chemosensing agents in embedded form in solid matrix materials (Malcik, & Caglar, 1997; Zhang et al., 2007; Pons, Forteza, & Cerd, 2005; Pulido-Tofin˜o, Barrero-Moreno, & Pe´rez-Conde, 2000; Oter et al, 2007; Wu, Chen, & Sung, 2011; Wang et all, 2002; Oter et all, 2007) expecting enhanced sensitivity, robustness and longer lifetimes.

In these designs, optical chemical sensing of Fe³⁺ ions is performed with a chromoionophore (or an ionophore and a chromophore) immobilized on a polymeric

support, a resin, glassy matrix material, or very rarely, on a nanomaterial. Those kinds of sensing materials display analyte dependent optical properties such as absorbance, fluorescence or reflectance. Such sensors provided enhanced stability, reversibility and sensitivity with respect to the sensing efforts performed in the solution phase.

Development of new technologies toward selective and highly sensitive detection techniques is still very important for the researchers working in the field of analytical chemistry. Due to the promising characteristics, nanoscale sensors have been attracting considerable attention in recent years. However, the number of published works exploiting nanomaterials in sensing area is very limited.

Wang et al. (2002) was reported the first use of electrospun nano-fibrous membranes as fluorescence quenching-based optical sensors for metal ions. In this approach a functionalized fluorescent polymer (PAA-PM) was used as sensing material. Optical chemical sensors were fabricated by electrospinning of PAA-PM and thermally cross-linkable polyurethane latex mixture solutions.

In another work, Wang and co-workers (2004) combined the techniques of electrospinning and electrostatic adsorption. In the subjective work, a fluorescent probe; poly[2-(3-thienyl) ethanol butoxy carbonyl-methyl urethane] was electrostatically assembled onto the surface of cellulose acetate electrospun nanofibrous membranes. The fluorescence of these membranes can be quenched by extremely low concentrations (ppb) of methyl viologen and cytochrome *c* in aqueous solutions.

Later Liu, Kameoka, Czaplewski, & Craighead (2004) used a nonlithographic deposition process to form single polymeric nanowire chemical sensors. Oriented polyaniline nanowires, with diameters on the order of 100 nm, were deposited on gold electrodes. The devices showed a rapid and reversible resistance change upon exposure to NH₃ gas at concentrations as low as 0.5 ppm.

Manesh, Santhosh, Gopalan, & Lee (2007) used the nanofibrous membrane composed of poly (vinylidene fluoride) and poly(aminophenylboronic acid) for glucose sensing. Sawicka, Gouma, & Simon (2005) presented an innovative technique for enzyme immobilization. Nanocomposite fibers of urease and polyvinylpyrrolidone were prepared by the electrospinning technique. The produced nonwoven mat offered as a potential urea biosensor.

Applications of nanomaterials in optical chemical sensing looks like promising. In this respect, the usage of such nanomaterials is expected to offer good results in terms of sensitivity and other sensor dynamics like response time and reversibility in comparison to the previously published optical chemical sensors having the similar composition.

In this thesis, the electrospinning technique was used as a novel and simple way to fabricate highly responsive optical chemical sensors for iron. Matrix material of ethyl cellulose (EC) was used to produce nanofibrous mats and continuous thin films. The fluorescent dye N'-(4- cyanobenzylidene) isonicotinohydrazide (CBINH) was chosen as the indicator due to the selective response, high quantum yield, large Stoke's shift and excellent photostability (see Figure 7.1). The electrospun nanofibers were characterized using scanning electron microscopy (SEM) and their average diameters were evaluated. To our knowledge this is the first attempt using the fluoroionophore; N'-(4-cyanobenzylidene) isonicotinohydrazide (CBINH) along with the ionic liquid; 1- ethyl- 3-methylimidazolium tetrafluoroborate in form of nanofiber for iron sensing at femtomolar level.

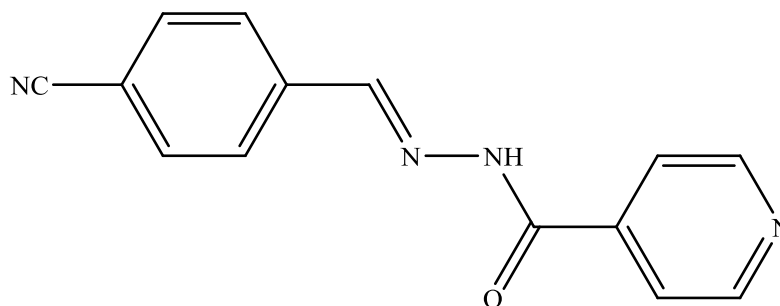


Figure. 7.1 N'-(4-cyanobenzylidene)isonicotinohydrazide (CBINH)

7.2 Spectral Evaluation, Photostability and Fluorescence Quantum Yield Calculations

A comparative spectral characterization of the employed dye was performed both in solvent and in polymer matrices. Absorption, excitation and emission spectra of the chrominophore were recorded in solvents of THF, EtOH, DMF, and in toluene/ethanol mixture (80:20 (v/v)). Similar data of the dye was also acquired exploiting thin film form of EC. The gathered absorption and excitation-emission spectra of the CBINH dye in different solvents were shown in Figure 7.2 I and II, respectively. Other spectral characteristics of the dye were given in Table 7.1. CBINH exhibited efficient absorbance and high molar extinction coefficients around 310 nm and 320 nm in all the employed solvents and solid matrices, respectively. In agreement with literature (Ertekin et al, 2000) molar extinction coefficients (ϵ_{\max}) of CBINH increased in the EC with respect to ϵ_{\max} values of CBINH measured in the solution phase (See Table 7.1). Upon excitation, the dye displayed maximum emission wavelengths of 470, 325, 340 and 433 in the solvents of THF, EtOH, To:EtOH (80:20) and DCM, respectively. Fluorescence quantum yield values (ϕ_F) of the CBINH were calculated employing the comparative William's method (Williams, Winfield, & Miller, 1983). Quinine sulphate (in 0.05M H₂SO₄, $\phi_F=0.546$) was used as reference standard. The dye displayed enhanced fluorescence emission quantum yield and red shifted excitation wavelength in immobilized form compared to the (ϕ_F) and λ_{\max} values recorded in THF (see Table 7.1).

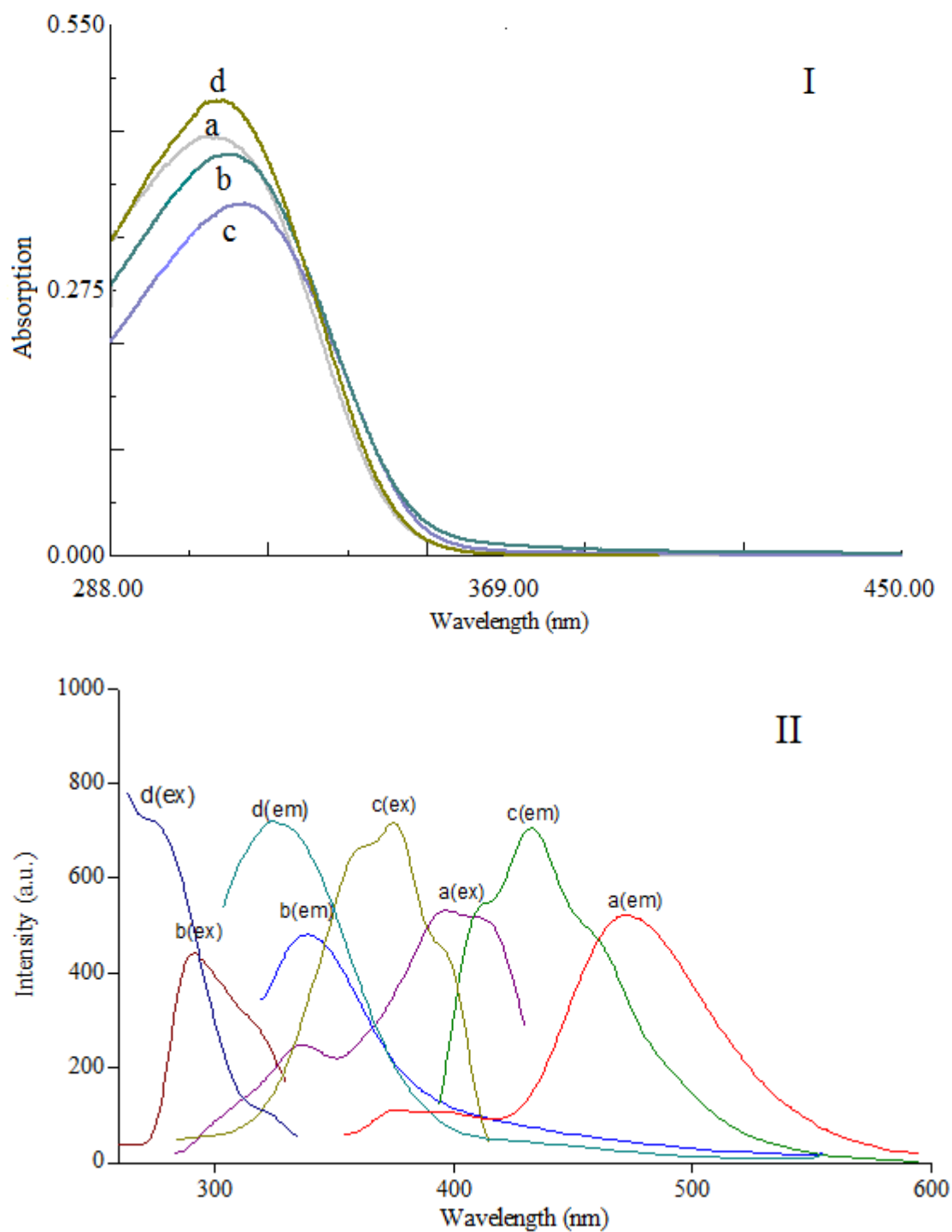


Figure 7.2 **I**: Absorption spectra of the dilute solutions of CBINH dye (a) in THF, (b) To:EtOH(80:20), (c) DMF, (d) EtOH **II**: excitation/ emission spectra recorded in same the solvents.

Table 7.1 Spectral characterization of CBINH dye in the solvents of EtOH, DMF, THF and toluene/ethanol mixture (80:20) and in solid matrices of EC

Compound	Matrix	λ_{abs}	ϵ_{max} (λ_{abs})	$\lambda_{\text{max}}^{\text{em}}$	$\lambda_{\text{max}}^{\text{ex}}$	$\Delta\lambda_{\text{ST}}$ (Stokes' s shift)	ϕ_{F} (Quantum yield)
CBINH	THF	309	43400	470	396	74	8.6×10^{-2} in THF
	EtOH	310	47200	325	272	43	
	To: EtOH	312	41400	340	290	50	
	DMF	315	36400	433	375	58	
	EC	320	116618	405	350	55	0.16

The short time photostability performance of CBINH dye doped EC electrospun nanofiber was checked with a steady-state spectrofluorimeter in time based mode. Molecule was excited at 350 nm. The data were acquired at emission maximum of the dye; 405 nm during 80 minutes of monitoring. In the employed media the dye exhibited excellent short-term photostability. Figure 7.3 reveals performance of the dye doped EC based electrospun nanofibers. The long term stability of CBINH ionophore in the employed matrix material was excellent and when stored in the ambient air of the laboratory there was no significant drift in signal intensity after 6 months. Our long term-stability tests are still in progress.

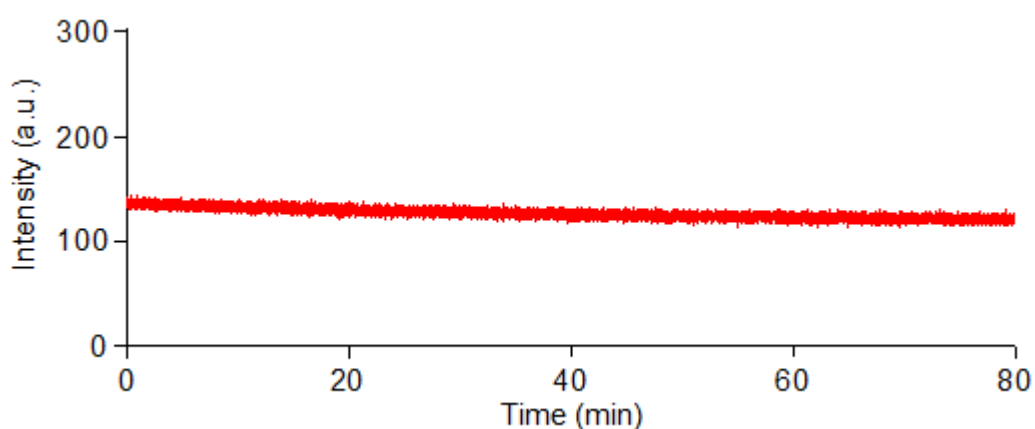


Figure 7.3 The photostability test of CBINH dye doped EC based electrospun nanofiber.

7.3 SEM Displays

The precursor compositions were optimized to form bead-free EC based continuous nanofibers by varying the amount of plasticizer, polymer and ionic liquid (IL) in the composites. The resulting composites were prepared by mixing 240 mg of polymer (EC, with an ethoxy content of 46%), 192 mg of plasticizer (DOP), 48 mg of ionic liquid (IL) and 2 mg of dye in THF. The electrospun fibers exhibited good adhesion and structural stability. The solution flow rate was maintained at 0.5 mL/h using the syringe pump. An electric potential of 25 kV was applied between the needle of the syringe and the substrate. The scanning electron microscope (SEM) images of an electrospun membrane were shown in Figure 7.4. Average fiber diameters were measured for all samples by using at least 40 representative data points and were reported as 457 ± 78 nm.

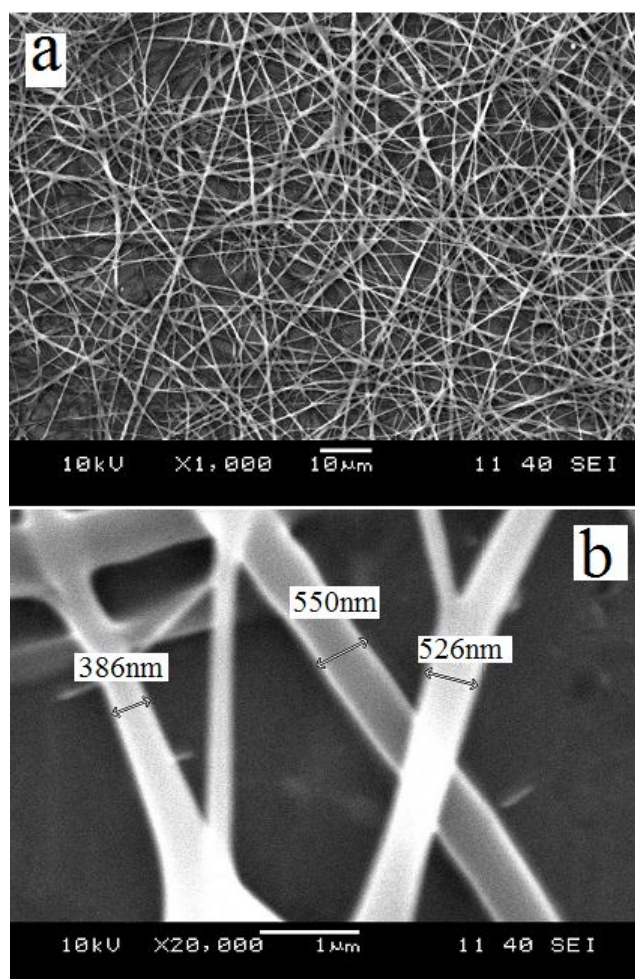


Figure 7.4 SEM images of EC based electrospun nanofibers (a) and (b); EC based nanofibers at different magnifications such as $\times 1\,000$ and $\times 20\,000$.

7.4 Explanation of Effect of pH on the response for Fe³⁺

The electronic absorption, fluorescence emission, and sensing efficiency of the CBINH dye slightly effects from the pH of the environment. Notwithstanding the slight pH dependency, we investigated the optimum conditions of pH separately at constant concentrations of Fe²⁺ and Fe³⁺ ions. The analytical signal ($I-I_0/I_0$) produced by the Fe³⁺ was approximately 10-fold of the signal produced by Fe²⁺ in the pH range of 3.0–6.0 (see Figure 7.5). Distribution of the Fe³⁺ related chemical species in the working conditions was theoretically checked with chemical equilibrium software programme (Visual MINTEQ) at pH 4.5 in presence of acetate ions. The ion distribution was as following: [(CH₃COO⁻(aq): 35.73%, CH₃COOH(aq): 64.27%, Fe³⁺(aq); 0.05%, Fe(OH)⁺²(aq); 14.68% and Fe(OH)₂⁺(aq); 82.26%]. The Fe³⁺ ions were in coordinated form; Fe(OH)⁺²(aq) and Fe(OH)₂⁺(aq) rather than naked Fe³⁺(aq). Similar tests were also performed for Fe²⁺ ions [(CH₃COO⁻(aq): 35.62 %, CH₃COOH(aq): 64.4 % and Fe²⁺(aq); 99.99%]. In contrast to the Fe³⁺, 99.99% of the Fe²⁺ ions were in non-coordinated form in acetic acid/acetate buffer at pH 4.5. Due to the solubility considerations, [Acetate¹⁻, Fe³⁺, Fe²⁺ and H¹⁺; dissolved 100%] acetic acid/ acetate buffered solutions of pH 4.5 was chosen further studies.

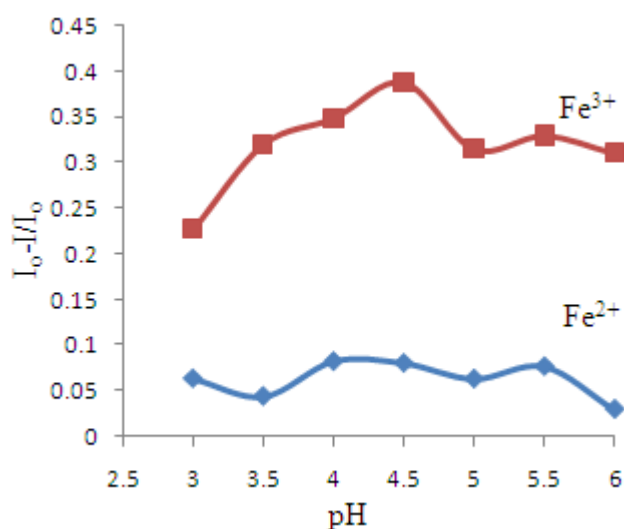


Figure 7.5 The pH dependency of CBINH dye in presence of iron (III) and iron (II) ions between pH 3.0-6.0.

7.5 Dynamic Working Range and Fe³⁺ Response

The dye-doped membranes and nanofibers exhibited remarkable fluorescence intensity quenching upon exposure to Fe³⁺ ions at pH 4.5. Figure 7.7 I-II shows the change in fluorescence spectrum of thin film and electrospun nanofiber as a function of different concentrations of iron ions. The observed intensity decrease at 405 nm is known to be due to the quenching of the CBINH dye by Fe³⁺ ions.

The CBINH dye is supposed to be formed a non-fluorescent complex with Fe³⁺ and statically quenched in ground state. According to the theory, the steady-state absorption spectrum of the chromophore is expected to be perturbed in the presence of quencher that interacts with the chromophore in the ground state. For this reason the nature of the ground state was investigated by studying the molecule's steady state absorption spectrum (see Figure 7.6). Curves a and b are the absorption spectra of the CBINH dye in the EtOH in absence and presence of the quencher. Absorption spectra of the CBINH dye in EtOH solution exhibits an appreciable increase in the intensity and an accompanying integral change in presence of 10⁻⁵ M quencher (See Figure 7.6, curves a and b).

This observation reveals the possibility of the formation of a ground state complex between the CBINH dye and Fe³⁺ and the quenching is of static type.

The CBINH doped electrospun nanofibers demonstrated a linear response over range of 10⁻¹²-10⁻⁶ M for Fe³⁺ ions. The tested sensor compositions exhibited large relative signal change, excellent linearity and very good sensitivity to Fe³⁺ ions. The regression results yielded an absolute linear response with coefficient of regression (R²) of 0.9988 for EC electrospun nanofibers. (see Table 7.2, Figure 7.7 II).

The limit of detection (LOD) for Fe³⁺ was defined as the concentration at which the signal is equal to the blank signal plus 3 σ and found to be 0.07 fM (7 \times 10⁻¹⁴ Molar) for EC based electrospun nanofiber. The detection limits of 6 fM were calculated for continuous thin film form of the same compositions (see Table 7.2).

We also tested whether it has been possible to determine the two oxidation states of iron: Fe^{2+} and Fe^{3+} . Calibration sets for speciation of iron species; Fe^{2+} and Fe^{3+} were prepared separately. The relative signal changes observed for Fe^{2+} and Fe^{3+} ions for same concentration range were 1.1% and 78% respectively. The Fe^{2+} species did not induce significantly the fluorescence signal either in thin film form or in nanomaterial at pH4.5. This result confirms that Fe^{2+} and Fe^{3+} can be distinguished with an error of 12.5% quantitatively in the region assessed. Figure 7.5 summarizes selectivity comparison of Fe^{3+} over Fe^{2+} in separate solutions at pH 4.5. It can be concluded that, the CBINH dye was effectual in reversible binding of Fe^{3+} but ineffectual in binding of Fe^{2+} in immobilized form. The selective uptake of Fe^{3+} over Fe^{2+} by the membrane may partly be attributed to the Pearson's HSAB principle. Theory states that "*hard* [Lewis] acids prefer to bind to *hard* [Lewis] bases and that *soft* [Lewis] acids prefer to bind to *soft* [Lewis] bases" to give complexes. Fe^{3+} ion is a harder acid in the sense of hard-soft acid-base (HSAB) theory than Fe^{2+} , Cu^{2+} , Hg^{+} , Pb^{2+} , Sn^{2+} , Cd^{2+} , Co^{2+} and Ni^{2+} (Pearson, 1973).

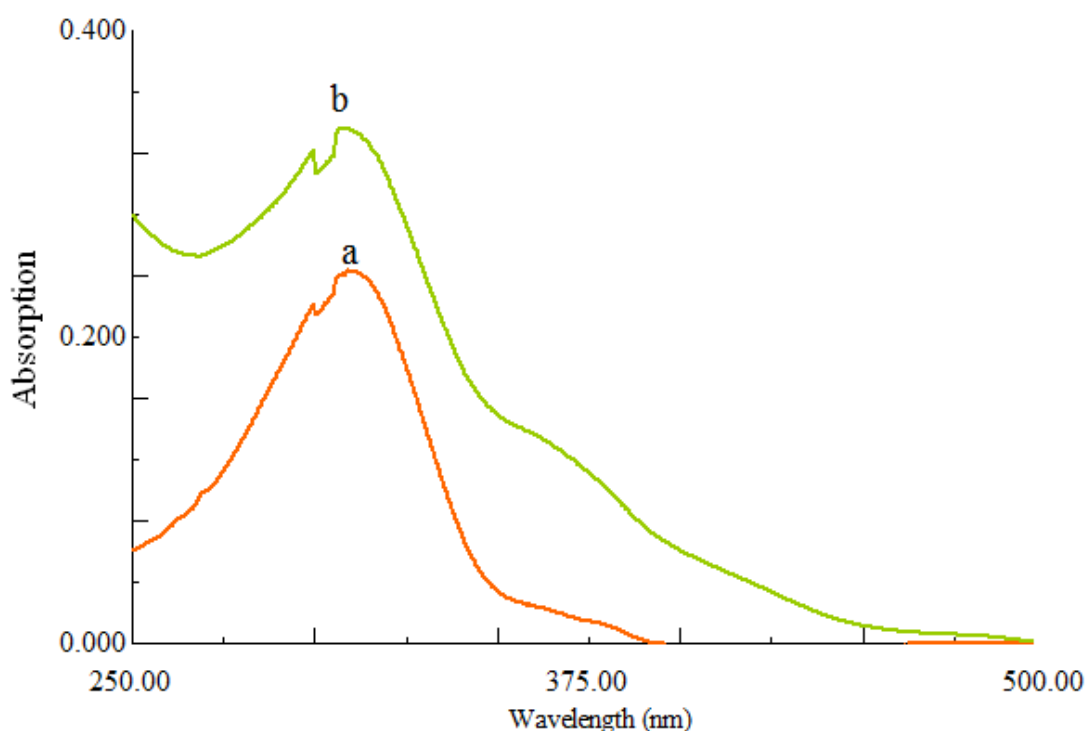


Figure 7.6 Absorption spectra of CBINH dye: (a) in EtOH ($\lambda_{\text{max}} = 310 \text{ nm}$), (b) in EtOH, in presence of $10^{-5} \text{ M Fe}^{3+}$ ($\lambda_{\text{max}} = 310 \text{ nm}$)

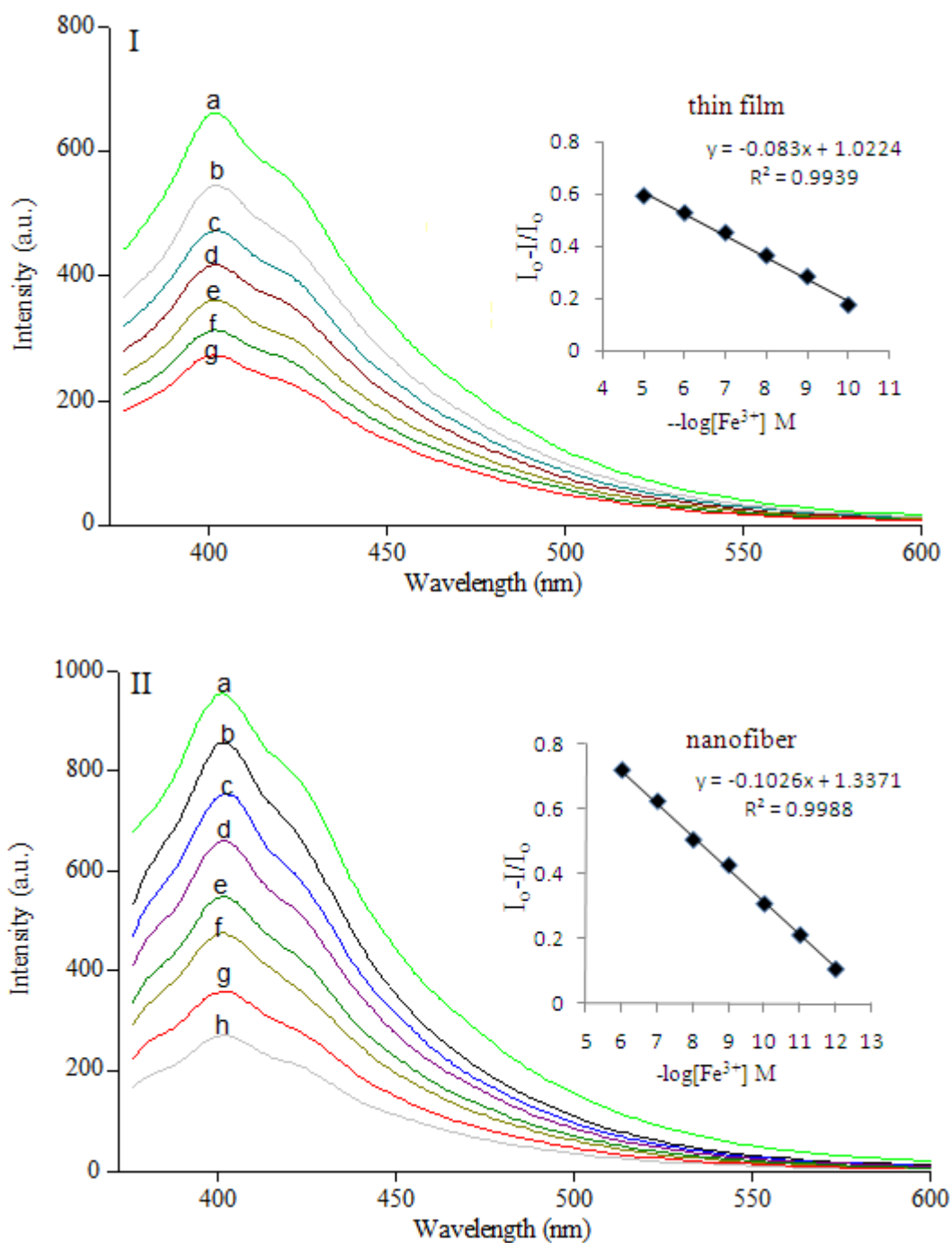


Figure 7.7 I. Excitation-emission based response of the dye-doped EC based thin film to Fe^{3+} ions at pH 4.5. (a) Fe^{3+} -free buffer, (b) 10^{-10} , (c) 10^{-9} , (d) 10^{-8} , (e) 10^{-7} , (f) 10^{-6} , (g) 10^{-5} M Fe^{3+} , Inset: Calibration plot for the concentration range of 10^{-10} - 10^{-5} M Fe^{3+} . **II.** Response of the EC based nanofiber to Fe^{3+} ions at pH 4.5. (a) Fe^{3+} -free buffer, (b) 10^{-12} , (c) 10^{-11} , (d) 10^{-10} , (e) 10^{-9} , (f) 10^{-8} , (g) 10^{-7} , (h) 10^{-6} M Fe^{3+} , Inset: Linearized calibration plot for the concentration range of 10^{-12} - 10^{-6} M Fe^{3+} .

Table 7.2 Calibration characteristics of EC based electrospun nanofibers and thin films.

Indicator Dye	Matrix /form	Linear Range (Mol/L)	Regression Coefficient (R^2)	LOD (Molar)	LOD (femtoM)
CBINH	EC/ electrospun nanofiber	1.0×10^{-12} to 1.0×10^{-6}	0.9988	7.0×10^{-14}	0.07
	EC / thin film	1.0×10^{-10} to 1.0×10^{-5}	0.9939	6.0×10^{-12}	6.0

7.6 Stern-Volmer Analysis

The quenching process of chemical sensors based on fluorescence quenching can be described by the well-known Stern-Volmer equation (Demas, DeGraff, & Xu, 1995);

$$I_0/I = 1 + K_{sv} [Q] \quad (7.1)$$

I_0 and I are the fluorescence intensities in the absence and presence of quencher respectively, $[Q]$ is the quencher concentration, and K_{sv} is the Stern-Volmer quenching constant. The constant K_{sv} defines the efficiency of quenching. When all other variables are held constant, the higher the K_{sv} , the lower the concentration of quencher required to quench the luminescence (Lakowicz, 1999; Turro, 1978).

The data obtained exploiting Stern-Volmer analysis for both; electrospun nanomaterials and continuous thin films are shown in Figure 7.8 and Table 7.3.

Stern- Volmer constants (K_{sv}) of the nanofiber and continuous thin film, calculated from slopes of the plots were found to be 1.00×10^8 (M^{-1}) and 1.56×10^5 (M^{-1}) respectively. The K_{sv} value calculated for nanomaterial is approximately 660 fold greater than that of obtained from the thin film sensors. The significant enhancement in the sensitivity of the sensor can be attributed to the nanostructure of the electrospun membranes.

Here we demonstrated that sensitivity and response related other sensor dynamics can be manipulated by controlling the quencher diffusion rate to fluorophores encapsulated in the polymer via the microstructural properties of the sensing agent. The offered nano-structure was quite beneficial for both the sensitivity and dynamic characteristics of the sensor due to its large specific area, which has high number of active sites for diffusion of Fe^{3+} ions towards the solid phase with respect to the thin films made up of same material. In these structures the possibility of interaction of the analyte ions with the Fe^{3+} selective chromoionophore molecules is higher than that of observed in conventional thin films. The attained LOD values exploiting nano-materials for the offered design (7.0×10^{-14} M for nanofiber and 6.0×10^{-12} M for thin film) is an evident of the enhanced sensitivity (see Table 7.2).

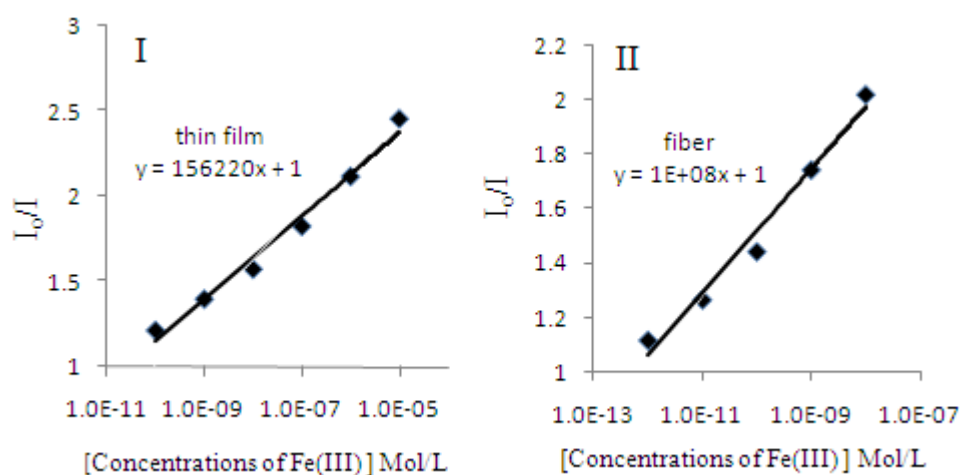


Figure 7.8 Stern-Volmer plots of EC based thin film (I) and electrospun nanofibers (II) as a function of different quencher concentrations.

Table 7.3 The Stern-Volmer plot related data of EC based electrospun nanofibers and thin films.

Indicator Dye	Matrix /form	Linear Regression Equation	Ksv Constant
CBINH	EC/ electrospun nanofiber	$y = 1 \times 10^8 x + 1$	1.00×10^8
	EC / thin film	$y = 1.56 \times 10^5 x + 1$	1.56×10^5

7.7 Specification of Selectivity and Interference Effect

Calcium, magnesium, potassium and sodium, which are the most abundant ions in natural water samples as well as physiologically relevant species, could be potential interferents for iron determination (Malcik, & Caglar, 1997; Oter et al., 2007; Jezek et al., 2007). On the other hand Cu^{2+} is third most abundant element (after Fe^{3+} and Zn^{2+}) among the essential heavy metal ions in the human body. In chemosensing based approaches, affinity of the chromoionophores for above mentioned metal ions is still a problem. In order to determine the selectivity of the proposed method, the influence of a number of cations were investigated. Tests were performed for Ag^+ , Al^{3+} , Ba^{2+} , Ca^{2+} , Co^{2+} , Cr^{3+} , Cu^{2+} , Fe^{3+} , Fe^{2+} , Hg^{2+} , Li^+ , K^+ , Mn^{2+} , Mg^{2+} , Na^+ , NH_4^+ , Ni^{2+} , Pb^{2+} , Sn^{2+} and Zn^{2+} ions in acetic acid/acetate buffer solutions at pH 4.5. From Figure 7.9-I, it can be concluded that, the sensing membrane is capable of determining iron ions (Fe^{3+}) with a high selectivity over other ions. The fluorescence was dramatically quenched in the presence of Fe^{3+} at 405 nm exhibiting a relative signal change (RSC) ratio of 70%. However, the response to Al^{3+} is markedly different from the response to other metal ions and fluorescence of CBINH is affected appreciably by Al^{3+} at concentrations of $\geq 10^{-3} \text{ mol L}^{-1}$.

The interference effects of the anions; F^- , Cl^- , Br^- , NO_3^- , NO_2^- , SO_4^{2-} and PO_4^{3-} were also tested. Relative signal changes of less than 2% were observed for EC doped films at pH 4.5 (see Figure 7.9-II).

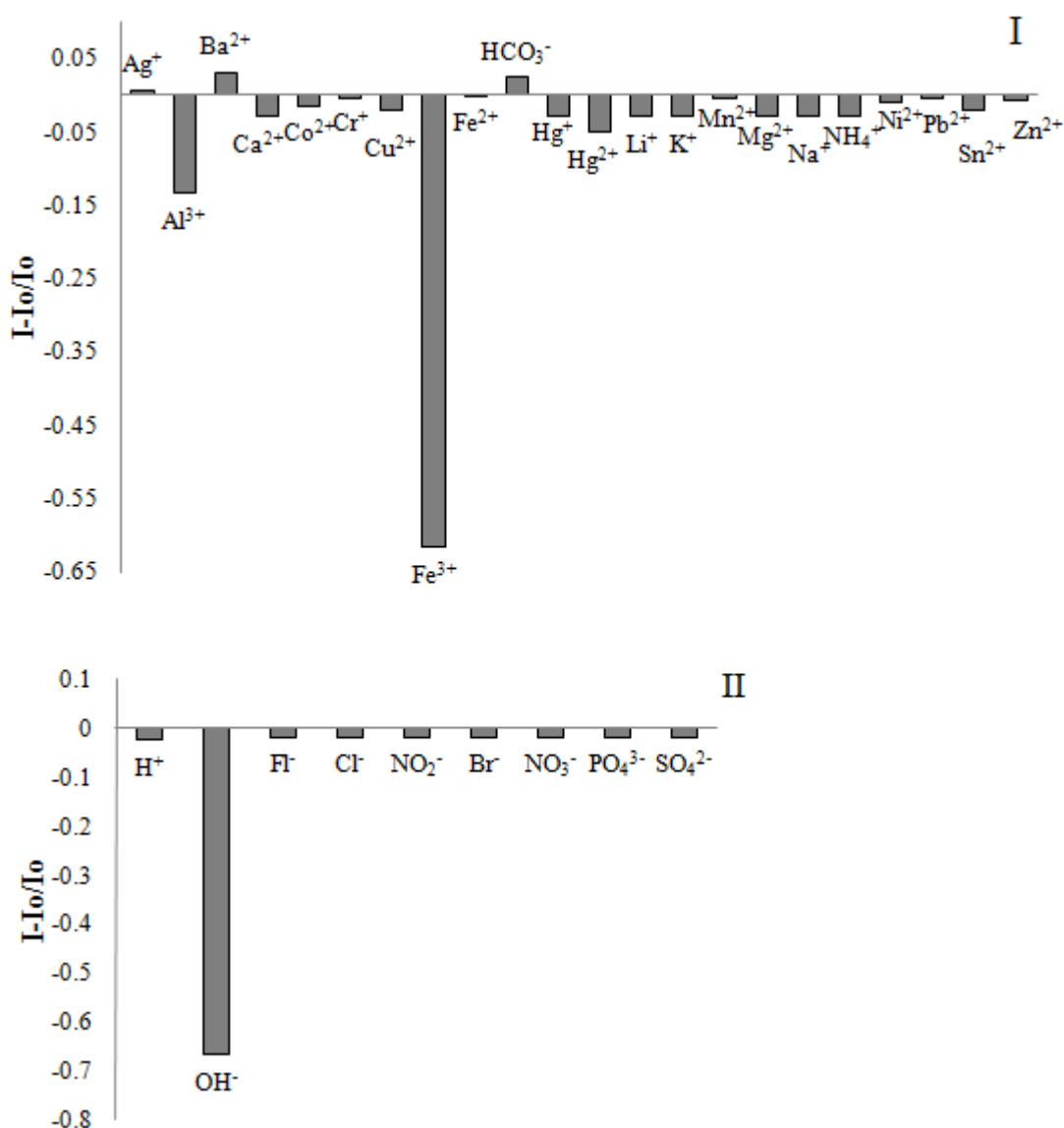


Figure 7.9 I: Metal ion response of EC based nanofibers at pH 4.5.

II: Anion response of the same composition.

7.8 Response Time, Regeneration and Reproducibility

The sensor has a response time of <30 s. Regeneration experiments were carried out in 0.01M CH₃COOH/CH₃COO⁻ buffer at pH: 4.5 and 0.1 M HCl solutions, respectively. Approximately 100% regeneration performance was succeeded with 0.1 M HCl and 0.01 M CH₃COOH/ CH₃COO⁻ buffer. For further regeneration treatments 0.01 M CH₃COOH/ CH₃COO⁻ buffer at pH: 4.5 was preferred. The

sensor was fully reversible and only a slight drift (1.98%) of the upper signal level has been observed after the fifteen cycles. Regeneration time is <60 s (see Figure 7.10). The regeneration time for thin film based structures was measured between 6-10 min. The attained regeneration time exploiting nanostructures is at least six times better than that of the ones measured with thin films. The nano-scale sensor size enhanced the response based dynamics as well as sensitivity. The measured response and regeneration times are good evidences of the above discussion. The reproducibility of the optical responses was assessed by repeatedly introducing a sample of 5.0×10^{-5} M Fe^{3+} in 5.0×10^{-3} M acetic acid/acetate buffer at pH 4.5. Between the 1st and 15th cycles, the level of reproducibility achieved was quite good and exhibited a SD of 305.47 ± 6.07 and RSD % 1.98 for upper signal level, respectively (see Figure 7.11).

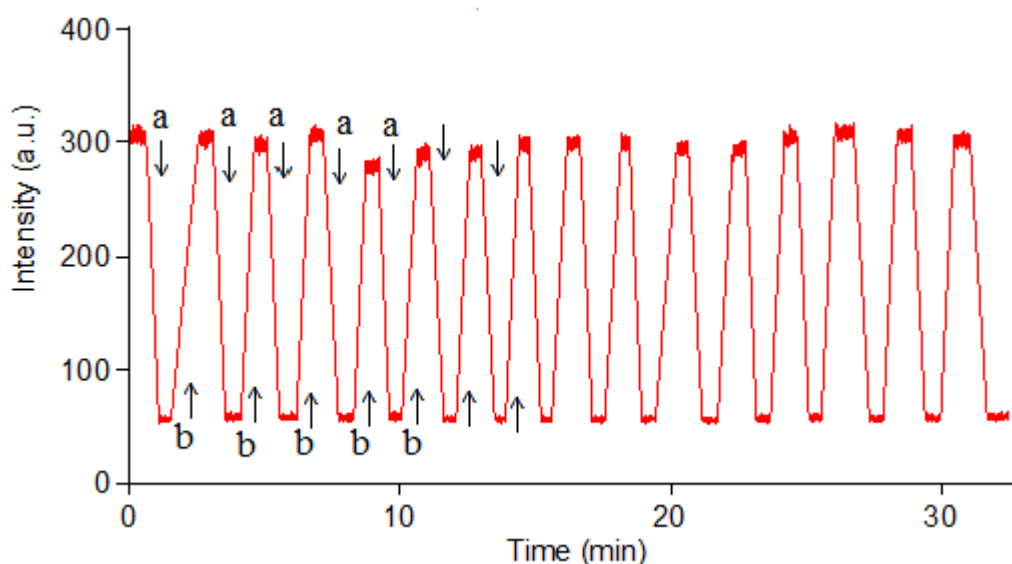


Figure 7.10 Rejuvenation characteristics of the sensor in an alternating concentration of 5.0×10^{-5} M Fe^{3+} solution 0.01 M $\text{CH}_3\text{COOH}/\text{CH}_3\text{COO}^-$ buffer. **a:** 5.0×10^{-5} M Fe^{3+} solution **b:** Rejuvenation of 0.01 M $\text{CH}_3\text{COOH}/\text{CH}_3\text{COO}^-$ buffer.

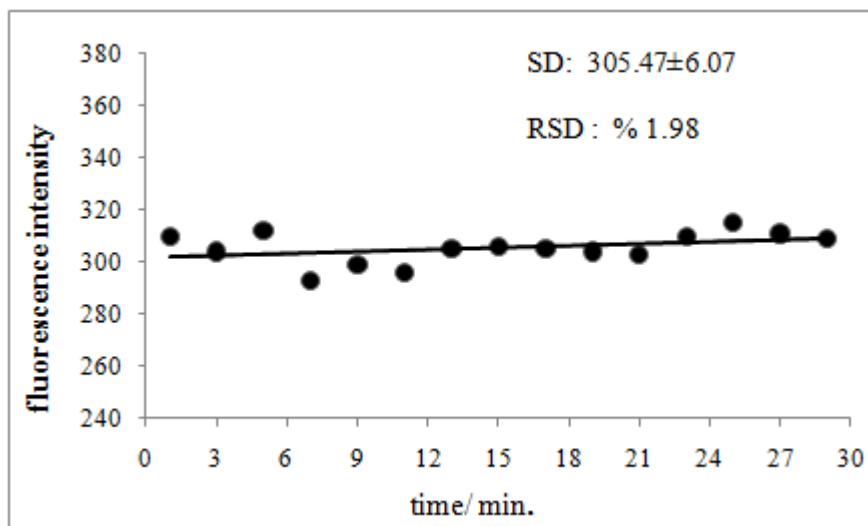


Figure 7.11 The level of reproducibility for upper signal level between the 1st and 15th cycles.

7.9 Conclusion

Electrospinning was used as a novel and facile method to fabricate optical chemical sensor devices. With respect to continuous thin films, electrospun nanofibers offered enhanced sensitivity, lower LOD values and faster response in optical chemical sensing of Fe^{3+} .

In this paper, we introduce highly responsive fluorescent sensors using functional electrospun nanofibers based on fluorescence quenching of an iron selective fluorophore. The CBINH dye was used for the first time as a chemosensor in the optical sensing of Fe^{3+} . The CBINH dye doped nanofibers in EC can be used at pH 4.5 for quantitative determination of Fe^{3+} in the concentration range of 10^{-12} - 10^{-6} M. A quite good LOD (0.07 fM) was reached. The sensor has a response time of <30 s and was fully reversible.

CHAPTER EIGHT

FIBER OPTIC HYDROXYL (OH⁻) SENSING WITH LONG WAVELENGTH EXCITABLE IONOPHORE DOPED IN NANOFIBERS

8.1 Introduction

Such important analytes as hydroxyl (OH⁻) is of vital importance for measuring and controlling physiological parameters in medicine, laboratory animals and humans, as well as in environmental analysis. Continuous monitoring is necessary to maintain tight control of this parameter. Except that of electrochemical pH sensors, there are limited number of optical sensors can quantify hydroxide concentrations with high sensitivity within large dynamic range. Optical nanosensors based on fluorescence are became increasingly popular devices for such applications. (Borisova, Herrod, & Klimanta, 2009; Vasylevska, Borisov, Krause, & Wolfbeis, 2006; Kocincova, Borisov, Krause, & Wolfbeis, 2007; Pringsheim, Zimin, & Wolfbeis, 2001; Vasylevska, Karasyov, Borisov, & Krause, 2007; Peng et al, 2007; Clark, Hoyer, Parus, Philbert, & Kopelman, 1999; Clark, Kopelman, Tjalkens, & Philbert, 1999)

However, most of the fluorescent pH probes work near neutral or acidic regions of the pH scale. In this work, we have prepared nanosensors using electrospinning technique based on fluorescent ionophore, 9-butyl-bis-3-(4-(dimethylamino) phenyl) allylidene)-9H-carbazole-3,6-diamine (BCDA) that allow pH measurements in the alkaline region. Matrix material of ethyl cellulose (EC) was used to produce nanofibrous mats and continuous thin films.

The long wavelength excitable BCDA dye (9-butyl-bis-3-(4-(dimethylamino) phenyl) allylidene)-9H-carbazole-3,6-diamine, $\lambda_{ex} = 590$ nm) was chosen as the indicator due to the selective response, high quantum yield, and excellent photostability. Chemical structure of the exploited dye was shown in Figure 8.1. Response of the BCDA was fully reversible within the dynamic working range. The response times were between 4–14 min. A relative signal change of 95% and 96% have been achieved for sensor dyes of BCDA.

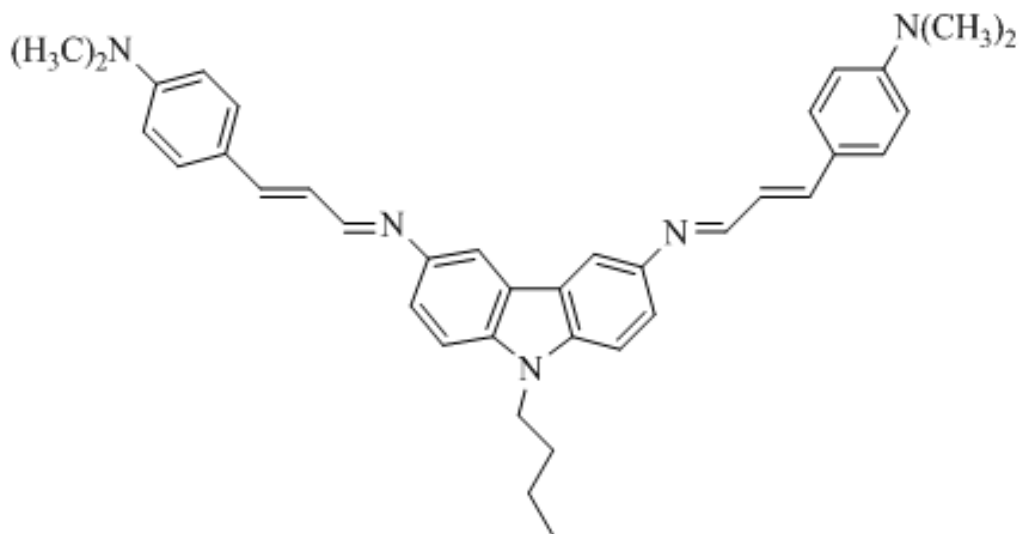


Figure 8.1 BCDA: 9-butyl-bis-3-(4-(dimethylamino)phenyl)allylidene-9H-carbazole-3,6-diamine

8.2 Photocharacterization of Newly Synthesized BCDA Dyes and Assessment of Quantum Yield

For spectral characterization of the BCDA, absorption, excitation and corrected emission spectra were determined in conventional solvents of EtOH, DCM, THF, DMF and toluene/ethanol (To: EtOH; 80:20) mixture (see Figure 8.2 and 8.3). The UV-Vis spectroscopy related data (absorption maxima; λ_{Abs} , and molar extinction coefficient; ϵ), were shown in Table 8.1 and Table 8.2. BCDA exhibited very efficient absorbance and high molar extinction coefficients around 590 nm in EC matrices. In agreement with literature (Ertekin et al., 2000) molar extinction coefficients (ϵ_{max}) of BCDA were increased in EC with respect to (ϵ_{max}) of BCDA in solution phase (see Table 8.1, Table 8.2). These data can be taken as proofs that BCDA molecules absorb better in plasticized EC matrices.

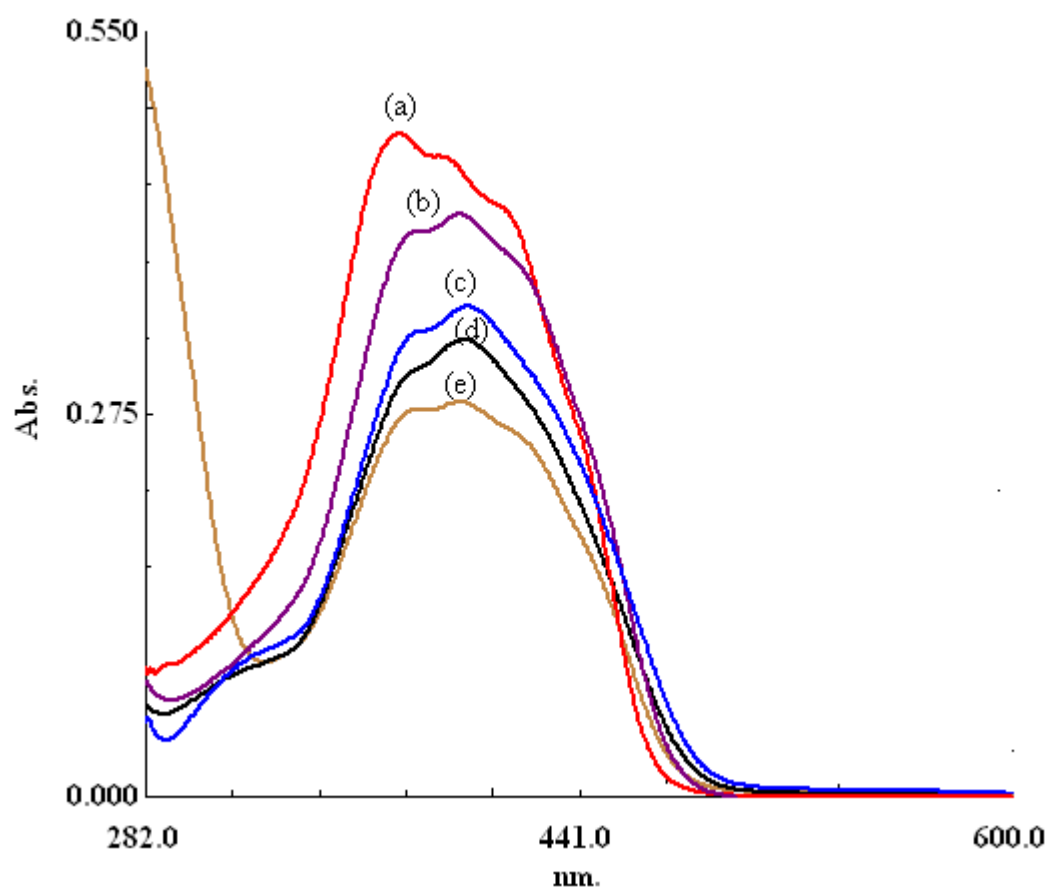


Figure 8.2 Absorption spectra of the BCDA dye (10^{-6} M dye or 2 mM dye/kg polymer). a) THF b) DCM c) To: ETOH d) ETOH e) DMF

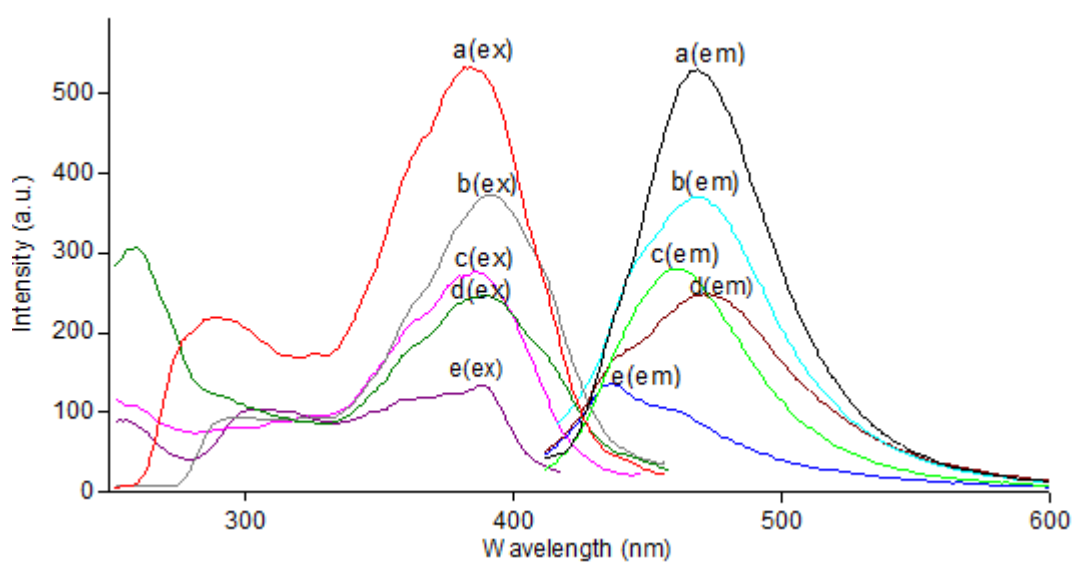


Figure 8.3 Excitation and corrected emission spectra of the BCDA dye (10^{-6} M dye or 2.5 mmol dye/kg polymer). a) DMF b) To: ETOH c) DCM d) ETOH e) THF.

Table 8.1 UV-Vis spectra related data of BCDA in the solvents of EtOH, DCM, THF, DMF and toluene/ ethanol mixture (80:20) and in solid matrices of EC.

Compound	Solvent/Matrix	λ_{abs}^1	$\varepsilon_{\text{max}} (\lambda_{\text{abs}}^1)$
BCDA	EtOH	400	33000
	DCM	397	42000
	THF	377	48000
	To: EtOH	400	35000
	DMF	398	27500
	EC	590	454029

Table 8.2 The excitation–emission spectra related characteristics of the BCDA acquired in conventional solvents, and in thin film form of EC.

Compound	Matrix	$\lambda_{\text{max}}^{\text{em}}$	$\lambda_{\text{max}}^{\text{ex}}$	$\Delta\lambda_{ST}$ (Stoke's shift)	ϕ_F (Quantum yield)
BCDA	EtOH	471	390	81	0.072 in EtOH
	DCM	460	390	70	
	THF	437	390	47	
	To:EtOH	469	395	74	
	DMF	470	390	80	
	EC	645	590	55	0.62

Fluorescence quantum yields (ϕ_F) of BCDA were calculated employing the comparative William's method, which involves the use of well-characterized standards with known ϕ_F values. For this scope, the UV–vis absorbance and corrected emission spectra of different concentrations of reference standards and samples were recorded. In solution phase studies, 8-hydroxypyrene-1,3,6-trisulfonic acid (HPTS) ($\lambda_{\text{ex}} = 390$ nm, quantum yield = 1 in acidic water) were used as reference standards for BCDA. In thin film studies the quantum yield Standard Rose

Bengal ($\lambda_{\text{ex}} = 525 \text{ nm}$, quantum yield = 0.11 in alkaline EtOH) was used as reference.

The integrated fluorescence intensities were plotted versus absorbance for the reference standards and BCDA. The gradients of the plots were proportional to the quantity of the quantum yield of the studied molecules.

In agreement with literature (Ertekin et al, 2003), fluorescence quantum yield of BCDA in EC; $\phi_F = 0.62$ increased 10-fold, with respect to ϕ_F of BCDA in solvents which can be concluded as proofs that the BCDA exhibit better fluorescence in immobilized EC matrix (See Figure 8.4, 8.5 and Table 8.3).

Table 8.3 Quantum yield related data for BCDA in EtOH and EC matrices.

Dye	Refractive index, n	Equations of plots	Gradient Of the plots	Quantum Yield, ϕ_f
HPTS (in water)	1.3328	$y = 4136512x$	4136512	1
Rose Bengal (in EtOH)	1.3590	$y = 43846x$	43846	0.11
BCDA (in EtOH)	1.3590	$y = 28870x$	28870	0.072 (calculated)
BCDA (in EC)	1.4790	$y = 209415x$	209415	0.62 (calculated)

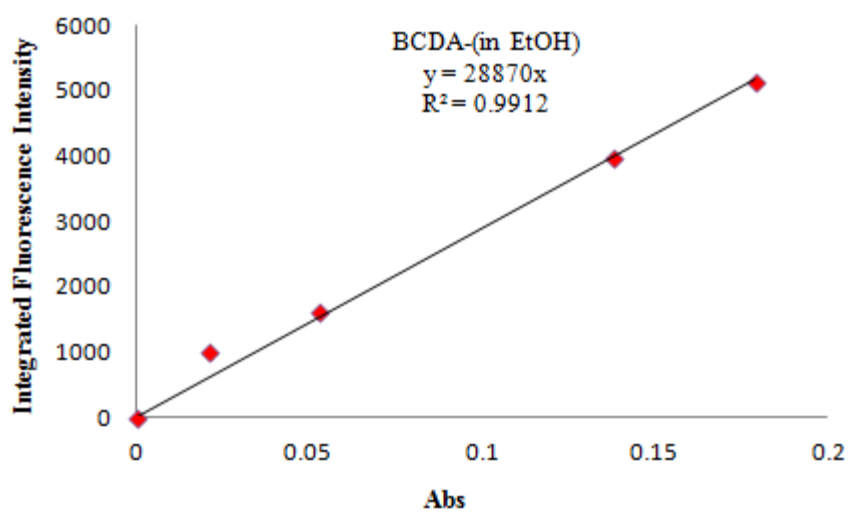


Figure 8.4 The integrated fluorescence intensities vs absorbance values of BCDA in EtOH (excitation at 390 nm).

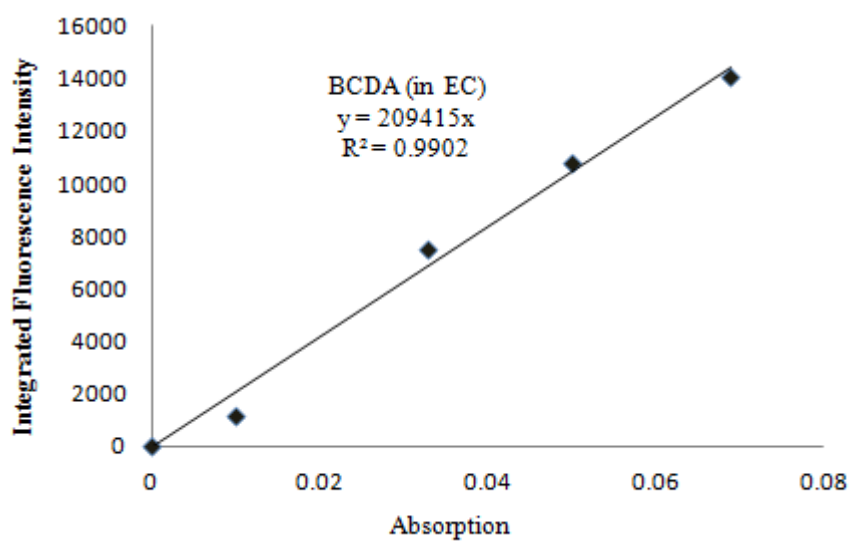


Figure 8.5 The integrated fluorescence intensities vs absorbance values of BCDA in EC (excitation at 590 nm).

8.3 SEM Images of Electrospun Membranes

The SEM images of EC based electrospun membranes at various magnifications are denoted in Figure 8.6. The membrane has a 3-D structure with a random fiber

orientation that is evenly distributed on the substrate. It can be seen from Figure 8.6 that the diameters of the fibers were between 372 and 598 nm.

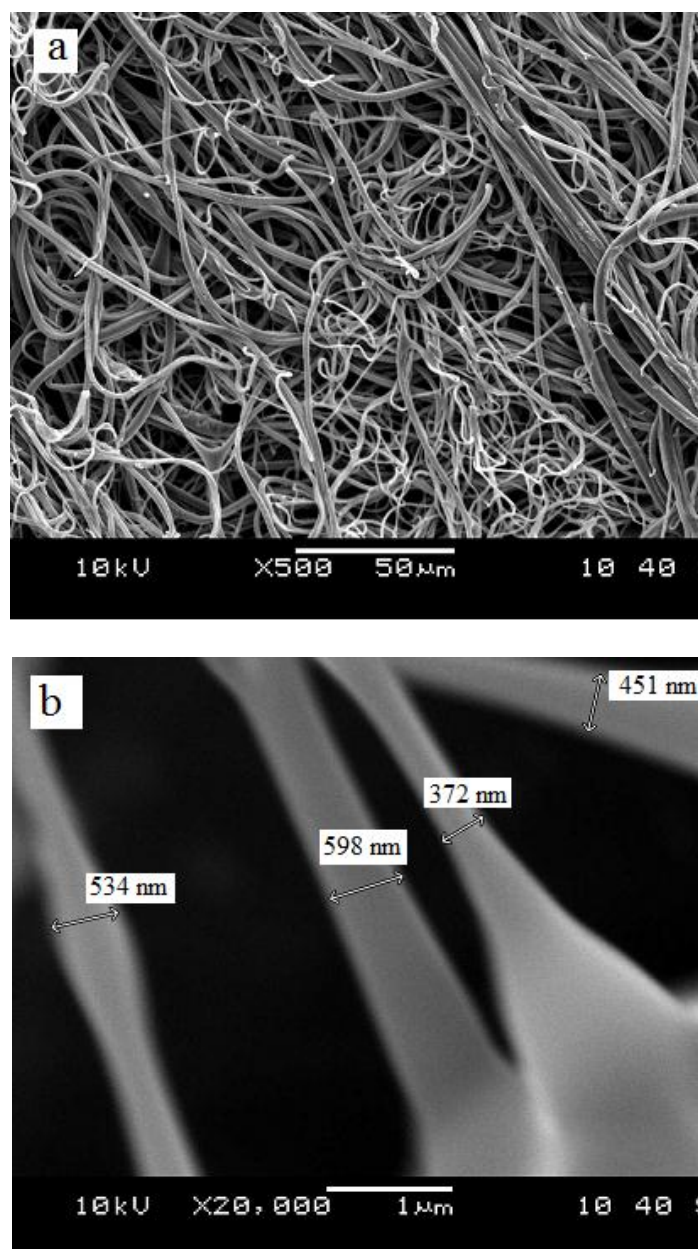
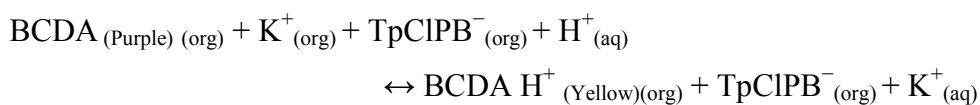


Figure 8.6 SEM images of EC based electrospun nanofibers (a) and (b); EC based nanofibers at different magnifications such as $\times 500$ and $\times 20\,000$.

8.4 Discussions Related to Possible Sensing Mechanism of BCDA

BCDA dye contains available active centers for proton attacks and is appropriate for use as pH probes in the alkaline region. When doped in plasticized EC together

with the anionic additive; potassium tetrakis-(4-chlorophenyl) borate; the BCDA become pH sensitive probe. In these systems, slightly acidic or near neutral pHs the H^+ ions are selectively extracted into the optode membrane by the anionic additive meanwhile potassium ions diffuse from the membrane into the aqueous phase due to the mechanism of ion-exchange. The first-step of response mechanism of BCDA can be explained by the following ion-exchange pathways. Following successive protonation steps are possible.



However, when exposed to alkaline solutions the dye becomes de-protonated. After the stepwise de-protonation of the pH-sensitive moieties, the color turns from purple to yellow for BCDA dye (See Figure 8.7).

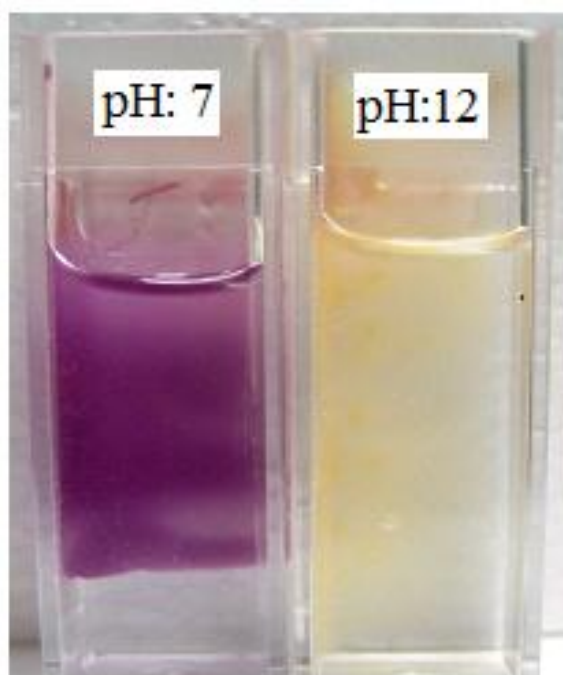


Figure 8.7 Images of stepwise protonation of the acid-sensitive moieties

8.5 pKa Calculations of BCDA in EtOH

The knowledge of dissociation constant (pKa) of BCDA is of fundamental importance in order to provide information on chemical reactivity range of the indicator dyes. In order to evaluate the availability of BCDA molecules for sensing purposes, determination of the acidity constants has been performed in different media. The sensor dyes irreversibly responded to H^+ ions in EtOH solutions. Figure 8.8 and 8.10 reveals the absorption and emission based response of the BCDA dye to H^+ ions in EtOH, respectively. The effective pKa values were determined to be $K_a = 4.40$ for BCDA in EtOH.

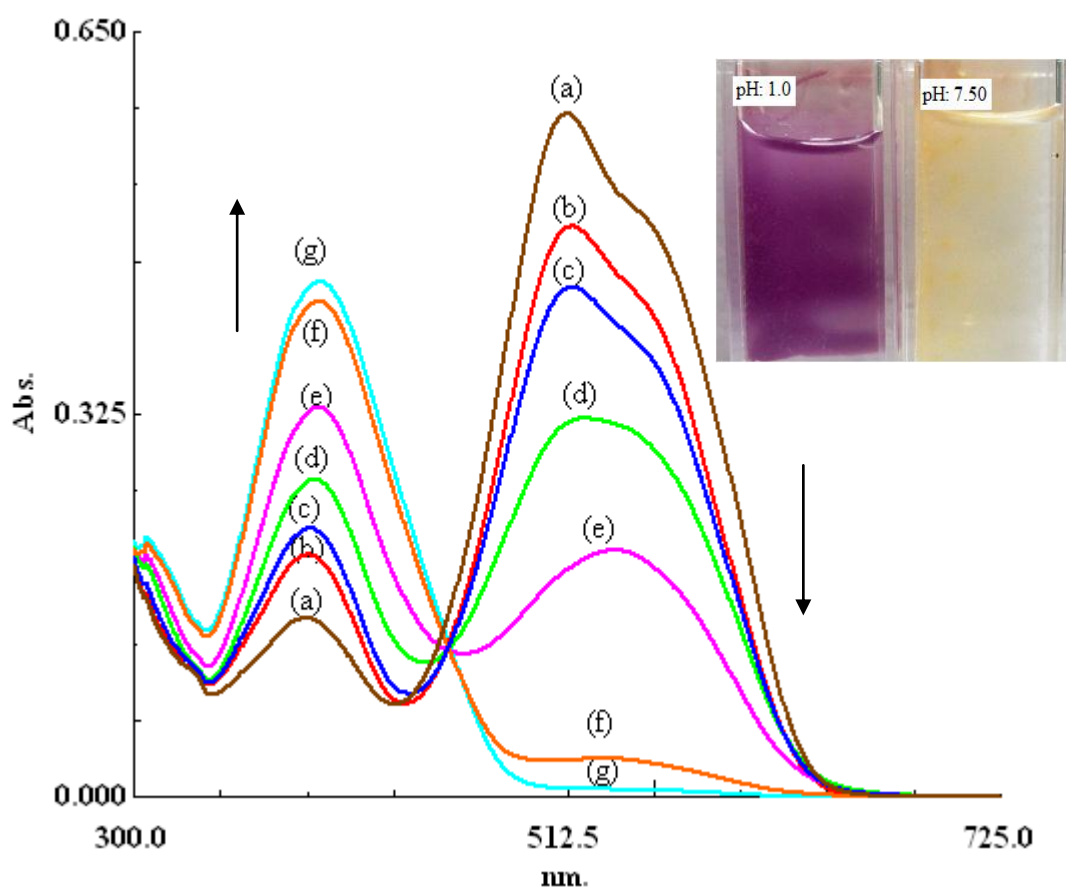


Figure 8.8 Absorption spectra of BCDA in EtOH after addition of acid and basic solutions in the pH range of 1.00-12.00 pH: a) 1.00 b) 2.00 c) 3.20 d) 4.40 e) 5.30 f) 6.20 g) 7.50 - 8.00 - 9.00 - 10.00 - 11.00 - 12.00

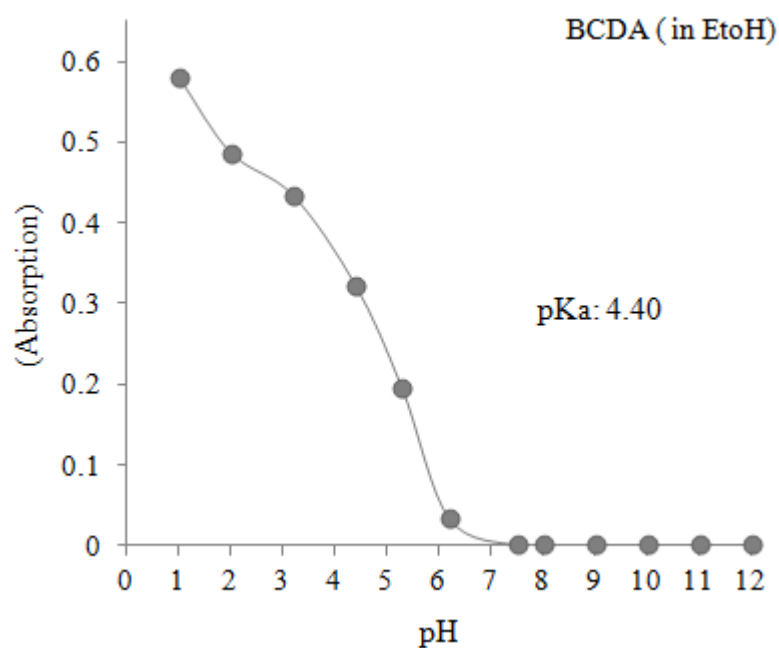


Figure 8.9 Absorption based sigmoidal response of BCDA in the pH range of 1.00-12.00

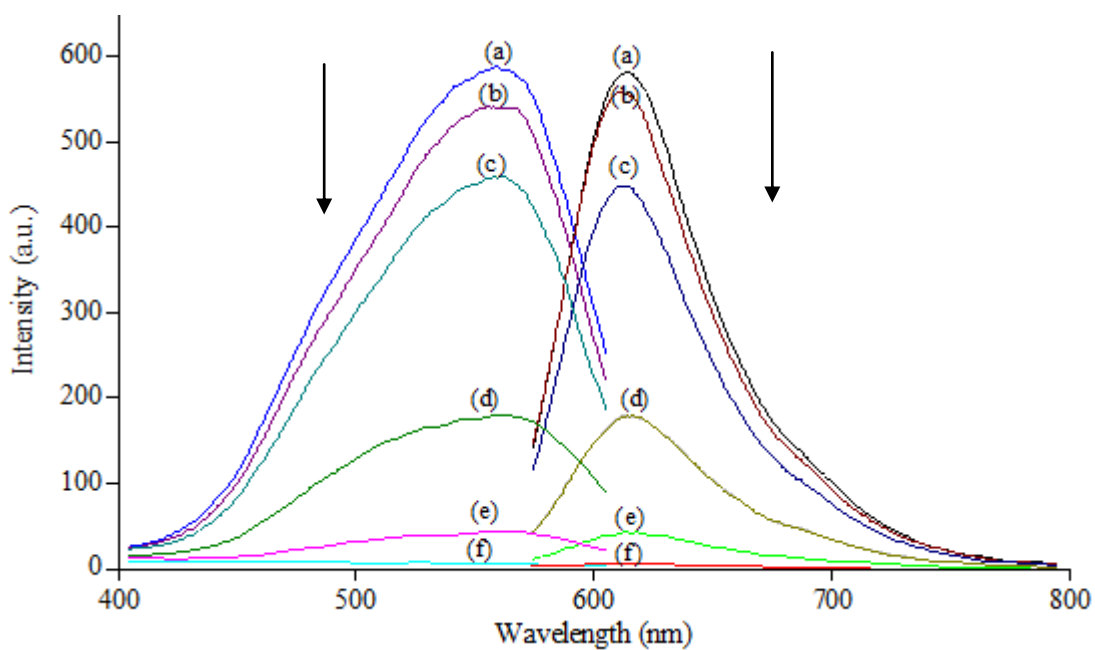


Figure 8.10 pH induced emission based spectral response of BCDA in EtOH after addition of acid and basic solutions in the pH range of 1.00-12.00 pH: a) 1.00 b) 2.00 c) 3.20 d) 4.40 e) 5.30 f) 6.20 - 7.50 - 8.00 - 9.00 - 10.00 - 11.00 - 12.00

8.6 pKa Calculations of BCDA in EC Matrix

Dissociation constants (pKa) of BCDA in ethyl cellulose (EC) matrix were calculated from the excitation/emission based measurements. BCDA doped EC exhibited a parallel decrease both in emission and excitation intensity after exposure to different concentrations of base solutions in the pH range of 7.00 to 12.00. In EC doped thin film, the pKa values of BCDA were found to be 9.50. Figure 8.11 and 8.12 show pH induced emission/excitation based spectral response and sigmoidal response of the EC doped BCDA in the pH range of 7.00-12.00, respectively.

Depending on the matrix, the pKa values of BCDA exhibited differences. In EtOH, apparent pKa values were obtained for BCDA ($K_a = 4.40$), whereas, pKa value was observed for BCDA in solid matrices of EC which are 9.50. The differences in pKa can be attributed to the microenvironment of the indicator dye.

The BCDA exhibited the pKa values of 4.40 and 9.50 in EtOH and EC, respectively. pKa value of BCDA is lower by approximately 5 pKa units in EtOH than that in EC. This can be attributed to the polarity differences of the matrices as well as the structure of the dye. The OH groups of ethyl cellulose probably interact with the immobilized BCDA dye making weak hydrogen bonds or via the acid sensitive moieties of the dye complexes. Interactions between support material and the dye can be beneficial to sensor performance giving stability.

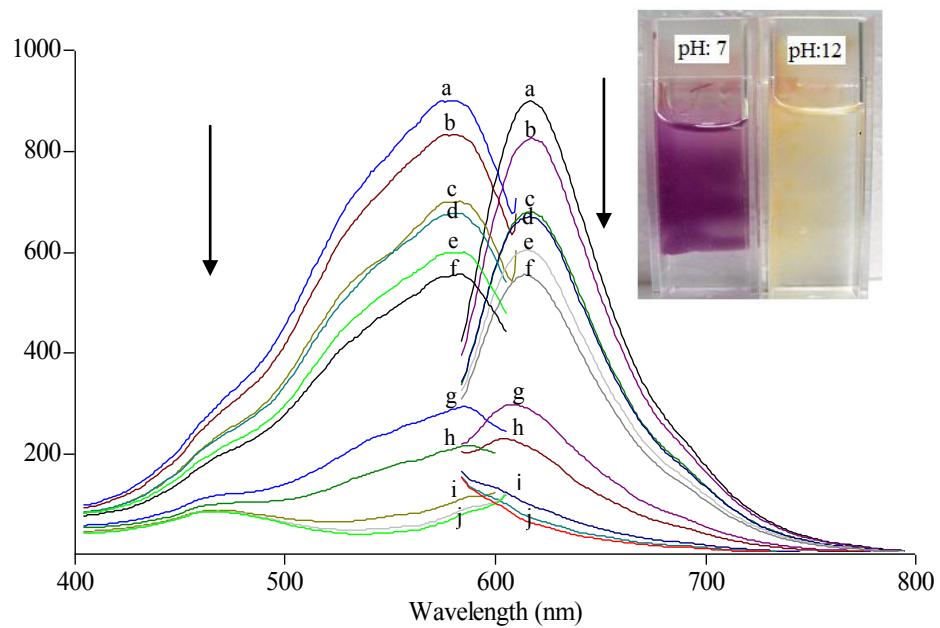


Figure 8.11 pH induced emission based spectral response of BCDA in EC matrix after addition of basic solutions in the pH range of 7.00-12.00 pH: a) 7.00 b) 7.50 c) 8.00 d) 8.50 e) 9.00 f) 9.50 g) 10.00 h) 10.50 i) 11.00 j) 11.50 – 12.00

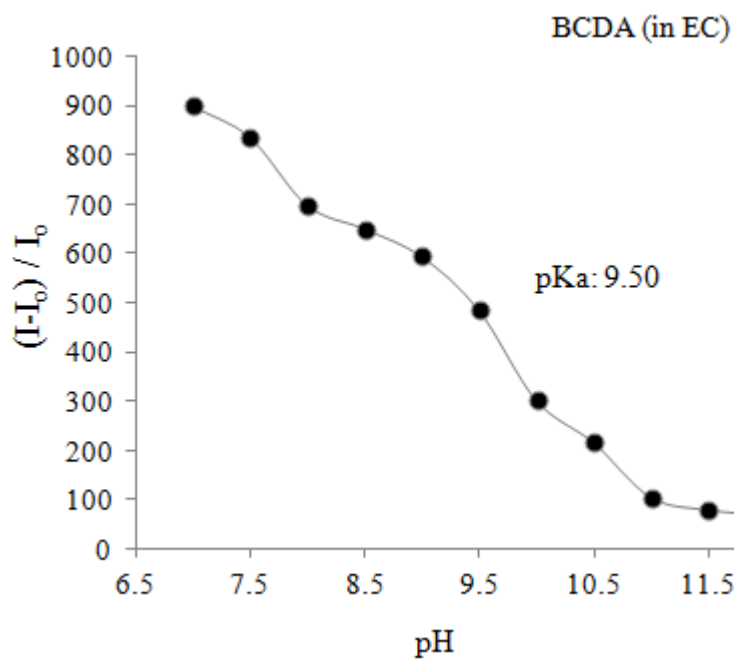


Figure 8.12 Emission based sigmoidal response of BCDA in the pH range of 7.00-12.00

8.7 Dynamic Working Range and Sensor Response

The sensor slides were found to give reproducible results on absorption and fluorescence emission measurements when pH was varied within the dynamic working range. The response of BCDA to protons was investigated in buffered solutions. Figure 8.13 and 8.14 shows the relative signal change and reversibility performance of the BCDA doped EC thin film and nanofiber sensor, respectively. Relative signal changes of 100 % have been achieved for sensor dyes of BCDA in the EC matrix. Regeneration was accomplished with concentrated buffer solutions at opposite pHs in the range of 7.00-12.00. The BCDA dye doped thin film and nanofiber was found to reach 90% of the signal intensity (t_{90}) between 4.0 - 8.0 min and 6.5 - 13.5 min, respectively.

Between the first and sixth cycles, the level of reproducibility of the upper signal level was quite good with a S.D. of 74.7 ± 1.6 and R.S.D % 2.1 and S.D. of 109.4 ± 0.7 and R.S.D % 0.6 for thin film form and nanofiber form, respectively.

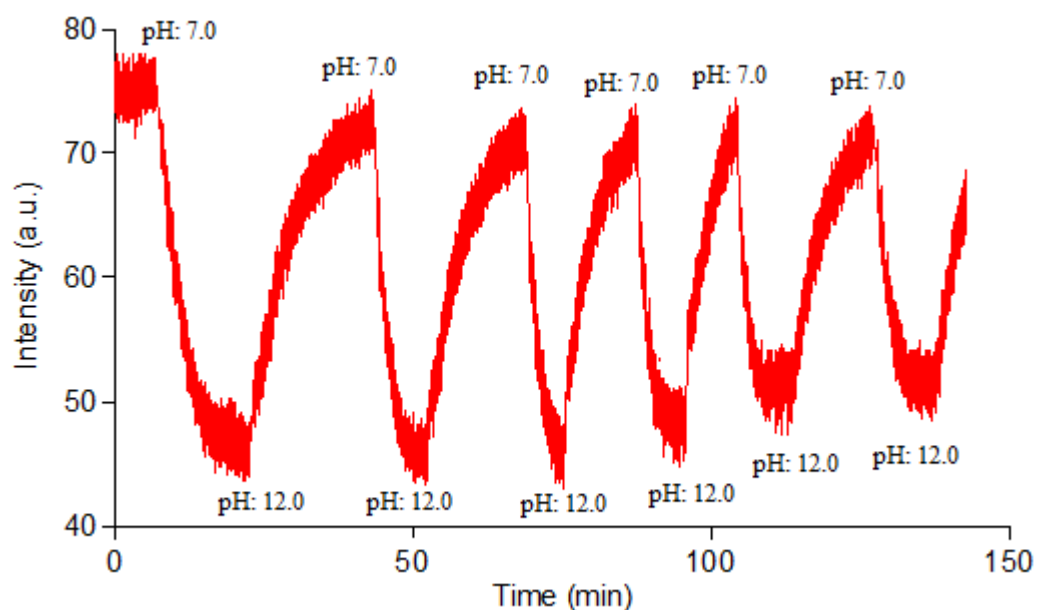


Figure 8.13 Response curve and regeneration performance of EC doped BCDA thin film sensor. Data were acquired with fiber optic probe which is in contact with flow system.

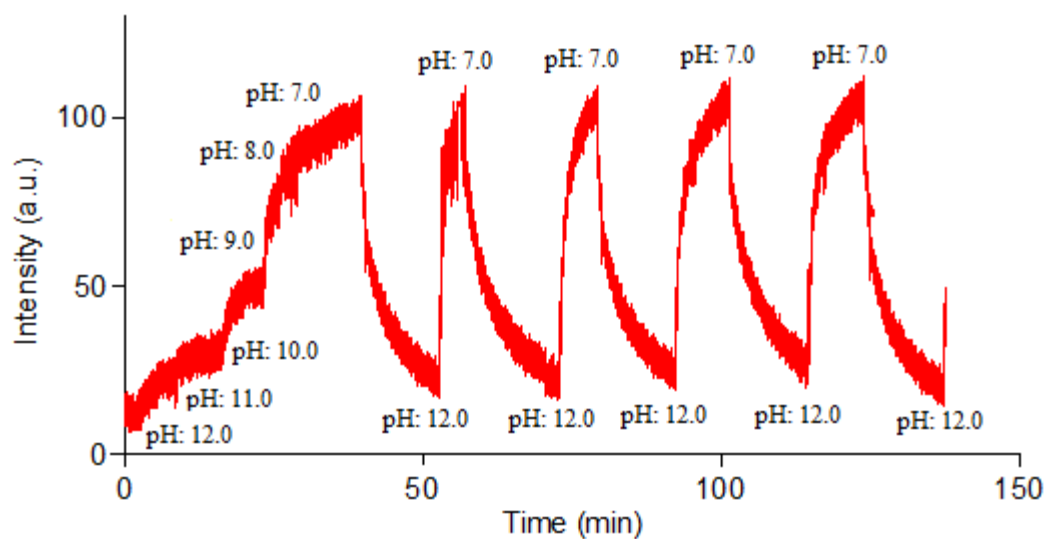


Figure 8.14 Response curve and regeneration performance of EC doped BCDA nanofiber sensor. Data were acquired with fiber optic probe which is in contact with flow system.

8.8 Possible Interference Effects

The cross-sensitivity of the BCDA dye doped EC nanofiber used in this study to many polyvalent metal ions and anions was investigated by exposure to 5×10^{-5} M solutions of Ag^+ , Al^{3+} , Ba^{2+} , Ca^{2+} , Co^{2+} , Cr^{3+} , Cu^{2+} , Fe^{3+} , Fe^{2+} , Hg^{2+} , Li^+ , K^+ , Mn^{2+} , Mg^{2+} , Na^+ , NH_4^+ , Ni^{2+} , Pb^{2+} , Sn^{2+} and Zn^{2+} , H^+ and OH^- . The interference effects of the anions; F^- , Cl^- , Br^- , NO_3^- , NO_2^- , SO_4^{2-} and PO_4^{3-} were also tested. Relative signal changes of less than 5% were observed for EC doped nanofibers at pH 5.5. Figure 8.15 reveals intensity based response of BCDA to the metal cations and anions in acetic acid/acetat buffered solutions at pH 5.5.

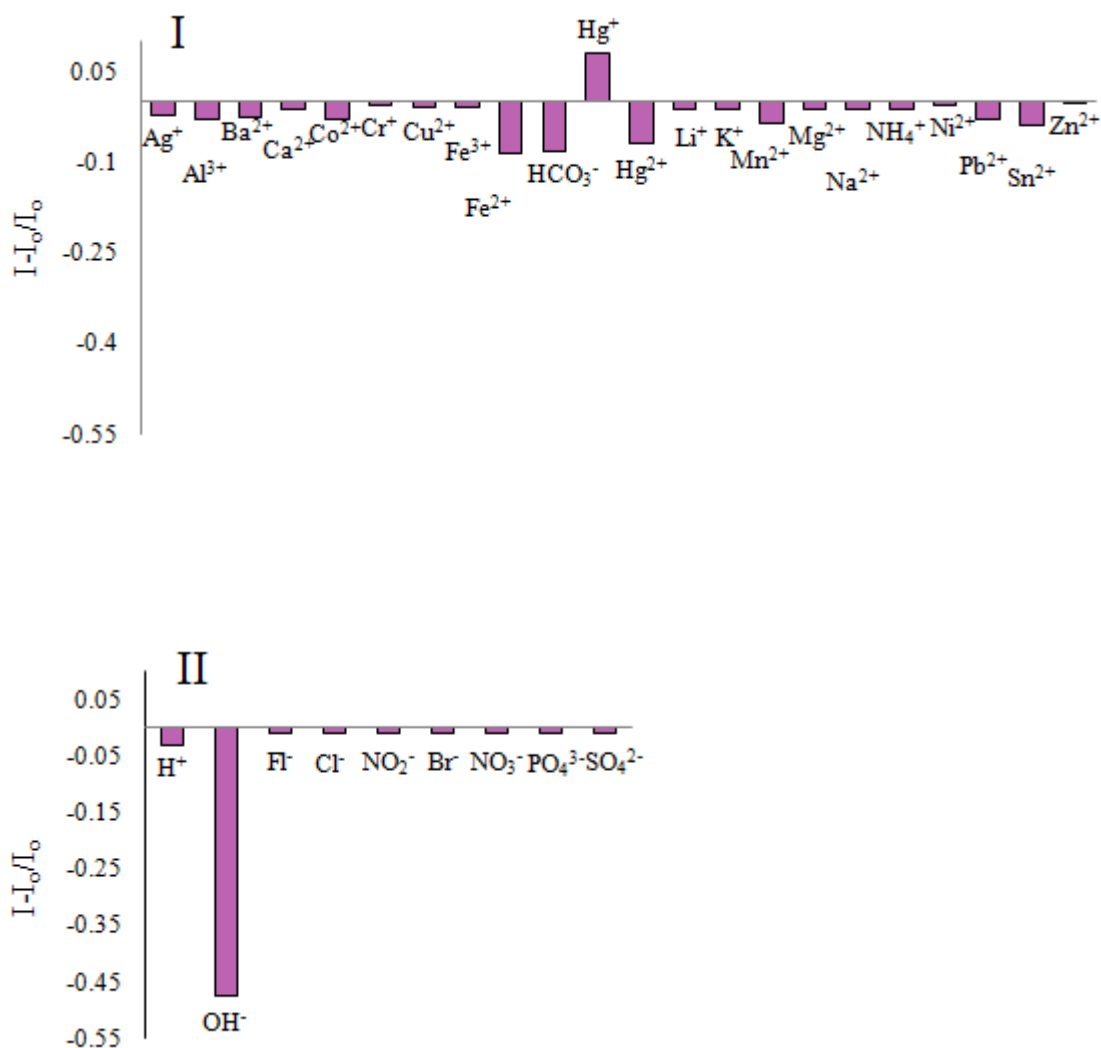


Figure 8.15 (I) Metal ion response of EC based nanofibers at pH 5.5. (II) Anion response of the same composition near neutral solutions.

8.9 Conclusion

There are only a limited number of fluorescence pH indicators available for the high pHs. We demonstrate that, the BCDA dye contain available active centers for proton attacks and are appropriate for use as fluorescent pH probes for alkaline region between pH 7.0–12.0. Response of the BCDA was fully reversible within the dynamic working range. The response times were between 4–14 min. Relative signal changes of 95% and 96% have been achieved for sensor dyes of BCDA. The pK_a value of 9.50 make the BCDA promising indicator dye for gaseous and dissolved

CO₂ sensing in environmental and physiological samples. The compatibility of the employed Schiff bases with the solid-state optical components (in particular LED's emitting in the wavelength range of 550–590 nm and fiber optics) can be useful in construction of inexpensive and field available instrumentation.

CHAPTER NINE

DESIGN OF A NOVEL FLUORESCENT OPTICAL SENSOR USING NANOFIBROUS MEMBRANES FOR Ca (II)

9.1 Introduction

The measurement of ionized calcium continues to be a field of active research, because of the environmental and biological importance. In addition to this, the selective detection of this cation in the presence of others, especially in existence of Mg^{2+} ions, in aqueous environment remains a challenging task.

However, as the concentrations of Ca^{2+} and Mg^{2+} are usually much greater than all other ions in watery samples, and as the selective examination of calcium is difficult and total amount of these two ions has been accepted as hardness, and can be determined by EDTA titrimetric method. The Standard method for the determination of water hardness is compleximetric titration, but is affected by several metal ions, is time-consuming (Cheney, Curran, & Fletcher, 1980).

Atomic absorption spectroscopy (AAS) and recently inductively coupled plasma-optical emission spectrometry (ICP-OES) are also used for the determination of Ca^{2+} and Mg^{2+} ions in water but is difficult, costly and necessarily laboratory based techniques. Ion selective electrodes and UV-vis spectrophotometry based techniques are other alternatives for calcium ion sensing. Spectrofluorometric sensing of Ca^{2+} ions is another good alternative.

Even though, there are most of the proposed chemicals and biological sensors for this ion (Ji, & Rosenzweig, 1999; Cotiis et al., 2008; Blachford, Celic, Petri, & Ehrlich, 2009; He, Jenkins, & Lin, 2008; Citterio et al., 2004; Beging et al. 2010; Vallvey, GaÁlvez, Ramos, & CastanÁeda, 2000) nowadays the design of nanomaterial-based sensors have attracted too much attention.

In this chapter of thesis, we proposed a new method to determine calcium in aqueous environment by the first use of Ethyl Cellulose (EC) based electrospun nanofibers as highly responsive fluorescence optical sensor for the determination of nanomolar levels of Ca (II) ions. DMK-OFD-BIS (2,2'-{1,2-phenylenebis[nitrilomethylylidene]}diphenol) dye was used as chromoionophore in fabrication of Ca (II) sensing nanofibers. Chemical structure of the exploited dye was shown in Figure 9.1.

Ethyl Cellulose based nanofibers, allows a calibration response for Ca (II) ions over a wide concentration range of 1.0×10^{-10} to 1.0×10^{-4} M. It has a response time of ≈ 90 s. The electrospun nanofiber sensors exhibited excellent selectivity for Ca (II) with respect to thin film sensor. It is expected that this high surface area of the nanofibrous membrane structures will provide high sensitivity in sensing applications.

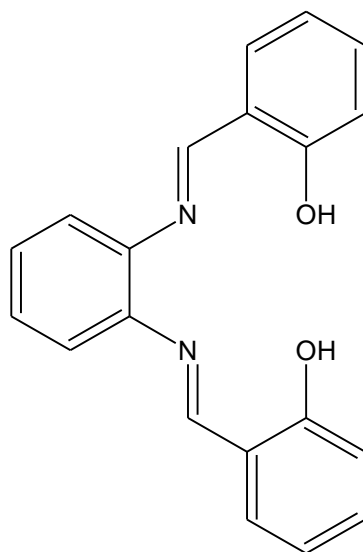


Figure 9.1 Schematic structure of the calcium sensing molecule, DMK-OFD-BIS; 2,2'-{1,2-phenylenebis[nitrilomethylylidene]}diphenol

9.2 Spectral Evaluation of DMK-OFD-BIS Dye and Quantum Yield Calculations

In order to perform spectral evaluation of the DMK-OFD-BIS dye; absorption, excitation and corrected emission spectra were recorded in the solvents of THF, EtOH, DMF, and toluene/ethanol (To: EtOH; 80:20) mixture and in EC matrix. The gathered absorption, excitation and emission spectra of the DMK-OFD-BIS dye were shown in Figure 9.2 and 9.3. Absorption spectra related molar extinction coefficients (ϵ) and maximum absorption wavelengths (λ_{Abs}) of the dye in employed solvents and EC were given in Table 9.1. DMK-OFD-BIS dye exhibited efficient absorbance and high molar extinction coefficients around 330 nm and 375 nm in all of the employed solvents and solid matrices of EC, respectively. Table 9.2 reveal emission based spectral characteristics of DMK-OFD-BIS dye in the employed solvents (EtOH, DMF, THF and To: EtOH) and in EC.

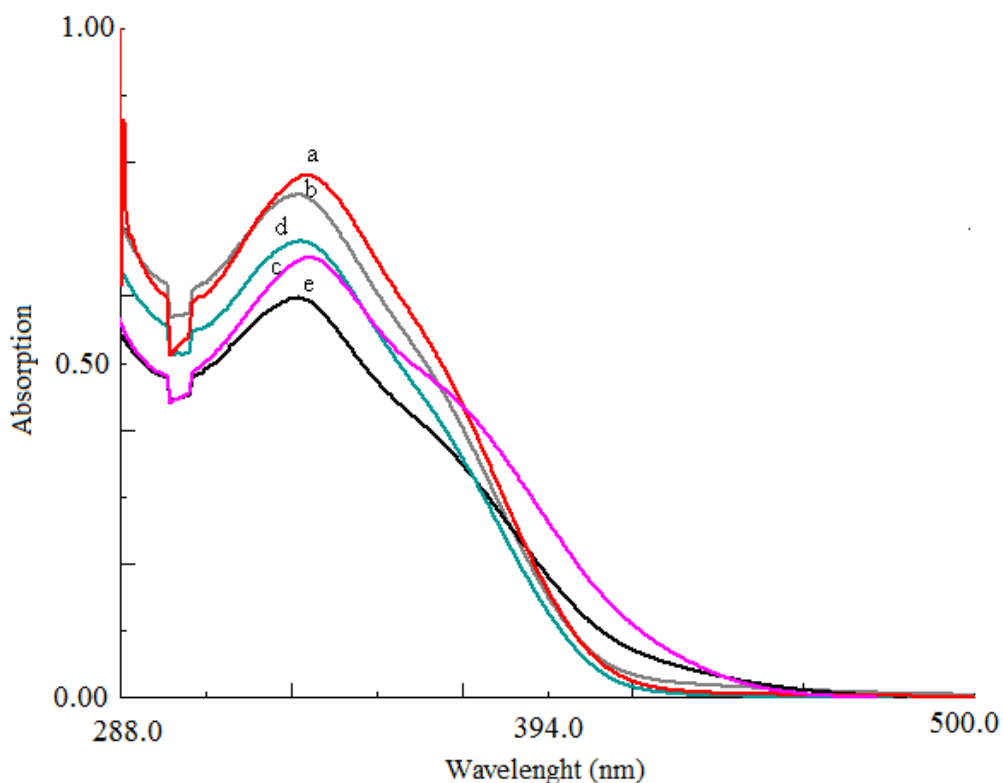


Figure 9.2 Absorption spectra of the DMK-OFD-BIS dye (10^{-6} M dye or 2 mM dye/kg polymer). a) THF b) EtOH c) To: EtOH d) DCM e) DMF

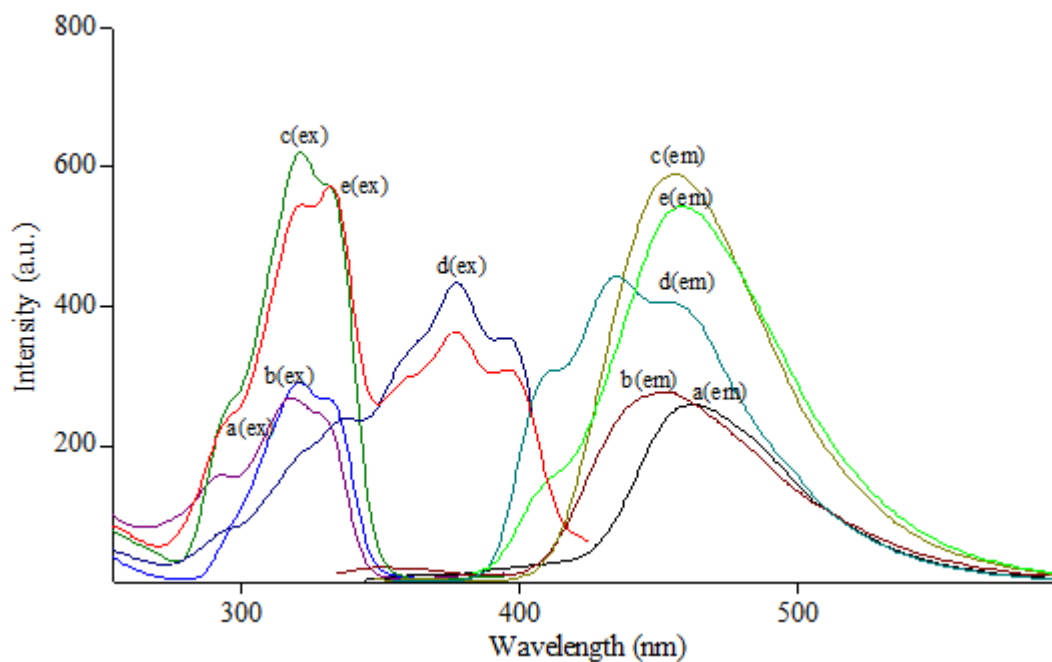


Figure 9.3 Excitation and corrected emission spectra of the DMK-OFD-BIS dye (10^{-6} M dye or 2.5 mmol dye/kg polymer). a) THF b) EtOH c) To: EtOH d) DCM e) DMF

Table 9.1 UV-Vis spectra related data of DMK-OFD-BIS in the solvents of THF, EtOH, To: EtOH (toluene/ ethanol mixture (80:20)), DCM, DMF and in solid matrices of EC.

Compound	Solvent/Matrix	λ_{abs}^1	$\epsilon_{\text{max}} (\lambda_{\text{abs}}^1)$
DMK-OFD-BIS	THF	334	78400
	EtOH	332	75400
	To: EtOH	335	65800
	DCM	333	68200
	DMF	332	60000
	EC	333 / 375	188700 / 117130

Table 9.2 The excitation–emission spectra related characteristics of the DMK-OFD-BIS acquired in conventional solvents, and in thin film form of EC.

Compound	Matrix	λ_{\max}^{em}	λ_{\max}^{ex}	$\Delta\lambda_{ST}$ (Stoke's shift)	ϕ_F (Quantum yield)
DMK-OFD-BIS	THF	460	320	140	0.056 in THF
	EtOH	451	318	133	
	To: EtOH	455	322	133	
	DCM	435	378	57	
	DMF	460	330	130	
	EC	390	325	65	0.30

For calculation of Fluorescence quantum yield (θ_F) of DMK-OFD-BIS dye, which involves the use of well-characterized standards with known (θ_F) values, The comparative William's method was employed. Quinine Sulfate ($\lambda^{ex} = 348$ nm, quantum yield = 0.546 in H_2SO_4) were used as reference standards for DMK-OFD-BIS dye. The integrated fluorescence intensities were plotted versus absorbance for the reference standards, DMK-OFD-BIS. The gradients of the plots were proportional to the quantity of the quantum yield of the studied molecules. Figure 9.4 shows that the integrated fluorescence intensities vs absorbance for the reference standard; Quinine Sulfate, the DMK-OFD-BIS dye in EC and DMK-OFD-BIS dye in THF matrices.

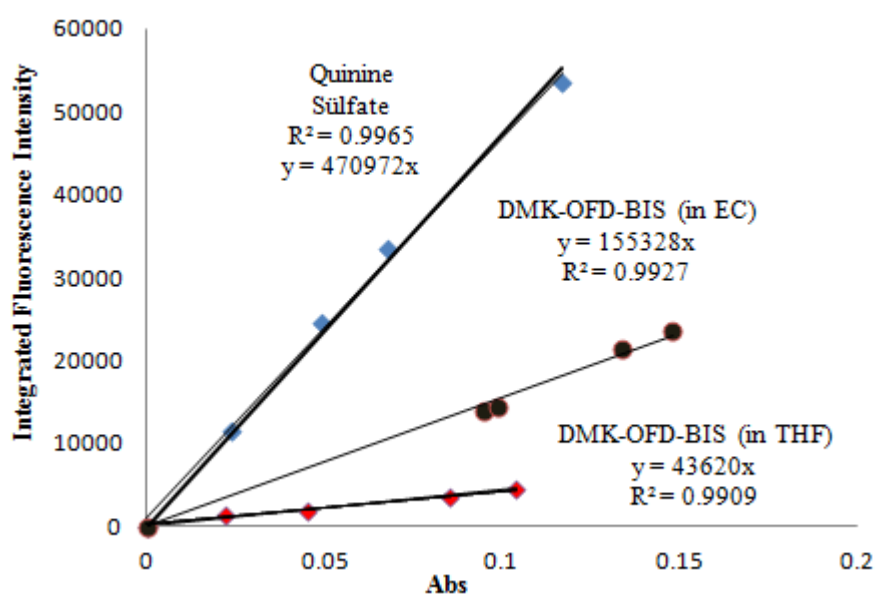


Figure 9.4 The integrated fluorescence intensities vs absorbance for the reference standard; Quinine Sulfate, the DMK-OFD-BIS dye in EC and DMK-OFD-BIS dye in THF matrices.

9.3 pKa Calculations of DMK-OFD-BIS in EC Matrix

The immobilized DMK-OFD-BIS dye responded to H^+ ions in EC matrix. The relative signal change of emission spectra was monitored after addition of certain concentrations of buffered acid solutions at different pH ranges. Figure 9.5 reveals pH induced changes observed in emission spectrum. The immobilized DMK-OFD-BIS dye exhibited the best response to different concentrations of acid solutions between pH=7.0-2.00 in the direction of an increase in signal intensity at 330 and 390 nm and a decrease at 470 nm, respectively. Upon exposure to the solutions between pH 7.0–2.0, the DMK-OFD-BIS dye exhibited a 95% relative signal change (see Figure 9.5-I).

The dye exhibited two different pKa values in immobilized form. The pKa values were calculated as explained earlier and were found to be 3.5 and 6.0 respectively. Figure 9.5 –II reveals to different slopes and corresponding pKa values.

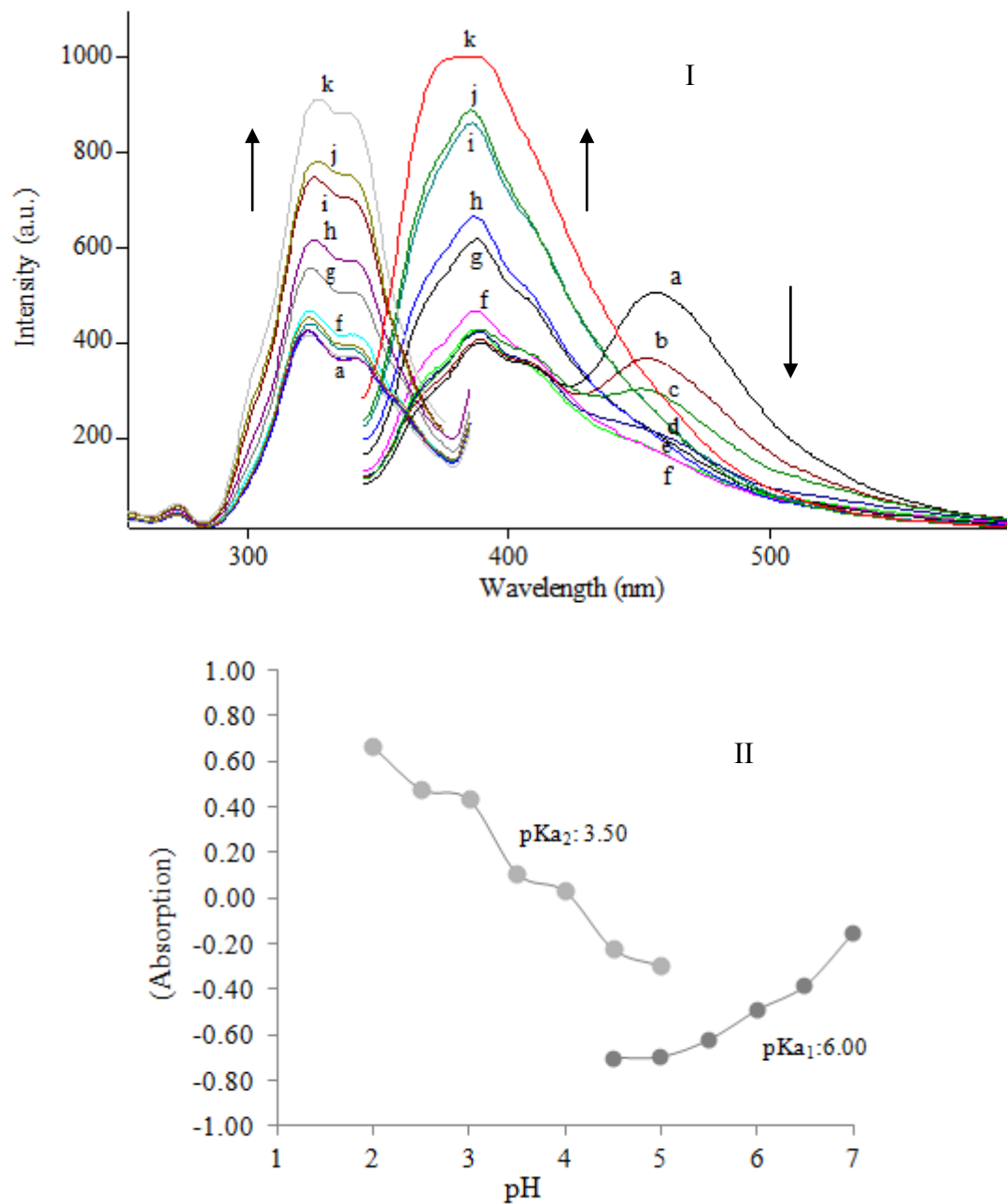


Figure 9.5 pH induced emission characteristics and sigmoidal calibration curve of DMK-OFD-BIS doped EC membrane in the pH range of 7.0–2.0 (a) pH=7.0 (b) pH=6.5 (c) pH= 6.0 (d) pH= 5.5(e) pH= 5.0 (f) pH= 4.5 (g) pH= 4.0 (h) pH= 3.5 (i) pH= 3.0 (j) pH= 2.5 (k) pH= 2.0 ($pK_{a1}=6.00$; $pK_{a2}=3.50$).

9.4 SEM Images of Electrospun Membranes

The SEM images of EC based electrospun membranes at various magnifications are denoted in Figure 9.6. The membrane has a 3-D structure with a random fiber

orientation that is evenly distributed on the substrate. It can be seen from Figure 9.6 that the diameters of the fibers were between 372 and 598 nm.

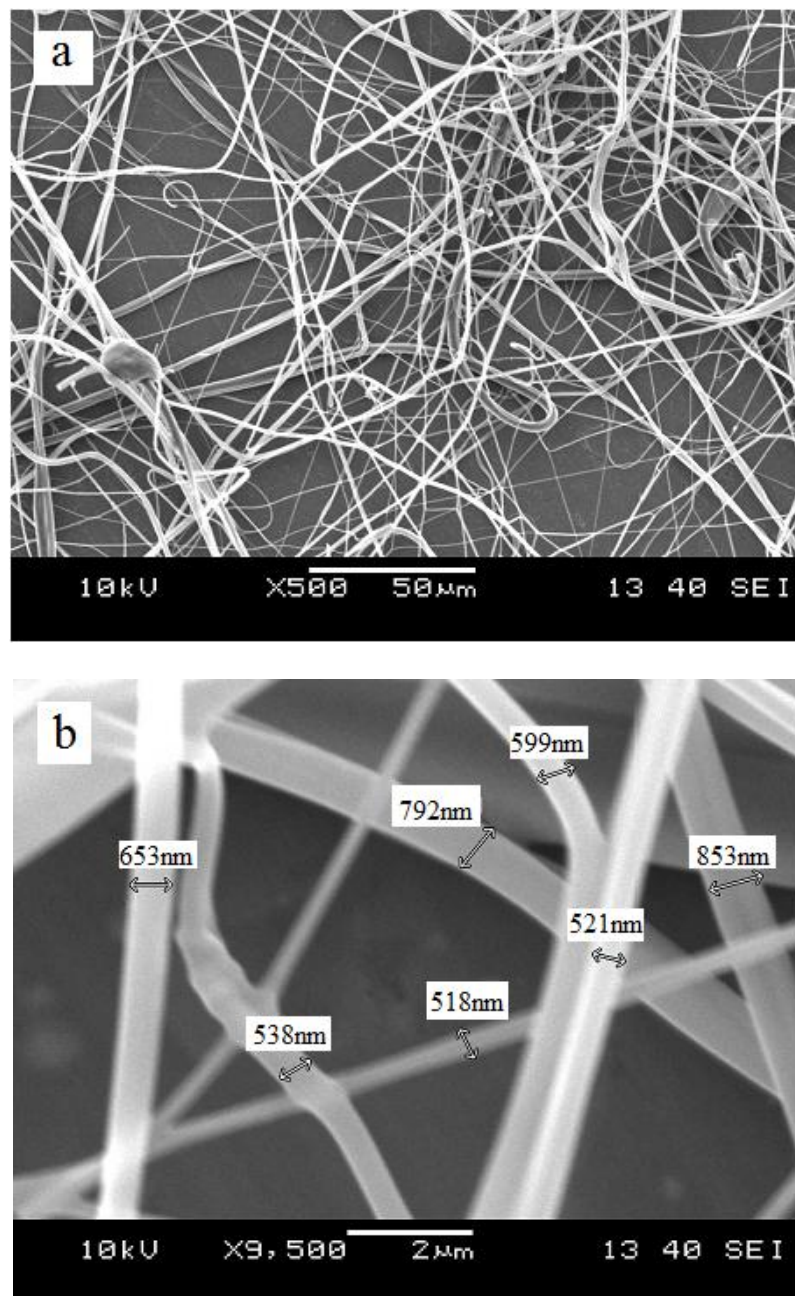


Figure 9.6 SEM images of EC based electrospun nanofibers (a) and (b); EC based nanofibers at different magnifications such as $\times 500$ and $\times 9500$.

9.5 Interference Effects

In order to test the selectivity of the proposed method for calcium ions, the influences of a number of cations were investigated. Interference tests were performed for Ag^+ , Al^{3+} , Ba^{2+} , Ca^{2+} , Co^{2+} , Cr^{3+} , Cu^{2+} , Fe^{3+} , Fe^{2+} , Hg^{2+} , Li^+ , K^+ , Mn^{2+} , Mg^{2+} , Na^+ , NH_4^+ , Ni^{2+} , Pb^{2+} , Sn^{2+} and Zn^{2+} ions in acetic acid/acetate buffer solutions at pH 4.0. From Figure 9.7 I, it can be concluded that, the sensing membrane is capable of determining Calcium ions (Ca^{2+}) with a high selectivity over other cations. The interference effects of the anions; F^- , Cl^- , Br^- , NO_3^- , NO_2^- , SO_4^{2-} and PO_4^{3-} were also tested. Relative signal changes of less than 2% were observed for EC doped films at pH 4.0 (see figure 9.7 - II).

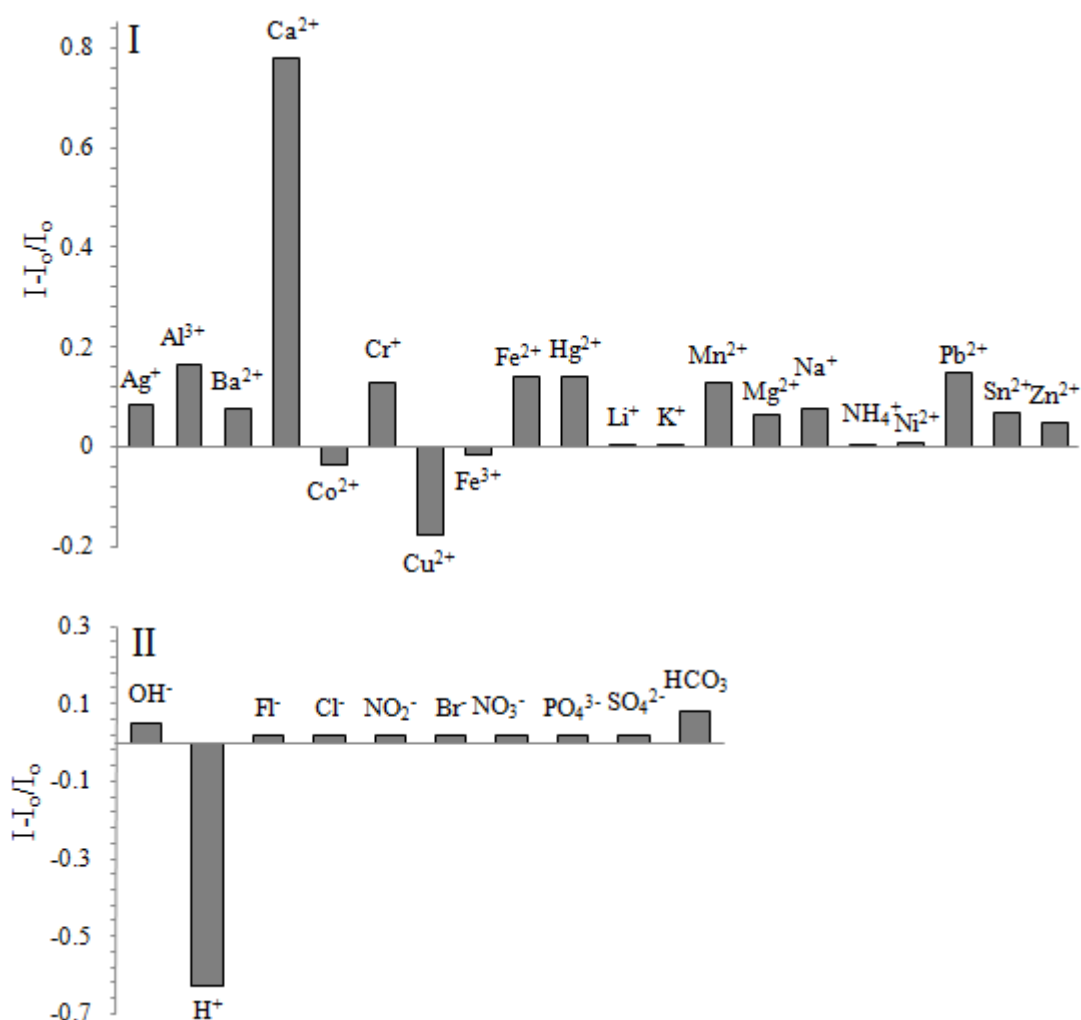


Figure 9.7 **(I)** Metal ion response of EC based nanofibers at pH 4.0. **(II)** Anion response of the same composition near neutral solutions.

9.6 Effect of pH on the Calcium Response

Optimum conditions of pH were investigated separately at constant concentrations of Ca^{2+} ions. Distribution of the Ca^{2+} related chemical species in the working conditions was theoretically checked with chemical equilibrium software programme (Visual MINTEQ) at pH 4.0 in presence of acetate ions. [$\text{CH}_3\text{COO}^-(\text{aq})$: 14.893 %, $\text{CH}_3\text{COOH}(\text{aq})$: 85.107%, $\text{Ca}^{2+}(\text{aq})$; 100%]. Due to the solubility considerations, [Acetate⁻¹, Ca⁺² and H⁺¹; dissolved range 100%] acetic acid/ acetate buffered solutions of pH 4.0 was chosen further studies.

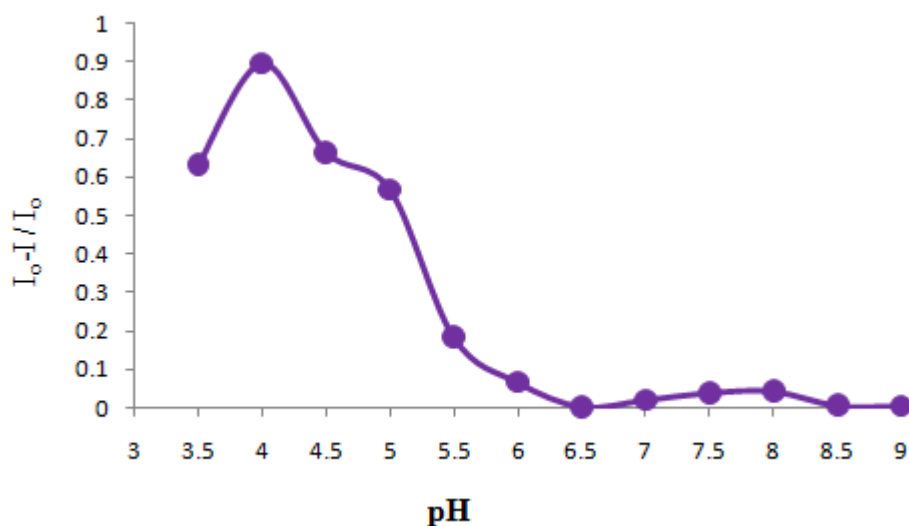


Figure 9.8 pH dependent response of DMK-OFD-BIS dye doped EC membran to Ca (II) at pH 3.5-9.0

9.7 Dynamic Working Range and Ca (II) Response

The dye-doped membrane and/or nanofibers exhibited remarkable fluorescence intensity change upon exposure to Ca^{2+} ions at pH 4.0. Figure 9.9 shows the absorption spectrum of the DMK-OFD-BIS dye in the absence and presence of Ca^{2+} ions. The absorption band around 320 nm exhibited a decrease in signal intensity upon exposure to Ca^{2+} . When the linear shape of the fluorescence intensity based response and absorption spectroscopy related data were evaluated together, the mechanism between DMK-OFD-BIS and Ca (II) can be concluded as “complex formation”.

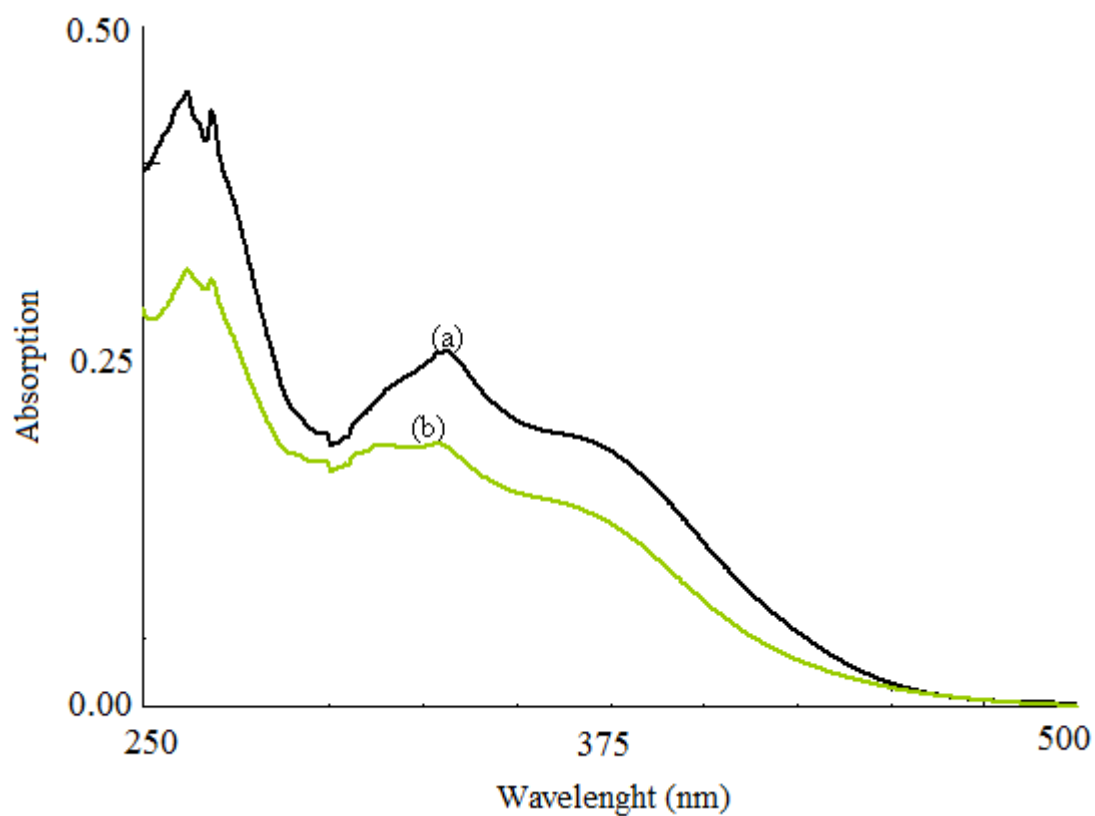


Figure 9.9 Absorption spectrum of the DMK-OFD-BIS dye in ethanol (a) Ca (II) free , (b) in presence of 5×10^{-5} M Ca (II)

Figures 9.10 I / II and 9.11 I / II show the changes in fluorescence spectra of thin film and electrospun materials as a function of different concentrations of calcium ions. The observed intensity increase at 390 nm is known to be due to the complex formation between the DMK-OFD-BIS dye and Ca (II) ions.

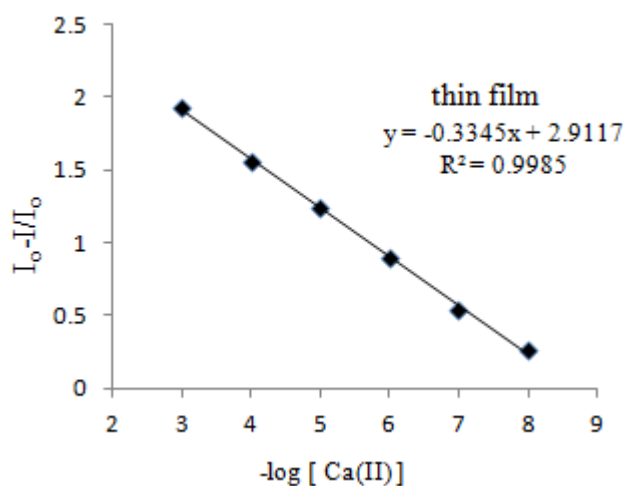
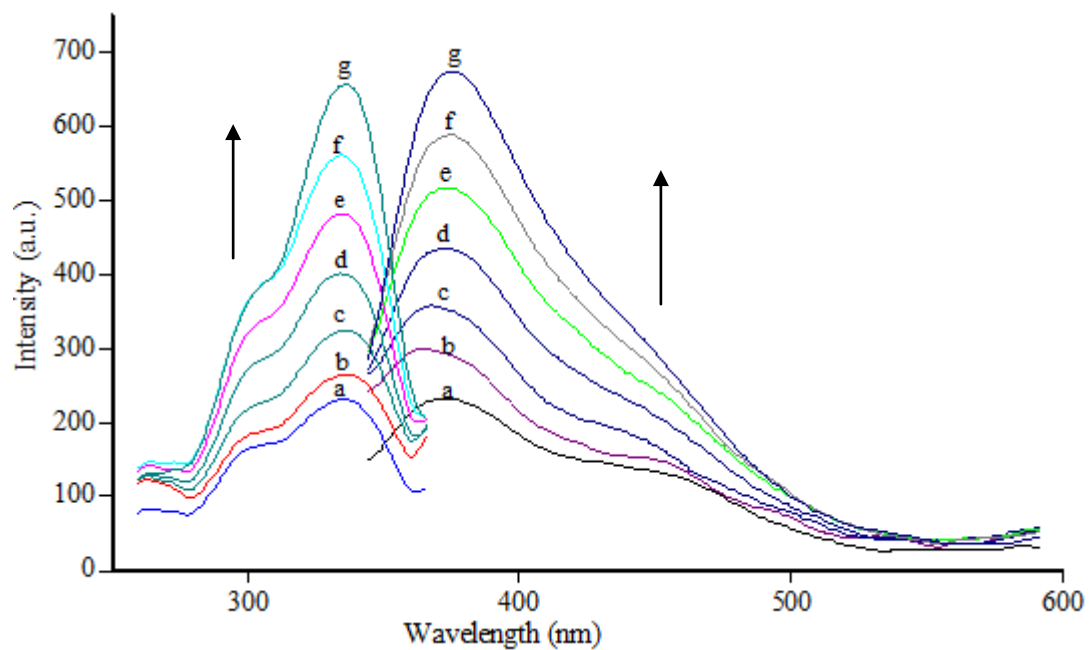


Figure 9.10 Fluorescence response of the DMK-OFD-BIS doped EC based thin film to Ca (II) ions at pH 4.0. (a) Ca-free buffer (b) 1×10^{-8} (c) 1×10^{-7} (d) 1×10^{-6} (e) 1×10^{-5} (f) 1×10^{-4} (g) 1×10^{-3} Mol/L Inset: Calibration plot for the concentration range of 10^{-8} - 10^{-3} M Ca (II). (66% Relative signal change)

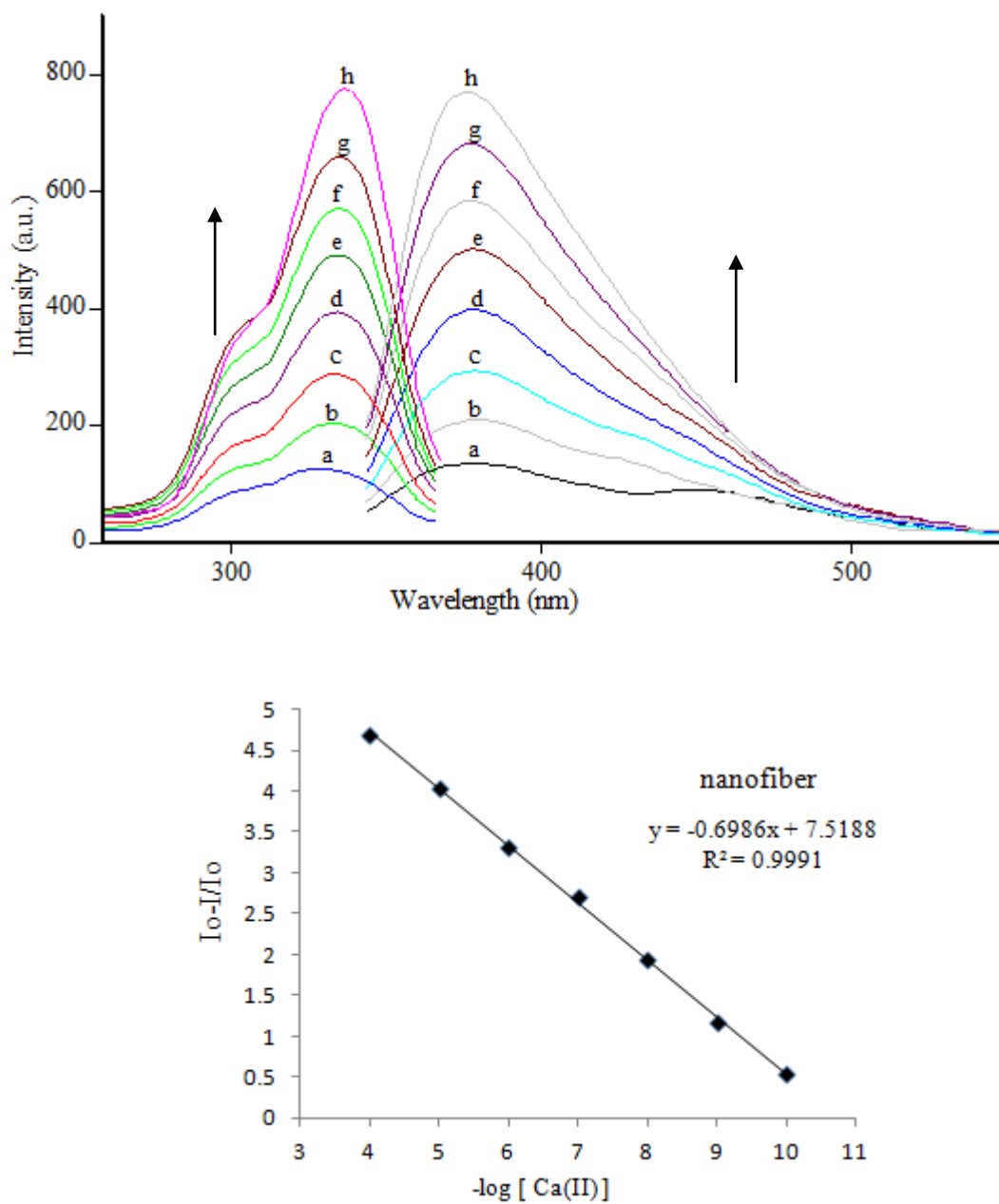


Figure 9.11 Response of the EC based nanofiber to Ca (II) ions at pH 4.0. (a) Ca free b) 1×10^{-10} c) 1×10^{-9} d) 1×10^{-8} e) 1×10^{-7} f) 1×10^{-6} g) 1×10^{-5} h) 1×10^{-4} Mol/L Inset: Linearized calibration plot for the concentration range of 10^{-10} - 10^{-4} M Ca (II).

(83% Relative signal change)

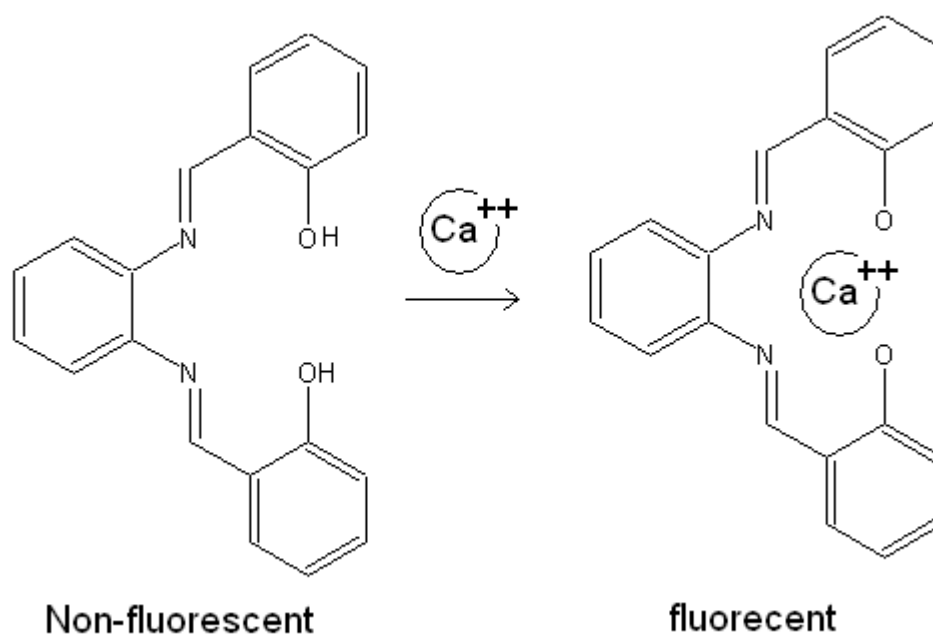


Figure 9.12 Possible interactions between DMK-OFD-BIS dye and Ca (II) ions.

From figure 9.12 it can be concluded that the ionic radius of hydrated Ca ions fit to the cavity of chromoionophore and enhances the conjugation within the molecule upon binding. The selectivity of the ionophore on Ca^{2+} ion over Mg^{2+} can be attributed to this behavior.

The DMK-OFD-BIS doped eletrospun nanofibers demonstrated a linear response over range of 10^{-10} - 10^{-4} M for Ca (II) ions. The tested sensor compositions exhibited large relative signal change, excellent linearity and very good sensitivity to Ca (II) ions. The regression results yielded an absolute linear response with coefficients of regression (R^2) of 0.9991 for EC electrospun nanofibers (See Table 9.3).

The limit of detection (LOD) for Ca^{2+} was defined as the concentration at which the signal is equal to the blank signal plus 3σ and found to be 0.016 nM (1.60×10^{-11} M) for EC based electrospun nanofiber. The detection limits of 1.75 nM were calculated for continuous thin film form of the same compositions (see Table 9.3).

Table 9.3 Calibration related characteristics of EC based electrospun nanofibers and thin films

Indicator Dye	Matrix /Form	Linear Range (Ca(II) Mol/L)	Regression Coefficient (R^2)	LOD (Molar)	LOD (nano molar)
DMK-OFD-BIS	nanofiber	$1.0 \cdot 10^{-10}$ to $1.0 \cdot 10^{-4}$	0.9991	$1.60 \cdot 10^{-11}$ M	0.016
	thin film	$1.0 \cdot 10^{-8}$ to $1.0 \cdot 10^{-3}$	0.9985	$1.75 \cdot 10^{-9}$ M	1.75

The time based response data of the sensor membrane for the determination of Ca^{2+} was acquired in the concentration range from $1.0 \cdot 10^{-10}$ to $1.0 \cdot 10^{-4}$ M (see Figure 9.13).

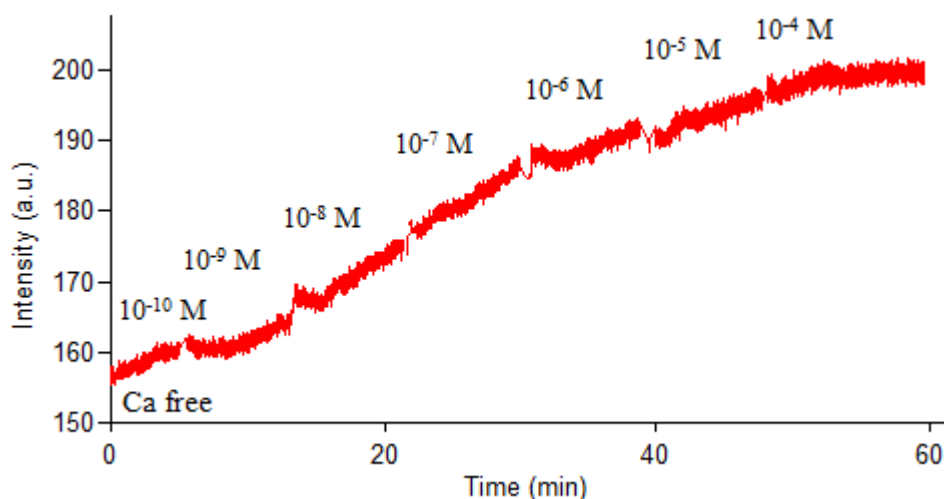


Figure 9.13 Time dependent response of the nanofiber sensor after injection of certain concentration of Ca^{2+} solutions from $1.0 \cdot 10^{-10}$ to $1.0 \cdot 10^{-4}$ M.

9.8 Conclusion

A novel fluorescent optical sensor using electrospun polymeric nanofibrous membrane for the quantitative analysis of Ca (II) ion was presented. Electrospinning was used as a novel and facile method to fabricate optical chemical sensor devices. With respect to continuous thin films, electrospun nanofibers offered enhanced sensitivity, lower LOD values and reactivity in optical chemical sensing of Ca (II).

The DMK-OFD-BIS dye was used for the first time as a fluoroionophore in the optical iron sensing. The DMK-OFD-BIS dye doped nanofibers in EC can be used at pH 4.0 for quantitative determination of Ca (II) in the concentration range of 10^{-10} - 10^{-4} M. A quite good LOD (0.016 nM) was reached.

CHAPTER TEN

A NOVEL FLUORESCENT QUENCHING-BASED Cu (II) NANOSENSOR

10.1 Introduction

Chemical analysis in minimal volumes for copper ion is very important issue in the field of environmental and biological samples. Because, In humans this trace element is third in abundance, after Fe (III) and Zn (II), among the essential heavy metals and is essential in several biological pathways including electron transport, O₂ metabolism and enzymatic catalysis (Barceloux, 1999; Rapisarda, Volentini, Farias, & Massa, 2002).

The detection methods of copper ions in watery samples include spectrophotometric methods, flame (FAAS) or graphite furnace atomic absorption spectroscopy (GFAAS), inductively coupled plasma emission or mass spectrometry (ICP-ES, ICPMS), total reflection X-ray fluorimetry (TXRF) and anodic stripping voltammetry (ASV) (Förstner, & Wittmann, 1981; Fresenius, Quentin, & Schneider, 1988, Klockenkampfer, 1997; Merian, 1991). However, only some of them have found application in routine analysis. Detection limits for copper in watery samples are 10⁻⁷ and 10⁻¹⁴ M for FAAS and GFAAS respectively. The GFAAS offers good limits of detection, but is an expensive and difficult method. Recently the chemical optical sensors combined with fiber optic systems became popular as small and inexpensive devices that can enable on-line and field monitoring. On the other hand, their selectivity and detection limits have to be developed so the synthesis of new probes selective to copper ions with lower detection limits and wide response concentration range is of great importance.

Mayr, Klimant, Wolfbeis, & Werner (2002) offered a dual lifetime referenced optical sensor membrane for the determination of copper (II) ions. The dual lifetime referencing system uses the indicator lucifer yellow and an inert reference luminophore; a ruthenium complex entrapped in polyacrylonitrile beads.

Mahendra, Gangaiya, Sotheeswaran, & Naratanaswamy (2002) offered a fiber optic sensor for Cu (II) based on the use of fast sulphon black F (FSBF) immobilized onto XAD-7 (methyl methacrylate copolymer). They obtained a linear response to the Cu(II) in the concentration range of 11–127 ppm at pH 9.5 with a reflectance spectrometry.

Yeh, Tien, & Chau (2001) was constructed A fiber optic evanescent-wave absorption sensor. They doped the propyl-ethylenediamine triacetate (PEDTA) with the sol-gel processing into anorganofunctional silicon alkoxide. The sensor worked in a dynamic range of 0.5–100 ppm and exhibited a detection limit of 56 ppb for Cu(II).

Malcik, Caglar, Narayanaswamy, & Quim (2000) offered optical Cu (II) ion sensors, based on several reagents such as 1-nitroso-2-naphthol (NN), 2,4-dinitrosoresorcinol (DNR), 4-(2-pyridylazo)resorcinol (PAR), 1-(2-pyridylazo)-2-naphthol (PAN), immobilized on a variety of polymeric materials such as XAD-4, XAD-7 and Dowex resin.

Thompson, Ge, Patchan, Huang, Fierke (1996) introduced a fiber optic biosensor for Co(II) and Cu(II) based on fluorescence energy transfer with an enzyme transducer, carbonic anhydrase. The non-specific photometric metal ion indicator pyrocatechol violet (PV) was modified with tetraoctylammonium cation and immobilized in a plasticized PVC membrane by Steinberg et al. After an exposure time of 10 min they measured the Cu(II) in the concentration range of 1–100 M with absorption spectrophotometry (Steinberg, Lobnik, & Wolfbeis, 2003). The copper sensitive phenanthroline-based Phen Green FL indicator which has been commercialized by Molecular Probes™ Invitrogen Detection Technologies, is a general purpose heavy metal sensor capable of detecting a broad range of metal ions, including both Cu^{2+} and Cu^+ (Chavez, Garrido, & Ahearn, 2001; Kuhn, Hoyland, Carter, Zhang, & Haugland, 1995).

Fluorescence based sensors are powerful techniques and has many advantages as small and inexpensive devices that can enable on-line and field monitoring for the measurement of copper ion concentrations (Cano-Raya, Capit'an-Vallvey, & Fern'andez-Ramos, 2006; Oter, Ertekin, Kirilmis, & Koca, 2006; Rapisarda, Volentini, Farias, & Massa, 2002; Cody, & Fahrni; 2004; Dumas, Grabchev, Stoikova, Chauvin, & Chovelon, 2009; Kim, & Choi, 2001).

Additionally, development of new approaches toward highly sensitive sensors with lower detection limits and wide response concentration ranges has still great importance. For this purpose, researchers working for miniaturization attempts and nanoscale structures allowed improvements in functionality, sensitivity, and low response time of the sensors.

Here, we designed a novel optical chemical nanosensor using electrospinning technique and then combined with fiber optic systems that allow the determination of picomolar of Cu (II) ions. Additionally, we used this combination for the first time for copper sensing. Ethyl Cellulose based nanofibers together with chromoionophore acted as highly sensitive copper probe and displayed a calibration response for Cu (II) ions over a wide concentration range of 5.0×10^{-12} to 5.0×10^{-5} M. It has a response time of ≈ 90 s. The electrospun nanofiber sensors exhibited excellent selectivity and sensitivity for Cu (II) with respect to thin film sensor. It is expected that this high surface area of the nanofibrous membrane structures will provide high sensitivity in sensing applications. Figure 10.1 shows chemical structure of the exploited dye for copper ion sensing in EC.

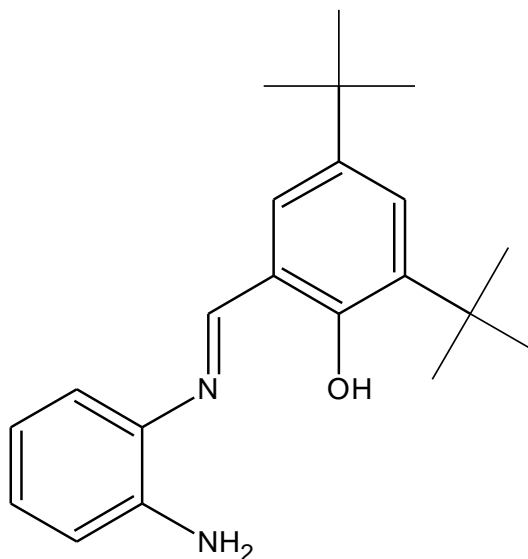


Figure 10.1 Structure of copper sensing fluoroionophore; DMK-OFD-7; 2-[[2-aminophenyl]imino]methyl]-4,6-di-*tert*-butylphenol

10.2 Spectral Evaluation of the DMK-OFD-7 Dye

In order to spectral characterization of the DMK-OFD-7; absorption, excitation and emission spectra were examined in the solvents of THF, EtOH, DCM, DMF, and toluene/ethanol (To: EtOH; 80:20) mixture and in EC matrix. The gathered absorption and excitation-emission spectra of the DMK-OFD-7 were shown in Figure 10.2 and 10.3.

Absorption spectra related molar extinction coefficients (ϵ) and absorption maxima (λ_{Abs}) of the dye in the employed solvents and EC were given in Table 10.1. DMK-OFD-7 dye exhibited efficient absorbance, high Stoke's shift (160 in EC) and high molar extinction coefficients around 340-380 nm in all of the employed solvents and solid matrix of EC, respectively. Table 10.2 reveals emission based spectral characteristics of DMK-OFD-7 in the employed solvents (EtOH, DMF, DCM, THF and To: EtOH) and in EC.

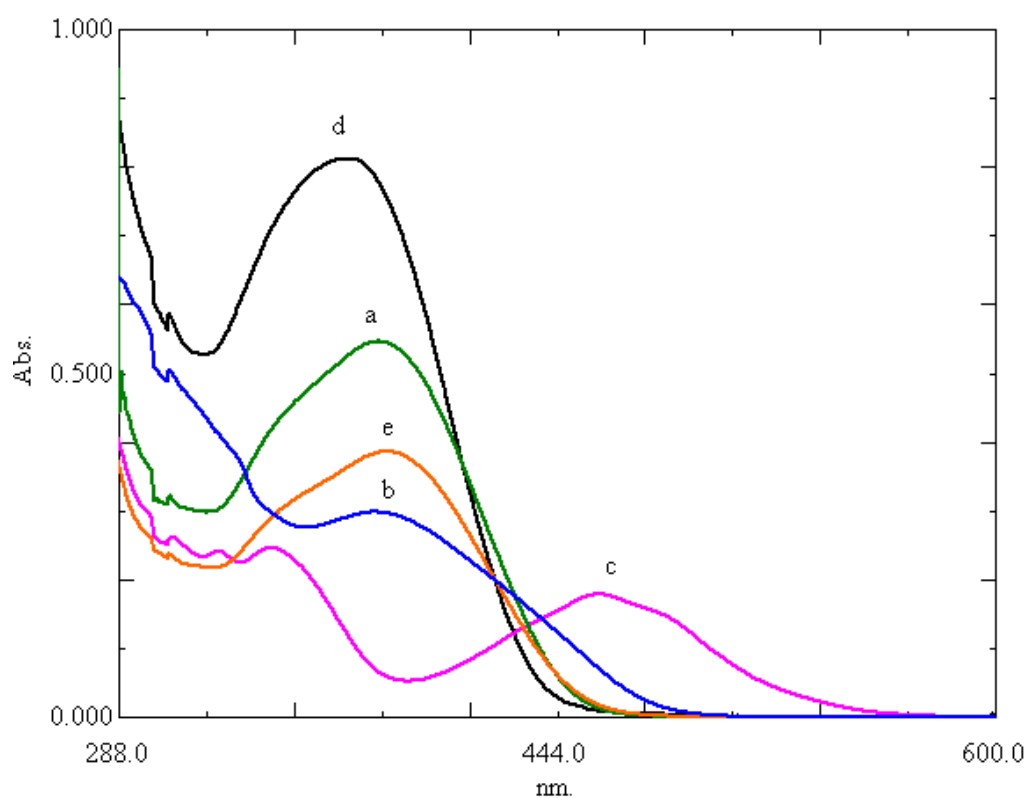


Figure 10.2 Absorption spectra of the DMK-OFD-7 dye (10^{-6} M dye or 2 mM dye/kg polymer). a) THF b) EtOH c) To: EtOH d) DCM e) DMF

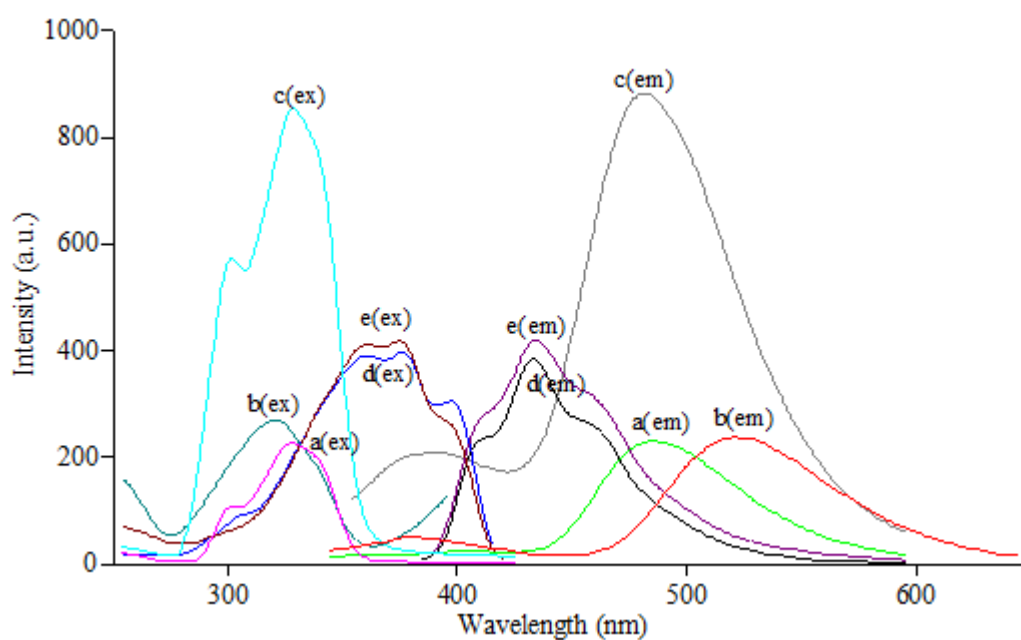


Figure 10.3 Excitation and corrected emission spectra of the DMK-OFD-7 dye (10^{-6} M dye or 2.5 mmol dye/kg polymer). a) THF b) EtOH c) To: EtOH d) DCM e) DMF

Table 10.1 UV-Vis spectra related data of DMK-OFD-7 in the solvents of THF, EtOH, To: EtOH (toluene/ ethanol mixture (80:20)), DCM, DMF and in solid matrices of EC.

Compound	Solvent/Matrix	$\lambda^1_{\text{abs(nm)}}$	$\epsilon_{\text{max}}(\lambda^1_{\text{abs}})$
DMK-OFD-7	THF	381	55000
	EtOH	380	30100
	To: EtOH	343	25100
	DCM	370	81500
	DMF	384	39000
	EC	340	190000

Table 10.2 Spectral characterization of DMK-OFD-7 dyes. $\lambda^{\text{em}}_{\text{max}}$: maximum emission wavelength in nm; $\lambda^{\text{ex}}_{\text{max}}$: maximum excitation wavelength in nm; $\Delta\lambda_{ST}$: Stoke's shift and ϕ_F : Quantum yield

Compound	Solvent/Matrix	$\lambda^{\text{em}}_{\text{max}}$	$\lambda^{\text{ex}}_{\text{max}}$	$\Delta\lambda_{ST}$ (Stoke's shift)	ϕ_F (Quantum yield)
DMK-OFD-7	THF	490	330	160	9.0×10^{-2} in THF
	EtOH	520	330	190	
	To: EtOH	480	328	152	
	DCM	430	370	60	
	DMF	435	375	60	
	EC	490	330	160	0.14

10.3 Calculation of Fluorescence quantum yield (θ_F)

The comparative William's method was employed for calculation of fluorescence quantum yield (θ_F) of DMK-OFD-7 dye, which involves the use of well-

characterized standards with known (θ_F) values. For this purpose, the UV-vis absorbance and corrected emission spectra of different concentrations of reference standards and samples were recorded. In solution phase studies, Quinine Sulfate ($\lambda^{\text{ex}} = 348 \text{ nm}$, quantum yield = 0.546 in H_2SO_4) were used as reference standard for DMK-OFD-7. The integrated fluorescence intensities were plotted versus absorbance for the reference standards, and DMK-OFD-7. The gradients of the plots were proportional to the quantity of the quantum yield of the studied molecules.

Quantum yield (θ_F) values were calculated according to the following equation where ST and X denote standard and sample, respectively. Grad is the gradient of the plot and n is the refractive index of the solvent or polymer matrix material.

$$\theta_F = \theta_{\text{ST}} (\text{Grad}_X / \text{Grad}_{\text{ST}}) (n_x^2 / n_{\text{ST}}^2)$$

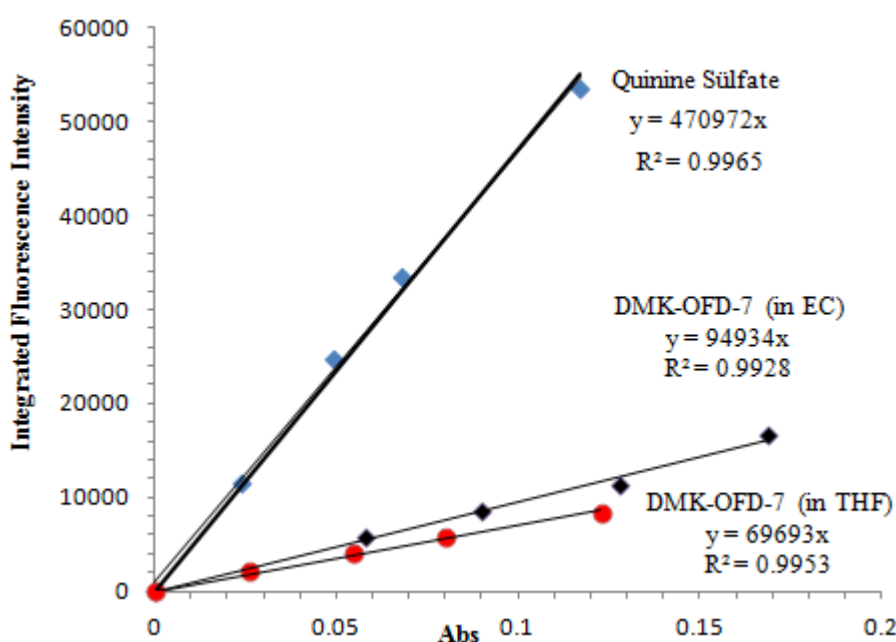


Figure 10.4 The integrated fluorescence intensities vs absorbance values of Quinine Sulfate in H_2SO_4 , DMK-OFD-7 dye in EC and DMK-OFD-7 dye in THF.

10.4 pKa Calculations of DMK-OFD-7 in EC Matrix

The immobilized DMK-OFD-7 dye reversibly responded to H^+ ions in EC. The relative signal change of emission spectra of the DMK-OFD-7 was monitored after

addition of certain concentrations of buffered acid solutions at different pH ranges. pH induced emission spectra of DMK-OFD-7 doped EC in the pH range of 7.00-2.00 was shown in Figure 10.5.

The pKa value of the indicator immobilized in EC thin films is calculated to be pKa= 3.75 by using non-linear fitting algorithm of Gauss-Newton-Marquardt method (Mills, & Chang, 1992).

$$\text{pKa} = \text{pH} + \log [(I_x - I_b)/(I_a - I_x)] \quad (4.1)$$

where I_a and I_b are the intensities of acidic and basic forms and I_x is the intensity at a pH near to the pKa.

$$\text{pKa} = 4.0 + \log[(380-481)/(199-380)]$$

$$\text{pKa} = 4.0 + \log [0.56]$$

$$\text{pKa} = 3.75 \quad (\text{for indicator immobilized EC})$$

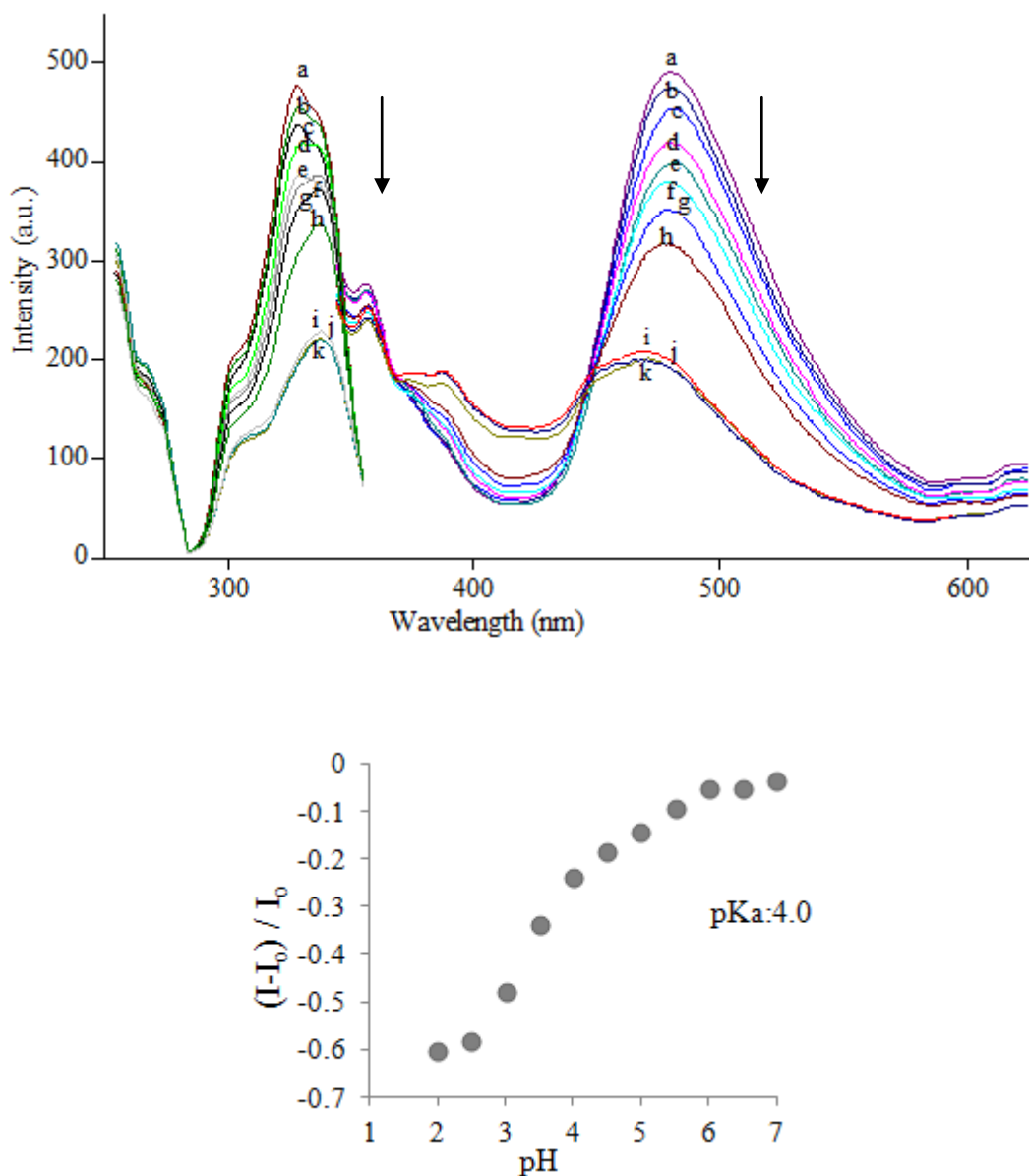


Figure 10.5 pH induced emission based spectral response of DMK-OFD-7 in EC matrix after addition of acidic solutions in the pH range of 7.00-2.00 pH: a) 7.00 b) 6.50 c) 6.00 d) 5.50 e) 5.00 f) 4.50 g) 4.00 h) 3.50 i) 3.00 j) 2.50 k) 2.00

10.5 Photostability Study

The short time photostability performance of DMK-OFD-7 dye doped EC electrospun nanofiber was checked with a steady-state spectrofluorimeter in time-based mode. Molecule was excited at 330 nm. The data were acquired at emission maximum of the dye; 475 nm during 40 minutes of monitoring. In the employed media the dye exhibited excellent short-term photostability. Figure 10.6 reveals performance of the dye doped EC based electrospun nanofibers.

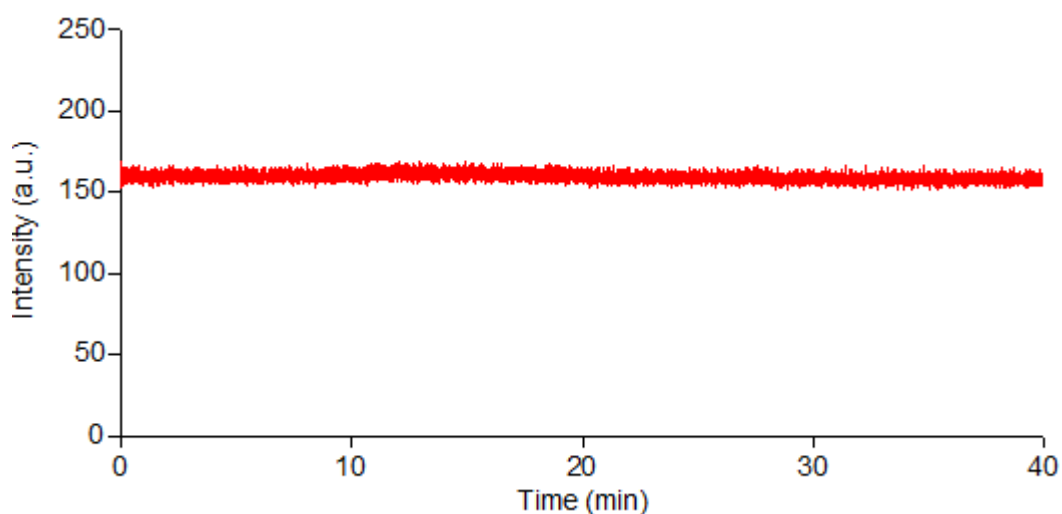


Figure 10.6 The photostability test of DMK-OFD-7 dye doped EC based electrospun nanofiber.

10.6 Investigation of Interference Effects

In order to investigate the selectivity and interference effects of the proposed method, the influence of a number of cations were examined. Tests were performed for Ag^+ , Al^{3+} , Ba^{2+} , Ca^{2+} , Co^{2+} , Cr^{3+} , Cu^{2+} , Fe^{3+} , Fe^{2+} , Hg^{2+} , Li^+ , K^+ , Mn^{2+} , Mg^{2+} , Na^+ , NH_4^+ , Ni^{2+} , Pb^{2+} , Sn^{2+} and Zn^{2+} ions in acetic acid/acetate buffer solutions at pH 5.5. From Figure 10.7 I, it can be concluded that, the sensing membrane is capable of determining Copper ions (Cu^{2+}) with a high selectivity over other ions. The interference effects of the anions; F^- , Cl^- , Br^- , NO_3^- , NO_2^- , SO_4^{2-} and PO_4^{3-} were also tested. Relative signal changes of less than 2% were observed for EC doped films at pH 5.5 (see figure 10.7 II).

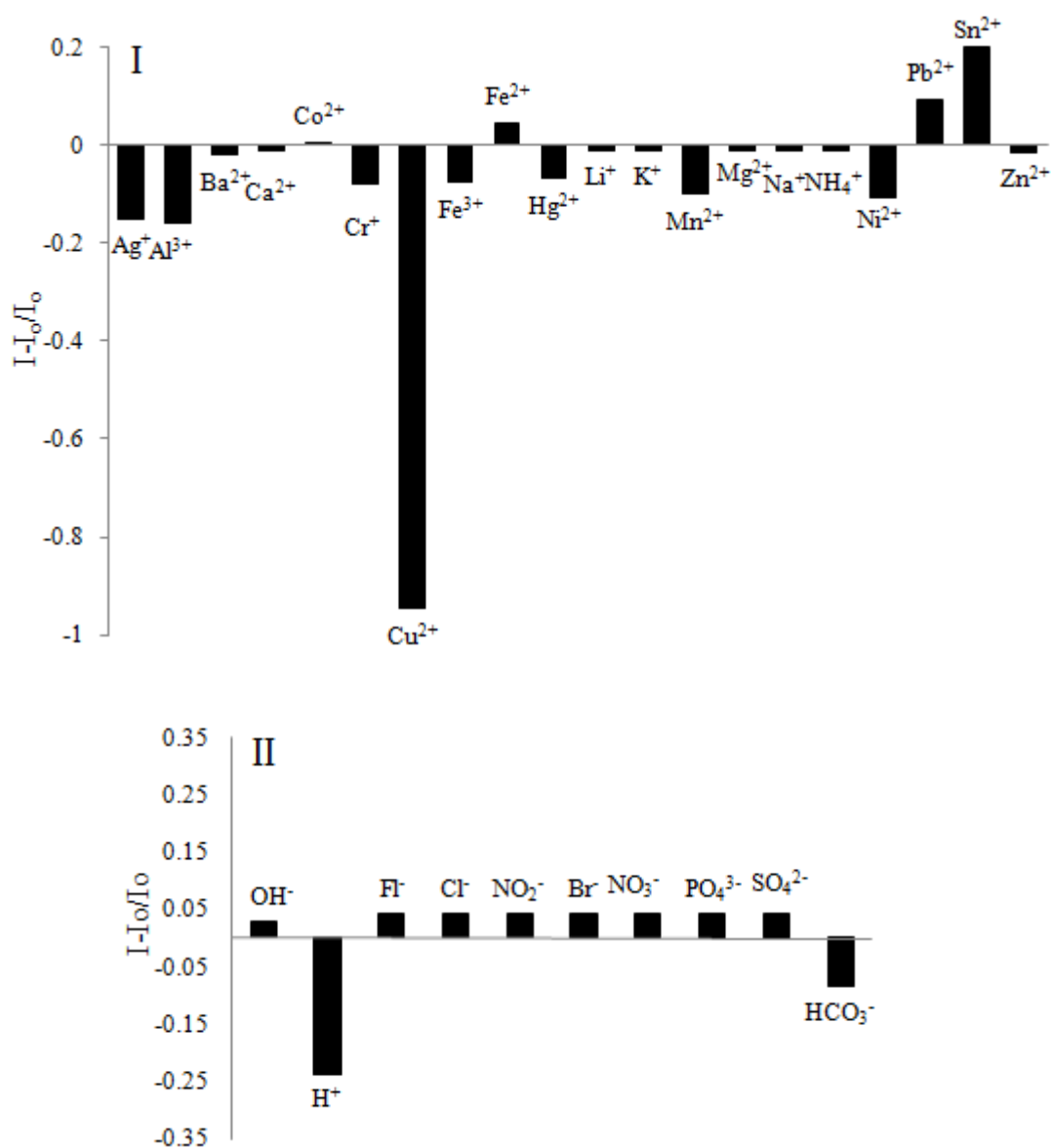


Figure 10.7 (I) Metal ion response of EC based nanofibers at pH 5.5. (II) Anion response of the same composition near neutral solutions.

10.7 Effect of pH on the Copper Response

For specification, pH effect was investigated at different pH values for constant concentrations of Cu²⁺ ions. Figure 10.8 shows pH dependent response of DMK-OFD-7 dye to Cu (II) between pH 3.5-8.0. Distribution of the Cu²⁺ related chemical species in the working conditions was theoretically checked with chemical equilibrium software programme (Visual MINTEQ) at pH 5.5 in presence of acetate ions. [(CH₃COO⁻(aq): 84.713 %, CH₃COOH (aq): 15.287%, Cu²⁺ (aq); 99.007%,

$\text{CuOH}^+(\text{aq})$; 0.993%, Due to the solubility considerations, [Acetate⁻¹, Cu⁺² and H⁺¹; dissolved range 100%] acetic acid/ acetate buffered solutions of pH 5.5 was chosen further studies.

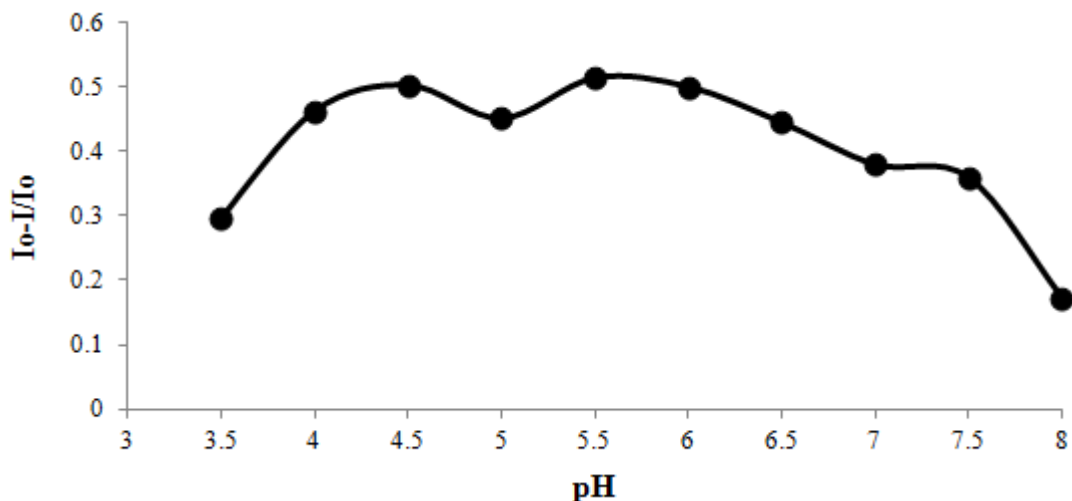


Figure 10.8 pH dependent response of DMK-OFD-7 dye doped EC membrane to Cu (II) at pH 3.5-8.0

10.8 Dynamic Working Range and Cu (II) Response

If doped into modified EC matrices along with the anionic additive; potassium tetrakis- (4-chlorophenyl) borate; the DMK-OFD-7 dye becomes a Cu (II) selective probe. In this system, Cu (II) ions are extracted into the polymer phase by the anionic additive simultaneously two of potassium ions diffuse from the membrane into the aqueous phase via the mechanism of ionexchange due to the electroneutrality consideration. Physical aspect of the ion-exchange pathway can be explained by the following equation.

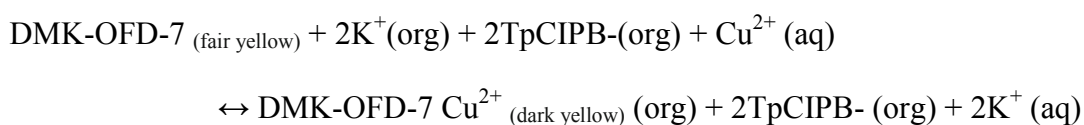


Figure 10.9 shows the absorption spectrum of the DMK-OFD-7 dye in the absence and presence of Cu²⁺ ions in EtOH. The absorption band around 340 nm to turn 435 nm exhibited a dramatic increase in signal intensity upon exposure to Cu²⁺.

Figure 10.10 I / II and 10.11 I / II shows the change in fluorescence spectra of thin film and electrospun materials as a function of different concentrations of copper ions. When the linear shape of the fluorescence intensity based response and absorption spectroscopy related data were evaluated together, the mechanism between DMK-OFD-7 and Cu (II) can be concluded as quenching of the DMK-OFD-7 dye by Cu (II) ions.

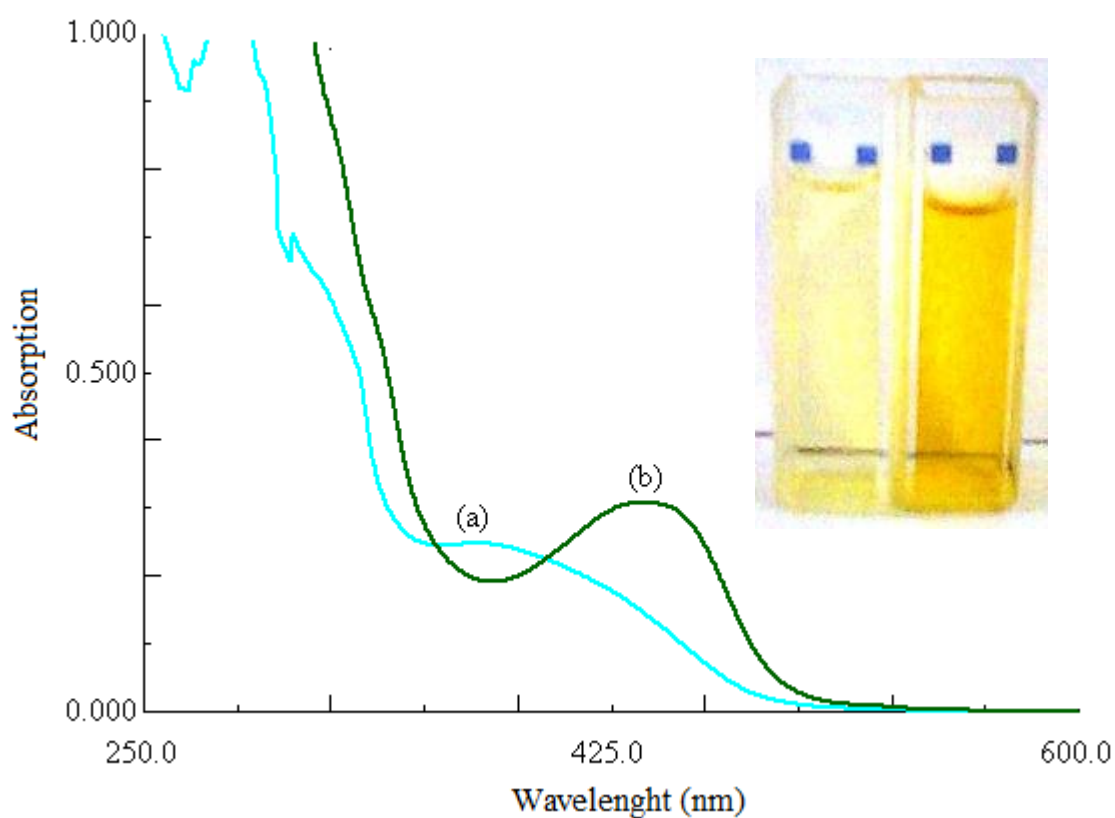


Figure 10.9 Absorption spectrum of the DMK-OFD-7 dye in ethanol (a) Cu (II) free , (b) in presence of 5×10^{-5} M Cu (II)

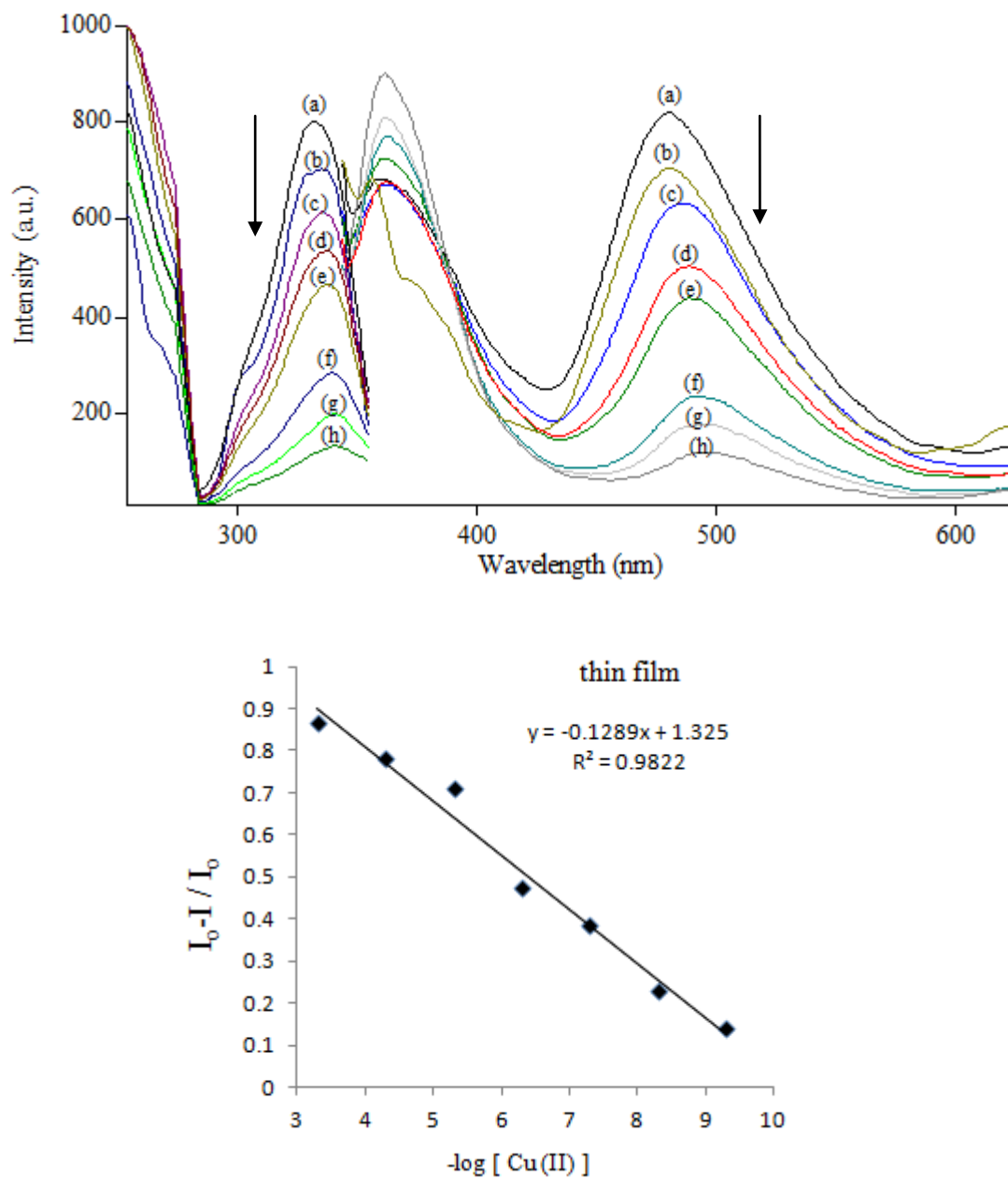


Figure 10.10 Fluorescence response of the DMK-OFD-7 doped EC based thin film to Cu (II) ions at pH 5.5. (a) Cu-free buffer (b) 5×10^{-10} (c) 5×10^{-9} (d) 5×10^{-8} (e) 5×10^{-7} (f) 5×10^{-6} (g) 5×10^{-5} (h) 5×10^{-4} Mol/L Inset: Calibration plot for the concentration range of 5×10^{-10} - 10^{-4} M Cu (II). (84% Relative signal change)

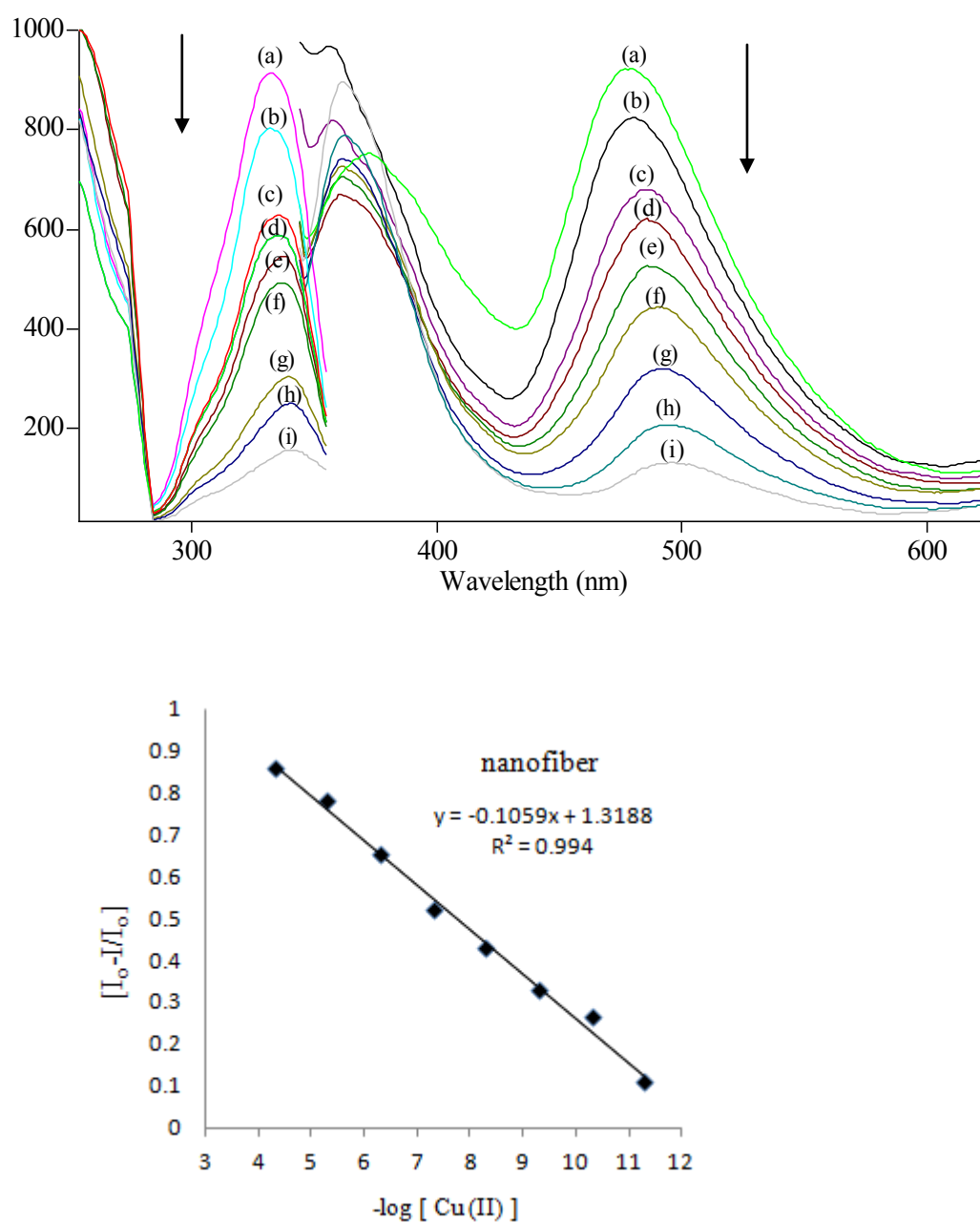


Figure 10.11 Response of the EC based nanofiber to Cu (II) ions at pH 5.5. (a) Cu free b) 5×10^{-12} c) 5×10^{-11} d) 5×10^{-10} e) 5×10^{-9} f) 5×10^{-8} g) 5×10^{-7} h) 5×10^{-6} i) 5×10^{-5} Mol/L Inset: Linearized calibration plot for the concentration range of 5×10^{-12} - 5×10^{-5} M Cu (II). (86% Relative signal change)

The DMK-OFD-7 doped eletrospun nanofibers demonstrated a linear response over range of 5×10^{-12} - 5×10^{-5} M for Cu (II) ions. The tested sensor compositions exhibited large relative signal change, excellent linearity and very good sensitivity to

Cu (II) ions. The regression results yielded an absolute linear response with coefficients of regression (R^2) of 0.9940 for EC electrospun nanofibers (See Table 10.3). The limit of detection (LOD) for Cu^{2+} was defined as the concentration at which the signal is equal to the blank signal plus 3σ and found to be 0.33 pM (3.30×10^{-13} M) for EC based electrospun nanofiber. The detection limits of 46 pM were calculated for continuous thin film form of the same compositions (See Table 10.3).

Table 10.3 Calibration characteristics of EC based electrospun nanofibers and thin films.

Indicator Dye	Matrix /form	Concentration Range Cu(II) Mol/L)	Regression Coefficient (R^2)	LOD (Molar)
DMK-OFD-7	EC/ nanofiber	5.0×10^{-12} to 5.0×10^{-5}	0.9940	3.3×10^{-13} M
	EC / thin film	5.0×10^{-10} to 5.0×10^{-4}	0.9822	4.6×10^{-11} M

10.9 Stern-Volmer Analysis

The quenching process of chemical sensors based on fluorescence quenching can be described by the well-known Stern-Volmer equation;

$$I_0/I = 1 + K_{sv} [Q] \quad (10.1)$$

I_0 and I are the fluorescence intensities in the absence and presence of quencher respectively, $[Q]$ is the quencher concentration, and K_{sv} is the Stern-Volmer quenching constant. The constant K_{sv} defines the efficiency of quenching. When all other variables are held constant, the higher the K_{sv} , the lower the concentration of quencher required to quench the luminescence.

The data obtained exploiting Stern-Volmer analysis for both; electrospun nanomaterials and continuous thin films are shown in Figure 10.12 and Table 10.4.

Stern- Volmer constants (K_{sv}) of the nanofiber and continuous thin film, calculated from slopes of the plots were found to be 2.00×10^7 (M^{-1}) and 2×10^6 (M^{-1}), respectively. The K_{sv} value calculated for nanomaterial is approximately 10 fold greater than that of obtained from the thin film sensors. The significant enhancement in the sensitivity of the sensor can be attributed to the nanostructure of the electrospun membranes. Here we demonstrated that sensitivity and response related other sensor dynamics can be manipulated by controlling the quencher diffusion rate to fluorophores encapsulated in the polymer via the microstructural properties of the sensing agent. The offered nano-structure was quite beneficial for both the sensitivity and dynamic characteristics of the sensor due to its large specific area, which has high number of active sites for diffusion of Cu^{2+} ions towards the solid phase with respect to the thin films made up of same material. In these structures the possibility of interaction of the analyte ions with the Cu^{2+} selective chromoionophore molecules is higher than that of observed in conventional thin films. The attained LOD values exploiting nano-materials for the offered design ($3.3 \times 10^{-13} M$ for nanofiber and $4.6 \times 10^{-11} M$ for thin film) is an evident of the enhanced sensitivity (see Table 10.3).

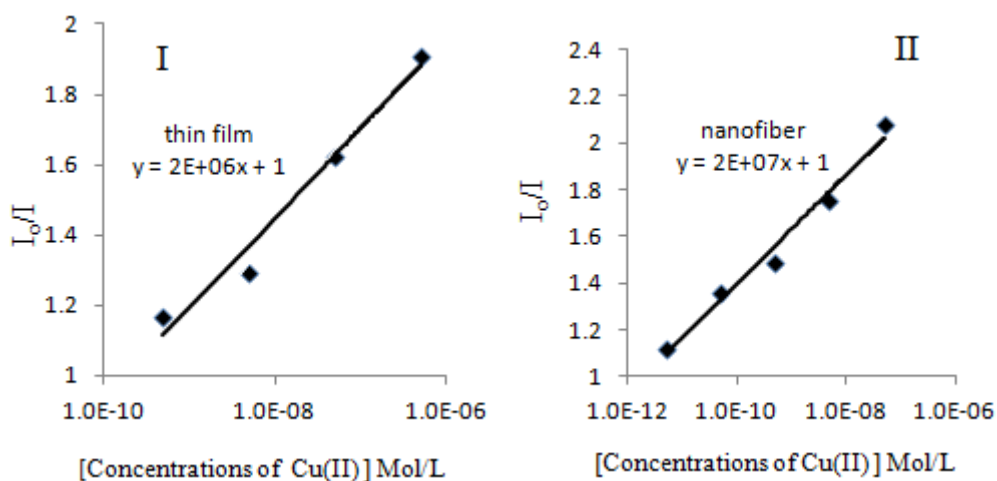


Figure 10.12 The Stern Volmer plot of EC based **I**: thin films and **II**: electrospun nanofibers.

Table 10.4 The Stern Volmer plot and Ksv Constant of EC based electrospun nanofibers and thin films.

Indicator Dye	Matrix /form	Linear Regression Equation	Ksv Constant
DMK-OFD-7	EC/ nanofiber	$y = 2 \cdot 10^7 x + 1$	$2.0 \cdot 10^7$
	EC / thin film	$y = 2 \cdot 10^6 x + 1$	$2.0 \cdot 10^6$

10.10 SEM Images of Electrospun Membranes

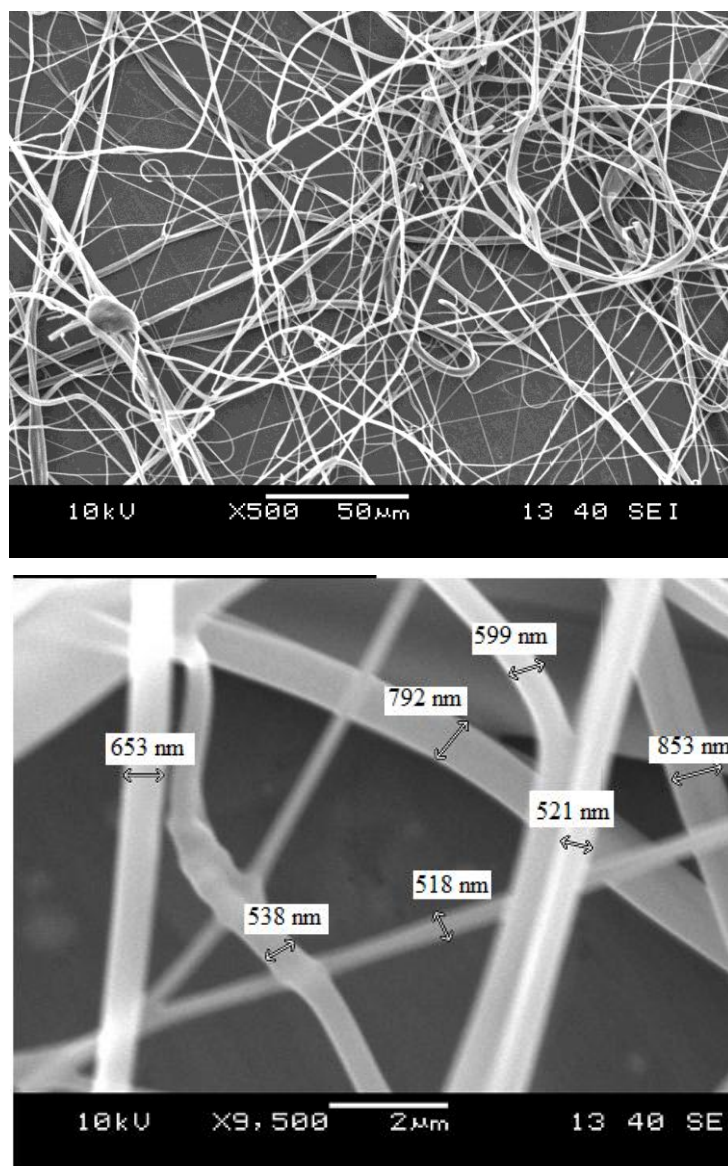


Figure 10.13 SEM images of EC based electrospun nanofibers (a) and (b); EC based nanofibers at different magnifications such as ×500 and ×9500.

The SEM images of EC based electrospun membranes at various magnifications are denoted in Figure 10.13. The membrane has a 3-D structure with a random fiber orientation that is evenly distributed on the substrate. It can be seen from Figure 10.13 that the diameters of the fibers were between 518 and 853 nm.

10.11 Conclusion

It has been fabricated a fiber optic sensor system for selective and sensitive detection of Cu (II) at picomolar level. The system was based on quenching of an indicator. In this research, the exploited polymer based nanofiber produced by electrospinning. With respect to continuous thin films, electrospun nanofibers offered enhanced sensitivity, lower LOD values and reactivity in optical chemical sensing of Cu (II). The DMK-OFD-7 dye was used for the first time as a fluoroionophore in the optical copper ion sensing. The DMK-OFD-7 dye doped EC nanofibers can be used at pH 5.5 for quantitative determination of Cu (II) in the concentration range of 5×10^{-12} - 5×10^{-5} M. A quite good LOD (0.33 pM) was reached and the sensor characteristics was investigated such as response time, reversibility, linear working range, effect of pH and interference effect.

CHAPTER ELEVEN

CONCLUSIONS

The thesis describes the design of optical chemical sensors based on electrospun nanomaterials for the subnanomolar determination of some cation and anions in aqueous samples. A sensing scheme for the selective determination of cations or anions based on fluorescence intensity changes was presented. Highly selective and sensitive nanosensors for Silver (I), Mercury (II), Iron (III), OH⁻, Calcium (II) and Copper (II) ions were developed. The sensor performance characteristics and interference effects of common metal ions for proposed optical sensors were also investigated.

In chapter 4, we introduced design of an emission based optical chemical nanosensor exploiting fluoroionophore encoded as M-AZM for the determination of silver (I) ion at sub-nanomolar level. A dynamic working range of 1.0×10^{-14} to 1.0×10^{-7} M was attained for silver (I) ions. By the help of the nanotechnology a limit of detection of 3.40×10^{-16} M was obtained. To our knowledge this is the first attempt using the fluoroionophore-doped electrospun nano-fibrous materials for silver sensing at femtomolar level (Kacmaz et. al., 2011).

In chapter 5, we tested and developed an EC doped selective fluorescent molecular probes in form of nanofiber for Hg (II) ion sensing. The DC-AZM dye was used for the first time as a fluoroionophore in the optical sensing of mercury (II) ions. The EC based nanofibers can be used at pH 4.0 for quantitative determination of Hg (II) in the concentration range of 1.0×10^{-10} - 1.0×10^{-4} Mol. L⁻¹. A quite good LOD (0.07 nM) was reached. The mercury levels as low as 0.01 and 0.07 nM can be measured with the offered system (Kacmaz et. al., 2012)

In chapter 6, a newly synthesized fluorescent probe is presented for Ag⁺ sensing that is based on the changes in the fluorescence intensity of the TM-AZM dye. The

quantum yield of the dye in EC and PMMA is reasonably high (0.23 and 0.79, respectively). The TM-AZM dye doped nanofibers in EC and PMMA can be used at pH 6.0 for quantitative determination of Ag (I) in the concentration range of 3.51×10^{-7} to 1.43×10^{-2} and 1.0×10^{-7} to 1.0×10^{-2} mol L⁻¹ with an outstanding high selectivity, whereas mercury (II) was the only interferent.

In chapter 7, we introduced highly responsive fluorescent sensors using functional electrospun nanofibers based on fluorescence quenching of an iron selective fluoroionophore. The CBINH dye was used for the first time as a chemosensor in the optical sensing of Fe³⁺. The CBINH dye doped nanofibers can be used at pH 4.5 for quantitative determination of Fe³⁺ in the concentration range of 10⁻¹²-10⁻⁶ M. A quite good LOD (0.07 fM) was reached. The sensor has a response time of <30 s and was fully reversible.

In chapter 8, We offered the BCDA dye as a chemosensor for sensing of OH⁻ ions. The dye contains available active centers for proton attacks and is appropriate for use as fluorescent pH probes for alkaline region between pH 7.0–12.0. Response of the BCDA was fully reversible within the dynamic working range. The response times were between 4–14 min. A relative signal change of 95% and 96% has been achieved for sensor dye of BCDA. The pK_a value of 9.50 makes the BCDA a promising indicator for gaseous and dissolved CO₂ sensing in environmental and physiological samples. The compatibility of the employed Schiff bases with the solid-state optical components (in particular LED's emitting in the wavelength range of 550–590 nm and fiber optics) can be useful in construction of inexpensive and field available instrumentation.

In chapter 9, a novel fluorescent optical sensor using electrospun polymeric nanofibrous membranes for the quantitative analysis of Ca (II) ion is presented. Electrospinning was used as a novel and facile method to fabricate optical chemical sensor devices. With respect to continuous thin films, electrospun nanofibers offered enhanced sensitivity, lower LOD values and reactivity in optical chemical sensing of Ca (II). The DMK-OFD-BIS dye was used for the first time as a fluoroionophore in the optical sensing of calcium. The DMK-OFD-BIS dye doped nanofibers in EC can

be used at pH 4.0 for quantitative determination of Ca (II) in the concentration range of 10^{-10} - 10^{-4} M. A quite good LOD (0.016 nM) was reached.

In chapter 10, a picomolar level sensitive and selective electrospun nanosensor was designed for Cu (II) ion sensing. The system was based on quenching of the fluorescent probe; DMK-OFD-7 upon exposure to copper ions. With respect to continuous thin films, electrospun nanofibers offered enhanced sensitivity, lower LOD values and reactivity in optical chemical sensing of Cu (II). The DMK-OFD-7 dye was used for the first time as a fluoroionophore in the optical copper sensing. The DMK-OFD-7 dye doped EC nanofibers can be used at pH 5.5 for quantitative determination of Cu (II) in the concentration range of $5 \cdot 10^{-12}$ - $5 \cdot 10^{-5}$ M. A quite good LOD (0.33 pM) was reached and the sensor characteristics was investigated such as response time, reversibility, linear working range, effect of pH and interference effect.

REFERENCES

- Alwayn, V. (2004). *Optical Network Design and Implementation* (1st ed.). Cisco Press: Networking Technology.
- Ambroziak, K., & Szypa, M. (2007). A synthesis of unsymmetrical chiral salen ligands derived from 2-hydroxynaphthaldehyde and substituted salicylaldehydes, *Tetrahedron Letters*, *48*, 3331–3333.
- Arienzo M., & Capasso, R. (2000). Analysis of metal cations and inorganic anions in olive oil mill waste waters by atomic absorption spectroscopy and ion chromatography. Detection of metals bound mainly to the organic polymeric fraction. *Journal of Agricultural and Food Chemistry*, *48* (4), 1405–1410.
- Babakhanian, A., Gholivand, M. B., Mohammadi, M., Khodadadian, M., Shockravi, A., Abbaszadeh, M., & Ghanbary, A. (2010). Fabrication of a novel iron(III)–PVC membrane sensor based on a new 1,1-(iminobis(methan-1-yl-1-ylidene))dinaphthalen-2-ol synthetic ionophore for direct and indirect determination of free iron species in some biological and non-biological samples. *Journal of Hazardous Materials*, *177*, 159–166.
- Bacon, J. R., & Demas, J. N. (1987). Determination of oxygen concentrations by luminescence quenching of a polymer-immobilized transition-metal complex. *Analytical Chemistry*, *59*, 2780–2785.
- Baldini, F., Chester, A. N., Homola, J. & Martellucci, S. (2004). *Optical Chemical Sensors*. Italy: Springer.
- Barceloux, D.G. (1999). Copper. *Clinical Toxicology*, *37*, 217–230.
- Beging, S., Mlynek, D., Hataihimakul, S., Poghossiana, A., Baldsiefen, G., Busch, H., Laube, N., Kleinene, L., & Schöninga, M. J. (2010). Field-effect calcium sensor for the determination of the risk of urinary stone formation. *Sensors and Actuators B*, *144*, 374–379.

- Biala, N. (2001). *An Introduction to Fiber-Optic Sensors*. Omron Electronics.
- Blachforda, C., Celic, A., Petri, E. T., & Ehrlich, B. E. (2009). Discrete proteolysis of neuronal calcium sensor-1 (NCS-1) by calpain disrupts calcium binding. *Cell Calcium*, *46*, 257–262.
- Borisov, S. M., Herrod, D. L., & Klimant, I. (2009). Fluorescent poly(styrene-block-vinylpyrrolidone) nanobeads for optical sensing of pH. *Sensors and Actuators B: Chemical*, *139*, 52–58.
- Bottari, B., Maccari, R., Monferto, F., Ottana, R., Rotondo, E., & Vigorita, M. G. (2000). Isoniazid-related copper(II) and nickel(II) complexes with antimycobacterial in vitro activity. *Bioorganic & Medicinal Chemistry Letters*, *10*, 657-60.
- Cano-Raya, C., Fern'andez-Ramos, M. D., G'omez-S'Anchez & Capit'An-Vallvey, L. F. (2006). Irreversible Optical Sensor For Mercury Determination Based On Tetraarylborate Decomposition. *Sensors and Actuators B: Chemical*, *117*, 135-142.
- Cano-Raya, C., Fern'andez-Ramos, M.D., & Capit'an-Vallvey L.F. (2006). Fluorescence resonance energy transfer disposable sensor for copper(II). *Analytica Chimica Acta*, *555*, 299–307.
- Capita'An-Vallvey, L. F., Alvarez de Cienfuegos-Ga'Alvez, P., Fern'andez Ramos, M.D., & Avidad-Castan'eda, R. (2000). Determination of calcium by a single-use optical sensor. *Sensors and Actuators B: Chemical*, *71*, 140-146.
- Carraway, E. R., Demas, J. N., DeGraff, B. A., & Bacon, J. R. (1991). Luminescence quenching mechanism for microheterogeneous systems. *Analytical Chemistry*, *63*, 337–342.
- Celin, S. M., Pandit, M., Kapoor, J. C. & Sharma, R. K. (2003). Studies on photodegradation of 2,4-dinitro toluene in aqueous phase. *Chemosphere*, *53*, 63-69.

- Chambers, J., Krieger, C. G., Kay, L., & Stroud, R. (1974). Silver ion inhibition of serine proteases: crystallographic study of silver–trypsin. *Biochemical and Biophysical Research Communications*, 59, 70–74.
- Chavez, C. P., Garrido, N., & Ahearn, G. A. (2001). Copper transport by lobster hepatopancreatic epithelial cells separated by centrifugal elutriation: measurements with the fluorescent dye, Phen Green. *The Journal of Experimental Biology*, 204, 1433-1444.
- Chen, J., & Teo K. C. (2001). Determination of cobalt and nickel in water samples by flame atomic absorption spectrometry after cloud point extraction. *Analytica Chimica Acta*, 434 (2), 325-330.
- Chen, L. H., Mcbranch, D. W., Wang, H. L., Helgeson, R., Wudl, F. D. & Whitten, G. (1999). Highly sensitive biological and chemical sensors based on reversible fluorescence quenching in a conjugated polymer. *Proceedings of the National Academy of Sciences*, 96, 12287-12292.
- Chen, Z., Megharaj, M., & Naidu, R. (2007). Speciation of chromium in waste water using ion chromatography inductively coupled plasma mass spectrometry. *Talanta*, 72 (2), 394–400.
- Cheney, M. C., Curran, D. J., & Fletcher K. S. (1980). Simultaneous titrimetric determination of bismuth ion and free nitric acid concentrations. *Analytical Chemistry*, 52 (6), 940-942.
- Cheruvally, G., Kim, J. K., Choi, J. W., Ahn, J. H., Shin, Y. J., Manuel, J., Raghavan, P., Kim, K. W., Ahn, H. J., Choi, D. S., & Song, C.E. (2007). Electrospun polymer membrane activated with room temperature ionic liquid: novel polymer electrolytes for lithium batteries. *Journal of Power Sources*, 172, 863–869.
- Citterio, D., Omagari, M., Kawada, T., Sasaki, S., Suzuki, Y., & Suzuki, K. (2004). Chromogenic betaine lariat for highly selective calcium ion sensing in aqueous environment. *Analytica Chimica Acta*, 504, 227–234.

- Clark, H. A., Hoyer, M., Parus, S., Philbert, M. A., Kopelman, R. (1999). Optochemical nanosensors and subcellular applications in living cells. *Mikrochimica Acta*, 131, 121–128.
- Clark, H. A., Kopelman, R., Tjalkens, R., Philbert, M. A. (1999). Optical nanosensors for chemical analysis inside single living cells. 2. Sensors for pH, calcium, and the intracellular application of PEBBLE sensors. *Analytical Chemistry*, 71, 4837–4843.
- Cody, J., & Fahrni, C. J. (2004). Fluorescence sensing based on cation-induced conformational switching: copper-selective modulation of the photoinduced intramolecular charge transfer of a donor–acceptor biphenyl fluorophore. *Tetrahedron*, 60, 11099–11107.
- Coskun, A., & Akkaya, E. U. (2005). Ion sensing coupled to resonance energy transfer: a highly selective and sensitive ratiometric fluorescent chemosensor for Ag (I) by a modular approach. *Journal of the American Chemical Society*, 127, 10464–10465.
- Cotiis, D. A. D., Woll, M. P., Fox, T. E., Hill, R. B., Levenson, R., & John M. (2008). Flanagan Optimized expression and purification of myristoylated human neuronal calcium sensor 1 in E. Coli. *Protein Expression and Purification*, 61, 103–112.
- Crafts, C., Bailey, B., Plante, M., & Acworth, I. (2009). Evaluation of Methods for the Simultaneous Analysis of Cations and Anions Using HPLC with Charged Aerosol Detection and a Zwitterionic Stationary Phase. *Journal of Chromatographic Science*, 47 (7), 534-539.
- Deitzel, J. M., Kleinmeyer, J., & Tan, N. C. B. (2001). The effect of processing variables on the morphology of electrospun nanofibers and textiles, *Polymer*, 42, 261–272.

- Demas, J. N., DeGraff, B. A., & Xu, W. (1995). Modeling of Luminescence Quenching-Based Sensors: Comparison of Multisite and Nonlinear Gas Solubility Models. *Analytical Chemistry*, *67*, 1377-1380.
- Derinkuyu, S., Ertekin, K., Oter, O., & Ergun, Y. (2010). pH-Driven Fluorescent Switch Behavior of Azometine Dyes in Solid Matrix Materials. *Spectroscopy Letters*, *43*, 500.
- Derinkuyu, S., Ertekin, K., Oter, O., Denizalti, S., & Cetinkaya, E. (2008). Emission based fiber optic pH sensing with Schiff bases bearing dimethylamino groups. *Dyes Pigments*, *76*, 133–141.
- Dhami, S., Mello A. J., Rumbles, G., Bishop, S. M., Phillips, D. & Beeby, A. (1995). Phthalocyanine fluorescence at high concentration: dimers or reabsorption effect. *Photochemistry and Photobiology*, *61*, 341.
- Ding, B., Kim, J., Miyazaki, Y. & Shiratori, S. (2004a). Electrospun nanofibrous membranes coated quartz crystal microbalance as gas sensor for NH₃ detection. *Sensors and Actuators B: Chemical*, *101*, 373-380.
- Ding, B., Yamazaki, M. & Shiratori, S. (2004b). Electrospun fibrous polyacrylic acid membrane-based gas sensors. *Sensors and Actuators B: Chemical*, *106*, 477-483.
- Dumasa, S., Grabchev, I., Stoikova, P., Chauvinc, J., & Chovelona, J. M. (2009). Synthesis of benzanthron derivatives for selective detection by fluorescence of copper ions. *Journal of Photochemistry and Photobiology A: Chemistry*, *201*, 237–242.
- El Naschie, M. S. (2006). Nanotechnology for the developing world. *Chaos, Solitons & Fractals*, *30* (4), 769-773.
- Environment Protection Agency, (EPA) 4405-80-071, (1980). *Ambient Water Quality Criteria For Silver*, Office of Water Regulations, Washington, DC.

- Ertekin K, Alp S, Karapire C, Yenigul B, Henden E, & Icli S. (2000). Fluorescence emission studies of an azlactone derivative embedded in polymer films; An optical sensor for pH measurements. *Journal of Photochemistry and Photobiology A: Chemistry*, 137, 155-161.
- Ertekin, K., Karapire, C., Alp, S., Yenigul, B., & Icli, S. (2003). Photophysical and photochemical characteristics of an azlactone dye in sol-gel matrix; a new fluorescent pH indicator. *Dyes Pigments*, 56, 125-133.
- Ertekin, K., Oter, O., Ture, M., Denizalti, S., & Cetinkaya, E., (2009). A Long Wavelength excitable fluorophore; chloro phenyl imino propenyl aniline (CPIPA) for selective sensing of Hg (II). *Journal of Fluorescence*, 20, 533-540.
- Fan, C., Plaxco, K. W., & Heeger, A. J. (2002). High-efficiency fluorescence quenching of conjugated polymers by proteins. *Journal of the American Chemical Society*, 124(20), 5642-5643.
- Fana, J., Guoa, K., Penga, X., Dua, J., Wang, J., Suna, S., & Li, H. (2009). A Hg²⁺ fluorescent chemosensor without interference from anions and Hg²⁺ imaging in living cells. *Sensors and Actuators B: Chemical*, 142, 191–196.
- Forstner, U., & Wittmann, G. T. (1981). *Metal Pollution in the Aquatic Environment*. Springer: Berlin.
- Forstner, U., & Wittmann, G. T. (1981). *Metal Pollution in the Aquatic Environment*. Springer: Berlin .
- Fresenius, W., Quentin, K. E., & Schneider, W. (1988). *Water Analysis*. Springer: Berlin.
- Fresenius, W., Quentin, K. E., & Schneider, W. (1988). *Water Analysis*. Springer: Berlin.
- Galinski, M., Lewandowski, A., & Stepniak, I. (2006). Ionic liquids as electrolytes, *Electrochimica Acta*, 51, 5567–5580.

- Gibson, P., Schreuder-Gibson, H., & Rivin, D. (2001). Transport properties of porous membranes based on electrospun nanofibers. *Colloids Surface A*, 187/188, 469–481.
- Gouma, P.I. (2003). Nanostructured polymorphic oxides for advanced chemosensors, *Reviews On Advanced Materials Science*, 5, 147-154.
- Greenberg, A. A., Clesceri, L. S., Eaton, A. D. (1992). *Standard Methods for the Examination of Water & Wastewater* (18nd Ed). Amer Public Health Assn.
- Grigoras, M., & Antonoaia, N. C. (2005). Synthesis and characterization of some carbazolebased imine polymers. *European Polymer Journal*, 41, 1079–1089.
- Gupta, V. K., Jain, A. K., Agarwal, S., Maheshwari, G. (2007). An iron (III) ion-selective sensor based on a -bis(tridentate) ligand. *Talanta*, 71, 1964–1968.
- Haghi, A. K., & Zaikov, G. (2011). *Advances in Nanofibre Research*. Smithers: Rapra.
- Harris, H. H, Pickering, I. J, & George, G. N. (2003). The chemical form of mercury in fish. *Science*, 301, 1203.
- He, H., Jenkins, K., & Lin, C. (2008). A fluorescent chemosensor for calcium with excellent storage stability in water. *Analytica chimica acta*, 611, 197–204.
- He, J., Liu, Y., Mo, L., Wan, Y., & Xu, L. (2008). *Electrospun Nanofibres and Their Applications*. Smithers Rapra Technology.
- Hiissa, T., Sirén, H., Kotiaho, T., Snellman, & M. Hautojärvi, A. (1999). Quantification of anions and cations in environmental water samples: Measurements with capillary electrophoresis and indirect-UV detection. *Journal of Chromatography A*, 853(1–2), 403–411.
- Hu, Z., Feng, Y., Huang, H., Ding, L., Wang, X., Lin, C., Li, M., & Ma, C. (2011). Fe³⁺ selective fluorescent probe based on rhodamine B and its application in bioimaging. *Sensors and Actuators B: Chemical*, 156, 428–432.

- Hulanicki, A., Geab, S., & Ingman F. (1991). Chemical sensors definitions and classification. *Pure and Applied Chemistry*, 63 (9), 1247-1250.
- Iyoshi, S., Taki, M., & Yamamoto, Y. (2008). Rosamine-based fluorescent chemosensor for selective detection of silver (I) in an aqueous solution. *Inorganic Chemistry*, 4, 3946–3948.
- Jackson, P. E. (2001). Determination of inorganic ions in drinking water by ion chromatography. *Trends in Analytical Chemistry*, 20 (6–7), 320–329.
- Jezek, J., Dilleen, J. W., Haggett, B. G. D., Fogg, A. G., & Birchi, B. J. (2007). Hexacyanoferrate (III) as a mediator in the determination of total iron in potable waters as iron(II)-1,10-phenanthroline at a single-use screen-printed carbon sensor device. *Talanta*, 71, 202–207.
- Jin, J., & Rosenzweig, Z., (1999). Fiber optic pH/Ca²⁺ fluorescence microsensor based on spectral processing of sensing signals. *Analytica Chimica Acta*, 397, 93–102.
- Jung, H., Singh, N., Lee, D. Y., & Jang, D. O. (2010). Single sensor for multiple analytes: chromogenic detection of I⁻ and fluorescent detection of Fe³⁺. *Tetrahedron Letters*, 51, 3962–3965.
- Kacmaz, S., Ertekin K., Suslu, A. Ergun, Y., Celik, E., & Cocen, U. (2012). Sub-nanomolar sensing of ionic mercury with polymeric electrospun nanofibers. *Materials Chemistry and Physics*, 133, 547–552.
- Kacmaz, S., Ertekin, K., Suslu, A., Ozdemir, M., Ergun, Y., Celik, E., & Cocen, U. (2011). Emission based sub-nanomolar silver sensing with electrospun nanofibers. *Sensors and Actuators B: Chemical*, 153, 205–213.
- Kandaz, M., Güney, O., & Senkal, B. F. (2009). Fluorescent chemosensor for Ag (I) based on amplified fluorescence quenching of a new phthalocyanine bearing derivative of benzofuran. *Polyhedron*, 28, 3110–3114.

- Kim, H., & Choi, H. (2001). Spectrofluorimetric determination of copper(II) by its static quenching effect on the fluorescence of 4,5-dihydroxy-1,3-benzenedisulfonic acid. *Talanta*, 55, 163–169.
- Kimura, K., Yajima, S., Tatsumi, K., Yokoyama, M., & Oue, M. (2000). Silver ion-selective electrodes using coordinate calix[4]arene derivatives as soft neutral carriers. *Analytical Chemistry*, 72, 5290–5294.
- Klockenkampfer, R. (1997). *Total-Reflection X-ray Fluorescence Analysis*. Wiley: New York.
- Klockenkampfer, R. (1997). *Total-Reflection X-ray Fluorescence Analysis*. Wiley: New York.
- Koca, A., Gonca, E., & Gül, A. (2008). Voltammetric and spectroelectrochemical characterization of porphyrazines: electrochemical metal sensor. *Journal of Electroanalytical Chemistry*, 612, 231–240.
- Kocincova, A.S., Borisov, S.M., Krause, Ch., & Wolfbeis, O.S. (2007). Fiber-optic microsensors for simultaneous sensing of oxygen and pH, and of oxygen and temperature. *Analytical Chemistry*, 79, 8486–8493.
- Kuhn, M. A., Hoyland, B., Carter, S., Zhang, C., & Haugland, R. P. (1995). *Fluorescent ion indicators for detecting heavy metals*. Proc. SPIE-Int'l Soc. Opt. Eng. 238, 2388.
- Kuswandia, B. & Narayanaswamy, R. (2001). Selective pool optode for mercury ion sensing in aqueous solution. *Sensors and Actuators B-Chemical*, 74, 131-137.
- Kwoun, S. J., Lee, R. M., Han, B. & Ko, F. K. (2000). A novel polymer nanofiber interface for chemical sensor applications. *Int. Frequency Control Symp. Exh*, 52-57.
- Kwoun, S. J., Leo, R. M., Han, B., & Ko, F. K. (2001). Polymer nanofiber thin films for biosensor applications. *Proc of the IEEE 27th Annual Northeast Bioengineering Conference*, 9-10.

- Lakowicz, J. R. (1999). *Principles of Fluorescence Spectroscopy*. Plenum Press: New York and London.
- Lala, N. L., Ramaseshan, R., Ramakrishna, S. (2005). A novel nanofiber based material system for glucose biosensor application. *Journal of Nanoengineering and Nanosystem Part N*, submitted.
- Lee, S. H., Ku, B. C., Wang, X., Samuelson, L. A. & Kumar, J. (2002b). Design, synthesis and electrospinning of a novel fluorescent polymer for optical sensor applications. *Materials Research Society Symposium Proc*, 708, pp. BB10.45.1-BB10.45.6.
- Liang, P., Qin, Y., Hu, B., Peng, T., & Jiang, Z. (2001). Nanometer-size titanium dioxide microcolumn on-line preconcentration of trace metals and their determination by inductively coupled plasma atomic emission spectrometry in water. *Analytica Chimica Acta*, 440 (2), 207–213.
- Lin W, Long L, Yuan L, Cao Z, & Feng J. (2009). A novel ratiometric fluorescent Fe^{3+} sensor based on a phenanthroimidazole Chromophore. *Analytical Chimica Acta*, 634, 262–266.
- Liu, H., Kameoka, J., Czaplewski, D. A. & Craighead, H.G. (2004). Polymeric nanowire chemical sensor. *Nano Letter*, 4 (4), 671-675.
- Lohani CR, & Lee K. (2010). The effect of absorbance of Fe^{3+} on the detection of Fe^{3+} by fluorescent chemical sensors. *Sensors and Actuators B: Chemical*, 143, 649–654.
- Lv, J., Ouyang, C., Yin, X., Zheng, H., Zuo, Z., Xu, J., Liu, H., & Li, Y. (2008). Reversible and highly selective fluorescent sensor for mercury (II) based on a water-soluble poly(*para*-phenylene)s containing thymine and sulfonate moieties. *Macro Rapid Communication*, 29, 1588.

- Mahendra, N., Gangaiya, P., Sotheeswaran, S., & Narayanaswamy, R. (2002). Investigation of a Cu(II) fibre optic chemical sensor using fast sulphon black F (FSBF) immobilised onto XAD-7. *Sensors and Actuators B: Chemical*, 81, 196-201.
- Malcik N, & Caglar P. (1997). The operational parameters of a new fibre-optic sensor for ferric ions in aqueous media. *Sensors and Actuators B: Chemical*, 38-39, 386-389.
- Malcik, N., Caglar, P., & Narayanaswamy, R. (2000). Investigations into optical sensing of cupric ions using several immobilized reagents. *Quimica Analitica*, 19, 94-98.
- Manesh, K. M., Santhosh, P., Gopalan, A., & Lee, K. (2007). Electrospun poly(vinylidene fluoride)/poly(aminophenylboronic acid) composite nanoweb membrane as a novel glucose sensor. *Analytical Biochemistry*, 360, 189–195.
- Mayr, T., Klimant, I., Wolfbeis, O. S., & Werner, T. (2002). Dual lifetime referenced optical sensor membrane for the determination of copper (II) ions. *Analytica Chimica Acta*, 462 (1), 1-10.
- Mélares, C., & Gandini, A. (1996). Polymeric schiff bases bearing furan moieties 2. polyazines and polyazomethines. *Polymer International*, 40, 33–39.
- Merian, E. (1991). *Metals and Their Compounds in the Environment*, VCH:Weinheim.
- Merian, E. (1991). *Metals and Their Compounds in the Environment*. VCH: Weinheim.
- Miller J. C., Seratto, R., & Cardences, J. M. R. (2005). *The handbook of nanotechnology*. New Jersey: John Wiley & Sons.
- Mills A., Chang Q., & McMurray N. (1992). Equilibrium studies on colorimetric plastic film sensors for carbon dioxide. *Analytical Chemistry*, 64, 1383.

- Motlagh, M. G., Taher, M. A., & Ahmadi, A. (2010). PVC membrane and coated graphite potentiometric sensors based on 1-phenyl-3-pyridin-2-yl-thiourea for selective determination of iron(III). *Electrochimica Acta*, 55(22), 6724-6730.
- Murkovic, I. & Wolfbeis, O. S. (1997). Fluorescence-based sensor membrane for mercury (II) detection. *Sensors and Actuators B: Chemical*, 38-39, 246-251.
- Oter, O., Ertekin K., Kirilmis, C. & Koca, M. (2007). Spectral characterization of a newly synthesized fluorescent semicarbazone derivative and its usage as a selective fiber optic sensor for copper(II). *Analytica Chimica Acta*, 584, 308–314.
- Oter, O., Ertekin, K., & Derinkuyu, S. (2008). Ratiometric sensing of CO₂ in ionic liquid modified ethyl cellulose matrix. *Talanta*, 76, 557–563.
- Oter, O., Ertekin, K., Kılıncarslan, R., Ulusoy, M., & Cetinkaya, B. (2007). Photocharacterization of a novel fluorescent Schiff Base and investigation of its utility as an optical Fe³⁺ sensor in PVC matrix. *Dyes and Pigments*, 74, 730-5.
- Oter, O., Ertekin, K., Kirilmis, C., Koca, M., & Ahmedzade, M. (2007). Characterization of a newly synthesized fluorescent benzofuran derivative and usage as a selective fiber optic sensor for Fe(III). *Sensors and Actuators B: Chemical*, 122, 450–456.
- Oter, O., Ertekin, K., Topkaya, D., & Alp, S. (2006) Emission-based optical carbon dioxide sensing with HPTS in green chemistry reagents: room-temperature ionic liquids. *Analytical And Bioanalytical Chemistry*, 386, 1225–1234.
- Parker, C. A. (1968). *Photoluminescence of Solutions*. Elsevier: Amsterdam.
- Pearson RG. (1973). *Hard and Soft Acids and Bases*. Hutchinson and Ross Inc. in: Dowden (Ed.), Stroudsburg.
- Peng, J., He, X., Wang, K., Tan, W., Wang, Y., & Liu, Y. (2007). Noninvasive monitoring of intracellular pH change induced by drug stimulation using silica nanoparticle sensors. *Analytical and Bioanalytical Chemistry*, 388, 645–654.

- Pons, C., Forteza, R., & Cerd, V. (2005). Optical fibre reflectance sensor for the determination and speciation analysis of iron in fresh and seawater samples coupled to a ultisyringe flow injection system. *Analitical Chimica Acta*, 528, 197–203.
- Pringsheim, E., Zimin, D., & Wolfbeis, O. S. (2001). Fluorescent beads coated with polyaniline. A novel nanomaterial for optical sensing of pH. *Advanced Material*, 13, 819–822.
- Pulido-Tofin˜o, P., Barrero-Moreno, J. M., & Pe´rez-Conde, M.C. (2000). A flow-through fluorescent sensor to determine Fe(III) and total inorganic iron. *Talanta*, 51, 537–545.
- Ramarkrishra, S., Fujihara, K., Teo, W., Lim, T., & Ma, Z. (2005). *An introduction to electrospinning and nanofibers* (3th ed.). Singapore: World Scientific.
- Rapisarda, V. A., Volentini, S. I., Farias, R. N., & Massa, E. M. (2002). Quenching of bathocuproine disulfonate fluorescence by Cu(I) as a basis for copper quantification. *Analytical Biochemistry*, 307, 105–109.
- Reneker, D. H. & Chun. I. (1996). Nanometre diameter fibres of polymer, produced by electrospinning. *Nanotechnology*, 7 (3), 215-216.
- Reneker, D.H., & Chun, I. (1996). Nanometer diameter fibers of polymer produced by electrospinning. *Nanotechnology*, 7, 216–223.
- Rocha, F. R. P., Martelli, P. B., & Reis B. F. (2004). Simultaneous in-line concentration for spectrophotometric determination of cations and anions. *Journal of the Brazilian Chemical Society*, 15 (1), 38-42.
- Romano, J. P., & Krol J. (1993). Capillary ion electrophoresis, an environmental method for the determination of anions in water. *Journal of Chromatography A*, 640 (1–2), 403–412.
- Sawicka K, Gouma P, & Simon S. (2005). Electrospun biocomposite nanofibers for urea biosensing. *Sensors and Actuators B: Chemical*, 108, 585–8.

- Scaiano, J. C. (1989). *Handbook of Organic Photochemistry*. CRC Press.
- Schmidt, W. (1994). *Optische Spektroskopie*. VCH: Weinheim.
- Selid, P. D., Xu, H. Y., Collins, E. M., Face-Collins, M. S., & Zhao, J. X. (2009). Sensing mercury for biomedical and environmental monitoring. *Sensors*, *9*, 5446–5459.
- Shamsipur, M., Alizadeh, K., Hosseini, M., Caltagirone, C.V., & Lippolis, B. (2006). A selective optode membrane for silver ion based on fluorescence quenching of the dansylamidopropyl pendant arm derivative of 1-aza-4,7,10-trithiacyclododecane ([12]aneNS3). *Sensors and Actuators B*, *113*, 892–899.
- Sperling, M., Xu, S., & Welz, B. (1992). Determination of chromium (III) and chromium (VI) in water using flow injection on-line preconcentration with selective adsorption on activated alumina and flame atomic absorption spectrometric detection. *Analytical Chemistry*, *64* (24), 3101–3108.
- Steinberg, I. M., Lobnik, A., & Wolfbeis, O. S. (2003). Characterisation of an optical sensor membrane based on the metal ion indicator Pyrocatechol Violet. *Sensors and Actuators B: Chemical*, *90* (1), 230-235(6).
- Szigeti, Z., Malon, A., Vigassy, T., Csokai, V., Grün, A., Wygladacz, K., Ye, N., Xu, C., Chebny, V. J., Bitter, I., Rathore, R., Bakker, E., & Pretsch, E. (2006). Novel potentiometric and optical silver ion-selective sensors with subnanomolar detection limits. *Analytical Chimica Acta*, *572*, 1–10.
- Taylor, G. (1964). *Dispersion of soluble matter in solvent flowing through a tube*. Proceedings of the Royal Society of London Series A.
- Thompson, R. B., Ge, Z. F., Patchan, M., Huang, C. C., & Fierke, C. A. (1996). Fiber optic biosensor for Co (II) and Cu(II) based on fluorescence energy transfer with an enzyme transducer. *Biosensors and Bioelectronics*, *11* (6/7), 557-564.

- Topal, S. Z., Gürek, A. G., Ertekin, K., Atilla, D., Yenigül, B., & Ahsen, V. (2010). Silver and proton driven fluorescent multiple-mode molecular logic gates employing phthalocyanines. *Materials Chemistry and Physics*, *121*, 425–431.
- Topal, S. Z., Yüksel, F., Gürek, A. G., Ertekin, K., Yenigül, B., & Ahsen, V. (2010). Fluorescent probes for silver detection employing phthalocyanines in polymer matrices. *Sensor Letters*, *8*, 1–8.
- Turro NJ. (1978). *Modern Molecular Photochemistry*. The Benjamin/ Cummings Publishing Co.: Menlo Park, CA.
- Vasylevska, A.S. Karasyov, A.A., Borisov, S.M., Krause, Ch. (2007). Novel coumarin-based fluorescent pH indicators, probes and membranes covering a broad pH range. *Analytical and Bioanalytical Chemistry*, *387*, 2131-2141.
- Vasylevska, G. S., Borisov, S. M., Krause, Ch., & Wolfbeis, O. S. (2006). Indicator-loaded permeation-selective microbeads for use in fiber optic simultaneous sensing of pH and dissolved oxygen. *Chemistry of Material*, *18*, 4609–4616.
- Wan, Q., Feng, X. B., Lu, J., Zheng, W., Song, X. J., Han, S. J., & Xu, H. (2009). Atmospheric mercury in Changbai Mountain area, northeastern China I. The seasonal distribution pattern of total gaseous mercury and its potential sources. *Environmental Research*, *109*, 201–206.
- Wang, H. H., Xue, L., Qian, Y. Y., & Jiang, H. (2010). Novel ratiometric fluorescent sensor for silver ions. *Organic Letters*, *12*, 292–295.
- Wang, X., Drew, C., Lee, S. H., Senecal, K. J, Kumar, J., & Samuelson, L. A. (2002). Electrospun nanofibrous membranes for highly sensitive optical sensors. *Nano Letter*, *2*, 1273–1275.
- Wang, X., Drew, C., Lee, S., Senecal, K. J., Kumar, J., & Samuelson, L. A. (2002). Electrospun Nanofibrous Membranes for Highly Sensitive Optical Sensors. *Nano Letter*, *2*, 1273-1275.

- Wang, X., Kim, Y. G., Drew, C., Ku, B. C., Kumar, J., & Samuelson, L.A. (2004). Electrostatic assembly of conjugated polymer thin layers on electrospun nanofibrous membranes for biosensors. *Nano Letter*, 4 (2), 331-334.
- Wang, X., Kim, Y., Drew, C., Ku, B., Kumar, J., & Samuelson, L.A. (2004). Electrostatic assembly of conjugated polymer thin layers on electrospun nanofibrous membranes for biosensors. *Nano Letter*, 4, 331-334.
- Water Project*. (n. d.) Retrieved May, 12, 2012, from http://water157.narod.ru/clear/root_e.htm
- Williams, A. T. R., Winfield, S. A., & Miller, J. N. (1983). Relative fluorescence quantum yields using a computer controlled fluorescence spectrometer. *Analyst*, 108, 1067–1071.
- Wolfbeis, O. S. (1991). *Fiber Optic Chemical Sensors and Biosensors*. CRC, Press: London.
- Wu, S., Chen, Y., & Sung, Y. (2011). Colorimetric detection of Fe³⁺ ions using pyrophosphate functionalized gold nanoparticles. *Analyst*, 136, 1887.
- Yang, J. S. & Swager, T. M. (1998). Fluorescent Porous Polymer Films as TNT Chemosensors: Electronic and Structural Effects. *Journal of American Chemical Society*, 120 (46), 11864-11873.
- Yarasir, M. N., Kandaz, M., Senkal, B. F., Koca, A., & Salih, B. (2007). Metal-ion sensing aggregation studies on reactive phthalocyanines bearing soft-metal receptor moieties: synthesis, spectroscopy and electrochemistry. *Polyhedron*, 26, 5235–5242.
- Yari, A., & Papi, F. (2009). Highly selective sensing of mercury (II) by development and characterization of a PVC-based optical sensor. *Sensors and Actuators B: Chemical*, 138, 467–473.

- Yeh, T. C., Tien, P., & Chau, L.K. (2001). Cladding fiber-optic evanescent-wave absorption copper (II) sensor based on sol-gel-derived organofunctionalized silica cladding. *Applied Spectroscopy*, 55 (10), 1320-1326.
- Yuan, M., Li, Y., Li, J., Li, C., Liu, X., Lv, J., Xu, J., Liu, H., Wang, S., & Zhu, D. (2007). A colorimetric and fluorometric dual-modal assay for mercury ion by a molecule. *Organic Letter*, 9, 2313-2316.
- Zhang, X., Chenga, G., Zhang, W., Shen, G., & Yu, R. (2007). A fluorescent chemical sensor for Fe³⁺ based on blocking of intramolecular proton transfer of a quinazolinone derivative. *Talanta*, 71, 171–177.
- Zhu, M., Yuan, M., Liu, X., Xu, J., Lv, J., Huang, C., Liu, H., Li, Y., Wang, S. & Zhu, D. (2008). Visible Near-Infrared Chemosensor for Mercury Ion. *Organic Letter*, 10 (7), 1481-1484.
- Zhu, X. J., Fu, S., & Wong, W. Y. (2008). A near-infrared fluorescent chemodosimeter for silver(I) ion based on an expanded porphyrin. *Tetrahedron Letters*, 49, 1843–1846.